Università degli Studi di Milano

Department of Pharmacological and Biomolecular Sciences

PhD School of Experimental and Clinical Pharmacological Sciences

XXXIII Cycle

Oxidized LDL/CD36/PPARγ circuitry is a trigger of adipogenesis in Arrhythmogenic Cardiomyopathy.

Ilaria Stadiotti

Student ID: R11936

Tutor: Prof. Marina Camera

Co-Tutor: Prof. Giulio Pompilio

Coordinator: Chiar.mo Prof. Alberico Luigi Catapano

A.A. 2019/2020

Table of contents

List of Figures and Tables

Abbreviations

13HODE: 13-hydroxy-octadecadienoic acid

9-HODE: 9-hydroxyoctadecadienoic acid

ACE: angiotensin-converting enzyme

ACM: arrhythmogenic cardiomyopathy

ACOT1: acyl-CoA thioesterase 1

AF: allele frequency

Akt: protein kinase B

AM: adipogenic medium

AP-1: activator protein 1

ARVC/D: arrhythmogenic right ventricular cardiomyopathy/dysplasia

BS: Brugada syndrome

CD: chow diet

CDH2: N-cadherin

CE: esterified cholesterol

CMR: cardiac magnetic resonance

C-MSC: cardiac mesenchymal stromal cells

CPTV: cathecholaminergic polymorphic ventricular tachycardia

CTNNA3: α-T-catenin

CVDs: cardiovascular diseases

Cx43: connexin 43

DCF: 2′,7′-Dichlorofluorescein diacetate

DCM: dilated cardiomyopathy

DES: desmin

DSC2: desmocollin-2

DSG2: desmoglein-2

DSP: desmoplakin

EB: embryoid bodies

ECG: electrocardiogram

EF: ejection fraction

ENDO: endocardium

EPI: epicardium

ERK1/2: extracellular signal-regulated kinase 1/2

FBS: fetal bovine serum

FC: free cholesterol

FDR: false discovery rate

FFA: free fatty acids

FLNC: filamin C

GLC: gas-liquid chromatographer

GM: growth medium

GSH: reduced glutathione

GSK3β: glycogen synthase kinase-3β

GSSG: oxidized glutathione

HC: healthy control

HDL: high-density lipoproteins

HFD: high fat diet

HIF-1α: hypoxia-inducible factor 1α

hiPSC-CM: human induced pluripotent stem cell-derived cardiomyocytes

HO-1: heme oxygenase-1

ICD: implantable cardioverter defibrillator

ID: intercalated disks

IDL: intermediate density lipoproteins

IF: immunofluorescence

IL-1: interleukin 1

IL-6: interleukin 6

IMDM: Iscove's modified Dulbecco's media

JNK: c-Jun N-terminal kinase

KO: knockout

LBBB: left bundle branch block

LC-MS/MS: liquid chromatography-tandem mass spectrometry

LDL: low density lipoproteins

LDLR: LDL receptor

LMNA: lamin A/C

LOX1: lectin-like oxLDL receptor-1

LV: left ventricle

MACE: major arrhythmic cardiovascular events

MAE: major arrhythmic events

MAPK: p38 mitogen-activated protein kinase

MDA: malondialdehyde

MFI: median fluorescence intensity

MGST3: microsomal glutathione S-transferase 3

n: number of subjects

na: not available

NAC: N-acetylcysteine

NFAT: nuclear factor of activated T-cells

NFkB: nuclear factor kappa-light-chain-enhancer of activated B cells

NR: nile red

Nrf2: nuclear factor erythroid 2–related factor 2

ORO: oil red o

OxLDL: oxidized low density lipoproteins

PBMC: peripheral blood mononuclear cells

PCA: principal component analysis

PDGFRα: platelet-derived growth factor receptor α

PG: plakoglobin

PGC-1α: peroxisome proliferator-activated receptor γ coactivator-1α

PI3: phosphoinositide 3-kinase

PKP2: plakophilin-2

Pkp2+/-: *Pkp2* heterozygous knock-out mice

PLIN1: perilipin 1

PLN: phospholamban

PPARγ: peroxisome proliferator-activated receptor γ

RBBB: right bundle branch block

RLE: relative log expression

ROC: receiver operating characteristic

ROS: reactive oxygen species

RT: room temperature

RV: right ventricle

RVIDd: right ventricular internal diameter in diastole

RVIDs: right ventricular internal diameter in systole

RVOT: right ventricular outflow tract

RYR2: ryanodine receptor-2

SCN5A: voltage-gated sodium channel alpha subunit 5

SP-1: specificity protein 1

SR: sarcoplasmic reticulum

SR: scavenger receptors

SSFP: steady state free precession

STAT 1/3: signal transducer and activator of transcription 1 and 3

TCF/LEF: T cell/lymphoid-enhancing binding

TG: triglycerides

TGFB3: transforming growth factor-beta 3

TJP1: tight junction protein-1

TLR4: toll-like receptor-4

TMEM43: transmembrane protein 43

TNF: tumor necrosis factor

TnTI: troponin I

TTN: titin

VA: ventricular arrhythmias

VLDL: very low density lipoproteins

VT: ventricular tachycardia

WB: western blot

WT: wild type

YAP: yes-associated protein

Abstract

English version

Rationale and hypothesis. Arrhythmogenic Cardiomyopathy (ACM) is a cardiac condition hallmarked by ventricular tissue fibro-adipogenic alterations, contributing to progressive function deterioration and arrhythmias. Although genetically-determined, mainly by mutations in desmosomal genes (*e.g. PKP2*), ACM clinical phenotypes are highly variable for poorly understood reasons. More data on molecular phenotype modulators, clinical prognosticators and etiological therapies are awaited. We hypothesized that oxidized low density lipoproteins (oxLDL)-dependent activation of peroxisome proliferator-activated receptor γ (PPARγ), a recognized effector of ACM adipogenesis, may contribute to disease pathogenesis.

Methods and results. ACM patients showed higher plasma concentration of oxLDL vs. matched healthy controls (HC) and vs. ACM mutation-carrier healthy relatives. Moreover, we found higher lipid peroxidation indexes in cardiac bioptic tissues of ACM vs. HC subjects.

By using ACM patient-derived cardiac mesenchymal stromal cells and induced pluripotent stem cell-derived cardiomyocytes, we demonstrated that oxLDL and their component 13-hydroxy-octadecadienoic acid (13HODE) are major cofactors of cardiac adipogenesis. Mechanistically, the increased lipid accumulation is mediated by oxLDL cell internalization through the scavenger receptor CD36, ultimately resulting in PPARγ upregulation.

By boosting oxLDL plasma concentration in a *Pkp2* heterozygous knock-out ACM mouse model, through high fat diet feeding, we confirmed *in vivo* the dependency of cardiac adipogenesis and right ventricle dysfunction on oxidized lipid metabolism. Conversely, atorvastatin treatment prevented these phenotypes. Importantly, high oxLDL plasma levels predict a severe clinical phenotype in terms of fat infiltration, ventricular dysfunction and risk of major arrhythmic events in ACM patients.

Conclusions. The modulatory role of oxidized lipids in ACM adipogenesis, as demonstrated at cellular, mouse and patient levels, represents a novel molecular pathogenic mechanism relevant for patients' risk stratification and for new pharmacological strategies.

Italian version

Razionale e ipotesi. La Cardiomiopatia Aritmogena (ACM) è una patologia cardiaca caratterizzata da sostituzione fibro-adiposa del miocardio ventricolare e aritmie maligne. Nonostante sia geneticamente determinata, soprattutto da mutazioni in geni desmosomiali (ad esempio mutazioni in *PKP2*), i fenotipi clinici ACM sono altamente variabili e i meccanismi molecolari alla base della variabilità fenotipica non sono del tutto noti. Abbiamo ipotizzato che le lipoproteine a bassa densità ossidate (oxLDL), agendo sul recettore gamma attivato dai proliferatori dei perossisomi (PPARγ), il principale regolatore del processo adipogenico nell'ACM, possano contribuire alla patogenesi della malattia.

Metodi e risultati. I pazienti ACM hanno mostrato un'elevata concentrazione plasmatica di oxLDL rispetto a controlli sani (HC) matchati per sesso, età e fattori di rischio cardiovascolari, e rispetto a loro famigliari portatori della stessa mutazione causativa ma asintomatici. Inoltre, abbiamo ottenuto una maggiore perossidazione lipidica nel tessuto cardiaco di pazienti ACM rispetto a HC.

Utilizzando come modelli *in vitro* cellule mesenchimali stromali cardiache ottenute da pazienti e cardiomiociti derivati da cellule staminali pluripotenti indotte, abbiamo dimostrato che le oxLDL e il loro componente acido 13-idrossi-octadecadienoico (13HODE) sono cofattori di adipogenesi nell'ACM. Dal punto di vista meccanicistico, l'aumento dell'accumulo lipidico dipende dall'internalizzazione di oxLDL nelle cellule attraverso il recettore CD36, provocando l'aumento di PPARγ.

Inducendo l'aumento delle oxLDL plasmatiche nel modello murino ACM eterozigote knock-out per *Pkp2*, attraverso una dieta ad alto contenuto di grassi e colesterolo, abbiamo confermato *in vivo* l'effetto del metabolismo dei lipidi ossidati sull'adipogenesi cardiaca e disfunzione ventricolare. Il trattamento con atorvastatina, invece, ha prevenuto questi fenotipi.

Alti livelli plasmatici di oxLDL predicono un fenotipo clinico severo, in termini di infiltrazione adiposa, disfunzione ventricolare e rischio di eventi aritmici maggiori, nei pazienti ACM.

Conclusioni. Il ruolo dei lipidi ossidati nell'adipogenesi ACM, come dimostrato *in vitro*, *in vivo* e sui pazienti, rappresenta un nuovo meccanismo di patogenesi, rilevante per la stratificazione del rischio dei pazienti e per nuove strategie farmacologiche.

Introduction

1. Arrhythmogenic Cardiomyopathy

1.1 Definition

Arrhythmogenic Cardiomyopathy (ACM) is a genetic disease characterized by fibro-adipose substitution of the ventricular myocardium that often predisposes patients to life-threatening ventricular arrhythmias and causes progressive ventricular dysfunction (1).

Initially, ACM was considered a disease of the right ventricle (RV), with left ventricular (LV) involvement only at later stages. For this reason, the classical name of the disease was Arrhythmogenic Right Ventricular Cardiomyopathy/Dysplasia (ARVC/D) (2). Currently, the impairment of the RV still predominates, but left-dominant and biventricular forms of ACM are increasingly recognized (1).

ACM patients present a structurally normal heart at birth. Usually, the first symptom appears between the second and fifth decades of life (1). In the early phases of the disease, non-specific symptoms (*e.g.* palpitations and syncope) often occur without overt structural alterations (3). The morpho-functional changes (*e.g.* ventricular dilation, regional wall-motion abnormalities and systolic dysfunction) usually follow electrocardiographic (ECG) signs and worsen with disease progression (3). In up to 50% of cases, sudden cardiac death is the first symptom (1). Interestingly, ACM is the primary cause of sudden death in young people and athletes (3). In Italy, ACM is responsible for over 20% of sudden cardiac death cases in young athletes (4). Other patients may remain relatively asymptomatic (2). Definitely, disease manifestation and progression are extremely variable in ACM patients (2).

The global prevalence of ACM is 1:2000-1:5000 (1), depending on geographical differences, and it affects men more than women (ratio 3:1) (1). In the North of Italy, especially in Veneto region, the prevalence is considerable (1:2000) (1).

1.2 Clinical manifestations

Typically, ACM clinical manifestation progresses in 4 recognized phases (3) (5):

- The “concealed phase”, a long preclinical phase usually starting from birth until young adulthood, with minimal or absent myocardial abnormalities; the patient is already at risk of sudden cardiac death.
- The “pre-symptomatic phase”, with electrical abnormalities (ECG changes and premature ventricular contractions). In some cases, structural defects, as ventricular dilation and dysfunction, can be detected. Cases of syncope are reported and sudden death risk remains.
- The “symptomatic phase” characterized by the full-blown manifestation of the disease with severe and frequent ventricular arrhythmias (VA). Cardiac substrate impairment is evident, and cardiac function deteriorates.
- In the last phase, heart failure can occur.

1.2.1 Arrhythmic manifestations

The electrical instability is the main determinant of ACM patients’ prognosis, and a typical arrhythmic age-related behaviour is described. During the early phases of ACM, ventricular fibrillation is more frequently reported, whereas sustained ventricular tachycardia is common after disease progression (3) (6) (7). Since the myocardial substrate degenerates over time, the arrhythmic phenotype could depend on the progressive nature of the disease: ventricular fibrillation may be associated with acute electrical instability, with a primarily electrical cause or depending on clinically silent changes at histologic level (8) (9) (10); sustained ventricular tachycardia is provoked by re-entry circuits around fibro-fatty myocardial areas, typical of more advanced stages of ACM (11).

1.2.2 Substrate remodelling

The myocardial remodelling in ACM hearts is due to cardiomyocyte death, fibro-adipose substitution, and inflammatory infiltrates (Figure I1).

Cardiomyocyte death, dependent on both apoptotic and necrotic mechanisms, is reported in ACM hearts, provoking a progressive myocardial atrophy and consequent arrhythmia worsening (12) (13) (14) (15). The contractile cells are replaced by fibro-adipose tissue, that is considered the hallmark of ACM, with a

segmental or patchy patterns (1). It usually extends in the so-called “triangle of dysplasia,” comprising the RV inflow tract, outflow tract and apex, although the latter is compromised only in advanced cases of ACM (16). LV alterations mainly affect the postero-lateral and postero-septal areas, with a lesser extent than those of RV (13) (17). The ventricular septum is rarely compromised, possibly because it is not a sub-epicardial structure. Indeed, the fibro-fatty tissue progresses from the epicardium towards the endocardium, ultimately creating transmural lesions with focal or diffuse wall thinning (18). The weakening of the ventricular wall leads, in some cases, to aneurysmal dilation. Typically, fibro-fatty areas infiltrate between islands of surviving myocytes (13) (19), impairing ventricular conduction and worsening the electrical instability.

The source of adipocytes in ACM hearts are cardiac mesenchymal stromal cells (C-MSC; **Figure I2**), a heterogeneous population of multipotent cells able to differentiate towards the adipogenic phenotype as a result of ACM causative mutations (20). The contribution of C-MSC in adipose substitution partially explains also the preferential involvement of RV in ACM, because they have been found in higher amounts in the RV than in the left one (21).

ACM cardiac fibrosis is less characterized, but it presumably depends by fibroblast differentiation to myofibroblasts. The underlying mechanisms and specific triggers are still not elucidated (22).

Patchy inflammatory infiltrates, consisting of neutrophils, macrophages, T-lymphocytes, and mast cells, have been reported in about 70% of ACM hearts, mainly in fibro-adipose areas (13) (23) (24) (25). They are often present in both ventricles even when the disease is confined to the RV (19). The abundance of inflammatory cells in ACM hearts may be misdiagnosed as myocarditis (13).

Figure I1. Gross and histological features of ACM.

a) Graphic representation of the most commonly affected ventricular regions in ACM; b) gross images of ACM right (RV) and left (LV) ventricles. Black arrowheads highlight epicardial fat deposition; c) histological analysis of ACM adipogenesis and cardiomyocyte loss (left; trichrome stain), fibrosis (middle; trichrome stain) and inflammation (right; haematoxylin and eosin stain). ENDO, endocardium; EPI, epicardium.

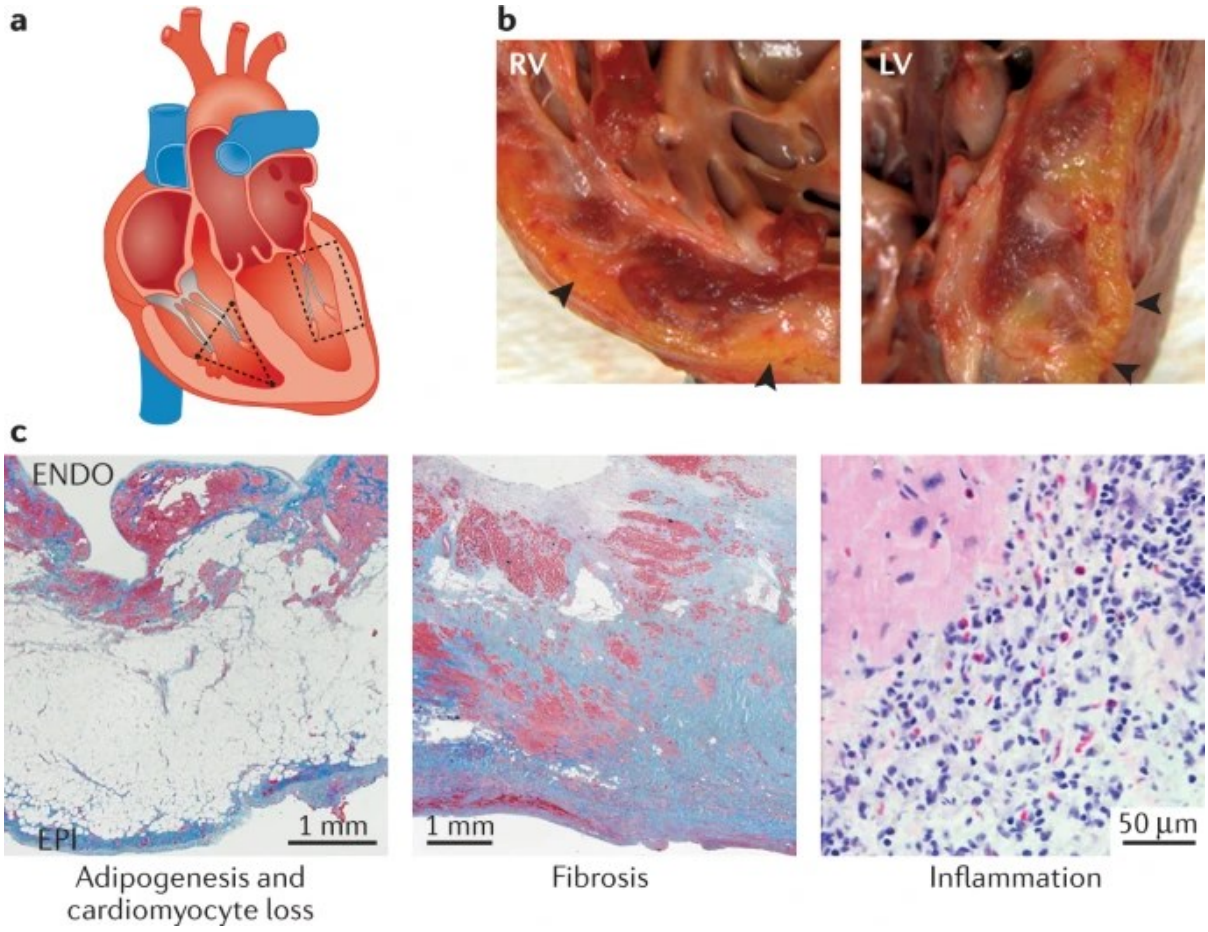

From Austin et al., Nature Reviews Cardiology; 2019; doi: 10.1038/s41569-019-0200-7.

Figure I2. Cardiac mesenchymal stromal cells are a source of adipocytes in ACM.

A) Immunostaining of sections of ACM explanted hearts define that the cells undergoing adipogenic differentiation, marked with PLIN1 antibody, express the mesenchymal markers CD29 and CD105. Nuclei are stained with Hoechst 33258. The scale bar indicates 10 µm. B) No cardiomyocytes, marked with α-sarcomeric actin, express PLIN1, indicating that they do not contribute to adipogenic differentiation in ACM hearts. Nuclei are stained with Hoechst 33258. The scale bar indicates 20 µm.

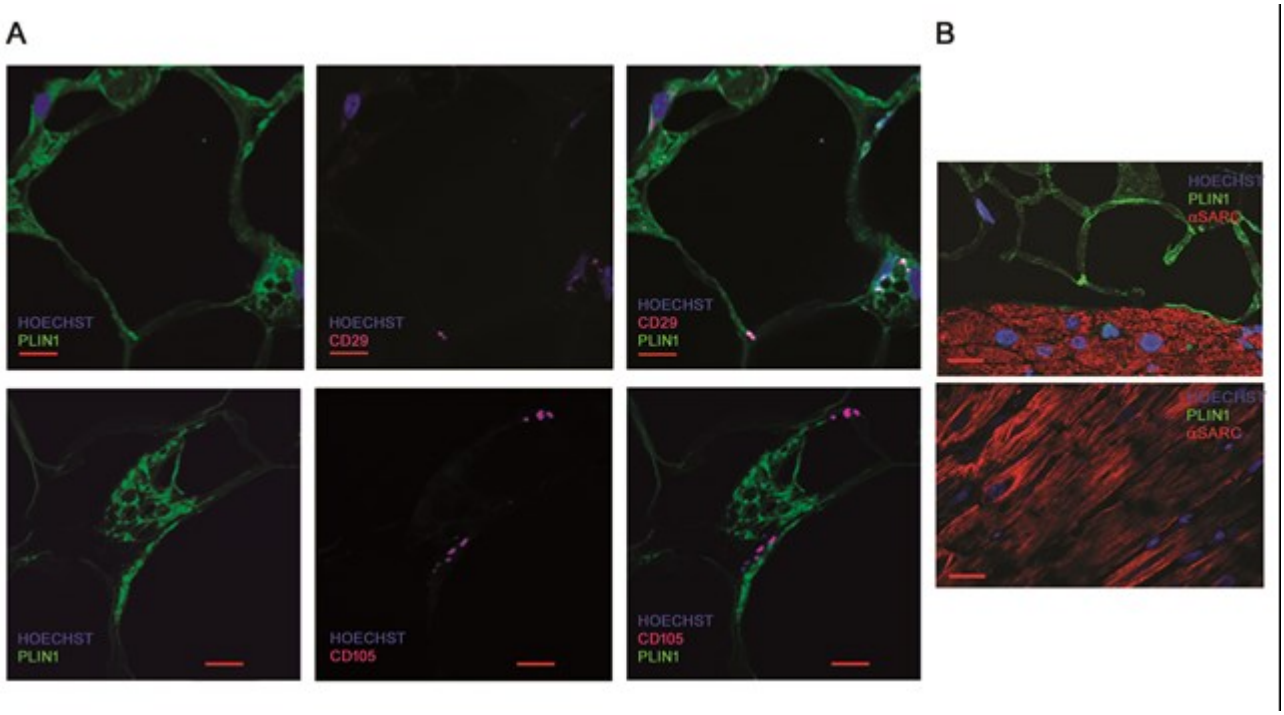

From Sommariva et al., European Heart Journal; 2016; doi: 10.1093/eurheartj/ehv579.

1.2.3 Disease phenotypes

1.2.3.1 *Right dominant phenotype*

The "classic" RV phenotype accounts for about 30% of ACM cases and is characterized by (1) ECG repolarization abnormalities, such as T-wave inversions in right precordial leads; (2) ECG depolarization abnormalities, such as epsilon waves or prolonged QRS complex; (3) premature ventricular contractions or ventricular tachycardia with left bundle branch block and superior axis morphology; (4) RV wall motion abnormalities and RV dilation or dysfunction.

The interventricular septum and LV myocardium can be involved but only in the advanced stages of the disease (26).

1.2.3.2 *Left dominant phenotype*

Left dominant ACM is characterized by the fibro-adipose replacement of LV, without RV impairment or only with mild RV alterations (17) (27) (28). Noticeable features of the LV forms of ACM are (1) left deviation of the QRS complex or T-waves in the lateral and/or inferior leads, at ECG; (2) ventricular arrhythmias of right branch block morphology, according to LV origin; (3) LV dysfunction at imaging, including sub-epicardial/mid-myocardial distribution of scar tissue mainly in the inferior/infero-lateral LV walls (29) (30). Often, the interventricular septum is involved (17).

1.2.3.3 *Biventricular phenotype*

The "biventricular" pattern is identified by early and parallel involvement of both ventricles, recapitulating the typical features of both LV and RV dominant forms (29).

1.3 Genetics

A genetic cause is identified in 30-60% of ACM cases and often a family history is recognized (31). ACM is usually inherited with autosomal dominant traits (1). However, recessive forms of ACM are known, called Naxos disease and Carvajal syndrome, mostly associated to a cardio-cutaneous phenotype (32). The study of these particular forms of ACM were of key importance to unravel ACM genetic basis. Indeed, following the discovery of the causal role of *JUP* mutations in Naxos disease (33), different ACM-associated mutations were found (Table I1).

Up to two-thirds of ACM patients harbour a mutation in desmosomal genes (34) (35). Desmosomes are intercellular junctions that guarantee cell-to-cell adhesion. Intracellularly, they are linked to the intermediate filament cytoskeleton, providing mechanical strength. Thus, they are particularly abundant in tissues subjected to significant mechanical stress, such as the epidermis and the heart (36). For the latter, the interaction in the extracellular space is mediated by the desmosomal cadherins desmoglein-2 (DSG2) and desmocollin-2 (DSC2). On the intracellular face, the armadillo proteins plakophilin-2 (PKP2) and plakoglobin (PG) provide stability to the complex. Desmoplakin (DSP), a cytoskeletal adaptor protein, tethers the intermediate filament network and the desmosomal complex (37). Mutations in desmosome components perturb cell adhesion, particularly in areas subjected to high stress and stretch, such as the "triangle of dysplasia" (25).

Desmosomes are abundant in cardiomyocytes, where they reside at the intercalated disks (ID; Figure I3). ID are areas of specialization at the site of cell-cell contact, comprising, in addition to desmosomes, *fascia adherens*, gap junctions, and ion channels. However, desmosomal proteins are also expressed in non-myocytes, such as epithelial cells and cardiac mesenchymal stromal cells (C-MSC) (20) (38).

PKP2 mutations represent the most prevalent in ACM, accounting for 30-80% of ACM total cases (6) (39) (40) (41) (42). They are often heterozygous and lead to premature termination of the protein or abnormal splicing (6) (39). Usually, ACM *PKP2* variants appears in more conserved regions of the protein if compared to *PKP2* variants in control populations (43). Beside PKP2 role in desmosome stabilization, it also regulates

genes associated with calcium handling, fibrosis and adipogenesis, key ACM features (44) (45) (46). Indeed, like other armadillo proteins, plakophilins can also be localized into the nucleus, where they mediate a transcriptional regulation (47).

In general, the impairment of desmosomal proteins can be responsible, not only of a junctional destabilization, but also of other alterations in the cells. As an example, DSP loss provokes the reduction of the gap junction protein Connexin 43 (Cx43) levels (48) (49), thus causing conduction defects.

Additional ACM-causative mutations reside in genes encoding for other ID proteins (50), among which α-T-catenin (*CTNNA3*) (51), N-cadherin (*CDH2*) (52), tight junction protein-1 (*TJP1*) (53), voltage-gated sodium channel alpha subunit 5 (*SCN5A*) (54), and transmembrane protein 43 (*TMEM43*) (55). Moreover, genes coding for calcium handling proteins, located at the sarcoplasmic reticulum, can be mutated in ACM patients, such as the cardiac ryanodine receptor-2 (*RYR2*) (56) and phospholamban (*PLN*) (57). Also mutations in titin (*TTN*) (58), lamin A/C (*LMNA*) (59), transforming growth factor-beta 3 (*TGFB3*) (60), desmin (*DES*) (61), and filamin C (*FLNC*) (62) are reported. Interestingly, most of the ACM-associated non-desmosomal genes are also linked to other cardiomyopathies, such as the dilated or hypertrophic, and arrhythmic syndromes, overcoming the one gene-one disease paradigm (63).

Pathogenic ACM mutations are frequently truncating. One report indicated that 83% are nonsense, frameshift or splice site mutations, while 14% are missense variants (64).

Although knowledge about ACM genetics is constantly growing, 30-40% of ACM cases are sporadic and a mutation cannot be identified (35). In addition, even if ACM is considered a monogenic disorder, disease penetrance can be affected by the contribution of a second mutation and of environmental factors. Indeed, the relevant role of compound and digenic heterozygosity has been demonstrated, with an occurrence range of 4-21% of total cases (6) (35) (65) (66). The frequency of some ACM-associated variants is greater than expected in the general population, given their phenotype prevalence, suggesting that these variants alone are not monogenic causes of ACM (67). Moreover, the variant pathogenicity is not always clear (43). The ACM genetic database classify about 70% of variants in ACM-associated genes as unknown or of uncertain pathogenicity (68).

Figure I3. Overview of ACM-associated protein localization and interactions in adjacent cardiomyocytes. The zoom of the desmosome is provided.

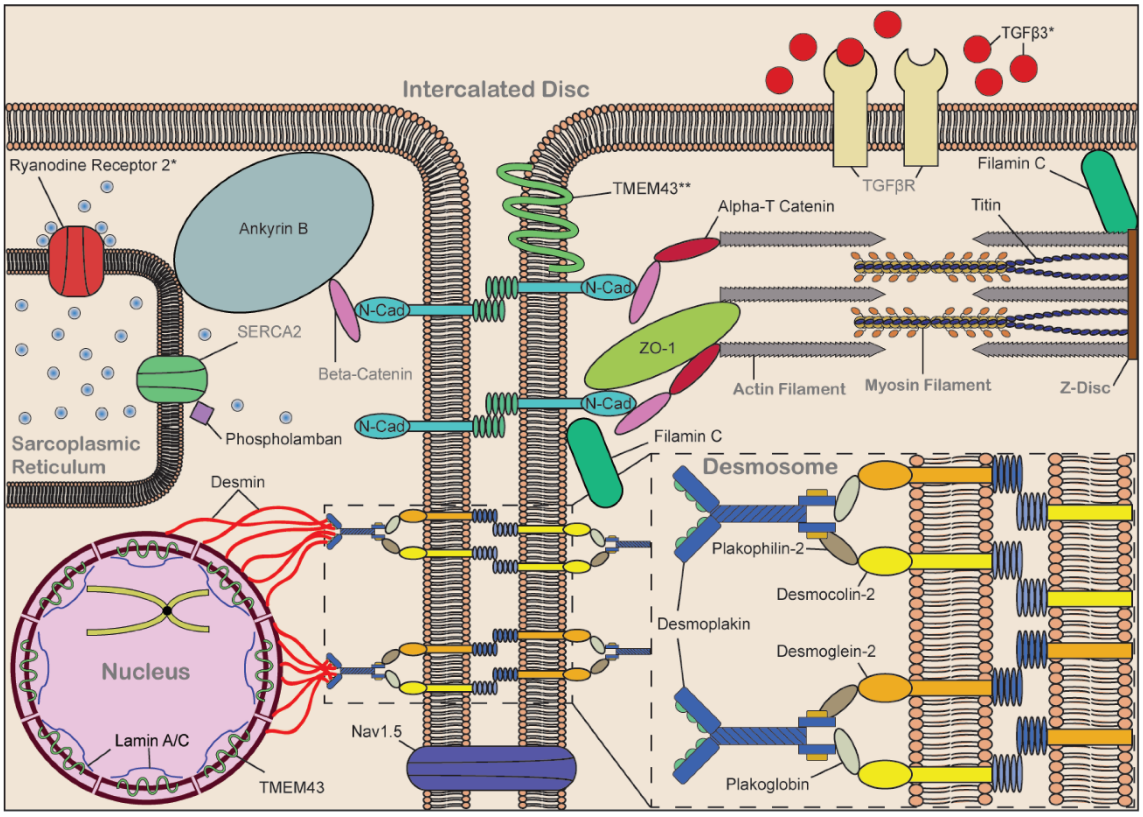

From Stevens et al., Journal of Cardiovascular Development and Disease; 2020; doi:10.3390/jcdd7020021.

1.3.1 Genotype-phenotype correlations

A better understanding of the risk of developing clinical phenotypes associated with the different mutations is needed. Thus, several studies have tried to correlate specific genetic mutations to definite phenotypes (Table I1). Generally, it is accepted that patients with mutations in known ACM-causative genes often have earlier disease onset (7) (35) (69). To date, no relevant differences in clinical manifestation and disease progression seem to be present between ACM patients with or without an identifiable mutation (35), but a recent meta-analysis recognised some common features of ACM patients with desmosomal mutations, such as inverted anterior pre-cordial T-waves, epsilon waves, or arrhythmias with left-bundle branch block morphology (69). Overall, *DSG2* variants seem to be associated with more severe cardiac dysfunction and higher risk of heart failure (31). In addition, a prevalent involvement of LV dysfunction and heart failure amongst *FLNC*, *DSP* and *PLN* mutation carriers has been found (6) (29) (70). Moreover, multiple mutation carriers have a higher risk of malignant ventricular arrhythmias (VA) and sudden death (6) (71) (72).

Despite the advances, there are still many difficulties in understanding the phenotypes associated with specific pathogenic mutations, thus the assessment of a reliable prognosis is not feasible. Desmosomal versus non-desmosomal mutation downstream effects can be compared in the same cell type, as an *in vitro* surrogate, to better understand the involved disease mechanisms and consequent phenotypes (73).

Table I1. List of the genes linked to ACM.

Gene	Protein	Structure or Location	ACM Prevalence *	Phenotype
PKP2	Plakophilin-2	ID/desmosome	23.4–57.6%	RV dominant ACM
DSP	Desmoplakin	ID/desmosome	1.6–15.7%	RV, LV, and biventricular ACM, Carvajal syndrome (recessive), palmoplantar keratoderma.
DSG2	Desmoglein-2	ID/desmosome	4.0–20.4%	RV and biventricular ACM
DSC2	Desmocollin-2	ID/desmosome	1.0–8.3%	RV, LV, and biventricular ACM
JUP	Plakoglobin	ID/desmosome	<1–3.0%	RV dominant ACM, Naxos disease (recessive).
CTNNA3	α-T-catenin	ID/area composita	<2.6% (among ACM cases without common mutation)	RV dominant ACM
DES	Desmin	Intermediate filaments/cytoskeleton	<1–2.2%	RV and biventricular ACM.
LMNA	Lamin A/C	Nuclear envelope	3.5–3.7%	RV and biventricular ACM.
PLN	Phospholamban	Sarcoplasmic reticulum	2.2–12.4%	RV, LV, and biventricular ACM.
TMEM43	Transmembrane protein 43	Nuclear envelope/ID	<1–2.2%	RV, LV, and biventricular ACM.
TTN	Titin	Sarcomere	<1% (18.4% of ACM cases negative for variants in common genes)	RV and biventricular ACM.
FLNC	Filamin C	Sarcomere/ID	<1% (7.5% of ACM cases negative for variants in common genes)	RV, LV, and biventricular ACM.
SCN5A	Sodium channel Nav1.5	Cell membrane/ ID	<1–1.8%	RV dominant ACM.
TJP1	Zonula occludens 1	ID/tight junction	<1% (<5% of ACM cases negative for variants in common genes)	RV, LV, and biventricular ACM
CDH2	N-Cadherin	ID/adherens junction	<1% (2.7% of ACM cases negative for variants in common genes)	RV and biventricular ACM
ANK2	Ankyrin B	Z-lines/T-tubules	Unknown	RV dominant ACM.

* Prevalence calculated by the percentage of ACM cases with an identified mutation in the gene of interest vs. total ACM cases. Abbreviations: ACM, arrhythmogenic cardiomyopathy; ID, intercalated discs; LV, left ventricle; RV, right ventricle.

1.3.2 Phenotype variability

Incomplete penetrance and variable expressivity often characterize ACM families, strengthening the concept that other genetic and/or environmental factors may play a modifying role (1) (74) (75) (76) (77). Indeed, also patients that are carriers of the same causative mutations can have different manifestation of the disease. In studies of ACM monozygotic twins, differences in symptom onset, disease severity and arrhythmic risk were reported (78) (79). Thus, the understanding of which cofactors can modulate the manifestation of the disease represent a key clinical need. The identification of modifiable risk factors and genetic markers will improve ACM prognosis, by providing novel therapeutic targets.

1.3.2.1 Compound and digenic heterozygosity

The co-inheritance of different disease alleles of a single gene (compound heterozygosity) and the co-inheritance of disease alleles of two different genes (digenic heterozygosity) contribute to ACM expression and penetrance (39) (65) (71) (80) (81). Xu et al., screening 198 ACM patients for desmosomal gene variants, found 38 patients, carriers of *PKP2* variants. Among them, 9 were carriers of additional variants in *PKP2* itself (compound heterozygosity), whereas 13 carried variants in other desmosomal genes (digenic inheritance). Relatives harbouring only one variant were asymptomatic (65). The study of Rasmussen et al. corroborated these findings: analysing 12 ACM families, he found that only subjects with digenic heterozygosity clinically expressed the disease (82). Indeed, subjects with multiple mutations can have a mixed clinical manifestation of the disease, but generally show more severe phenotypes, such as LV and RV dilation, than subjects carrying a single mutation (81). In addition, this complex genetic status represents an independent risk factor for malignant arrhythmias and SCD, in a “dose-dependent” manner (71).

The frequency of compound and digenic heterozygosity in ACM probands could imply that pathogenic variants potentially occur in the general population more frequently than previously supposed (81).

1.3.2.2 Modifier genes

Beside compound and digenic inheritance, also modifier genes could have a role in ACM. A modifier gene is defined as a contributing variant of unknown significance that can enhance the phenotypic expression of another putatively pathogenic variant (83). The impact of modifier genes may elicit strong effects ("monogenic-like model") or milder effects ("multifactorial-like model") (83) (Figure I4). However, despite the advanced genetic tools available today, the detection of genetic modifiers remains very challenging, due to the difficulty for certain diseases to clearly define the clinical phenotype, for which searching the modifier genes, and to choose the study population (83).

Sen-Chowdhry et al. have proposed that modifier genes can regulate various clinical parameters in ACM patients, among which LV and RV ejection fraction (84).

1.3.2.3 Exercise-induced mechanical stretch

A relevant lifestyle risk factor is physical exercise, exacerbating the risk of worst disease outcomes and sudden cardiac death. In particular, 25% of sudden cardiac death among athletes are secondary to ACM in Italy (85). Sen-Chowdhry et al. reported larger RV volumes and lower RV function in 11 endurance athletes compared to an ACM non-athletic cohort (29). Moreover, ACM athletes develop symptoms at younger age and have higher incidence of ventricular arrhythmias and heart failure, possibly dependent on β-adrenergic signalling activation (86) (87). Thus, it is accepted that mechanical stretch, caused by intense physical exercise, can be deleterious in a context of genetically compromised cell-to-cell adhesion, triggering cell disruption, necrosis and fibro-adipose replacement (88).

Physical activity has a greater impact on the RV than on the left one (89). Different studies demonstrated that intense exercise provokes a reduction in RV function without changes in LV (90) (91). Indeed, RV structure and cellular composition are suited to tolerate a small mechanical stress, leading to a disproportionate afterload increase and wall stress during intense exercise (89).

In addition, the amount of practiced exercise, both as intensity and duration, has to be taken into account. For ACM patients, an inverse relationship between the amount of performed exercise and RV and LV

ejection fraction was found (92). Moreover, the high-intensity exercise seems to be more deleterious than long-duration milder exercise for adverse outcomes (93). Therefore, it has been evaluated if the genetics of each patient could be useful to calculate the maximum amount of exercise that can be practiced, considering this dose-dependent impact. ACM patients with desmosomal mutations practicing exercise are more predisposed to early disease onset, worst structural abnormalities and stronger arrhythmic risk (86) (94). Non-desmosomal mutation carriers have to exercise more intensely to become clinically affected (95) (96). Multiple mutation carriers require very little exercise for ACM expression (**Figure I4**). Despite these results, in clinical practice, exercise restriction is still advised for all ACM genetic causes to reduce disease progression (1) (86).

In addition, the hypothesis of exercise-induced forms of ACM is increasingly accepted since repeated sessions of exercise, even in the absence of desmosomal mutations, may cause junction disruption (97). Indeed, a study demonstrated that patients with a clear ACM diagnosis but without an identifiable mutation and with no family history were for the majority high-level endurance athletes (95) (96).

1.3.2.4 β-adrenergic signalling

The sympathetic nervous system (SNS) is involved in many arrhythmic diseases (98). As part of the autonomous nervous system, it is responsible, also in physiological conditions, through the fight-or-flight response, of the regulation of involuntary processes, such as the heart rate or blood pressure (99). Adrenergic nerves, that are in contact with cardiac cells (100), release neurotransmitters (*e.g.* adrenaline and noradrenaline) that are sensed by the cardiac adrenoreceptors, inducing a positive inotropic heart response (101) (102) (103).

The role of SNS in ACM has been proposed due to the recurrent occurrence of ventricular tachyarrhythmias during exercise, mental stress, or catecholamine provocation. Moreover, the use of antiadrenergic agents as antiarrhythmic drugs confirms the involvement of the adrenergic system in ACM (104). Different studies demonstrated, using ^{123}I-Meta-Iodobenzylguanidine scintigraphy, that ACM patients have an abnormal LV and RV sympathetic innervation (105) (106). Moreover, ACM myocardium has a strongly reduced post-

synaptic β-adrenergic receptor density, possibly due to the increased firing rates of SNS efferent neurons rather than a defective presynaptic catecholamine uptake (107). These alterations seem to be independent of the extent of fibro-fatty substitution, although cardiac substrate alterations could induce anatomic denervation and re-innervation processes, enhancing the susceptibility to catecholamines (108). More likely, SNS dysfunction is possibly due to frequent premature ventricular contractions and wall stress that, boosting afferent sympathetic activity, provoke a significant reflex increase in the cardiac sympathetic efferent drive (108). In addition, desmosomal mutations affect intracellular calcium cycling, inducing catecholamine sensitivity (44), and some ACM-associated genes have adrenergic-dependent functions (109).

β-adrenergic signalling is counted among ACM phenotypic modulators. There is also a strict crosslink of β-adrenergic signalling with physical exercise, described above as the main cofactor of ACM expressivity (110), and emotional stress (111). Therefore, all these cofactors can cooperate worsening disease phenotypes.

1.3.2.5 Sexual hormones

ACM affects mainly men than women, with 3:1 ratio (1), although the disease is usually transmitted with an autosomal dominant trait. In addition, the disease expression differs between genders. Male ACM patients develop life-threatening ventricular arrhythmias at an earlier age as compared to females (112). Moreover, men have larger RV volumes, lower RV ejection fraction, and a more severe LV involvement than ACM female patients (112). Accordingly, mild forms are usually more frequent in women. This is in line with previous studies on healthy subjects, indicating larger ventricular volumes in men (113) (114).

Recently, Akdis et al. correlated the higher incidence of ACM in men than in women with sexual hormone levels, among which testosterone, independently of the causative mutation (115). In general, testosterone increases the risk of cardiovascular diseases (116), whereas estrogens (*e.g.* estradiol) seems to exert protective effects (117). Accordingly, in male ACM patients, the elevated serum levels of testosterone are associated with major arrhythmic cardiovascular events (MACE), while MACE-positive female patients have

significantly reduced estradiol levels (115) (118). Specifically, to obtain an optimum sensitivity and specificity for MACE prediction, the testosterone cut-off value has been setting to >13.5 nmol/l (115). The modulatory role of sexual hormones in ACM phenotypic manifestation has been confirmed i*n vitro*: testosterone treatment increased apoptosis and lipogenesis in human induced pluripotent stem cell-derived cardiomyocytes (hiPSC-CM), indicating its potential pathogenic role (115).

Interestingly, ACM manifestation usually occurs after pubertal development, during adolescence or young adulthood (119), corroborating sexual hormone role.

1.3.2.6 Inflammation

Inflammation has a key role in ACM pathogenesis and progression (120). Various studies have reported inflammatory infiltrates in ACM hearts (13) (24). Importantly, they are mostly found in ACM left-dominant or biventricular forms, often associated with severe manifestations of the disease (19). A genetic predisposition or susceptibility to infections cannot be excluded in ACM (13). The presence of myocardial inflammation can be non-invasively detected through ^{67}Ga scintigraphy (121), or analysing circulating pro-inflammatory cytokines (122).

Conflicting studies are present in literature regarding the role of inflammation as a primary event or a consequence of cell death in ACM (123) (124), but the presence of inflammatory infiltrates in the patients' hearts often indicate an ongoing myocardial damage (19). As for other cardiovascular conditions, the absence of resolution of the inflammatory process can over-stimulate the substrate remodelling, with pathological repercussions on fibrosis and arrhythmias (125). The interplay between different ACM phenotypic modulators could be proposed also in the context of ACM immune response (123).

Figure I4. Relative influence of genetics, sex and exercise in ACM pathogenesis.

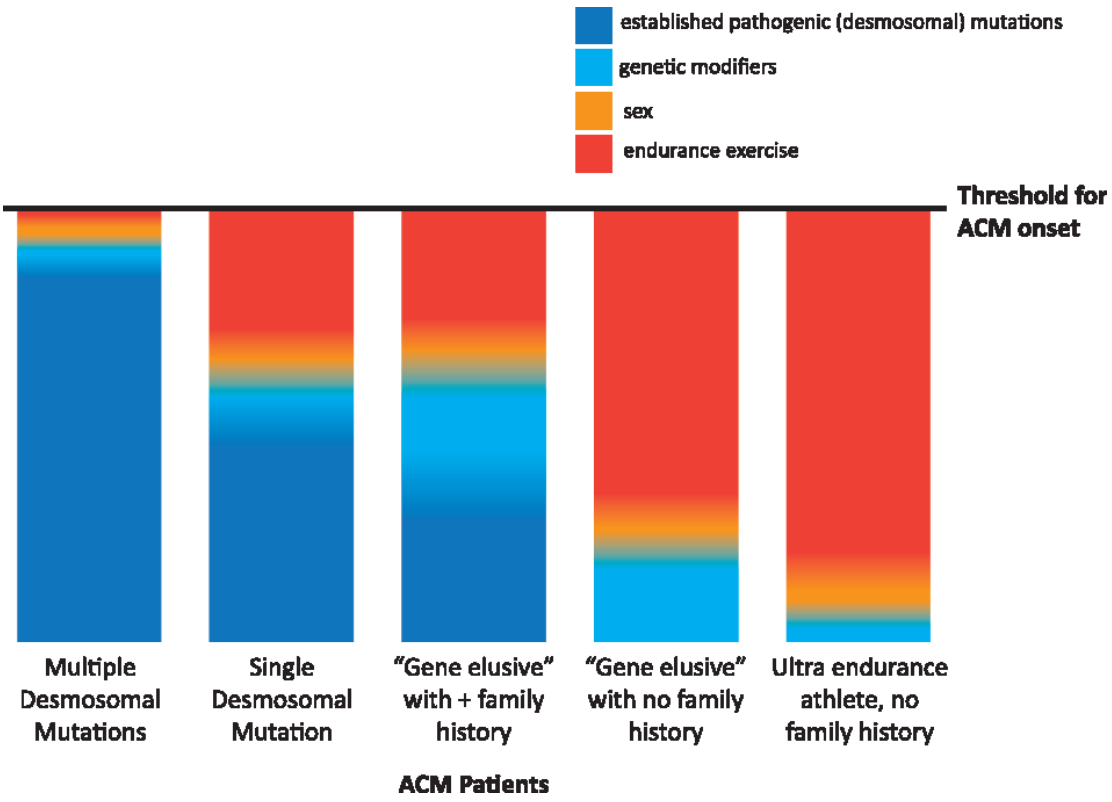

From Hoorntje et al., Cardiovascular Research, 2017; doi: 10.1093/cvr/cvx150

1.4 Pathogenic mechanisms

Several mechanisms participate to ACM pathogenesis and most of them are directly dependent on causative mutations (**Figure I5**). The desmosomal impairment leads to a reduced resistance of cardiac tissue to mechanical stress, provoking cell detachment. Cardiomyocyte loss is a key process in ACM pathogenesis, contributing to the progressive atrophy of the ventricular myocardium (126). It is mediated either by necrotic, as demonstrated by the sarcolemma disruption, myofilament disintegration and mitochondrial swelling (9), or apoptotic programmed cell death, as verified by chromatin condensation, nuclear fragmentation and presence of caspase 3 (127).

Inflammation contributes to ACM pathological characteristics (124) (123). Pro-inflammatory cytokines are known to induce fibrotic cardiac remodelling, stimulating the differentiation of fibroblasts in myofibroblasts (22) (125) (128) (129). In addition, infiltrating macrophages can replace resident cardiac macrophages, necessary to support electrical excitation propagation in physiological conditions, and thus contribute to the arrhythmogenic phenotype (130). The cytokine production seems not only restricted to inflammatory cells, but also performed, although for a limited extent, by cardiomyocytes and cardiac fibroblasts (123) (131). The autocrine action of cytokines may impair ion channel function, promoting arrhythmias (123). In addition, the adipose tissue, typically found in ACM hearts, could represent another source of pro-inflammatory cytokines (132).

The suppression of Wnt signalling pathway also participates to ACM pathogenesis (133). Wnt signalling pathway is involved in cell proliferation, cell polarity, cell fate determination, and tissue homeostasis in physiological conditions (134). The desmosomal protein PG has a key role in this context. Under normal conditions, PG is mainly found at the intercalated discs, but ACM desmosomal impairment can lead PG to translocate into the nucleus (135) (136). Due to its high homology to β-catenin, an important mediator of the canonical Wnt pathway, PG can compete with β-catenin for the binding of the Wnt pathway-associated transcription factors, named T cell/lymphoid-enhancing binding (TCF/LEF), inducing the transcription of pro-adipogenic genes, among which peroxisome proliferator activated receptor gamma (PPARγ) (133) (136).

In addition, Wnt/β-catenin pathway is cross-linked to Hippo signalling pathway. Hippo signalling pathway controls cell proliferation, survival, mobility, and differentiation (137). In ACM, intercalated disc remodelling decrease protein kinase C α levels, resulting in the activation of neurofibromin-2 (138). The latter phosphorylates Yes-associated protein (YAP), the Hippo pathway effector, causing YAP sequestering of β-catenin, and reinforcing the effect of Wnt pathway impairment in ACM (139).

Due to the wide nature of ACM-associated mutations, the involved pathogenic mechanisms extend beyond the desmosome to include the cellular mechano-transduction machinery (140) (141). Indeed, adhesion impairment alters cell mechano-transduction and mechano-sensing. Hippo pathway may have a role also in this context, regulating gene transcription basing on mechano-sensing, thus responding to mechanical forces generated from cell-cell contacts, cell-extracellular matrix interaction, and microenvironment (142).

The arrhythmic phenotype is caused both by re-entry conduction mechanisms due to cardiomyocyte death and fibro-adipose substitution, and by proper alterations in ion channel expression levels and localisation and in cell-cell electrical coupling. Functional gap junction formation and maintenance rely on stable mechanical connections between adjacent cells (143). In addition, PKP2 and the gap junction proteins coexist in the same macromolecular complex (144). In ACM, due to desmosomal alterations, gap junction remodelling occurs, with Cx43 mislocalization and Nav1.5 sodium channel reduction at intercalated discs (145) (146) (147) (148).

Moreover, PKP2 regulate the expression of proteins involved in calcium cycling, such as RyR, ankyrin-B, Cav1.2, and calsequestrin 2 (44), thus the remodelling of the calcium handling machinery is likely to be numbered among ACM pathogenic mechanisms (149) (150). In addition, mutations in genes encoding for the calcium cycling machinery, as *RYR2* and *PLN*, are reported as causative in ACM (149).

The activity of RhoA GTPase, involved in transcriptional regulation during cardiomyocyte differentiation, is under PKP2 control (151). RhoA is highly expressed in ACM myocardial tissue and leads to the overexpression of adipogenic differentiation inducers (152).

Also microRNAs are putatively involved in ACM pathogenesis. MiR-21-5p and miR-135b are differently expressed in ACM versus healthy control cardiac tissue (153), possibly with a role in fibrotic remodelling

(154). Both microRNAs can also modulate Wnt and Hippo signalling pathways (155) (156). PKP2 reduction in ACM decreases also miR-184 levels, provoking the upregulation of its target gene *PPARγ* and consequent enhanced adipogenesis (157). In ACM plasma samples, the reduction of mir-320a has also been reported (158), with a potential implication in the adipogenic process and Wnt pathway regulation (159) (160). Recently, the presence of circulating anti-DSG2 autoantibodies has been described in ACM patients, and speculations were presented about their possible role in gap junction functional impairment (161). Nevertheless, a broader knowledge of ACM pathogenic mechanisms still needs to be acquired, since other molecular players are likely involved.

Figure I5. Overview of the main pathogenic mechanisms of ACM.

a) In the healthy cardiomyocyte, desmosomes form strong intercellular connections with neighbouring cells. Connexin 43 (Cx43) and the sodium channel (Nav1.5) are appropriately positioned as a result of coordinated trafficking and membrane tethering. B-catenin has a structural function in adherens junctions as well as a role in modifying transcriptional activity through activation of Wnt-dependent gene expression. Cytoplasmic β-catenin is quickly degraded. The Hippo pathway is 'off', allowing transcription of genes promoting cardiomyocyte survival, function and growth. Calcium flux is well regulated in the sarcoplasmic reticulum; b) In ACM, multiple signalling pathways are perturbed: disruption of the desmosomes and adherens junctions leads to increased mechanical stress; plakoglobin can dissociate from the desmosome and inhibits Wnt-dependent gene transcription; activation of the Hippo pathway promotes a pro-apoptotic and adipogenic phenotype; microRNAs can modulate both Hippo and Wnt signalling; active Hippo signalling can further inhibit canonical Wnt signalling; dysregulation of calcium handling; abnormal shuttling and tethering of both the sodium channel and Cx43; increased pro-inflammatory and profibrotic cytokine production, including TGFβ1.

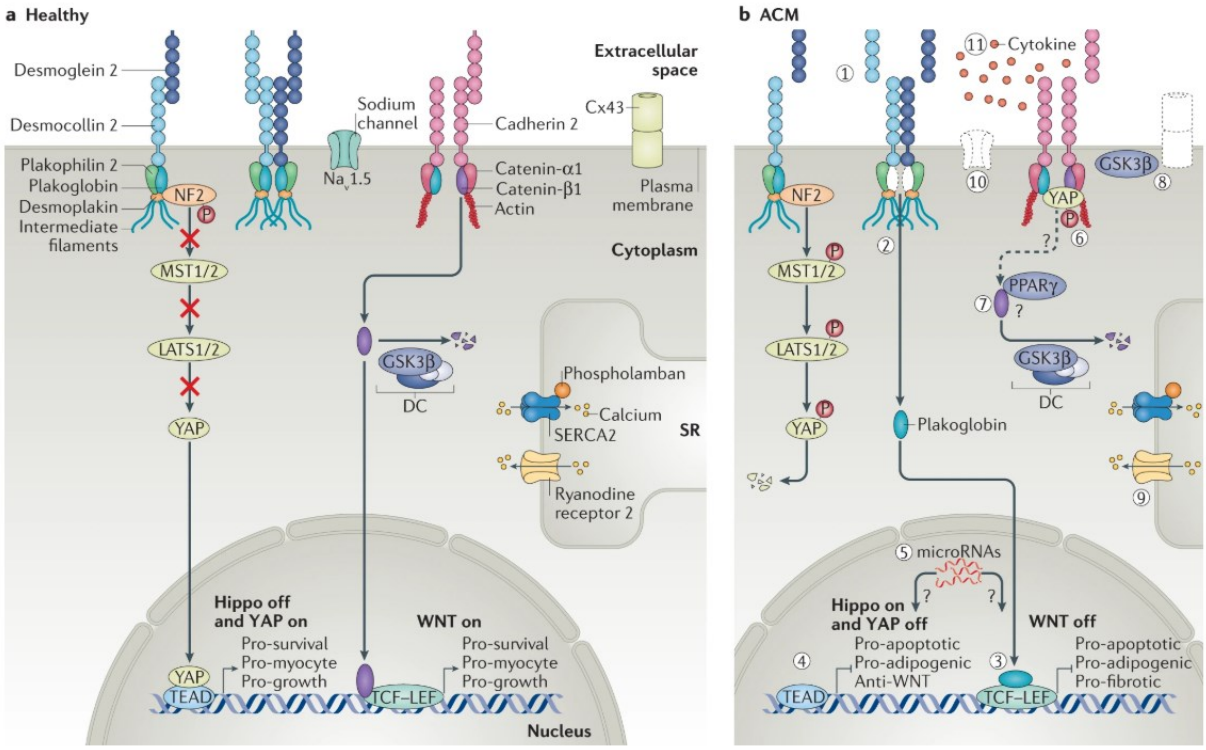

From Austin et al., Nature Reviews Cardiology, 2018; doi: 10.1038/s41569-019-0200-7.

1.5 Diagnosis

The clinical diagnosis of ACM is particularly challenging for the age-related progression, the huge phenotypic variability and the incomplete penetrance of the disease. For these reasons, a univocal gold-standard diagnostic test is absent. The diagnostic process is based on the fulfilment of the ACM Task Force Criteria, originally proposed in 1994 (162) and revised in 2010 (163), to increase their sensitivity for early and familial disease (164) (165). The criteria could be major or minor, according to the specificity to ACM features, and comprise ventricular structural and functional changes, depolarization and repolarization ECG abnormalities, arrhythmias, cardiac tissue characterization, familial/genetic background. A summary of current Task Force Criteria is reported in Figure I6. The diagnosis is confirmed when two major, one major and one minor, or four minor criteria are obtained. The "borderline" diagnosis is based on one major and one minor criterion, or three minor criteria. The "possible" ACM diagnosis includes one major or two minor criteria (163).

Unfortunately, although the 2010 revision of the diagnostic criteria, many issues regarding their complexity and high error probability are still present (166) (167). Different clinicians proposed a further simplification of the current criteria to reduce misdiagnosis risk (168), but they are still not transposed into clinical practice. An additional improvement of the Task Force Criteria is needed to enhance the recognition of early forms of ACM and to better characterize the non-classic presentations of the disease (169) (170).

1.5.1 Structural and functional changes

The use of non-invasive imaging approach, based on echocardiography and cardiac magnetic resonance, is essential to assess structural and functional changes (171). Parameters such as ventricular wall thickness and motion abnormalities, ejection fraction and fractional area shortening are measured since wall motion abnormalities, defined as regional akinesia, dyskinesia, or dyssynchrony, combined with RV dilation and/or RV dysfunction, are required for ACM diagnosis (163). The identification of mild structural changes in the RV seems not particularly reliable using conventional echocardiography (172), whereas cardiac magnetic

resonance represents the gold standard to measure ventricular volumes and function, with high intra-observer and inter-observer reproducibility (173) (174). It can also be implemented with late gadolinium enhancement, although its use is not included in the current Task Force Criteria for fibro-fatty tissue detection (173) (175) (176). Unfortunately, cardiac magnetic resonance is not applicable for patients with certain implanted cardiac devices.

1.5.2 ECG abnormalities

Fibro-adipose replacement can create repolarization and conduction defects, causing potentially life-threatening ventricular tachycardia (VT). ECG major criteria include inverted T-waves in V1- V3 precordial leads without complete right bundle branch block (RBBB), the presence of epsilon wave, and increased QRS complex duration. Minor criteria are inverted T-waves in V1- V2 leads, or V4, V5, V6 in the absence of complete RBBB, or inverted T-waves in V1- V4 leads in the presence of complete RBBB.

Nevertheless, about 30% of patients with morphological criteria for ACM does not fulfil the 2010 ECG criteria (177), because they may present less specific ECG abnormalities (*e.g.* ST-segment modifications or QRS fragmentation) (178) (179), indicating the need for further improvements of diagnostic criteria.

1.5.3 Arrhythmias

Ventricular arrhythmias are usually related to scar extent or abnormal adrenergic stimulation. They commonly occur as sustained or non-sustained ventricular tachycardia with a left bundle branch block (LBBB) pattern, compatible with the RV origin. They represent a major criterion if initiating from the RV inferior wall or RV apical sites, whereas a minor criterion if they originate from the RV outflow tract. In addition, frequent premature ventricular contractions can be present.

1.5.4 Tissue characterization

The analysis of cardiac biopsy specimens is performed to detect cardiomyocyte loss, fibrous tissue and inflammatory infiltrates (180). The recognition of adipose substitution is not anymore included in the

diagnostic parameters (181), although it could be determinant in borderline cases. The reduced amount of plakoglobin at cardiac tissue, although potentially useful, is still not used in the clinical practice, because of the lack of information about the reproducibility and diagnostic accuracy (135).

The diagnostic yield of endomyocardial biopsies is increased when is performed in combination to electroanatomic voltage-guide mapping, in order to confine the tissue sampling to pathological areas (182) (183) (184). Nevertheless, since the bioptic procedure is invasive and, in some cases, associated with clinical complications, it has to be avoided if not strictly necessary and it can be performed only in highly specialized centres (185).

1.5.5 Familial/genetic background

The evaluation of family history relies on the confirmation of ACM diagnosis in a first-degree relative for Task Force Criteria fulfilment, or at autopsy or surgery. Also the identification of a pathogenic mutation categorized as associated or probably associated with ACM in the patient is considered a major criterion (163).

Figure I6. Summary of 2010 Task Force Criteria.

	Major	Minor
I. Global or regional dysfunction and structural alterations	By 2D echocardiogram: Regional RV akinesia, dyskinesia, or aneurysm and 1 of the following (end-diastole): PLAX RVOT ≥32 mm (PLAX/BSA ≥19 mm/m^2) PSAX RVOT ≥36 mm (PSAX/BSA ≥21 mm/m^2) Or RFAC ≤33% By MRI: Regional RV akinesia or dyskinesia or dyssynchronous RV contraction and 1 of the following: RV end-diastolic volume/BSA ≥110 ml/m^2 (male) or ≥100 ml/m^2 (female) Or RV ejection fraction ≤40% By RV angiography: Regional RV akinesia, dyskinesia, or aneurysm	By 2D echocardiogram: Regional RV akinesia or dyskinesia, and 1 of the following (end-diastole): 29 ≤PLAX RVOT <32 mm (16 ≤PLAX/BSA <19 mm/m^2) 32 ≤PSAX RVOT <36 mm (18 ≤PSAX/BSA <21 mm/m^2) Or 33% < RFAC ≤40% By MRI: Regional RV akinesia or dyskinesia or dyssynchronous RV contraction and 1 of the following (end-diastole): 100 ml/m^2 ≤ RV end-diastolic volume/BSA <110 ml/m^2 (male) or 90 ml/m^2 ≤ RV end-diastolic volume/BSA <100 ml/m^2 (female) Or 40% < RV ejection fraction ≤45%
II. Tissue characterization of wall	Residual myocytes <60% by morphometric analysis (or <50% if estimated), with fibrous replacement of the RV free wall myocardium in ≥1 sample, with or without fatty replacement of tissue on endomyocardial biopsy	Residual myocytes 60% to 75% by morphometric analysis (or 50% to 65% if estimated), with fibrous replacement of the RV free wall myocardium in ≥1 sample, with or without fatty replacement of tissue on endomyocardial biopsy
III. Repolarization abnormalities	Inverted T waves in right precordial leads (V_1, V_2, and V_3) or beyond in individuals >14 yrs of age (in the absence of complete RBBB QRS ≥120 ms)	Inverted T waves in leads V_1 and V_2 in individuals >14 yrs of age (in the absence of complete RBBB) or in V_4, V_5, or V_6 Inverted T waves in leads V_1, V_2, V_3, and V_4 in individuals >14 yrs of age in the presence of complete RBBB
IV. Depolarization/conduction abnormalities	Epsilon wave in the right precordial leads (V_1 to V_3)	Late potentials by SAECG in ≥1 of 3 parameters in the absence of a QRS duration ≥110 ms on the standard ECG Filtered QRS duration ≥114 ms Duration of terminal QRS <40 μV (low-amplitude signal duration) ≥38 ms Root mean square voltage of terminal 40 ms ≤20 μV Terminal activation duration of QRS ≥55 ms measured from the nadir of the S-wave to the end of the QRS, including R', in V_1, V_2, or V_3, in the absence of complete RBBB
V. Ventricular Arrhythmias	Nonsustained or sustained VT of LBBB morphology with superior axis (negative or indeterminate QRS in leads II, III, and aVF and positive in lead aVL)	Nonsustained or sustained RVOT VT of LBBB morphology with inferior axis (positive QRS in leads II, III, and aVF and negative in lead aVL) or with unknown axis >500 ventricular extrasystoles per 24 h (Holter)
VI. Family history	ARVC/D confirmed in a first-degree relative who meets current TFC ARVC/D confirmed pathologically at autopsy or surgery in a first-degree relative Identification of a pathogenic mutation categorized as associated or probably associated with ARVC/D in the patient	History of ARVC/D in a first-degree relative in whom it is not possible or practical to determine whether the family member meets current TFC Premature sudden death (<35 yrs of age) due to suspected ARVC/D in a first-degree relative ARVC/D confirmed pathologically or by current TFC in second-degree relative

From Gandjbakhch et al., Journal of the American College of Cardiology, 2018; doi:10.1016/j.jacc.2018.05.065.

1.5.6 Differential diagnosis

The achievement of a conclusive diagnosis for ACM patients is often complicated by the several pathologic conditions with which ACM shares common features.

Idiopathic right ventricular arrhythmias originating from the right ventricular outflow tract (RVOT) are not easily distinguished from ACM-associated arrhythmias (186), both often presenting left bundle branch block morphology and inferior axis deviation. Different management procedures are performed for the two conditions, as RVOT patients have usually a benign course (187); thus, their discrimination is required (188).

Of highly diagnostic challenge is myocardial scarring associated with myocarditis or sarcoidosis, often difficult to be discriminated from ACM (189) (190) (191) (192).

ACM and Brugada Syndrome (BS) are both inherited disorders predisposing to sudden cardiac death with similar arrhythmic manifestations (193) (194). Also rare RV structural anomalies in BS patients have been reported (195). Interestingly, mutations in *SCN5A*, usually causative in BS context, have been found also in ACM patients (196), whereas *PKP2* mutations, typical of ACM, are reported also in BS patients (197). Thus, the genetic-based diagnosis appears further intricate.

An arrhythmogenic phenotype occurs in a large amount of dilated cardiomyopathy (DCM) patients (198), often fulfilling ACM Task Force Criteria (163).

Cathecholaminergic polymorphic ventricular tachycardia (CPTV) and ACM has been proposed as phenocopies (199), since mutations in *RYR2*, provoking calcium handling impairment, are associated with both the diseases (200).

In addition, the discrimination between ACM and athlete's heart is often devious, since endurance training provokes RV dilation and reduced function (201) (202) (203) (204). The extreme haemodynamic stress induced by exercise may also promote arrhythmogenic remodelling, mimicking ACM arrhythmic phenotype (89). Nevertheless, the impairment of RV systolic function, being usually associated only with ACM, could represent a useful diagnostic tool to discriminate between the two. Moreover, no wall motion abnormalities are usually identified in healthy athletes (205).

1.6 Management and prevention

ACM is characterized by a strong risk of malignant arrhythmias and sudden cardiac death. Thus, the main goal for ACM management is to avoid these worst consequences and prevent disease progression. The therapeutic approach comprises lifestyle changes, pharmacological intervention, use of implantable cardioverter defibrillator (ICD), ventricular arrhythmia ablation, and, if needed, heart transplantation (206) (207).

Sport restriction, especially for the participation in high-intensity endurance training, is advised to reduce the risk of malignant ventricular arrhythmias and disease progression (92) (208) (209).

To control the arrhythmic burden, the prescription of anti-arrhythmic drugs is necessary. No proper systematic assessments of the efficacy of anti-arrhythmic strategies exist in ACM context, but the available evidence advocates amiodarone and sotalol, alone or in combination with beta-blockers, the election drugs to prevent symptomatic arrhythmias (210). The treatment with calcium channel blockers is adopted in patients with catecholamine-triggered arrhythmias, but they have limited efficacy for re-entry arrhythmias management (211).

The only proper life-saving approach is constituted by ICD implantation, able to prevent sudden cardiac death and improving long-term prognosis, through the termination of life-threatening arrhythmias (207) (212). The efficacy and safety of ICD is reported in several observational studies on large ACM populations (213) (214) (215). Interestingly, a study reported that the concomitant treatment with anti-arrhythmic drugs does not protect against most ICD appropriate interventions, indicating that they may not confer adequate defence against SCD, and further confirming the unavoidability of ICD implantation (216).

Catheter ablation is additionally proposed to patients with frequent recurrence of ventricular arrhythmias, despite the anti-arrhythmic therapy. Scar regions, constituting arrhythmogenic substrates, can be identified by either electrophysiological or electroanatomical mapping (206). The combination of endocardial and epicardial ablation seems to be more effective in reducing the frequency of arrhythmic episodes (217) (218) (219) (220). Since catheter ablation does not demonstrate considerable effects on

SCD risk reduction and survival increase, it cannot be considered a valid substitute of ICD (221).

In the late phases of the disease, ACM patients may develop heart failure, thus their therapy is implemented with diuretics, angiotensin-converting enzyme (ACE) inhibitors or aldosterone inhibitors, and heart transplantation, in the worst scenarios (206).

Unfortunately, to date no mechanism-based therapies are available, and a definitive cure does not exist (123). Gene therapies could represent a possibility in the future (222). Moreover, the deepening of ACM molecular mechanism knowledge would be useful to propose new therapeutic strategies.

The identification of parameters determining the risk of worst clinical outcomes is particularly important in ACM context, also to ascertain the best management strategy both for ACM patients and family members (223). A prediction model to define individualized 5-year risk for ventricular arrhythmias in ACM has been recently created (www.arvcrisk.com) and may guide clinicians in the primary prevention choices (224).

Nevertheless, since ACM is a progressive disease, patients should undergo life-long periodical follow-up to re-examine the risk of SCD and optimize the therapeutic approach (206).

1.7 Cellular models

In vitro modelling of ACM, by using cardiomyocytes, cardiac progenitor cells, cardiac stromal cells, and non-cardiac cells, helped to unravel disease pathogenic mechanisms, including its genetic bases, as well as its cellular, signalling and molecular alterations (**Figure I7**) (73).

Figure I7. Cellular models for ACM *in vitro* studies.

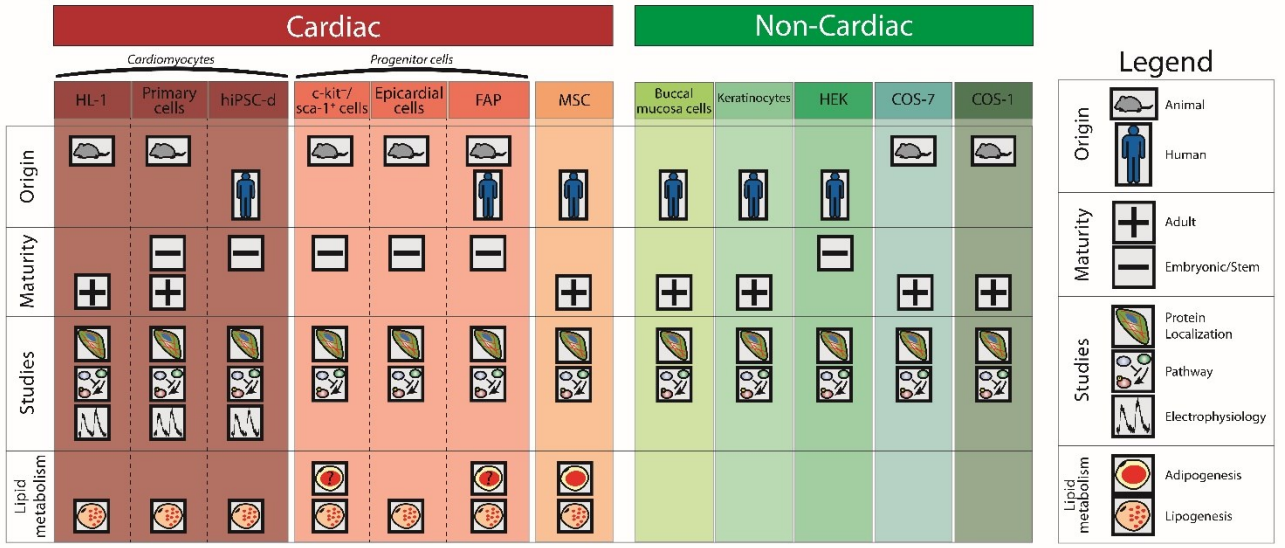

From Sommariva et al., Disease Model and Mechanisms, 2017; doi:10.1242/dmm.029363

1.7.1 Cardiomyocytes

Human adult cardiomyocytes are considered the ideal model for ACM modelling, but their isolation and maintenance in culture is challenging. Thus, many researchers have exploited murine immortalized cardiomyocytes, such as HL-1 line (225). The main advantages of using cell lines is their scarce variability among samples and the possibility to easily introduce genetic mutations of interest to evaluate the downstream effects. HL-1 cells facilitated the understanding of ACM causative mutation impact (226) (227) (228) (229) (230) (231) (232) (233), the impairment of Wnt and Hippo pathway (133) (139), and the gap junction remodelling (197) (234) (235) (236). Since HL-1 cells are of atrial origin, they are not able to fully recapitulate ventricular myocyte features. Moreover, showing disorganised sarcomeres and channel

selective expression, they are not suitable for contraction or electrophysiological studies.

Primary myocytes, both neonatal and adult, from ACM transgenic murine models have been characterized, also through electrophysiological studies (147) (237) (238). Although they provided further insights about ACM pathogenesis, they are limited by their non-human origin.

This limitation can be overcome by using human induced pluripotent stem cells-derived cardiomyocytes (hiPSC-CM) (239) (240) (241). This *in vitro* model is potentially unlimitedly available, suitable for high-throughput screening, and, since it carries patients' genome, appropriate for precision medicine studies. In contrast, the foetal-like phenotype of hiPSC-CM, the high variability among clones from the same donor, and handling difficulties represent shortcomings in their use.

3D micro-tissue models have the potential to improve disease modelling. Indeed, different cardiac cell types can be obtained from the same hiPSC-derived cardiac mesoderm, creating an isogenic multicellular model composed by CM, endothelial cells and cardiac fibroblasts. The presence of the three main cardiac cell types in the same model can induce CM maturation, without requiring specialized devices, mechanical load, or scaffolds (242).

1.7.2 Progenitor cells

Cardiac progenitor cells possess a stem-cell-like multipotency, thus they represent an interesting cell type to model the fibro-adipose substitution process in ACM. They are usually quiescent in the adult heart, but, after injuries, they can be activated and differentiate towards diverse phenotypes (243). Several resident progenitor populations have been described in the adult heart, characterized by different cell surface markers (73). C-kit+/Sca1+ cells are counted among them. In ACM context, murine C-kit+/Sca1+ cells from *JUP* transgenic mice helped to confirm the pivotal role of PG as mediator of myogenesis-to-adipogenesis switch (244).

Epicardial cells are considered progenitor cells because, after injuries, they are able to undergo epithelial-to-mesenchymal transition and differentiate into fibroblasts, smooth muscle and endothelial cells (245), as well as to secrete paracrine factors (246). In ACM context, they were advantageous to recognise Cx43

involvement (144), and to evaluate PKP2 loss effects as for lipid accumulation and myofibroblast differentiation (38).

Also murine fibro-adipocyte progenitors, connoted by platelet-derived growth factor receptor α (PDGFRα) expression, were useful to investigate ACM fibro-fatty substitution mechanisms (247).

1.7.3 Cardiac mesenchymal stromal cells

Cardiac mesenchymal stromal cells (C-MSC) are non-contractile cells, required to preserve cardiac functional homeostasis both in physiological and pathological conditions (248) (249). They are characterized by a residual multipotency toward mesenchymal lineages (250), thus they can differentiate into adipocytes and contribute to the adipose substitution in ACM hearts (20).

Human adult C-MSC constitute a good *in vitro* model to study ACM adipogenesis, since they can be directly isolated from ACM patient cardiac biopsies (185). As primary cells, isolated C-MSC carry patients' genetic background. Thus, their behaviour is influenced by ACM causative mutations, that induce PG translocation into the nucleus and the consequent Wnt pathway impairment, triggering C-MSC adipogenic differentiation (20).

1.7.4 Non-cardiac cells

Besides cardiac cell models, *in vitro* studies of ACM mechanisms were performed also with non-cardiac cell lines, such as HEK293T and COS cells, in order to simplify the modelling process and overcome the limitation of human myocardial sample paucity. Non-cardiac cell lines have been primarily exploited for functional tests on newly identified ACM-associated mutations (51) (251) (252).

1.8 Animal models

The only spontaneous animal model of ACM is represented by Boxer dogs, that widely resemble human clinical and pathological features (253) (254).

Thanks to genetic technology advances, other *in vivo* models have been developed for the systematic examination of the pathways involved in ACM pathogenesis (255).

The main advantage of animal model use relies on the possibility to analyse phenotypic changes dependent only by a specific genetic background, complemented, if appropriate, with the environmental cofactors of interest. However, ACM animal models do not fully recapitulate patient disease. For instance, no ACM *in vivo* models develop abundant cardiac adipose tissue. Nevertheless, ACM animal models have contributed to deepen disease molecular mechanisms and represent a good platform for drug testing.

1.8.1 Models of desmosomal mutations

PKP2 is the most frequently mutated gene in ACM patients (256) and several studies have tried to characterize its impairment in animal models. Whole *Pkp2* knockout (KO) mice shows embryonic lethality, being PKP2 essential for cardiac development (257). Conversely, *Pkp2* heterozygous KO mice (*Pkp2*+/-) are viable and fertile, thus available for research studies (257), but they display only a mild ACM cardiac phenotype, with impaired desmosomes and sodium current dysfunction upon provocative test (147) (258). The reduction of *Pkp2* affects the whole body in this murine model. The cardiac-specific and tamoxifen-inducible *Pkp2* KO model better recapitulate ACM features, as cardiac fibrosis, Cx43 impairment, and LV and RV dilation (44) (45). In addition, different transgenic models resemble the expression of PKP2 truncated protein and are characterized by cardiac remodelling if subjected to physical exercise (259) (260). Nevertheless, cardiac restricted full-length PKP2 loss results in more severe cardiac defects.

Zebrafish models have also been used to study *PKP2* mutations. *PKP2* zebrafish embryos showed decreased heart rate, a reduced number of ID, and abnormal ventricular looping. As demonstrated also in ACM murine models, *PKP2* have both a structural and a signalling role in heart development (261).

Different *Dsp* transgenic models, either homozygous and heterozygous, showed embryonic lethality (262) (263). However, cardiac-specific *Dsp* KO mice are available and display ventricular enlargement and biventricular cardiomyopathy, other than Cx43 defects (145). In addition, *Dsp* heterozygous KO mice have been generated. Despite the high mortality, they manifest Wnt pathway impairment, with PG delocalization into the nucleus (133). Further, Gomes et al. demonstrated that cardiomyocyte-specific *Dsp* haploinsufficiency lead to Cx43 reduction and alterations in conduction–repolarization kinetics prior to morphological changes (238). The cardiac-specific overexpression of R2834H *Dsp* mutation further confirm the deleterious effect of endurance exercise when desmosomes are impaired (264). Additionally, *Dsp*-deficient zebrafish recapitulate Wnt, TGFβ, and Hippo pathway alterations (265).

Dsg2 KO mice, besides the high mortality rate, display increased ventricular volume, reduced ejection fraction, arrhythmias, and cardiac fibrosis (266) (267) (268). In these mice, the inhibition of glycogen synthase kinase-3β (GSK3β), a modulator of the Wnt-β catenin pathway, moderated the pathologic phenotype (269). Different *Dsg2*-mutation overexpression animal models have been created, showing typical ACM clinical features, as ventricular arrhythmias and cardiac dysfunction (8) (9) (270).

To date, there is almost no model available to study *Dsc2* deficiency. The only existing transgenic mice are characterized by *Dsc2* cardiac overexpression, that, although not representative of any known ACM-linked variants, show biventricular dysfunction, necrosis, inflammation and fibrotic remodelling (271). Moreover, *Dsc2* KO zebrafish exhibit desmosomal structure alterations (272).

As most desmosomal gene homozygous KO models, also *Jup* deficiency provokes embryonic lethality (273) (274), but *Jup* heterozygous KO mice are viable and predisposed to ventricular arrhythmias, in absence of structural remodelling (275) (276). Also cardiac-specific conditional *Jup* KO models were generated, displaying cardiomyocyte loss, fibrosis and RV dilation (277) (278). Conversely, the cardiac overexpression of mutant PG increased mouse mortality (244).

1.8.2 Models of non-desmosomal mutations

Fewer ACM animal models have been generated to recapitulate ACM non-desmosomal mutations (31).

RYR2 mutations, although their association to ACM is still controversial, have been mimicked in different murine models (279) (280) (281), but only *Ryr2*-p.R176Q+/- knock-in mice partially recapitulate ACM phenotype, showing adrenergic-induced ventricular arrhythmias (280).

Different murine and zebrafish models carry *Scn5a* mutations and show conduction defects and biventricular cardiomyopathy (282) (283) (284) (285). *Scn5a* homozygous mice are embryonically lethal (286).

Phospholamban mutations, responsible of disturbed calcium homeostasis, have been introduced in transgenic mice, producing a phenotype covering both ACM and DCM. These murine models show ventricular dilation, myocardial fibrosis, and impaired calcium handling (287) (288).

The role of TMEM43 in ACM can be assessed by different mouse models (289) (290). The closest model to severe human phenotype is characterized by cardiac-specific *TMEM43*-p.S358L overexpression, showing a significant biventricular impairment, fibro-adipose substitution, and diminished survival (291).

Mouse models carrying *Lmna* missense mutations have been produced, but their phenotype does not overlap with those of ACM patients (292).

Des-deficient mice are characterized by fibrosis and myocardial degeneration, but they only partially mimic human ACM (293).

Cttna3 conditional KO mice are available and display a progressive cardiomyopathy phenotype, comprising LV dilation and reduced ejection fraction, due to junctional alterations (294).

The effects of reduced N-Cadherin can be studied by using cardiac-specific inducible *Cdh2* KO mice, that develop ventricular arrhythmias and conduction abnormalities (295) (296).

Only inducible cardiac-specific *Flnc* KO mice are available, showing cardiac fibrosis and dysfunction, because global and cardiac-specific KO are embryonically lethal (297).

Several zebrafish and murine models have been obtained to study *TTN* mutations (298) (299) (300) (301) (302). Most of them show phenotypical overlapping with DCM features with reduced systolic function.

Although the causative role of TGFβ3 in ACM needs to be confirmed, *Tgfβ3* KO mice have been developed, but they do not show a specific cardiac phenotype (303) (304).

In conclusion, non-desmosomal animal models do not recapitulate specifically ACM features, thus their applications are limited.

2. Oxidative stress

Reactive oxygen species (ROS) are oxygen-containing molecules, and include free radicals, species with one or more unpaired electrons (*e.g.* superoxide, O_2-; hydroxyl anions, OH-), and compounds which are convertible to radicals (*e.g.* hydrogen peroxide, H_2O_2) (305).

ROS are produced as cellular metabolites in physiological conditions (306). The main cell source of ROS are the mitochondria, during the so-called free-radical leak. Indeed, not all the electrons, in the mitochondrial electron transport chain, are transferred to O_2, the final electron acceptor, and this provokes ROS production (306). ROS can be produced also in the cytoplasm, cell membrane, endoplasmic reticulum, lysosomes, cytoskeleton, and peroxisomes (307). The key enzymes involved in oxidant production are NADPH oxidase, xanthine oxidase, myeloperoxidase, and lipoxygenase (308). During pathogen infections, ROS can act as host-defending compounds: immune cells produce ROS, after the recognition and internalization of pathogens, for their degradation via oxidative burst (309).

Due to their high reactivity, ROS are able to target any molecule in the cell, such as lipids, proteins, and nucleic acids. They also possess signalling properties, including the regulation of kinases, phosphatases, and transcription factors (310). In the heart, they control multiple physiological processes, among which excitation-contraction coupling, since different calcium channel activity is redox-sensitive (311), and cell proliferation and differentiation (312). Thus, at low concentration, ROS are fundamental to maintain cellular homeostasis. However, ROS effects depend on their levels and on exposure duration: at higher concentrations and as a result of long exposure, they can be deleterious, inducing modifications that disturb cell physiology (313).

The cells are usually able to balance ROS amount, in order to prevent damages, through two different strategies: minimization of free-radical leak, increasing mitochondrial respiratory complex expression, and production of antioxidants, able to scavenge ROS (312) (314). These latter include both enzymatic (*e.g.* superoxide dismutase, catalase, glutathione peroxidase, and glutaredoxins) and non-enzymatic compounds (*e.g.* vitamins E and C, reduced glutathione, lipoic acid, urate, and ubiquinone).

A dysregulation between ROS production and antioxidant mechanisms leads to oxidative stress and to the consequent activation of pathologic pathways: ROS may induce genetic mutations, alter protein structure, modify intracellular lipids through lipid peroxidation, and cause apoptosis (315) (316). Interestingly, during their reaction with target molecules, ROS can directly mediate a further increase of oxidative stress. For instance, the ROS-mediated oxidation of plasma membrane fatty acids produces a fatty acid peroxyl radical, in turn able to target the adjacent fatty acid, creating a chain reaction that alters membrane integrity and permeability (317) (318).

2.1 ROS in cardiovascular diseases

Due to the above described mechanisms, ROS overproduction is associated with the pathogenesis and progression of many pathological conditions, among which cardiovascular diseases (CVDs). The most common risk factors of CVDs, such as smoking, aging, and hypercholesterolemia, are associated with an increased ROS production (317). Different *in vitro* and *in vivo* studies have described ROS increment in the cardiovascular system in response to stressors and in failing hearts (319) (320) (321) (322) (323) (324). Due to the key role of myocardial oxygen consumption and availability to guarantee cardiac homeostasis, hypoxic conditions can be determinant in oxidative stress production: hypoxia-inducible factor 1α (HIF-1α) can modulate the transcription of downstream genes, among which ROS modulators (325) (326) (327).

CVDs characterized by elevated inflammation are associated with redox balance impairment, due to their reciprocal influence (328) (329) (330). Pro-inflammatory stimuli induce ROS production, through NADPH oxidase activation and mitochondrial activity enhancement. High amount of ROS mediates NF-kB and downstream inflammatory gene upregulation, with consequent cytokine secretion (306).

Interestingly, cardiac lipid accumulation, that occurs when there is an imbalance between lipid uptake and β-oxidation, increases ROS, due to the activation of fatty acid oxidation (331).

In addition, secondary products of ROS, such as 4-hydroxynonenal and malondialdehyde, can propagate oxidative stress effects (332) (333) (334).

Cardiomyocytes need a high amount of energy to sustain contraction, thus they possess a considerable greater number of mitochondria than other cell types (335). Cardiomyocytes produce more than 95% of the energy consumed by the heart (336). For this reason, they could be considered the main source of ROS in the heart, but also the contribution of non-myocyte cells to the cardiac oxidative status has been reported.

Oxidative stress is able to elicit cardiomyocyte dysfunction and apoptosis, leading to contractile alterations (320) (337). Cardiac hypertrophy is promoted by ROS, as well as cardiac fibrosis, due to fibroblast proliferation and secretion of collagen (320) (337). The main pathways that are activated by ROS to induce these changes are the extracellular signal-regulated kinase 1/2 (ERK1/2), c-Jun N-terminal kinase (JNK), p38 mitogen-activated protein kinase (MAPK), and phosphoinositide 3-kinase (PI3)/protein kinase B (Akt) pathways (338). In addition, oxidative stress is one of the major determinants of endothelial dysfunction, particularly relevant in atherosclerosis (339).

2.2 ROS-mediated low density lipoprotein oxidation

As discussed above, any molecule can be altered by ROS. Low density lipoproteins (LDL) are among those, becoming oxidized, in an oxidative stress environment. In physiological conditions, LDL oxidation occurs rarely in the blood or cell cytoplasm thanks to the abundance of antioxidant compounds (340). Much of the oxidation occurs in the sub-endothelial space of vessels, where the concentration of antioxidants is lower. Due to high LDL concentration and increased vascular permeability, also inflammation areas are sites of LDL oxidation (308).

LDL are the main carriers of cholesterol, and they are constituted by a lipid core, including triglycerides, cholesteryl esters and unesterified cholesterol, and by a surface monolayer mainly composed of phospholipids and the apolipoprotein ApoB-100, necessary for the interaction with the LDL receptor (LDLR) (341).

Although they carry also lipophilic antioxidants (341), LDL can be oxidized both on their lipid and protein components. The free radicals oxidize primarily the polyunsaturated fatty acids (*e.g.* arachidonic and

linoleic acids), whereas non-radical oxidants modify directly ApoB-100 (308). When the oxidation regards only LDL lipids, minimally-modified LDL are produced; when also Apo-B is subjected to oxidation, fully-oxidized LDL are obtained (Figure I8). Interestingly, the oxidation process to fully-oxidized LDL seems to be mediated by the consecutive activity of several oxidants (308). Moreover, the aldehyde products of oxidized LDL (oxLDL) lipid peroxidation (*e.g.* 4-hydroxynonenal and malondialdehyde) can further modify ApoB-100 residues (308).

Figure I8. Low density lipoprotein oxidation.

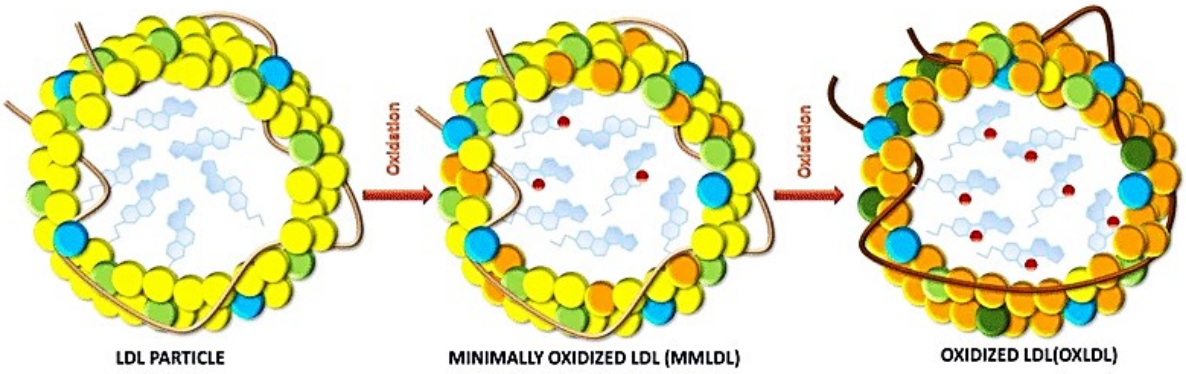

From Zmysłowski et al., Lipids in Health and Disease, 2017; doi:10.1186/s12944-017-0579-2

These modifications permanently alter LDL properties. They are no longer capable of binding the LDL receptor (LDLR), but they acquired affinity for different receptors among which scavenger receptors (SR). SR comprise two classes: SR class A, which includes two subtypes (I and II), and SR class B. SR-A I and II are well characterized in the atherosclerosis context, since they are expressed in macrophage-derived foam cells (342) (343) (344). Their presence has also been reported in smooth muscle cells and endothelial cells (345) (346) (347). However, the uptake of oxLDL by macrophages is largely attributed to CD36, a member of the class B of scavenger receptors (348) (349) (350). It is expressed in macrophages, platelets, fibroblasts, adipocytes, and endothelial cells (351) (352) (353). CD36 is able to bind not only fully-oxidized LDL, as

SR-A, but also minimally-modified LDL. OxLDL uptake by CD36 depends mostly on their lipid moiety (*e.g.* presence of lipid peroxidation), rather than ApoB-100 modifications (352) (349). SR-B1, highly expressed in the liver, is included in the class B scavenger receptors, but it binds native LDL and high-density lipoproteins (HDL), being involved in reverse cholesterol transport and cholesterol clearance (354) (355) (356) (357) (358).

Lectin-like oxLDL receptor-1 (LOX1) mediates oxLDL uptake mostly in endothelial cells, but its expression is inducible in smooth muscle cells and macrophages, and, in general, in vascular-rich organs (359) (360). Like SR-A I and II, it recognizes the modified ApoB-100 (361), but it has a higher affinity for the minimally-modified forms of LDL, possibly through the recognition of lipids covalently bound to the apolipoprotein (362). Toll-Like Receptor-4 (TLR4) is a further minimally-modified LDL receptor, expressed in endothelial cells (363), myocytes (364), and adipocytes (365). Its role in lipid accumulation induction has been described both *in vitro* and *in vivo* (366).

Based on the plurality of receptors and the extent of the oxidation, the biological responses prompted by oxLDL could be extremely different and, in some cases, conflicting (308). Indeed, both pro- and anti-inflammatory properties have been described. The pro-inflammatory response may be mediated by nuclear factor kappa-light-chain-enhancer of activated B cells (NFkB), activator protein 1 (AP-1), signal transducer and activator of transcription 1 and 3 (STAT 1/3), nuclear factor of activated T-cells (NFAT), and specificity protein 1 (SP-1) transcription factors (308) (340). The anti-inflammatory effects may depend on the activation of peroxisome proliferator-activated receptors (PPARs), nuclear factor erythroid 2–related factor 2 (Nrf2), and heme oxygenase-1 (HO-1) (308). In addition, oxLDL can induce autoimmune responses through adaptive and innate mechanisms (308).

In atherosclerosis, macrophages internalize oxLDL through CD36 receptor, causing their transformation into lipid-laden foam cells (367). Indeed, the internalized oxLDL, by means of their main components 13-hydroxyoctadecadienoic acid (13HODE) and 9-hydroxyoctadecadienoic acid (9HODE), activate the nuclear receptor PPARγ, involved in adipogenesis and lipogenesis (368). A feed forward loop is then created,

leading to the transcriptional increase of PPARγ itself and CD36, facilitating a further internalization of oxLDL (368) (369).

Also the pro-fibrotic effects of oxLDL, following LOX-1 binding, has been studied: oxLDL stimulates TGFβ1 expression and Smad pathway activation, increasing the synthesis and secretion of extracellular matrix proteins (370) (371).

oxLDL are also able to increase intracellular ROS production, stimulating NADPH oxidase activity, lipoxygenase/cyclooxygenase system, and mediating mitochondrial dysfunction (308) (372) (373) (374).

In addition, cell death, either for apoptosis and necrosis, has been reported in several *in vitro* models, following oxLDL treatment (375) (376), but the oxidation extent seems to be determinant. Indeed, by using minimally-modified LDL, the promotion of cell growth, rather than death, has been described in arterial smooth muscle cells, macrophages, and fibroblasts (377).

Also the effects on angiogenesis are debated and they likely depend on oxLDL concentrations: low amount of oxLDL may stimulate the pro-angiogenic factors, through p38-MAPK pathway activation (378) (379) (380), whereas high amount has possibly anti-angiogenic effects, due to sphingolipid-mediated mechanisms (379) (381).

2.3 oxLDL in ACM

Several features of ACM suggest a role of oxidative stress and oxLDL in disease pathogenesis, although their contribution has not been fully recognized yet.

ACM patients are often athletes, and physical exercise is an accepted cofactor contributing to disease progression (92). Despite the beneficial role of mild training, linked to HDL increase and transient production of ROS necessary to promote beneficial adaptive responses (382) (383), intense activity can induce ROS overproduction, thus increasing susceptibility of LDL to oxidation (384) (385) (386). Indeed, during high-intensity sport, the greater oxygen demand at tissue level leads to larger ROS leakage from the mitochondria, charging the environment with oxidative stress (387). In addition, cardiomyocyte mechanical stretch has been linked to ROS production (388). Endurance exercise promotes lipid peroxidation with

parallel reduced vitamin E (389). 9- and 13-HODE, which are oxLDL components, have been proposed as exercise-induced oxidative stress markers, thus their concentrations are likely increased also in ACM patients (390). In addition, 13HODE demonstrated *in vitro* the capability to induce, through PPARγ activation, lipid accumulation in iPS-derived cardiomyocytes, indicating its role as a lipogenesis stimulator (240). ACM cardiac remodelling includes adipose substitution of ventricular myocardium, mediated by PPARγ upregulation (20) (133) (240) (391), hence the contribution of 13HODE in ACM adipogenesis can be hypothesized. This is supported by Parhami et al. work, that demonstrated oxLDL effects on adipogenic differentiation of bone marrow mesenchymal stromal cells (392). Since, in ACM hearts, the main responsible of adipose substitution are C-MSC (20), increased concentrations of oxLDL could concur in their differentiation.

Moreover, oxLDL and 13HODE can induce apoptosis (393) (394) (395), corroborating the possible link with ACM cardiomyocyte death. One possible mechanism involves p53, which is able to reduce peroxisome proliferator-activated receptor γ coactivator-1α (PGC-1α) levels, leading to mitochondria dysfunction and apoptosis (396) (397).

The fibrotic remodelling of ACM hearts could be explained by oxidative stress effects: in other diseases, as heart failure, ROS trigger cardiac fibrosis (398) (399). Galectin-3 is involved in fibroblast activation to produce collagen (400) (401), and interestingly its levels are significantly elevated in ACM patients (402).

Inflammation often characterizes ACM patients, although it is still not clear if it represents a consequence of cardiomyocyte death or an initial trigger (123) (124). For other CVDs, the crosstalk between inflammation and oxidative stress has been described, both capable of stimulating each other (403) (404) (405). Pro-inflammatory cytokines, such as interleukin 6 (IL-6), interleukin 1 (IL-1) and tumor necrosis factor (TNF), promote oxidative stress (406), in turn ROS accumulation induces systemic inflammation via formation of immunogenic protein adducts, able to trigger the immune response (407) (408) (409).

Hypothesis and Aims

Incomplete penetrance and variable expressivity often characterize ACM families, strengthening the concept that other genetic and/or environmental factors may play a modifying role.

In this regard, several gaps in the literature need to be filled:

- to identify new molecular phenotype modulators;
- to detect clinical prognosticators;
- to obtain etiological therapies.

As described above, many hints point to a role of oxidative stress and oxLDL in ACM pathogenesis. The aim of the present project was to assess if oxLDL/CD36/PPARγ circuitry is a pathogenic trigger in ACM patients, focusing on cardiac adipose substitution process. In particular, we hypothesized that, beside the causative genetic mutation, higher oxLDL concentration and oxidative stress levels can aggravate the disease clinical manifestations, through PPARγ and CD36 hyperactivation (Synopsis figure).

To verify our hypothesis, we performed the following studies:

- patients' lipid profile characterization, ventricular tissue analysis and associations with clinical parameters;
- *in vitro* experiments, by using human primary C-MSC and hiPSC-CM, to unravel the oxLDL-activated mechanisms and test potential pharmacological intervention;
- *in vivo* studies on the plakophilin2 heterozygous knock-out model, to recapitulate disease phenotypes, in line with our hypothesis, and pharmacologically prevent them.

Synopsis figure.

ACM mutations are necessary but not sufficient for disease penetrance. oxLDL trigger ACM adipogenesis by a feed-forward circle: oxLDL components, as 13HODE, are internalized through the CD36 receptors and induce PPARγ, leading to further PPARγ and CD36 expression, thus stimulating higher adipogenesis, and facilitating oxLDL uptake.

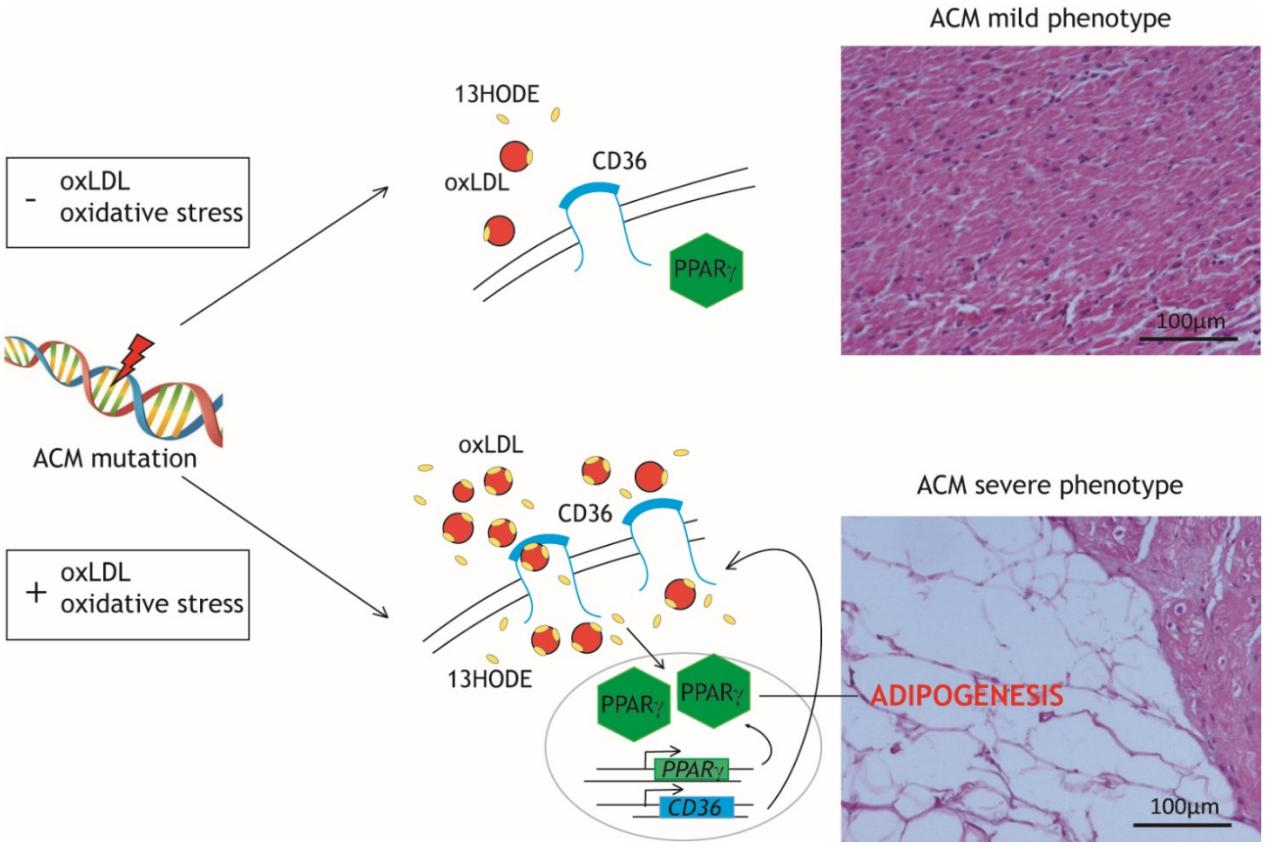

Materials and Methods

1. Ethics statement

This study complies with the Declaration of Helsinki and was approved by “IEO-CCM IRCCS” (12/06/2012) and by "South Tyrol Azienda Sanitaria" (13/03/2014, N. 1/2014) Ethics Committees. Written informed consent was obtained from all participants. Healthy control (HC) cardiac samples were obtained from donors (accidental death), from “Treviso Tissue Bank Foundation”.

2. Study patients’ population

A total of 67 ACM patients hospitalized at Centro Cardiologico Monzino IRCCS were enrolled for this study. ACM diagnosis was reached according to the 2010 International Task Force criteria (163). 36 patients out of the total cohort were matched for age, sex and cardiovascular risk factors to 36 HC without a previous history of heart disease for plasma analysis. We further enrolled for the plasma analysis 9 ACM patients’ relatives with *PKP2* mutations but no clinical signs of the disease. Since the group of relatives was not perfectly matched for sex and age with the ACM patients used for the comparison, the influence of these variables on the relationship of oxLDL and ACM has been excluded by multiple regression analysis ($p = 0.02$).

We obtained blood samples from all the recruited ACM patients and HC. ACM patients and HC taking statins or other lipid-lowering drugs were excluded from the analysis. Clinical data were collected for all ACM patients, as available: RV ejection fraction (EF) % was determined by cardiac magnetic resonance (CMR); RV dysfunction was defined as in (163); major arrhythmic events (MAE) are defined as sustained ventricular tachycardia, ventricular fibrillation, appropriate implantable cardioverter device (ICD) intervention, aborted sudden cardiac death.

RV endomyocardial samples were obtained by bioptic procedures from 19 ACM patients.

3. Plasma preparation

Blood samples (5 ml) were collected in EDTA coated tubes and centrifuged at 1500 x g for 15 minutes. Supernatants were collected, centrifuged again at 16000 x g for 15 minutes to obtain cells- and platelet-free plasma, and stored at -80 °C as 400 µl aliquots until usage.

4. oxLDL in human plasma samples

Plasma samples from ACM patients and HC were used for the determination of oxidized low density lipoproteins (oxLDL) quantity, using a specific Elisa kit (Immundiagnostik). The test recognizes MDA-modified apolipoprotein B100. The protocol recommended by manufacturers was observed and the absorption was determined with a spectrophotometer (Berthold Technologies) at 450 nm. Results were interpreted by constructing a dose/response curve according to the standards provided in the kit.

5. 13HODE quantification

The determination of plasma 13HODE levels was performed by a liquid chromatography-tandem mass spectrometry (LC-MS/MS) method. Briefly, plasma samples (100 µl) were acidified with 1% formic acid, mixed with the internal standard (d_4-13HODE, final concentration 50 pg/µl; Cayman Chemicals) and purified through HLB extraction cartridges (Oasis® HLB 1cc (30 mg), Waters). The eluted fraction was evaporated to dryness and reconstituted with 250 µl of water/methanol/acetonitrile (80:10:10, v/v/v) before the LC-MS/MS analysis. The LC-MS/MS analysis was performed using an Accela HPLC System (ThermoFisher Scientific) coupled to a triple-quadrupole mass spectrometer TSQ Quantum Access (ThermoFisher Scientific) outfitted with electrospray ionization source operating in negative mode. The chromatographic separation was achieved using an XBridge® C18 column (2.1 mm × 30 mm, particle size 2.5 µm, Waters) at 30 °C. The mobile phase was composed by 2 mM ammonium acetate in water/acetonitrile/methanol (87:10:3, v/v/v, at pH 8 by ammonium hydroxide) (solvent A) and 2 mM ammonium acetate in acetonitrile/water/methanol (87:10:3, v/v/v, at pH 8 by ammonium hydroxide)

(solvent B). The following gradient, at a flow rate of 250 µl/min, was used: 0 minutes – 10% B, 2 minutes – 35% B, 2.5 minutes – 90% B, 6 minutes – 90% B, 6.5 minutes – 10% B and 12 minutes – 10% B. The analytes were detected by multiple reaction monitoring and the transitions monitored (precursor ion > product-fragment ions) were: *m/z* 295.1 → *m/z* 276.8, 194.9 (13HODE) and *m/z* 299.1 → *m/z* 279.9, 197.8 (d_4-13HODE). A linear 6-points calibration curve (range 2-62.5 pg/µl) was used for the quantification.

6. Genetic analysis

To investigate a genetic predisposition for oxidized lipid increase in ACM-affected patients, we performed exome sequencing on 3 families with low ACM penetrance, in which causative *PKP2* mutations were identified, analyzing the co-segregation with the ACM phenotype of variants in a selected panel of genes associated with dyslipidemia and oxidative stress.

DNA samples from blood were prepared following the Nextera® Rapid Capture Exome Enrichment kit protocol. Libraries for all samples, except Fam3.I.3, Fam3.I.4, and Fam3.II.3, were sequenced on two lanes of an Illumina HiSeq in paired-end mode and a read length of 100 bp. The remaining three samples were sequenced subsequently on four lanes of an Illumina MiSeq in paired-end mode and a read length of 75 bp. Nextera adapters were trimmed off using SeqPrep (https://github.com/jstjohn/SeqPrep) and read quality was controlled with FastQC (http://www.bioinformatics.babraham.ac.uk/projects/fastqc/). Reads were aligned to reference genome GRCh37 with BWA version 0.7.15 (410). Duplicate marking was performed with picard tools version 2.8.1 (https://broadinstitute.github.io/picard/). Indels were realigned and base quality scores recalibrated using GATK 3.7 (411), following the GATK best practice guidelines (412). Quality of bam files was evaluated with QualiMap version 2.2.1 (413), sample contamination estimated with verifyBamId (414), and sex validated by inspection of the X chromosome coverage. Intermediate per sample gvcfs were generated with the GATK HaplotypeCaller, followed by joint genotyping on all individuals with GATK GenotypeGVCFs and additional samples not related to this study. Variants were called on the exonic target regions as defined by the Nextera protocol with a padding of 100 bp around the exons. Variants were annotated with Ensembl gene and variant consequence data using the

Dintor gcoords2cons tool (415). For each variant, the annotation of the transcript with the worst consequence type as according to Ensembl was selected.

First, using the Dintor MendelianFiltration tool, variants were selected that were present either in homo- or heterozygous form in all affected individuals of all three families, requiring a coverage of at least 10X at variant sites in the respective individuals.

Variants were restricted to those mapped to a gene of the oxidative stress and dyslipidemia gene panel. Further, variants were removed if their ExAC EUR allele frequency (AF) (416), their gnomAD NEF AF (416), or their 1000 Genomes phase 3 EUR AF (417) was greater than 0.3. Variants were not required to be in protein-coding genes.

Next, each family was analyzed individually. Using the Dintor MendelianFiltration tool, variants were selected if present in families' affected *PKP2* carriers, but absent in the same families' healthy *PKP2* carriers, requiring a coverage of at least 10X at the variant sites in the relevant individuals. For the selection, variants segregating in the affected *PKP2* carriers in either a dominant or a recessive mode of inheritance were accepted. Variants were restricted to those mapped to a gene of the oxidative stress and dyslipidemia gene panel. Further, variants were removed if their ExAC EUR allele frequency (AF) (416), their gnomAD NEF AF (416), or their 1000 Genomes phase 3 EUR AF (417) was greater than 0.05. Variants were not required to be in protein-coding genes.

Per sample, an average of 55 million ± 17 million reads mapped to reference genome, resulting in a mean coverage of 57X ± 21X, and 87% ± 4% of the exon target region covered at ≥ 10X. The sex of all samples was confirmed by inspection of the coverage of the X chromosome and sample contamination was below 1%.

7. Bioptic sampling

Endomyocardial biopsy sampling was performed in ACM-suspected patients for diagnostic purposes, guided by CARTO mapping, as previously described (184) (185). A bioptic sample from the RV acquired in the area adjacent to the electroanatomical scar was obtained from ACM patients and was processed to

obtain heart sections and cardiac mesenchymal stromal cells (C-MSC) (20). HC RV autoptic samples were treated with the same protocols.

8. Heart tissue section preparation and immunofluorescence analysis

Human ventricular samples were fixed in 4% paraformaldehyde (Santa-Cruz) in phosphate-buffered saline (PBS; Lonza) and processed for paraffin embedding. Paraffin-embedded sections (6 µm thick) were de-waxed in xylene and rehydrated in ascending alcohols. The immunofluorescence analysis was performed following antigen retrieval with incubation with target retrieval solution citrate pH 6/microwave (Dako). Sections were incubated with primary antibody anti-malondialdehyde (MDA; 1:2500; Abcam) and anti-CD36 (1:200; BD) at 4 °C overnight. After washing, sections were incubated with the fluorochrome-conjugated antibody goat anti-rabbit IgG Alexa 488 1:200 (AlexaFluor) for 1 hour at room temperature (RT) in the dark. Nuclear staining was performed by incubating sections with Hoechst 33342 (1:1000; Life Technologies). Sections were observed by Zeiss Axio Observer.Z1, with Apotome technology, and images acquired with the software AxioVision Rel. 4.8. For each explanted heart subject, 5 consecutive slices and at least 50 fields for each slice were examined. For ACM bioptic samples, all the samples were sliced and examined. See Table M1 for antibody list.

9. C-MSC isolation and culture

C-MSC were isolated and cultured as previously reported (20) (185) Figure M1. Briefly, ventricular samples were washed with PBS, cut into 2-3 mm pieces and incubated at 37 °C for 1.5 hours under continuous agitation in Iscove's Modified Dulbecco's Media (IMDM; Gibco) containing 3 mg/mL collagenase NB4 (Serva). The digested solution was then centrifuged at 400 x g for 10 minutes, washed with PBS and centrifuged again. The obtained pellet was re-suspended in growth medium (GM), consisting of IMDM supplemented with 20% fetal bovine serum (FBS; Euroclone), 10 ng/ml basic fibroblast growth factor (R&D Systems), 10000 U/ml Penicillin (Invitrogen), 10000 µg/ml Streptomycin (Invitrogen) and 20 mmol/L L-

Glutamine (Sigma-Aldrich). The cells were seeded onto uncoated Petri dishes (Corning). Non-adherent cells were removed after 24 hours.

The use of different C-MSC samples for different experiments is detailed in Table M2.

The characterization of isolated C-MSC was performed to confirm their mesenchymal lineage, through FACS analysis.

Figure M1. Summary of C-MSC isolation from endomyocardial biopsies procedure.

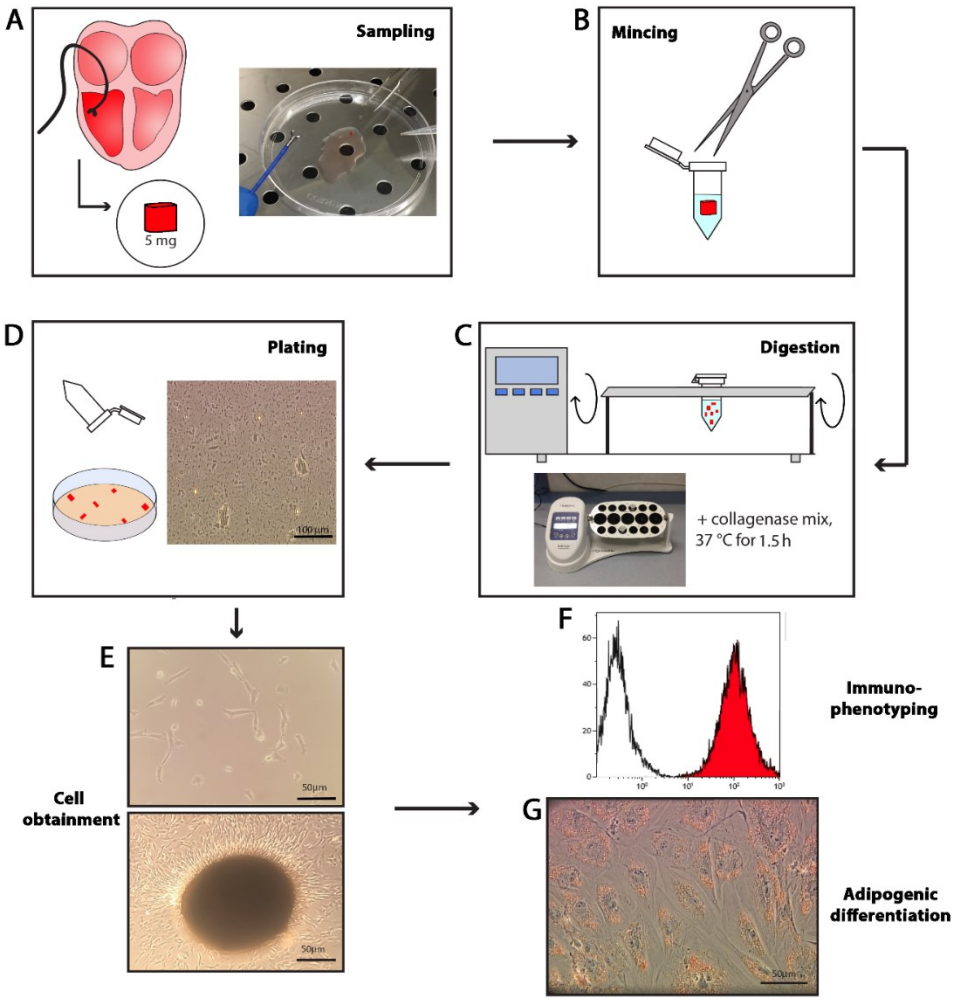

From Pilato et al., Journal of Visualized Experiments, 2018; doi: 10.3791/57263

10. C-MSC immunofluorescence analysis

C-MSC were plated on 1.8 cm^2 chamber slides (ThermoFisher Scientific) at a density of 20000 cells/cm^2. After 24 hours of culture in basal conditions, C-MSC were washed with PBS and fixed in 4% paraformaldehyde in PBS. After the blocking step in 10% goat serum (Sigma-Aldrich), cells were incubated with primary antibodies anti-MDA (1:2500; Abcam) and anti-CD36 (1:200; BD) at 4 °C overnight (see Table M1). After washing, sections were incubated with the fluorochrome-conjugated antibody goat anti-rabbit IgG Alexa 488 1:200 (AlexaFluor) for 1 hour at RT in the dark (see Table M1). Nuclear staining was performed by incubating sections with Hoechst 33342 (1:1000; Life Technologies). Sections were observed by Zeiss Axio Observer.Z1, with Apotome technology, and images acquired with the software AxioVision Rel. 4.8. For each dish, 10 fields were examined.

11. Glutathione quantification in C-MSC

Levels of reduced (GSH) and oxidized glutathione (GSSG) were determined by a previously described and validated LC-MS/MS method (418). Briefly, cells cultured in GM have been washed twice with PBS, detached with trypsin, and then collected and centrifuged at 400 x g for 10 minutes. The supernatant was removed, the pellet resuspended in 50 µL of PBS, and proteins were precipitated with 50 µL of 10% trichloroacetic acid with the addition of 1 mmol/L EDTA and stored at -80 °C until the analysis. Thawed samples were further diluted 1:10 with formic acid 0.1% before the LC-MS/MS analysis. The LC-MS/MS analysis was performed using an Accela HPLC System (ThermoFisher Scientific) coupled to a triple-quadrupole mass spectrometer TSQ Quantum Access (ThermoFisher Scientific) outfitted with electrospray ionization source operating in positive mode. The chromatographic separation was conducted on a Luna PFP column (2.0 mm × 100 mm, particle size 3.0 µm, Phenomenex) maintained at 35 °C. Analytes were eluted under isocratic conditions at 200 µL/min by 1% methanol in 0.75 mM ammonium formate adjusted to pH 3.5 with formic acid. The analytes were detected by multiple reaction monitoring and the transitions monitored (precursor ion > product-fragment ions) were: *m/z* 308.1 → *m/z* 76.2, 84.2, 161.9 (GSH) and

m/z 613.2 → *m/z* 230.5, 234.6, 354.8 (GSSG). A linear 6-points calibration curve (range 0.25-8 µM for GSH and 0.008-0.25 µM for GSSG) was used for the quantification.

12. C-MSC transcriptome sequencing

Total RNA of HC and ACM C-MSC was isolated using TRIzol Reagent (ThermoFisher Scientific), precipitated through the ammonium acetate/ethanol method and, then, treated with DNAse (TURBO DNAse; ThermoFisher Scientific) to remove genomic DNA contamination. The total RNA concentration and quality were assessed. Poly(A)$^+$ RNA enrichment was performed using Dynabeads mRNA DIRECT Micro Kit (ThermoFisher Scientific) starting from 6 µg of total RNA. Barcoded libraries were constructed using Ion Total RNA-Seq Kit v2.0 and Ion Express RNA-Seq Barcode kit (Thermo Fisher Scientific) following the manufacturer's instructions. Briefly, after poly(A)$^+$ RNA fragmentation using RNAse III, hybridization and ligation of barcoded adapters for stranded RNA sequencing were performed, followed by reverse transcription. cDNA fragments of 200 bp of each sample were amplified by 16 cycles of PCR using the specific "Barcode BC primers" for library demultiplexing and quantified on the 2100 Bioanalyzer system (Agilent Technologies, Santa Clara, CA, United States). One hundred pM diluted libraries were randomly pooled (six samples per pool). Templated Ion sphere particles preparation and chip loading were, then, performed by the automated Ion Chef System and Ion 550 Kit-Chef reagents and disposables. Loaded Ion 550 Chips were run on Ion GeneStudio S5 Prime System (all kits and instruments for sequencing were provided by Thermo Fisher Scientific).

Sequential aligning of raw reads was performed against the GRCh38 Human Genome reference with the most updated version of the "Spliced Transcripts Alignment to a Reference (STAR)" software (419) and with "Bowtie2" (420) to align locally any reads not mapped by STAR. Gene expression quantification and annotation were computed by "featureCounts" (421).

Raw count data were imported into the R software v3.5.0. and filtered to retain genes with a minimum of 10 counts in at least 50% of the samples. Differential expression analysis was performed by a negative binomial GLM approach (using the edgeR/Bioconductor package) (422) (423) along with the estimation of

latent variables, technical batch effects, or biological confounding variables, for adjusting the statistical model (using the RUVSeq R/Bioconductor package) (424). The number of K factors was chosen by comparing unadjusted vs. adjusted expression data by the use of diagnostic plots, i.e., relative log expression (RLE) plot, scatter plot of the first two principal components derived from PCA performed on total data, and histogram of the *P*-value distribution for testing the differential expression between LV vs. RV. A $K = 3$ factor of "unwanted variation" showed the best trade-off between data adjustment and the risk of data overcorrection and was, thus, used as covariates for model adjustment in a paired-sample data analysis. Genes were deemed as significantly different for FDR-adjusted P-value < 0.05. The reliability of the differential expression analysis results was further assessed by exploring the histograms of the *P*-value distribution, which showed a uniformly flat distribution across the unit interval (null *P*-values) with a peak near zero (*P*-values for alternative hypotheses) (425).

Functional inference analysis took advantage of prior biological knowledge of genes grouped by pathways and used for GSEA (software v4.0) (426). Gene sets of various pathway repositories were retrieved as a unique, merged Gene Matrix Transposed file format (*.gmt) from the Bader Lab gene-set collections[1] to perform a single GSEA run. A combined gene rank score (cs) was applied to weigh the relevance of the genes by taking into consideration both the magnitude [i.e., log2 fold change (FC)] and the statistical score of the gene expression differences [likelihood ratio (LR)] and was used as the gene-ranking metric for the GSEA pre-ranked tool option. Other GSEA parameters included 10,000 permutations and gene-set size limit ranging from 10 to 250 genes. To reduce redundancy and highlight grouping of functionally related gene sets, GSEA results were visualized through an enrichment network of the most significant pathways (FDR q-value < 0.05) with the Enrichment Map Software v.3.2.1 (427), implemented as a plug-in in the Cytoscape v.3.7.1 platform (428).

13. Flow cytometry - C-MSC

To confirm the mesenchymal lineage of C-MSC, cells cultured in the basal medium were detached with TrypLE™ Select Enzyme (ThermoFisher Scientific), incubated with FITC/APC/PE-conjugated antibodies in

100 µl PBS, and analyzed by flow cytometry (Gallios, Beckman Coulter). The antibodies used are the following: CD29, CD44, CD105, CD90, (mesenchymal markers), CD14, CD31, CD34, CD45 (endothelial and hematopoietic markers), and HLA-DR (immunogenicity marker).

To evaluate C-MSC oxidative status, cells cultured in basal medium were incubated 30 minutes with 10 µM 2′,7′-Dichlorofluorescein diacetate (DCF; Sigma-Aldrich), detached with TrypLE™ Select Enzyme (ThermoFisher Scientific) and analyzed by flow cytometry (Gallios, Beckman Coulter). The mean FITC fluorescence was measured.

To determine the correlation between CD36 expression and lipid accumulation, cells were stained using 12.5 ng/ml Nile Red (Invitrogen), to mark intracellular neutral lipids, and 2.5 µl of anti-CD36 antibody (Life Technologies; Table M1). The mean of the fluorescence was determined for Nile Red and CD36 for each sample.

To quantify the DiI oxLDL internalization, cells were treated with 10 µg/ml DiI oxLDL for 3 hours, detached with TrypLE™ Select Enzyme (ThermoFisher Scientific) and acquired with FACS Gallios (Beckman Coulter). The mean APC fluorescence was determined for each sample.

14. Western blot - C-MSC

Total proteins from C-MSC were obtained by Laemmli lysis buffer. After quantification with DC protein assay (Biorad), proteins were run on SDS-PAGE gel (NUpage precast 4-12%; Invitrogen) and transferred to nitrocellulose membrane (Biorad). The membrane was blocked in 5% skimmed milk-TBS for 1 hour at RT and incubated overnight at 4 °C with primary antibodies against GAPDH, PPARγ, CD36, TLR4, SR-A, LOX-1 (see Table M1). After washes, the membrane was incubated 1h at RT with the appropriate HRP-conjugated secondary antibody goat anti-rabbit or goat anti-mouse (GE healthcare). Blots were washed and developed with the ECL system (BioRad). Images were acquired with the Alliance Mini 2M System (UVITEC Cambridge) and densitometric analysis was performed using Alliance Mini4 16.07 software (UVITEC Cambridge). Data are normalized reporting to 1 the comparison group to highlight the differences between different groups or treatment.

15. OxLDL internalization assay - C-MSC

C-MSC were plated on 1.8 cm^2 chamber slides (ThermoFisher Scientific) at a density of 20000 cells/cm^2 either in growth (GM) or adipogenic medium (AM) for 3 days. 10 µg/ml DiI oxLDL (ThermoFisher Scientific) were added. After 3 hours, the cells were fixed for 5 minutes in 4% paraformaldehyde in PBS, stained with Hoechst 33342 (1:1000; Life Technologies) and the slides mounted. Pictures were acquired with Zeiss Axio Observer.Z1, with Apotome technology. For the quantification of intracellular DiI, other cells from the same cultures were treated as described above and acquired with FACS Gallios (Beckman Coulter).

16. Analysis of C-MSC lipids

Cell lipids were extracted by hexane/isopropanol 3:2, plus butylated hydroxytoluene 0.005% as antioxidant. Known amounts of proper internal standards (stigmasterol, cholesteryl heptadecanoate, tryheptadecanoin, nonadecanoic acid; Sigma Aldrich) were added for the analysis of free (FC) and esterified cholesterol (CE), triglycerides (TG) and free fatty acids (FFA), respectively. Lipid extracts were dried in a steam of nitrogen, aliquoted and conserved at -80 °C in the dark, until use.

An aliquot was loaded onto pre-run and activated channeled Silica TLC plates (BioMap) and run in hexane-diethyl ether-acetic acid (80:20:1 vol/vol/vol). The plates were then sprayed with dichlorofluorescein (0.15% in ethanol) and the spots corresponding to those of FC, FFA, TG and CE standards were identified by UV light and scraped out of the TLC.

Samples were analyzed by a gas-liquid chromatographer (GLC 1000; DANI Instruments) equipped with an autosampler HT300A (HTA), a fused silica column (MEGA-5 30 m length, 0.3 mm diameter, 0.15 µm film thickness; Mega Columns) and a flame ionization detector. Hydrogen flow was at a constant pressure of 1.2 bar. The oven temperature was constant (260 °C, 8 minutes run) for FC, while ranged from 120 °C to 300 °C for FFA, TG, CE (total run 45 minutes).

FC were resuspended in hexane/isopropanol and analyzed without derivatization. The other lipid classes were processed with methanolic acid 3 N at 30-80 °C for 30-120 minutes and analyzed for their fatty acid

content. Peaks were identified by comparing their retention times with those of standard and their area determined by a dedicated software (Clarity). To calculate the total mass of each lipid class, the areas of all the peaks corresponding to the fatty acids were summed and the real mass determined by comparison with the area of the internal standards. Results were normalized by the number of cells in each dish (µg lipid/10^6 cells).

17. oxLDL preparation

Fresh plasma purchased from healthy donors (Niguarda Ca' Granda Hospital, Milano) was brought to a density of 1.019 g/ml with KBr and subsequently centrifuged at 40,000 rpm for 16 hours to remove VLDL particles. After this operation, the gradient was adjusted to a density of 1.063 g/ml and samples centrifuged for further 24 hours at the same speed. LDL were then isolated, dialyzed for 48 hours at 4 °C, sterilized by filtration (0.22 µm; Millipore) and then characterized for their protein and cholesterol content. Aliquots of 2-3 ml were oxidized by addition of an equal volume of $CuSO_4$ (final concentration 2.7 mM) for 18 hours, under stirring. Oxidation was documented by agarose gel electrophoresis and by gas-liquid chromatography analysis, by which we monitored the specific disappearance of polyunsaturated fatty acids, namely linoleic-, arachidonic and eicosapentaenoic ones. OxLDL were then utilized for cell culture experiments, under sterile conditions.

18. C-MSC treatments

The medium used to prompt the adipogenic differentiation of C-MSC consists of IMDM supplemented with 10% FBS (Euroclone), 0.5 mmol/L 3-isobutyl-1-methylxanthine (Sigma-Aldrich), 1 µmol/L hydrocortisone (Sigma-Aldrich), 0.1 mmol/L indomethacin (Sigma-Aldrich), 10000 U/ml Penicillin (Invitrogen), 10000 µg/ml Streptomycin (Invitrogen) and 20 mmol/L L-Glutamine (Sigma-Aldrich). For the preparation of adipogenic medium (AM), refer to (185).

C-MSC were plated in AM at a concentration of 20000 cells/cm^2 and treated with 150 µg/ml oxLDL (see the paragraph "oxLDL preparation"), 20 µg/ml 13HODE (Cayman) or 5 mmol/L N-acetylcysteine (NAC; Sigma-

Aldrich), a known thiolic antioxidant (429). After 72 hours, treatment effects were evaluated by Oil Red O (ORO; Sigma-Aldrich) staining and western blot analysis.

19. C-MSC lipid staining

C-MSC were plated at a concentration of 20000 cells/cm^2 and cultured in AM. Fat accumulation was tested by ORO (Sigma-Aldrich) intracellular lipid staining. In detail, C-MSC were stained with 1% ORO (Sigma-Aldrich) solution in 60% isopropanol for 1 hour after 5-minute fixation with 4% paraformaldehyde in PBS. After 5 washes in PBS to ensure the removal of unbound dye, quantitative results were obtained by evaluating luminance in the 255 red channel with the ImageJ program (at least 10 fields were evaluated per condition per patient).

20. *PKP2* silencing

HC C-MSC were plated at a density of 12500 cell/cm^2 in growth medium and transduced with pooled lentiviral particles containing shRNAs targeting both variants of human *PKP2* (Gene ID 5381) in psi-LVRU6GP (with U6 promoter, eGFP reporter, puromycin resistance; Genecopeia) or with the correspondent scrambled control lentiviral particles (Genecopeia) for 24 hours. After checking the transduction efficiency by detection of the GFP signal, 2 µg/ml puromycin was added to select transduced cells.
After cell amplification, PKP2 reduction was assayed by Western Blot. Scrambled control and PKP2 shRNA C-MSC were plated in AM at a concentration of 20000 cells/cm^2 and treated with 150 µg/ml oxLDL. After 72 hours, treatment effects were evaluated by Oil Red O (ORO; Sigma-Aldrich) staining.

21. CD36 knockdown in C-MSC

C-MSC were cultured for 24 hours in low serum medium without antibiotics (IMDM, 2% FBS (Euroclone) and 20 mmol/L L-Glutamine (Sigma-Aldrich). 0.05 µM of Human Silencer Select Pre-designed CD36 siRNA (4392422-S2646 siRNA; Life Technologies) or 0.05 µM Silencer Select Negative Control (4390844 scramble; Life Technologies) and 4 µl lipofectamine RNAiMAX (Life Technologies) were added to 300 µl of Optimem

medium (Life Technologies). After 15 minutes at RT, the transfection reactions were added to the cells in 1.5 ml low-serum/no antibiotics medium. After 24 hours the medium was changed to AM supplemented with 150 µg/ml oxLDL for the following 72 hours. CD36 reduction was confirmed by Western blot at the end of the experiment. The effects of CD36 silencing were evaluated by ORO (Sigma-Aldrich) staining, western blot analysis and oxLDL internalization assay.

22. PPARγ antagonism in C-MSC

C-MSC were cultured for 72 hours in AM with 5 µM GW9662 (Sigma Aldrich). The treatment was added to the medium every 8 hours. To check oxLDL internalization, 10 µg/ml DiI oxLDL (ThermoFisher Scientific) were added 3 hours before the end of the experiment, following the protocol described above (see "OxLDL internalization assay"). Pictures were acquired with Zeiss Axio Observer.Z1, with Apotome technology and images acquired with the software AxioVision Rel. 4.8. For each biological sample, 10 fields were examined. The effects of PPARγ antagonism on CD36 expression were evaluated by western blot.

23. Generation of ACM and HC hiPSC

Two clones of hiPSC from one ACM patient, carrying the deletion of the whole *PKP2* exon 4 leading to a predicted truncated protein (p.N346Lfs*12), and one HC of the same family were obtained as previously described (430). Peripheral blood mononuclear cells (PBMCs) were isolated from human buffy coats after whole blood centrifugation. Every hiPSC line has been generated using episomal vectors carrying OCT3/4, SOX2, KLF4, and L-MYC. The obtained hiPSC were characterized for the expression of the pluripotency markers SSEA-4, OCT3/4, TRA-1-80, SOX-2, TRA-1-60 and alkaline phosphatase, and the karyotype analysis was performed.

24. Cardiomyogenic differentiation of hiPSC

hiPSCs were propagated on Matrigel® (Corning) coated plates and the cardiomyogenic differentiation was performed using PSC Cardiomyocyte Differentiation Kit (Thermo Fisher Scientific). After 30 days,

cardiomyocytes were dissociated at single cells using Multi Tissue Dissociation Kit 3 (Miltenyi Biotec) and enriched by magnetic separation with the QuadroMACS™ Separator and PSC-Derived Cardiomyocyte Isolation Kit (Miltenyi Biotec). Cells were then maintained in culture for additional 25 days in the following different conditions: growth medium (composed by High Glucose DMEM (Gibco), 2% of Hyclone Fetal Bovine Defined (GE Healthcare Life Sciences), 1% of Non-Essential Amino Acids, Penicillin/Streptomycin and 0,09% of β-mercaptoethanol), and Adipogenic Medium (growth medium supplemented with 50 µg/ml Insulin (Sigma-Aldrich), 0.5 µM Dexamethasone (Sigma-Aldrich), 0.25 mM 3-isobutyl-1 methylxanthine (IBMX) (Sigma-Aldrich), 200 µM Indomethacin (Sigma Aldrich) with 5 µM Rosiglitazone (Vinci-Biochem)). The culture medium was changed every other day. Cells were analyzed through immunofluorescence and FACS analysis.

25. hiPSC-CM immunofluorescence analysis

Cells were fixed with 4% paraformaldehyde for 15 minutes and then permeabilized (PBS with 0,1% Triton X100) for 10 minutes at RT. Cells were then blocked in PBS with 5% Goat serum for 1 hour at RT and incubated with anti-αSARC overnight at 4 °C (see Table M1). After washing, cells were incubated with the proper secondary antibody for 1 hour at 37 °C. Intracellular lipid droplet accumulation was evaluated using BODIPY 493/503 assay (D3922 Thermo Fisher Scientific; dilution 0.1 µg/ml in PBS) incubated for 20 minutes at RT and nuclei were stained with DAPI (Invitrogen R37606). The images were acquired using confocal microscopy (Leica Microsystem CMs GmBH Type: TCSSP8X) and analyzed with ImageJ software. Intensity fluorescence was normalized on nuclei number.

26. hiPSC-CM flow cytometry analysis

Cells were dissociated at single cell using Multi Tissue Dissociation Kit 3 (Miltenyi Biotec), following manufacturer's instructions and blocked in FACS buffer (PBS containing 0.5% FBS and 2 mM EDTA). Cells were incubated with anti-CD36 (see Table M1) for 15 minutes at 4 °C avoiding direct light and then washed and resuspended with FACS buffer. Cardiomyocytes were identified and gated based on their forward and

side scatter using the S3 Cell Sorter (Biorad); median fluorescence intensity (MFI) of PE was calculated on the gated cells. Data were analyzed using FlowJo software. Median intensity fluorescence is presented as MFI(PE) sample – MFI(PE) isotype.

27. hiPSC-CM transcriptome sequencing

The transcriptome sequencing of hiPSC-CM cultured in GM and AM+rosiglitazone was performed. RNA was extracted using TRIzol reagent (ThermoFisher Scientific). The concentrations and the quality of the samples were assessed. 500 ng of RNA for each sample were used for the preparations of the libraries, using the QuantSeq 3' mRNA-Seq Library Prep FWD (Lexogen). Samples were sequenced using the platform HiSeq2500, following the protocol SR1000. Raw reads were aligned against the genome (Homo Sapiens assembly GRCh38) using STAR. Gene quantification was carried out using HTSeq-count reporting all reads falling within exon boundaries of a gene. Subsequent statistical analysis was performed in R using the DESeq2 package employing a model adjusting for potential sex biases. Raw p-values for significance of differential expression were adjusted for multiple hypothesis testing using the method from Benjamini and Hochberg for a strong control of the false discovery rate (FDR).

28. ACM murine model: *Pkp2*+/- mice

C57Bl/6 *Pkp2* heterozygous knock-out mice (*Pkp2*+/-) were produced by Prof. Birchmeier, as described (257). The homozygous mice were embryonic-lethal, while heterozygous mice were healthy and fertile. For our experiments, we used 20 C57Bl/6 *Pkp2*+/- mice and 20 siblings C57Bl/6 wild type (WT), as controls. Experiments were authorized on 27/07/2015 by the Italian Ministry of Health, protocol n. 779/2015-PR.

29. Murine C-MSC isolation and culture

Explanted hearts from 5 WT and 5 *Pkp2*+/- mice (age: 10 weeks) were washed with PBS, cut into 2-3 mm pieces and incubated at 37 °C for 1 hour under continuous agitation in IMDM containing 3 mg/mL collagenase NB4. After a PBS wash, the pellet was re-suspended in GM and seeded. Non-adherent cells

were removed after 24 hours. AM medium was used to prompt the adipogenic differentiation of murine C-MSC for 6 days.

30. High fat diet

10 WT and 10 *Pkp2*+/- mice (age: 10 weeks) were fed for 3 months with a high-cholesterol (279.6 mg/kg) and high-fat (60% kcal) diet (HFD; OpenSource DIETS) (431).

5 WT and 5 *Pkp2*+/- mice were fed with chow diet (CD; OpenSource DIETS) and euthanized at 14.30 ± 1.46 months of age, when disease manifestation, if any, should have happened.

Heart volumes and functionality were assessed before the beginning of the diet and every month by echocardiography. Bodyweight was monitored every month. Blood samples were taken before and after the diet. At sacrifice, hearts were explanted after perfusion with saline solution. Sections of heart specimens were used for lipid accumulation analysis, PPARγ, MDA and CD36 immunofluorescence staining.

31. High fat diet plus atorvastatin

9 WT and 9 *Pkp2*+/- mice (age: 10 weeks) were fed for 3 months with a HFD (Open Source D12492) to which 20 mg/kg atorvastatin were added. Heart volumes and functionality were assessed before the beginning of the diet and every month by echocardiography. Bodyweight was monitored every month. Blood samples were taken before and after the diet. At sacrifice, hearts were explanted after perfusion with saline solution. Sections of heart specimens were used for lipid accumulation analysis, PPARγ, MDA and CD36 immunofluorescence staining.

32. Echocardiographic analysis

Transthoracic echocardiography was performed using the Vevo2100 high-resolution imaging system (VisualSonics) and a 40-MHz linear transducer with simultaneous electrocardiographic recording, as previously reported (432). Analyses were performed on mice lightly anesthetized with 0.5% to 1% isoflurane (heart rate: 480–550 beats/min) at the following time points: 1 day before starting the diet (pre-

diet) and on 1, 2 and 3 months of HFD or HFD+atorva, or at 14.30 ± 1.46 months of age for mice fed with CD.

RV parameters in systole and diastole were acquired from a parasternal long-axis view and measured from images acquired in M mode, using the depth interval (in millimeters) generic measurements tool (433) (434) (435).

Two-dimensional short-axis M-mode echocardiography was performed at the level of the midpapillary muscle to measure left ventricular (LV) parameters, in systole and diastole.

All measurements were averaged from a minimum of three cycles during diastole and systole corresponding to the electrocardiogram. Data and imaging were analyzed using the VisualSonics Cardiac Measurements Package by a blinded investigator. Parameters were normalized on mice heart weight.

33. Murine blood sampling

Mice were anesthetized with 4% isoflurane and maintained asleep with 1% isoflurane. The blood sampling was performed through tail vein using 25G needle, after tail pre-heating and local application of anesthetic. Whole blood was collected into EDTA–coated tubes (Fisher Scientific). Separated plasma was obtained after centrifugation for 15 minutes at 2000 x g at 4 °C and stored at -80 °C until the analysis.

34. Total cholesterol distribution in lipoproteins from mouse plasma

50 µl of mouse plasma have been injected twice in an HPLC system (Jasco 920; Jasco), with a pre-column (6mm ID x 4cm; Tosoh), two consecutive inverse phase, size-exclusion, anionic-exchange TSK-GEL LIPOPROPAK XL (7.8mm ID X 30cm) columns (Tosoh) and with a UV-VIS detector (Jasco). Readings were performed at a 280 nm. The mobile phase consisted of 6.9 g of sodium monobasic phosphate, 50 mg BRIJ and 30 ml isopropanol per liter (pH 8).

We divided each sample in 50 fractions (one every minute) and we collected those from #22 to #45, corresponding to VLDL, IDL, LDL, HDL. Each obtained fraction (1 ml) was frozen at -80 °C, lyophilized and

then reconstituted with 200 µl of water. On portions of these samples, total cholesterol was measured by commercial colorimetric kits (ABX Pentra) at 490 nm by a spectrophotometer (BioRad).

35. oxLDL in murine plasma samples

For the quantitative determination of oxLDL in murine plasma samples before and after the HFD or HFD+atorva, Mouse Oxidized Low Density Lipoproteins ELISA kit was used (CUSABIO), following manufacturer instruction. Absorbance was determined with a spectrophotometer (Berthold Technologies) at 450 nm. Results were inferred according to a calibration curve constructed using the standards provided in the kit.

36. Histological characterization of *Pkp2* +/- hearts.

Explanted hearts from WT and *Pkp2*+/- mice, both in CD, HFD and HFD+atorva conditions, were fixed in 4% paraformaldehyde (Santa-Cruz) overnight at 4 °C. The following day, after 3 washes in PBS, the hearts were transferred in 15% sucrose in distilled water overday at RT, and then in 30% sucrose in distilled water overnight at 4 °C. The explanted hearts were embedded in OCT (ThermoFisher Scientific) and stored at -80 °C until use. After sectioning with a cryostat (ThermoFisher Scientific), OCT embedded sections (6 µm thick) were de-frosted and washed twice in PBS. The immunofluorescence analysis was performed following blocking in 2% goat serum (Sigma-Aldrich) for 30 minutes. Sections were incubated with primary antibodies anti-PPARγ, anti-MDA, anti-CD36, anti-CD105, anti-troponin T and anti-perilipin1 at 4 °C overnight. After washing, sections were incubated with the fluorochrome-conjugated antibodies goat anti-rabbit IgG Alexa488 (1:200; AlexaFluor), Streptavidin-Alexa Fluor 594 (1:200; AlexaFluor), goat anti-rabbit 546 (1:200; AlexaFluor), goat anti-guinea pig 488 (1:200; AlexaFluor) for 1 hour at RT in the dark. Nuclear staining was performed by incubating sections with Hoechst 33342 (1:1000; Life Technologies). Sections were observed with Zeiss Axio Observer.Z1, with Apotome technology, and images acquired with the software AxioVision Rel. 4.8. For each explanted heart, at least 10 fields for 5 consecutive transversal slices were quantified. See **Table M1** for antibody list.

For the lipid accumulation analysis, the sections were stained with ORO (Sigma-Aldrich) for 1 hour at RT and then washed 5 times in PBS to ensure the removal of the aspecific dye. Quantitative results were obtained by evaluating red area vs. total tissue area (all the section surface of 5 consecutive slices for each sample were quantified).

37. Fat infiltration analysis at CMR

Intramyocardial fat mass was evaluated as previously described (436) (437) (438). Briefly, steady state free precession (SSFP) were used and the following acquisition parameters were applied: 30 phases, 10-25 views per segment, NEX 1, FOV 40 cm, a matrix of 224 x 224, a 60° flip angle, TR 3.6-4.2 and TE = TR/2. Images were acquired using a 1.5-T unit (Discovery MR450, GE-Healthcare, Milwaukee, MN). Fat in the ventricular myocardium appears as a hyperintense area surrounded by a hypointense band, the so called ‘‘Indian Ink’’ artifact (436). Manual contouring of the Indian Ink artifact (including the black contour) was drawn and its extent was measured.

38. Statistical analysis

Discrete variables are analyzed with Fisher’s exact test. Continuous variables are reported as mean ± standard error. Comparisons between normally distributed groups were performed using either paired or unpaired two-tailed Student's t-tests, whereas populations without a Gaussian distribution were compared using Mann-Whitney tests. Multiple regression analysis was performed to exclude the influence of confounding variables. Comparisons between three or more groups were performed with two way-ANOVA test, in association with Bonferroni multiple comparison post-tests. When both intragroup and intergroup values are tested, red lines and asterisks identify test differences within the same group, while intergroup differences are in black. X-Y correlation analyses have been determined. Comparison of slopes of linear regressions was performed with the following method: t= (b1-b2) / sb1, b2 where b1 and b2 are the two slope coefficients and sb1, b2 the pooled standard error of the slope. Receiver Operating Characteristic (ROC) plots was used to determine the oxLDL level cut-off value with optimal sensitivity and specificity in

discriminating ACM patients vs. HC individuals. Kaplan-Meier curves were performed to determine the actual risk of MAE, and analyzed through Log-rank (Mantel-Cox) test. Statistics were performed using GraphPad Prism software. Results were considered statistically significant for p values < 0.05.

Table M1. Antibody list.

	Protein	Antibody	Host	Company	Dilution
Anti-human	MDA	ab6463	Rabbit	Abcam	IF 1:2500
	CD36	610882	Mouse	BD	IF 1:200- WB 1:1000
	CD36	A15724 (clone CB38 – NL07)	Mouse	Life Technologies	FACS on C-MSC 1:50
	CD36	A15777 (clone TR9)	Mouse	Life Technologies	FACS on hiPSC-CM 1:100
	GAPDH	sc-25778	Rabbit	Santa Cruz	WB 1:1000
	PPARγ	sc-7273 (clone E-8)	Mouse	Santa Cruz	WB 1:60
	αSARC	A7732	Mouse	Sigma-Aldrich	IF 1:250
Anti-mouse	MDA	ab6463	Rabbit	Abcam	IF 1:2500
	CD36	RA25035	Rabbit	Neuromics	IF 1:200
	PPARγ	PA3-821A	Rabbit	Life Technologies	IF 1:200
	PLIN1	BP5015	Guinea Pig	OriGene	IF 1:100
	CD105	BAF1320	Goat	R&D System	IF 1:40
	Troponin T	ab92546	Rabbit	Abcam	IF 1:100
Secondary antibodies	Anti-rabbit IgG 488	A11034	Goat	Life Technologies	IF 1:200
	Anti-mouse IgG 488	A11001	Goat	Life Technologies	IF 1:200
	Anti-mouse IgG HRP	GENA9310	Sheep	GE Healthcare	WB 1:1000
	Anti-rabbit IgG HRP	GENA9340	Donkey	GE Healthcare	WB 1:1000
	Anti-mouse IgG 555	A28180	Goat	Life Technologies	IF 1:1000
	Anti-guinea pig 488	sc-2441	Goat	Santa Cruz	IF 1:200
	Anti-streptavidin 594	S32356	-	Life Technologies	IF 1:200
	Anti-rabbit 546	A11010	Goat	Life Technologies	IF 1:200

Table M2. List of the cardiac mesenchymal stromal cells obtained from ACM and Healthy Control (HC) individuals used for the *in vitro* experiments (dependent on availability and culture passage number).

13H: 13-hydroxy-octadecadienoic acid; ACM: Arrhythmogenic Cardiomyopathy; DCF analysis: 2′,7′-Dichlorofluorescein diacetate analysis; GSH/GSSG ratio: reduced glutathione/oxidized glutathione ratio; MDA IF: Malondialdehyde immunofluorescence; NAC: N-acetylcysteine; NR: Nile Red; oxLDL intern.: oxLDL internalization; WB: western blot.

Sample name	Sex	Age	DCF analysis	MDA IF	GSH/ GSSG ratio	WB in basal conditions	CD36/ NR FACS analysis	OxLDL intern.	OxLDL treatm.	13H/ NAC treatm.	CD36 siRNA	PPARγ inhib.	Lipid analysis
ACM1	M	52	X			X	X						X
ACM2	M	42	X			X	X						X
ACM3	M	40	X		X	X	X			X			X
ACM4	M	51	X		X	X	X			X			X
ACM5	M	57	X		X	X					X		X
ACM6	M	43				X				X		X	
ACM7	F	39				X				X			
ACM8	M	64				X				X		X	
ACM9	M	45				X			X			X	
ACM10	M	46			X	X			X	X	X		
ACM11	M	47			X	X			X	X	X		
ACM12	M	30			X	X			X	X	X		
ACM13	F	42		X	X	X				X			
ACM14	M	41		X		X			X	X	X		
ACM15	F	24		X		X			X	X			
ACM16	F	52		X		X			X	X			
ACM17	M	49			X	X		X	X				
ACM18	M	52				X		X	X	X	X		
ACM19	M	28				X		X	X		X		

Sample name	Sex	Age	DCF analysis	MDA IF	GSH/ GSSG analysis	WB in basal conditions	CD36/ NR FACS analysis	OxLDL intern.	OxLDL treatment	13H/ NAC treatment	Lipid analysis
HC1	M	51	X			X	X			X	X
HC2	M	48	X		X	X	X			X	X
HC3	M	44	X			X	X			X	X
HC4	M	56	X			X	X		X	X	X
HC5	M	40	X	X	X	X	X				X
HC6	F	25		X		X				X	
HC7	M	57		X	X	X					
HC8	F	50		X		X			X		
HC9	F	35		X	X	X			X	X	
HC10	M	41				X			X	X	
HC11	M	55			X	X			X	X	
HC12	M	17				X			X	X	
HC13	M	57			X	X					
HC14	F	58				X					
HC15	M	21			X	X		X			
HC16	M	49			X	X		X	X		
HC17	M	64				X			X	X	
HC18	F	48				X			X	X	
HC19	M	44				X		X	X	X	
HC20	M	28				X			X	X	

Results

1. Patients' studies

1.1 Patients' population characteristics

Table R1 summarizes baseline characteristics of 36 ACM patients and 36 HC enrolled in this study for plasma analysis. ACM diagnosis was reached according to the 2010 International Task Force criteria (163). HC without a previous history of heart disease, age-, sex- and risk factors-matched with ACM patients have been selected. The considered cardiovascular risk factors are physical exercise, smoking, familiarity for cardiovascular events, hypertension, obesity and diabetes. ACM patients and HC taking statins or other lipid-lowering drugs were not included in the cohort.

The male to female ratio in our population was 5:1 (n = 30 males; n = 6 females), 12 (33.3%) patients were athletes or very active people. A genetic analysis was performed in 19 patients (52.8%), of which 12 (63.1%) tested positive for an ACM-likely pathogenic variant; among those, *PKP2* was the most commonly mutated gene (n=7 (58.3%)).

Table R1. Clinical parameters of the individuals enrolled for plasma analysis.

Continuous variables are expressed as mean ± standard error. The indicated p value is the result of Fisher's exact test for discrete variables and Mann-Whitney test for continuous variables.

ACM: Arrhythmogenic Cardiomyopathy; HC: healthy controls; n: number of subjects; na: not available.

	HC	ACM	p value
n	36	36	-
Age (years)	44±2	46±2	p=0.55
Male gender (n)	30	30	p=1.00
Sport (>3 times/week) (n)	13	12	p>0.99
Smoking (n)	8	9	p>0.99
Familiarity for cardiovascular events (n)	5	7	p=0.75
Hypertension (n)	7	12	p=0.28
Obesity (n)	0	1	p>0.99
Diabetes (n)	0	1	p>0.99
Mutation in known ACM genes (n; %)	na	12 on 19 analyzed; 63.1%	-

We have further enrolled 9 ACM patients' relatives with *PKP2* mutations but no clinical signs of the disease. Since the group of relatives was not perfectly matched for sex and age (Table R2) with the ACM patients used for the comparison, the influence of these variables on the relationship of oxLDL and ACM has been excluded by multiple regression analysis (p=0.02).

Table R2. Characteristics of ACM patients with a known ACM associated mutations and their family members, carriers of the same mutation but clinically not affected by ACM.

Continuous variables are expressed as mean ± standard error. The indicated p value is the result of Fisher's exact test for discrete variables and Mann-Whitney test for continuous variables. * $p < 0.05$.

ACM: Arrhythmogenic Cardiomyopathy; n: number of subjects.

	Mutation carrier NON ACM	Mutation carrier ACM	p value
n	9	7	-
Age (years)	49±6	45±6	p=0.67
Male gender (n; %)	4; 44.4%	5; 71.4%	p=0.36
Obesity (n)	0	0	p=1.00
Mutation in known ACM genes (n; %)	9; 100%	7; 100%	-

1.2 Plasma lipid profile

To test the hypothesis of altered lipid metabolism in ACM, we obtained blood samples from 36 ACM patients and HC to characterize their lipid profile, focusing on total cholesterol, LDL cholesterol, oxLDL, and 13HODE plasma concentrations. As reported in **Table R3**, no differences in total cholesterol (n = 36 each; HC 191.50 ± 6.05 mg/dl vs. ACM 197.5 ± 6.51 mg/dl) and LDL cholesterol (n = 36 each; HC 118.50 ± 4.91 mg/dl vs. ACM 122.90 ± 5.93 mg/dl) have been identified between ACM patients versus HC. Conversely, the increased oxidation of LDL leads to the detection of a higher amount of oxLDL in ACM plasma samples, if compared to HC (n = 36 each; ACM 137.90 ± 20.85 vs. HC 66.74 ± 5.79 ng/ml; p = 0.015; **Figure R1A**). Accordingly, plasma 13HODE was found significantly higher in patients than controls (n = 27 each; ACM 44.42 ± 5.32 vs. HC 27.22 ± 2.44 ng/ml; p = 0.03; **Figure R1B**).

To test the potential association between ACM causative mutations and altered patients' plasma lipid profile, we compared ACM patients with and without mutations in known ACM genes, finding no different predisposition to higher oxLDL levels in the two cohorts (n = 12 vs. n = 7; mutated ACM patients 139.60 ± 42.75 vs. non-mutated ACM patients 122.60 ± 36.68; p = 0.75; **Figure R1C**).

However, a difference in oxLDL mean levels was observed between patients with overt ACM phenotype carrying ACM-related causative mutations and their relatives, carriers of the same mutations but not clinically affected by the pathology (n = 7 vs. n = 9; ACM 384.50 ± 139.1 vs. unaffected relatives 66.99 ± 17.09 ng/ml; p = 0.03; **Figure R1D**). Overall, this evidence points to an association between a fully penetrant disease and high oxLDL plasma concentration.

Table R3. Plasma lipid profile of the individuals enrolled for the study.

Continuous variables are expressed as mean ± standard error. The indicated p value is the result of Mann-Whitney test for continuous variables. * $p < 0.05$.

13HODE: 13-hydroxy-octadecadienoic acid; ACM: Arrhythmogenic Cardiomyopathy; HC: healthy controls; LDL: low density lipoproteins; n: number of subjects; na: not available; oxLDL: oxidized low density lipoproteins.

	HC	ACM	p value
n	36	36	-
Total cholesterol (mg/dl)	191.50±6.05	197.5±6.51	p=0.52
LDL cholesterol (mg/dl)	118.50±4.91	122.90±5.93	p=0.74
OxLDL (ng/ml)	66.74±5.79	137.9±20.85	* p=0.015
13HODE (ng/ml)	27.22±2.44	44.42±5.32	* p=0.03

Figure R1. ACM patients show high plasma oxLDL and 13HODE.

A) Plasma concentration of oxLDL in arrhythmogenic cardiomyopathy (ACM) patients and healthy controls (HC; n = 36 each). * $p < 0.05$ (Mann-Whitney test).

B) Plasma concentration of 13HODE in ACM patients and HC (n = 27 each). * $p < 0.05$ (Mann-Whitney test).

C) Plasma concentration of oxLDL in ACM patients with or without mutations in known ACM genes (n = 12 vs. n = 7). * $p < 0.05$ (Mann-Whitney test).

D) oxLDL plasma concentration in mutated arrhythmogenic cardiomyopathy (ACM; n = 7) and NON ACM subjects (ACM patients' relatives, carriers of the same causative mutation, but not clinically affected; n = 9). * $p < 0.05$ (Mann-Whitney test).

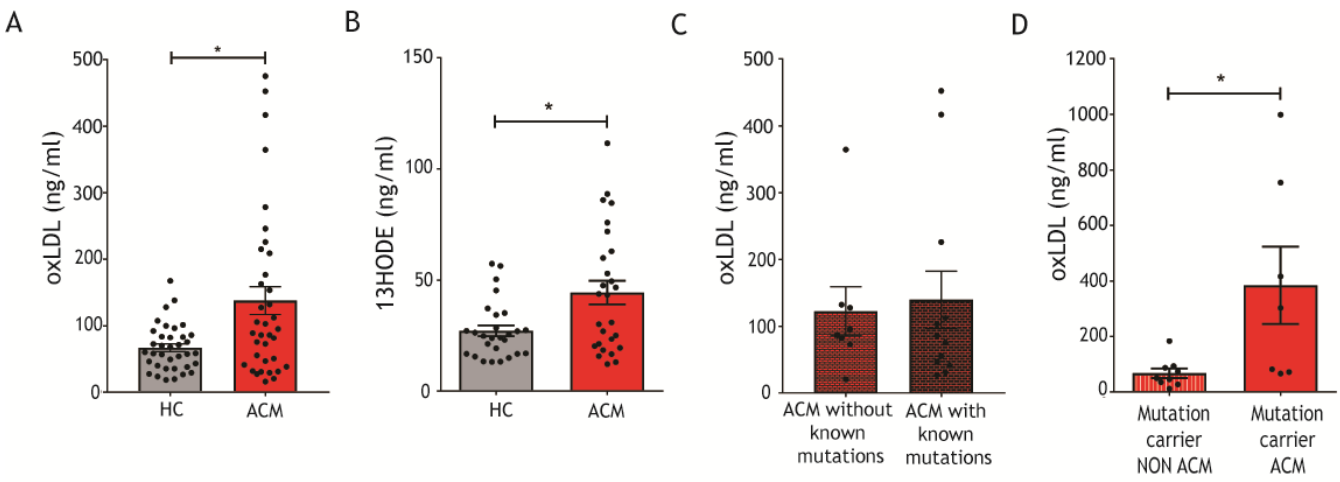

1.3 Genetic predisposition for oxLDL increase

Since the aforementioned results suggest that the main causative ACM mutation may not be responsible for augmented oxLDL (**Figure R1D**), we investigated a genetic predisposition, beyond the causative mutation, for oxidized lipid increase in ACM-affected patients. We, therefore, performed the exome sequencing on three families with low ACM penetrance, in which causative *PKP2* mutations were identified (**Figure R2**). We analyzed the presence and the co-segregation with the ACM phenotype of variants in a selected panel of genes associated with dyslipidemia and oxidative stress, with two different analysis criteria, either cumulative of the three families (**Tables R4A**), or separately in each family (**Tables R4B**). A variant in *MGST3* (Microsomal Glutathione S-Transferase 3) gene, which codifies for an enzyme with glutathione-dependent peroxidase activity towards lipid hydroperoxides, was segregating with disease phenotypes when the three families were analysed together (**Tables R4A**). By separately analysing each family (**Tables R4B**), two variants in genes associated with ROS detoxification and LDL internalization segregated with ACM phenotype in Family 1, ten variants in genes associated with ROS production, anti-oxidant defences, mitochondrial protection and contractility were obtained for Family 2, and one variant associated with oxidative stress and segregating with ACM phenotypes was found in Family 3. These results introduce the concept of a possible influence of the genetic background on the ACM phenotype.

Figure R2. Families in which investigation of oxidative stress and dyslipidemia as genetically determined secondary traits was conducted.

The pedigrees of three genotyped ACM families are represented. DNA of all numbered individuals underwent exome sequencing. Full red blocks represent subjects with ACM, black circles represent main causative mutations. ACM: arrhythmogenic cardiomyopathy.

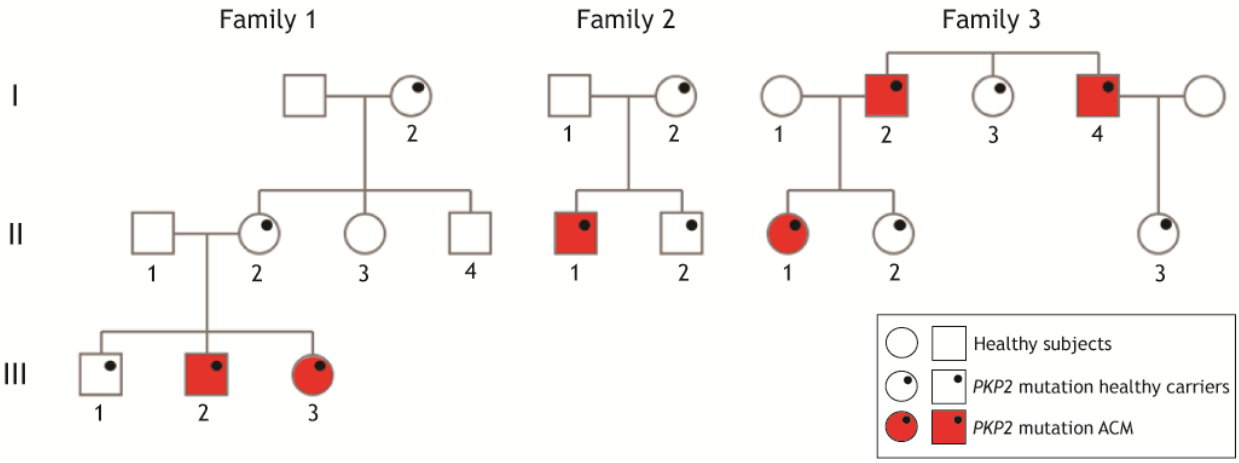

Table R4A. Variant in genes of the oxidative stress and dyslipidemia panel in all the three analyzed families.

Family	Variant	Allele frequency in the general population	Gene	Pathway	Classification	Allele frequency in healthy carriers	Allele frequency in affected carriers
ALL	rs77176546	0.22	*MGST3*	Glutathione-dependent peroxidase activity	Oxidative stress	0.3125	0.6667

Table R4B. Variant in genes of the oxidative stress and dyslipidemia panel found separately in each family.

LDL: low density lipoproteins; na: not available; redox: oxidation-reduction; ROS: reactive oxygen species.

Family	Variant	Allele frequency in the general population	Gene	Pathway	Classification
1	rs11087654	0.004691	*PRNP*	ROS detoxification	Oxidative stress
1	rs17248882	0.002529	*LDLR*	LDL internalization	Dyslipidemia
2	na	0.0008196	*VIMP*	Anti-oxidant function	Oxidative stress
2	rs199922141	na	*CYP2E1*	ROS generator	Oxidative stress
2	na	na	*TXNRD1*	Redox homeostasis	Oxidative stress
2	rs142623210	0.001156	*NFKB2*	Increase expression of antioxidant proteins	Oxidative stress
2	rs5742620	0.023	*IGF1*	Mitochondrial protection and antioxidant function	Oxidative stress
2	rs55676195	6.619e-05	*TTN*	Reduced cardiac contractility when oxidized	Oxidative stress
2	rs55886356	0.006771	*TTN*	Reduced cardiac contractility when oxidized	Oxidative stress
2	rs34070843	0.018	*TTN*	Reduced cardiac contractility when oxidized	Oxidative stress
2	rs115744476	0.005594	*TTN*	Reduced cardiac contractility when oxidized	Oxidative stress
2	rs185767460	na	*TTN*	Reduced cardiac contractility when oxidized	Oxidative stress
3	rs201428532	0.000313	*TRPM2*	Activated by oxidative stress	Oxidative stress

1.4 Total ventricular tissue analysis

To understand if high plasma oxLDL and 13HODE have a correspondence at cardiac tissue levels, we quantified the lipid peroxidation marker MDA on ACM and control RV sections, finding higher oxidative stress in ACM hearts (n = 4 each; MDA relative densitometric analysis/nuclei numbers ACM 36.25 ± 10.43 vs. HC 1.00 ± 0.72; p = 0.015; Figure R3A).

CD36 receptor has a central role in oxLDL uptake (439). CD36 immunostaining on RV tissue from ACM and HC donors revealed higher CD36 expression in ACM samples (n = 4 each; CD36 relative densitometric analysis/nuclei numbers ACM 14.72 ± 2.10 vs. HC 1.00 ± 0.40; p = 0.0007; Figure R3B), which was mainly distributed in adipose replacement tissue areas.

Figure R3. ACM patients show high cardiac lipid peroxidation and oxLDL receptor levels.

A) Representative images of malondialdehyde (MDA) immunostaining (green) on ventricular tissue sections of arrhythmogenic cardiomyopathy (ACM) patients and healthy controls (HC) and relative quantification (n = 4 each). Nuclei are counterstained with Hoechst 33342 (blue). * $p < 0.05$ (Two-tailed Student's t-test).

B) Representative images of CD36 immunostaining on ventricular tissue sections of ACM patients and HC and relative quantification (n = 4 each). Nuclei are counterstained with Hoechst 33342 (blue). *** $p < 0.001$ (Two-tailed Student's t-test).

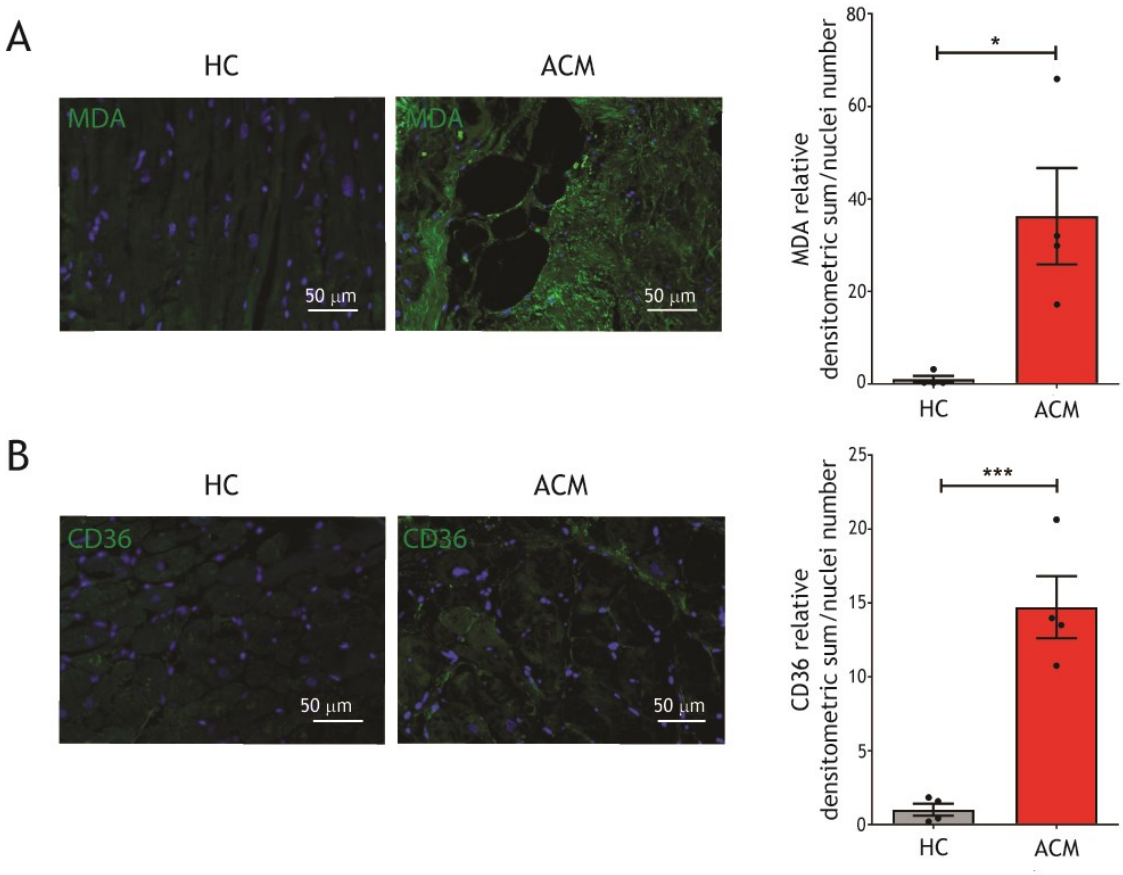

2. *In vitro* studies

2.1 C-MSC isolation

To test our hypothesis *in vitro*, we isolated ACM and HC C-MSC from human RV endomyocardial biopsies (n = 19 each; **Figure M1**), as previously described (185), since they represent a good primary cell model to study ACM adipogenesis.

To confirm their mesenchymal lineage, we characterized them (**Figure R4**), in line with the International Society for Cellular Therapy criteria (440). For both HC and ACM lines, we assessed the positive expression of the mesenchymal surface markers CD29, CD44, and CD105. The percentage of cells expressing the fibroblast marker CD90 resulted variable, as previously reported (185) (441). Almost no C-MSC expressed endothelial (CD31, CD34) and hematopoietic (CD14, CD45) markers, thus excluding the contamination of other cell types. Moreover, HLA-DR, a marker of alloreactivity, was not detected. For all the surface marker analysed, the cell populations obtained from ACM and HC cardiac biopsies have a comparable pattern of expression, indicating no differences in their mesenchymal identity.

Figure R4. Immuno-phenotyping of isolated C-MSC.

Representative images of FACS-based surface marker analysis of C-MSC. The histograms relative to the mesenchymal markers CD29, CD44, CD105, the fibroblast marker CD90, the endothelial markers CD31 and CD34, the hematopoietic markers CD14 and CD45, and the alloreactivity marker HLA-DR are shown.

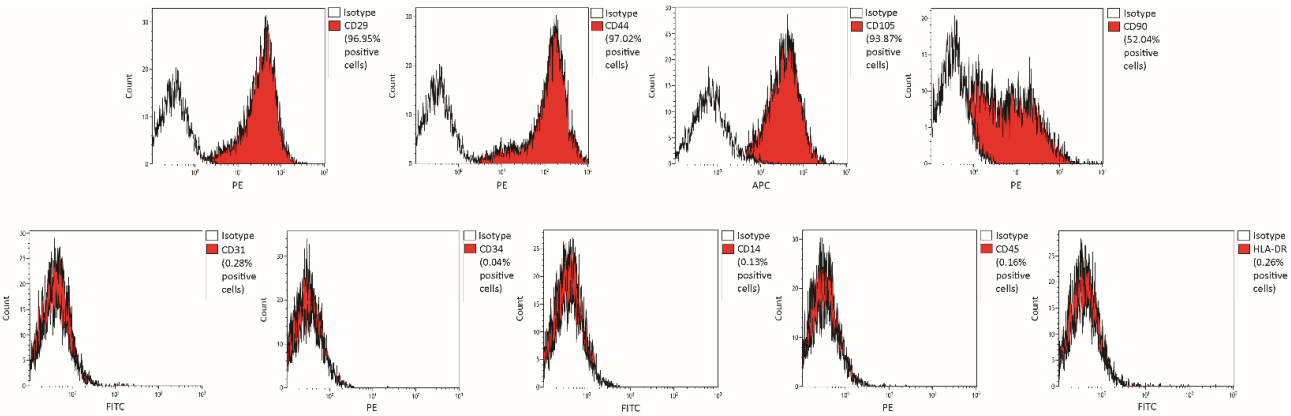

2.2 C-MSC characterization in growth conditions

To evaluate basal oxidative stress status of ACM cells, we cultured ACM and HC C-MSC in growth medium (GM) and treated with the Dichlorofluorescein probe. The conversion into the fluorescent dye 2′,7′-Dichlorofluorescein diacetate (DCF) by cell reactive oxygen species (ROS) was measured by FACS analysis. As shown in **Figure R5A**, we found that oxidative stress is significantly higher in ACM C-MSC compared to HC C-MSC (n = 5 each; relative mean DCF emission ACM 1.63 ± 0.26 vs. HC 1.00 ± 0.06; p = 0.049; **Figure R5A**). In particular, at least part of the ACM C-MSC oxidative stress is associated with lipid peroxidation, as shown by MDA cell immunofluorescence staining (n = 4 vs. n = 5; MDA relative densitometric analysis/nuclei number ACM 8.83 ± 2.78 vs. HC 1.00 ± 0.51; p = 0.017; **Figure R5B**). To understand if the elevated oxidative stress may be due to a defect in the cellular antioxidant capacity, we measured the ratio between reduced (GSH) and oxidized glutathione levels in HC and ACM C-MSC, obtaining no differences between the two groups (n = 8 each; **Figure R5C**).

Figure R5. ACM C-MSC show elevated oxidative stress.

A) Left panel: exemplificative FACS analysis of the FITC emission of unstained healthy control (HC) cardiac mesenchymal stromal cells (C-MSC; autofluorescence; white), HC C-MSC in growth medium (GM) treated with 2′,7′-Dichlorofluorescein diacetate (DCF; grey), arrhythmogenic cardiomyopathy (ACM) C-MSC in GM treated with DCF (red), and HC cells in GM treated with 2 mmol/l H_2O_2 as positive control (blue). Right panel: mean DCF emission of HC and ACM C-MSC in GM (n = 5 each). * $p < 0.05$ (Two-tailed Student's t-test).

B) Left panels: representative images of malondialdehyde (MDA) immunostaining (green) on ACM and HC C-MSC in GM. Nuclei are counterstained with Hoechst 33342 (blue). Right panel: image quantification (n = 4 ACM vs. n = 5 HC). * $p<0.05$ (Two-tailed Student's t-test).

C) Reduced and oxidized glutathione (GSH/GSSG) ratio quantification in HC and ACM C-MSC cultured in GM (n = 8 each).

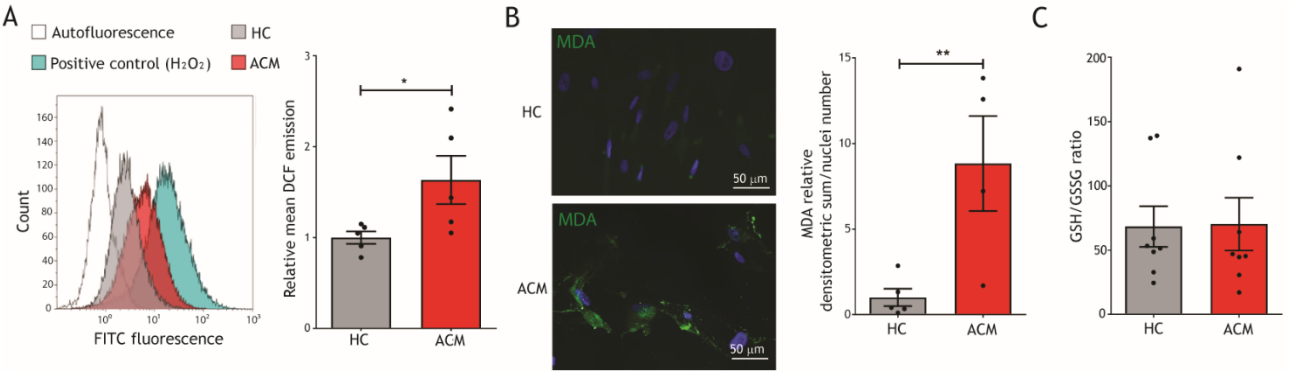

2.3 C-MSC transcriptome sequencing

To understand the reasons of excess oxidative stress in ACM C-MSC, as no differences in their antioxidant capacity were detected, we hypothesized the involvement of mitochondria, since they are the main cellular source of ROS (306). With this aim, we re-analysed an available transcriptome sequencing of total RNA extracted from ACM and HC C-MSC (n = 6 each) which identified differentially enriched pathways in ACM vs. controls. The transcriptome was analysed with a hypothesis-driven approach in order to evaluate the reasons of elevated oxidative stress in ACM cells and to confirm metabolic dysfunction. Most genes representing processes linked to mitochondria activity were more expressed in ACM than in control C-MSC. In particular, pathways associated with mitochondria respiratory chain complex assembly, respiratory electron transport chain and ATP synthesis and metabolic processes resulted significantly associated to ACM (**Figure R6**), indicating a potential mitochondria impairment in ACM.

Figure R6. Enrichment map for ACM C-MSC.

The enrichment network shows a selection of the pathway gene sets (nodes) that are significantly associated with ACM (false discovery rate < 0.05). Node size is proportional to the gene-set size. Edges connect related pathways. Edge thickness is proportional to the similarity between two pathways, for a cutoff = 0.25 of the combined Jaccard plus overlap coefficient.

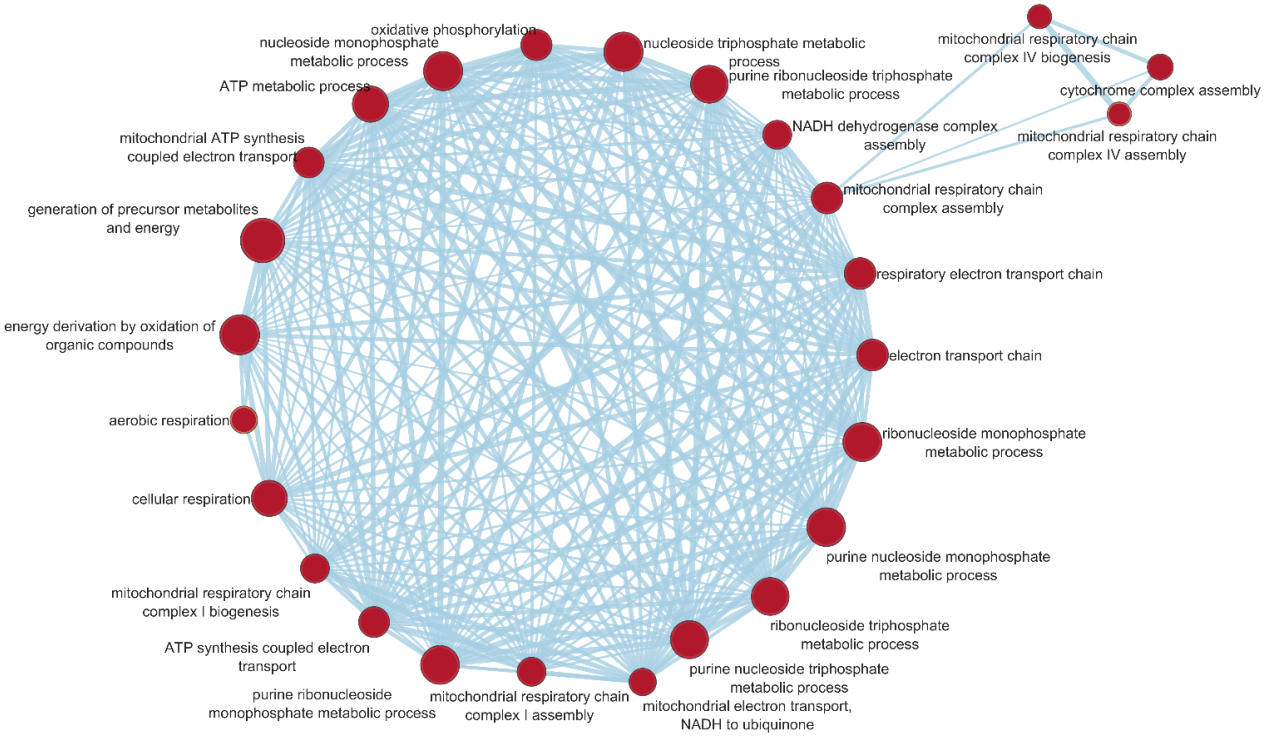

2.4 C-MSC protein expression analysis

In line with the hypothesis of oxLDL/PPARγ/CD36 involvement in ACM pathogenesis, we evaluated C-MSC PPARγ and CD36 protein expression in GM (**Figure R7A, B, C**). ACM C-MSC have higher PPARγ and CD36 levels compared to HC (n = 18 each; PPARγ/GAPDH densitometric analysis ACM 1.47 ± 0.12 vs. HC 1.00 ± 0.06; p = 0.002; **Figure R7B**; n = 17 vs. n = 16; CD36/GAPDH densitometric analysis ACM 1.52 ± 0.20 vs. HC 1.00 ± 0.16; p = 0.02; **Figure R7C**).

Conversely, ACM C-MSC did not show statistically significant differences in the expression of other oxLDL receptors, such as TLR4 (n = 4 vs. n = 3; TLR4/GAPDH densitometric analysis ACM 1.97 ± 0.48 vs. HC 1.00 ± 0.19; **Figure R7D**), SR-A (n = 4 vs. n = 3; SR-A/GAPDH densitometric analysis ACM 2.02 ± 0.88 vs. HC 1.00 ± 0.20; **Figure R7E**) and LOX-1 (n = 4 vs. n = 3; LOX-1/GAPDH densitometric analysis ACM 1.14 ± 0.23 vs. HC 1.00 ± 0.27; **Figure R7F**), with respect to HC cells, although, due to the small number of samples analysed and the high variability, further investigations are necessary.

Figure R7. ACM C-MSC show elevated PPARγ and CD36 expression in growth conditions.

A) Representative images of Western Blot analysis of proteins extracted from healthy control (HC) and arrhythmogenic cardiomyopathy (ACM) cardiac mesenchymal stromal cells (C-MSC) cultured in growth medium (GM), hybridized with anti-TLR4, anti-CD36, anti-SR-A, anti-PPARγ, anti-LOX-1 antibodies. Immunostaining of the housekeeping GAPDH is shown for normalization.

B) Densitometric analysis of PPARγ levels, normalized on the housekeeping protein GAPDH, in HC and ACM C-MSC (n=19 vs. n=20). ** $p < 0.01$ (Mann-Whitney test).

C) Densitometric analysis of CD36 levels, normalized on the housekeeping protein GAPDH, in HC and ACM C-MSC (n=19 vs. n=20). * $p < 0.05$ (Mann-Whitney test).

D) Densitometric analysis of TLR4 levels, normalized on the housekeeping protein GAPDH, in HC and ACM C-MSC (n=3 vs. n=4).

E) Densitometric analysis of SR-A levels, normalized on the housekeeping protein GAPDH, in HC and ACM C-MSC (n=3 vs. n=4).

F) Densitometric analysis of LOX-1 levels, normalized on the housekeeping protein GAPDH, in HC and ACM C-MSC (n=3 vs. n=4).

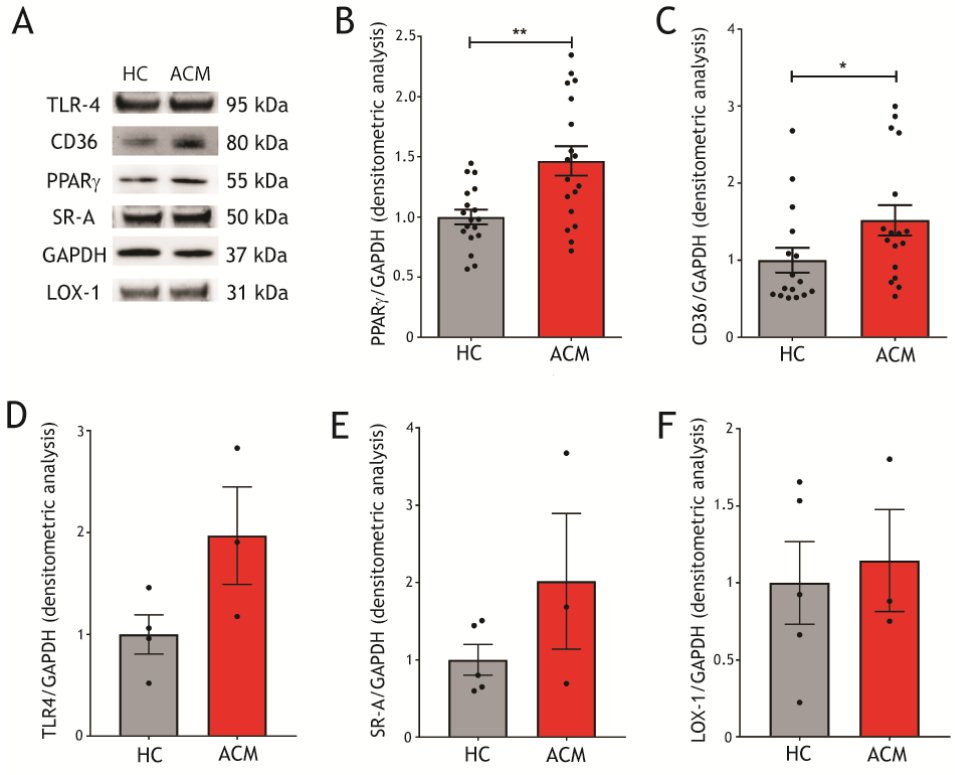

2.5 Lipid accumulation and CD36 levels in ACM C-MSC upon adipogenic stimulus.

Since corresponding transcription levels of CD36 and PPARγ, as well as lipid accumulation, is described for other cell types (368), we evaluated if ACM C-MSC, already predisposed to PPARγ activation (20), were more prone to expose CD36 on the plasma membrane during lipid accumulation. We performed a double staining with Nile Red, to mark neutral lipids, and anti-CD36 antibody in ACM and HC C-MSC, cultured in adipogenic medium (AM) for different time-points (0, 3, 6 and 10 days). **Figure R8A** shows that, during adipogenic differentiation, ACM C-MSC simultaneously increase CD36 and lipid content significantly more than HC cells. In both ACM and HC cells a linear correlation is present between these two parameters ($p = 0.008$ and 0.03, respectively), however a steeper slope in ACM C-MSC was evident ($n = 4$ vs. $n = 5$; ACM slope 1.33; $R^2 = 0.99$ vs. HC slope 0.69; $R^2 = 0.93$; slopes statistically different $p = 0.016$). To understand CD36 activity during adipogenic differentiation, we evaluated C-MSC oxLDL internalization, by assessing the intracellular fluorescence after 10 µg/ml DiI dye-conjugated oxLDL treatment (DiI-oxLDL), either in GM or in AM. ACM C-MSC internalized more DiI-oxLDL in AM compared to GM ($n = 3$ each; DiI internalization ACM GM 2.22 ± 0.16 vs. ACM AM 6.29 ± 0.65; $p = 0.002$) and 3-fold more than controls in AM ($p = 0.01$; **Figure R8B**).

Figure R8. ACM C-MSC show elevated CD36 levels and functionality, during adipogenic differentiation.

A) Results of a FACS analysis of arrhythmogenic cardiomyopathy (ACM) and healthy control (HC) cardiac mesenchymal stromal cells (C-MSC), cultured in growth medium (GM; time-point 0) or adipogenic medium (AM) for 3, 6 or 10 days (time-points 3, 6 and 10, respectively) and marked with anti-CD36 antibody and Nile red. The mean (ACM n = 4 vs. HC n = 5) fluorescence of CD36 and Nile Red is shown for each condition together with the relative regression line, its equation, R^2 and p value. * $p < 0.05$ (X-Y correlation).

B) Top panels: representative images of HC and ACM cells, cultured either in GM or in AM, and subjected to 10 µg/ml DiI-oxLDL treatment. The images show the internalization of oxLDL (red), effect of CD36 functionality. Nuclei are counterstained with Hoechst 33342 (blue). Bottom panel: quantification of the relative mean DiI fluorescence for each sample, measured by FACS analysis (n = 3 each). * $p < 0.05$, ** $p < 0.01$ (Two-Way Anova).

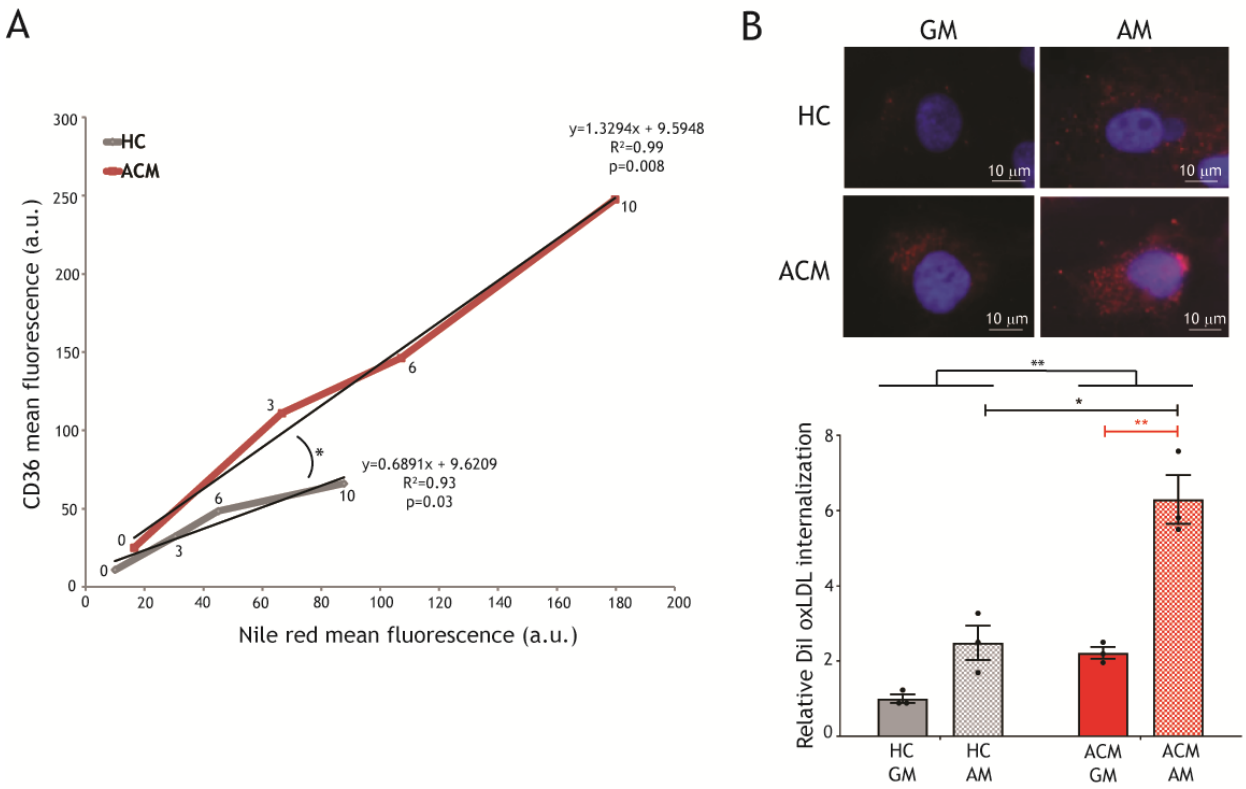

2.6 Comparison of the mass of different lipid classes accumulated during adipogenic differentiation.

We also performed a detailed quantitative and qualitative characterization of C-MSC lipid profile during 7 days of adipogenic differentiation, to better understand which metabolic pathways could be impaired in ACM. Lipidomic assays revealed mass increase of free cholesterol, triglycerides, esterified cholesterol and free fatty acids in ACM C-MSC. Interestingly, ACM cells accumulated significantly more free cholesterol (n = 5 vs. n = 4; µg free cholesterol/10^6 cells ACM 11.95 ± 1.05 vs. HC 8.24 ± 1.15; p = 0.05; Figure R9A) and triglycerides than HC C-MSC (n = 5 vs. n = 4; µg triglycerides/10^6 cells ACM 35.23 ± 5.38 vs. HC 18.64 ± 3.22; p = 0.04; Figure R9A). In all the lipid classes, included phospholipids (not shown), a trend toward an increase of monounsaturated fatty acids (mainly oleic acid) was documented.

These data are in line with the neutral lipid accumulation detected through Oil Red O (ORO) staining, as previously published (20). Indeed, we found a linear correlation between triglyceride quantity and ORO staining levels (Figure R9B). Triglycerides accumulation confirmed the ongoing transition of C-MSC toward an adipogenic lineage.

Figure R9. Mass increase of free cholesterol, triglycerides, esterified cholesterol and free fatty acids in ACM C-MSC.

A) Mass of free cholesterol, triglycerides, cholesteryl esters and free fatty acids accumulated by healthy control (HC; n = 4) and arrhythmogenic cardiomyopathy (ACM; n = 5) cardiac mesenchymal stromal cells (C-MSC) after 7 days of adipogenic differentiation. The masses are normalized on 10^6 cells. * $p < 0.05$ (Two-tailed Student's t-test).

B) Upper panel: correlation between triglyceride mass and percentage of Oil Red O (ORO) positive cells. Regression line, its equation, R^2 and p value are shown. Lower panel: dot plot of cholesteryl ester mass and percentage of ORO positive cells (X-Y correlation).

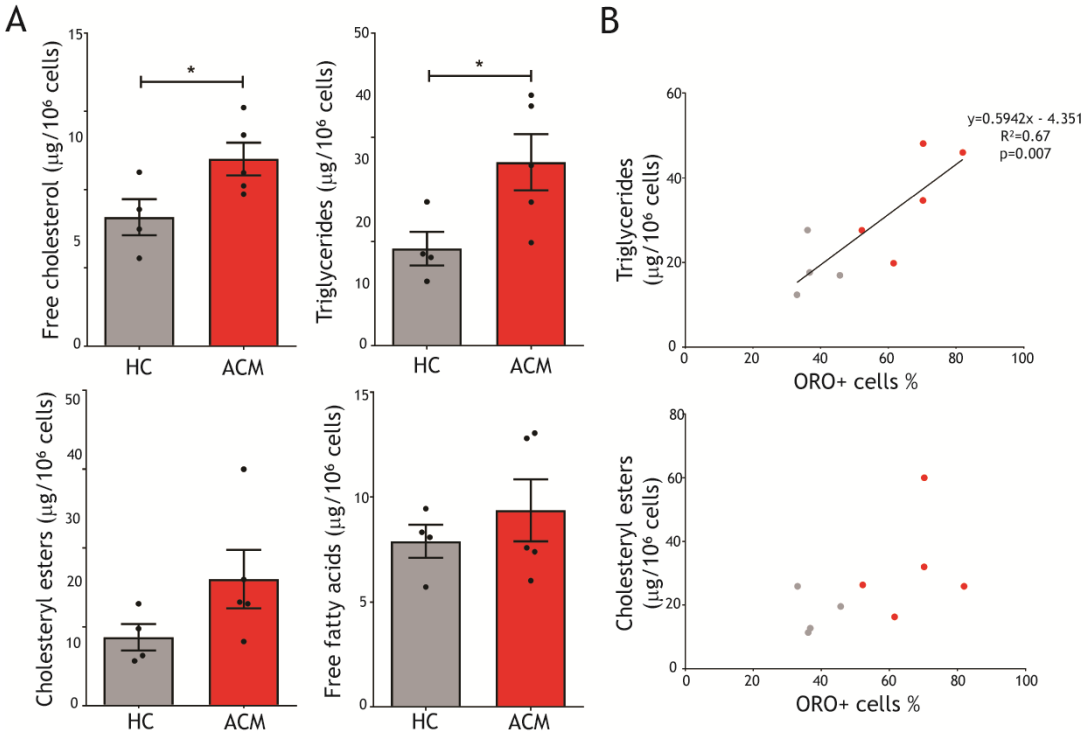

2.7 oxLDL and 13HODE effects on lipid accumulation in ACM C-MSC.

To test the hypothesis that oxLDL may exacerbate adipogenic propensity in ACM C-MSC through a vicious circle implicating CD36 and PPARγ, we treated ACM and HC C-MSC with or without 150 µg/ml oxLDL in AM. After 72 hours of incubation, the effect on lipid accumulation was assessed. In the presence of oxLDL addition, ACM C-MSC further increased lipid accumulation compared to AM only (n = 11 each; ORO relative lipid accumulation ACM AM 6.19 ± 0.83 vs. ACM AM + oxLDL 11.86 ± 2.64; p = 0.01; Figure R10A).

To understand 13HODE specific contribution to the increased adipogenic differentiation provoked by oxLDL in ACM cells, we cultured ACM and HC C-MSC for 72 hours in AM, with or without 20 µg/ml 13HODE. Importantly, the treatment with 13HODE significantly increased lipogenesis in ACM C-MSC only (n = 12 each; ORO relative lipid accumulation ACM AM 3.60 ± 0.82 vs. ACM AM + 13HODE 4.75 ± 0.92; p = 0.048; Figure R10B). In the same experiment, we evaluated the protein levels of PPARγ and CD36. We observed PPARγ and CD36 level upregulation after 13HODE treatment in ACM C-MSC (n = 8 each; PPARγ/GAPDH densitometric analysis ACM AM 1.67 ± 0.16 vs. ACM AM + 13HODE 2.17 ± 0.20; p = 0.047; n = 8; CD36/GAPDH densitometric analysis ACM AM 1.22 ± 0.06 vs. ACM AM + 13HODE 1.78 ± 0.20; p = 0.008; Figure R10C), as expected in light of the previously described feed-forward circle (393).

2.8 The antioxidant compound NAC effects on lipid accumulation in ACM C-MSC.

In an attempt to prevent the effects of oxidized agents on lipid droplet accumulation in ACM cells, we tested the effect of the antioxidant N-acetilcysteine (NAC). ACM and HC C-MSC, with or without 13HODE, were cultured in AM, either supplemented or not with 5 mmol/L NAC for 72 hours. As for lipid accumulation, NAC treatment was able to contain 13HODE effects (n = 12 each; ORO quantification ACM AM + 13HODE 4.75 ± 0.92 vs. ACM AM + NAC 2.38 ± 0.61; $p < 0.0001$; ORO quantification ACM AM + 13HODE 4.75 ± 0.92 vs. ACM AM + 13HODE + NAC 3.48 ± 0.78; $p = 0.02$; **Figure 10B**). Accordingly, both PPARγ and CD36 protein levels were reduced (n = 7; PPARγ/GAPDH densitometric analysis ACM AM + 13HODE 2.17 ± 0.20 vs. ACM AM + NAC 1.03 ± 0.08; $p < 0.0001$; PPARγ/GAPDH densitometric analysis ACM AM + 13HODE 2.17 ± 0.20 vs. ACM AM + 13HODE + NAC 1.31 ± 0.15; $p = 0.0001$; n = 8; CD36/GAPDH densitometric analysis ACM AM + 13HODE 1.72 ± 0.20 vs. ACM AM + NAC 0.95 ± 0.10; $p < 0.0001$; CD36/GAPDH densitometric analysis ACM AM + 13HODE 1.72 ± 0.20 vs. ACM AM + 13HODE + NAC 0.86 ± 0.15; $p < 0.0001$; **Figure 10C**).

Moreover, NAC addition to AM led to lipid accumulation reduction in ACM C-MSC compared to AM alone, suggesting that oxidative stress plays a role in the lipogenic process per se (n = 12 each; ORO quantification ACM AM 3.60 ± 0.82 vs. ACM AM + NAC 2.38 ± 0.61; $p = 0.03$; **Figure 10B**). Accordingly, NAC significantly reduced PPARγ levels (n = 7 each; PPARγ/GAPDH densitometric analysis ACM AM 1.67 ± 0.16 vs. ACM AM + NAC 1.03 ± 0.08; $p = 0.007$; **Figure 10C**), whereas a decrement trend was observed for CD36 (CD36/GAPDH densitometric analysis ACM AM 1.22 ± 0.06 vs. ACM AM + NAC 0.95 ± 0.10; **Figure 10C**). The effect is possibly due to a direct action of NAC on gene expression as previously described in macrophages during foam cell formation (442).

Figure R10. ACM C-MSC lipogenesis is increased with oxLDL or 13HODE and prevented by NAC treatment.

A) Left panels: representative images of Oil Red O (ORO) staining on arrhythmogenic cardiomyopathy (ACM) and healthy control (HC) cardiac mesenchymal stromal cells (C-MSC) in adipogenic medium (AM) supplemented or not with 150 µg/ml oxLDL. Right panel: image quantification (n = 11 each). * $p < 0.05$, *** $p < 0.001$ (Two-Way Anova).

B) Left panels: representative images of ORO staining on ACM and HC C-MSC in AM supplemented or not with 20 µg/ml 13HODE, 5mmol/L NAC or both the compounds. Right panel: image quantification (n = 13 each). * $p < 0.05$, ** $p < 0.01$, *** $p < 0.001$ (Two-Way Anova).

C) Left panel: representative images of Western Blot of CD36, PPARγ and GAPDH protein expression of ACM and HC C-MSC protein extracts in AM supplemented or not with 20 µg/ml 13HODE, 5 mmol/L NAC and both (n = 8 each). Right panels: densitometric analysis normalized on the housekeeping protein GAPDH. * $p < 0.05$, ** $p < 0.01$, *** $p < 0.001$ (Two-Way Anova).

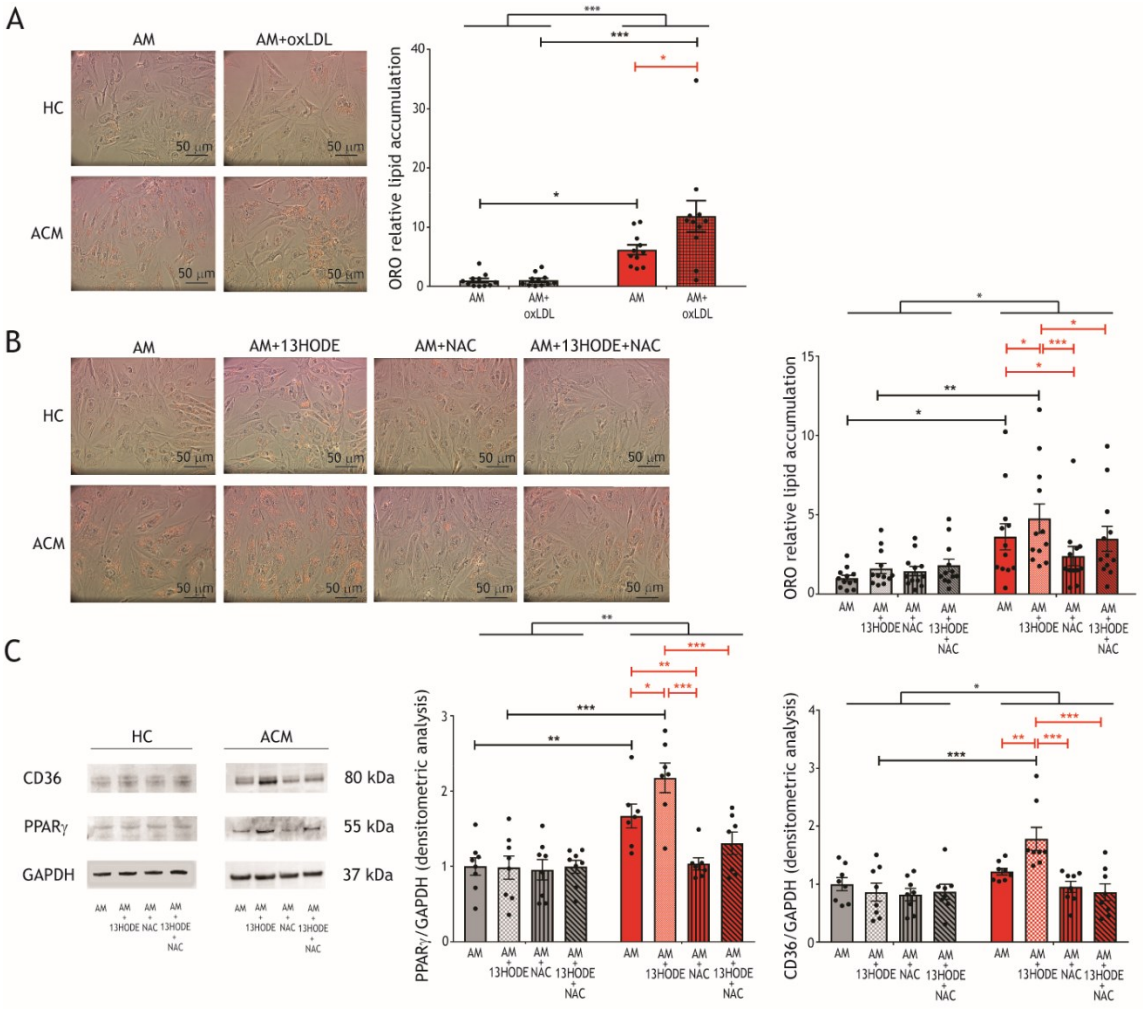

2.9 Susceptibility to oxLDL treatment of ACM C-MSC upon *PKP2* expression

To unravel the reasons of higher susceptibility to oxLDL treatment of ACM C-MSC, we evaluated its dependency upon *PKP2* expression. Indeed, most of our patients carry a genetic mutation in the *PKP2* gene, leading to its haploinsufficiency. Moreover, we previously demonstrated a lower expression of PKP2, even in ACM patients without a known causative mutation (20). To this purpose, we silenced PKP2 in HC cells, using lentiviral particles containing *PKP2* shRNA. A reduction of PKP2 to half of its original expression (**Figure R11A**) significantly increased lipid accumulation in response to oxLDL (n = 3 each; ORO quantification PKP2 shRNA AM 4.11 ± 0.09 vs. PKP2 shRNA AM+oxLDL 7.76 ± 0.67; p = 0.05; **Figure R11B**), whereas no changes in lipid accumulation were detected between scrambled control cells cultured in AM or AM+oxLDL. This indicates that susceptibility to oxLDL treatment is dependent upon PKP2 expression levels. As previously demonstrated in (20), we also confirmed that HC C-MSC can accumulate lipid when PKP2 expression is reduced (n = 3 each; ORO quantification scramble AM 1.00 ± 0.04 vs. PKP2 shRNA AM 4.11 ± 0.09; p = 0.001; **Figure R11B**).

Figure R11. *PKP2* silencing in HC C-MSC demonstrated the dependency of oxLDL/CD36/PPARγ axis on genetic causes.

A) Left panel: Western Blot of PKP2 and GAPDH protein expression of healthy control (HC) cardiac mesenchymal stromal cell (C-MSC) protein extracts treated with shRNA scrambled control or *PKP2* shRNA and cultured in growth medium (GM). Right panel: densitometric analysis normalized on the housekeeping protein GAPDH (n = 3 each). ** $p < 0.01$ (Two-tailed Student's t-test).

B) Oil Red O (ORO) staining quantification of HC C-MSC treated with shRNA scrambled control or *PKP2* shRNA and cultured in adipogenic medium (AM) with or without 150 µg/ml oxLDL for 72 hours (n = 3 each). * $p < 0.05$, *** $p < 0.001$ (One-Way Anova).

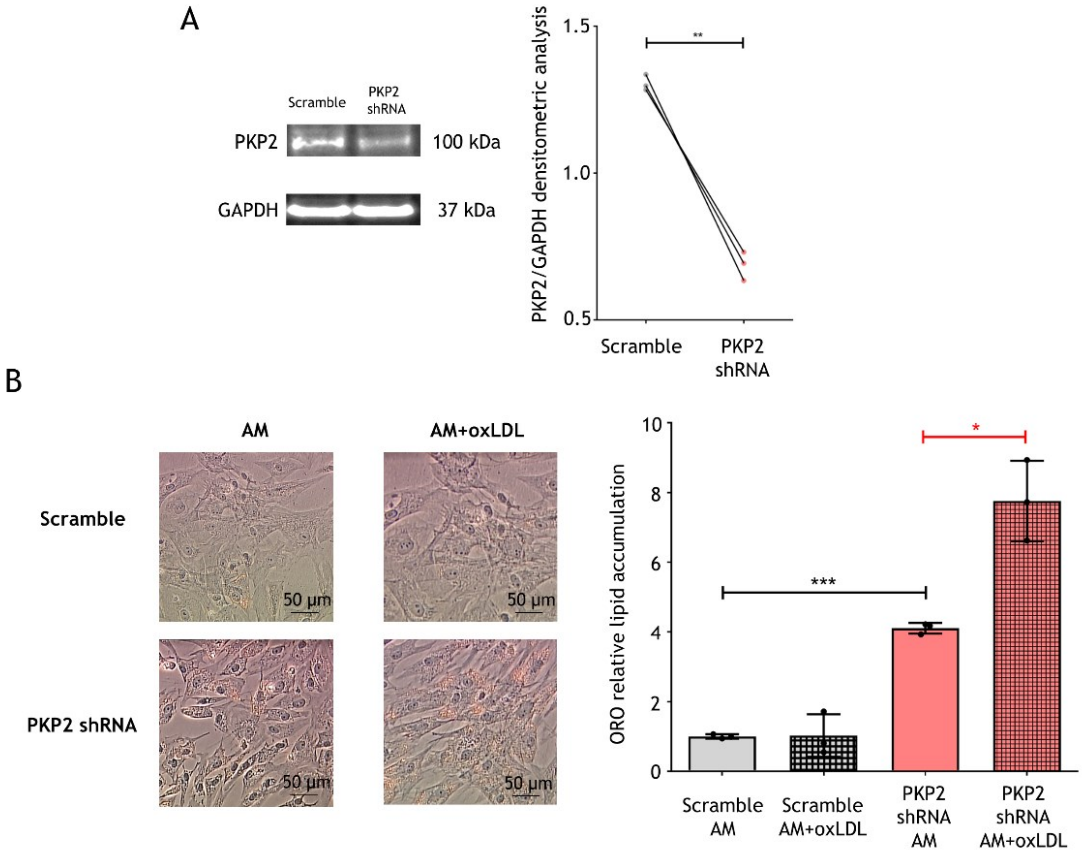

2.10 CD36 silencing in ACM C-MSC

To directly assess CD36 causal role in ACM cell adipogenic process, we performed CD36 siRNA-induced silencing in AM supplemented with oxLDL. 32% mean reduction in CD36 levels (n = 7; p = 0.014; **Figure R12A**) in ACM C-MSC was enough for inducing significantly less lipid accumulation if compared to the non-silenced counterparts (n = 7; ORO relative lipid accumulation scramble 1.00 ± 0.19 vs. siRNA 0.35 ± 0.10; p = 0.003; **Figure R12B**), along with PPARγ reduced levels (n = 7 each; PPARγ/GAPDH relative densitometric analysis scramble 1.00 ± 0.18 vs. siRNA 0.76 ± 0.15; p = 0.05; **Figure R12A**). In addition, CD36 levels (both with and without silencing) correlated with PPARγ (n = 14; slope = 1.05; R^2 = 0.76; p = 0.0002; **Figure R12C**) and to a lesser extent with ORO staining (n = 14; slope = 0.52; R^2 = 0.26; p = 0.07; **Figure R12C**). As expected, reduced CD36 levels determined a lower oxLDL internalization (n=3 each; DiI internalization scramble 7.34±1.31 vs. siRNA 0.63±0.13; p=0.04; **Figure R12D**).

Figure R12. CD36 silencing reduces lipid accumulation in ACM C-MSC.

A) Left panel: representative images of Western Blot of CD36, PPARγ and GAPDH expression of protein extracts of arrhythmogenic cardiomyopathy (ACM) cardiac mesenchymal stromal cells (C-MSC) treated with scramble siRNA or CD36 siRNA and cultured in adipogenic medium (AM) with 150 µg/ml oxLDL. Right panels: densitometric analysis normalized on the housekeeping protein GAPDH (n = 7 each). * $p < 0.05$ (Two-tailed Student's t-test).

B) Left panels: representative images of Oil Red O (ORO) staining on ACM C-MSC treated with scramble siRNA or CD36 siRNA and cultured in AM with 150 µg/ml oxLDL. Right panel: image quantification (n = 7 each). ** $p < 0.01$ (Two-tailed Student's t-test).

C) Left panel: correlation between CD36/GAPDH densitometric analysis and PPARγ/GAPDH densitometric analysis. Right panel: correlation between CD36/GAPDH densitometric analysis and ORO relative lipid accumulation. For both panels, regression lines, their equations, R^2 and correlation p values are shown (X-Y correlation).

D) Left panel: representative images of ACM C-MSC treated with scramble siRNA or CD36 siRNA, cultured in AM and subjected to 10 µg/ml DiI oxLDL treatment. The images show the internalization of oxLDL (red), effect of CD36 functionality. Nuclei are counterstained with Hoechst 33342 (blue). Right panel: quantification of the DiI fluorescence normalized on nuclei number for each sample (n= 3). * $p < 0.05$ (Two-tailed Student's t-test).

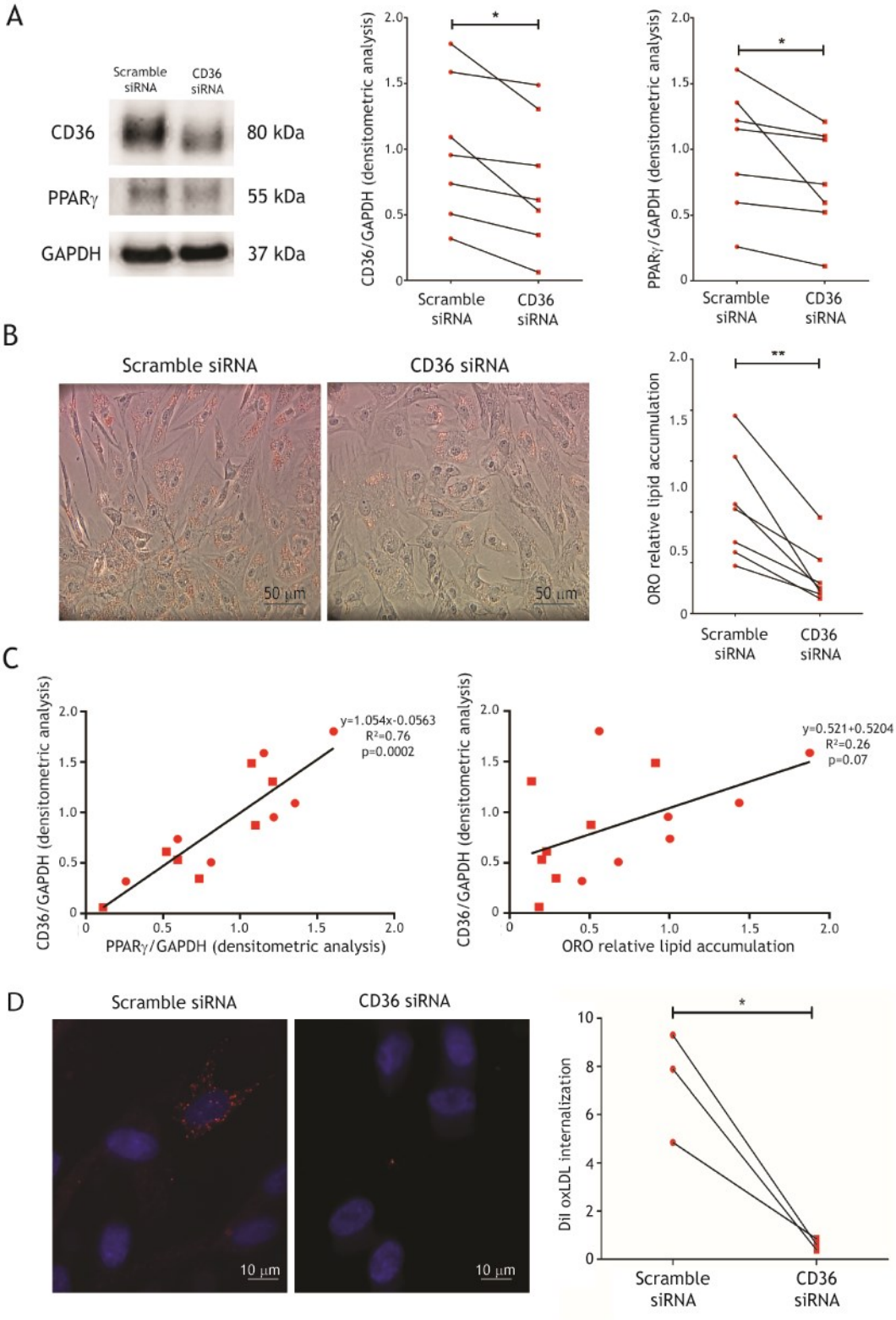
A
Scramble siRNA
CD36 siRNA
CD36
80 kDa
PPARγ
55 kDa
GAPDH
37 kDa
CD36/GAPDH (densitometric analysis)
PPARγ/GAPDH (densitometric analysis)
Scramble siRNA
CD36 siRNA
B
Scramble siRNA
CD36 siRNA
50 μm
ORO relative lipid accumulation
C
y=1.054x-0.0563
R²=0.76
p=0.0002
PPARγ/GAPDH (densitometric analysis)
y=0.521+0.5204
R²=0.26
p=0.07
ORO relative lipid accumulation
D
Scramble siRNA
CD36 siRNA
10 μm
DiI oxLDL internalization

2.11 PPARγ inhibition in ACM C-MSC

oxLDL/CD36/PPARγ interdependence in ACM cells was also confirmed by inhibiting PPARγ with the antagonist GW9662. This provoked a significant reduction of oxLDL internalization (n = 3; DiI internalization ACM AM 25137 ± 3567 vs. ACM AM + GW9662 10194 ± 3787 arbitrary units; p = 0.01; **Figure R13A**), together with a lower expression of CD36 (n = 3; CD36/GAPDH densitometric analysis ACM AM 1.26 ± 0.08 vs. ACM AM + GW9662 0.97 ± 0.14; p = 0.04; **Figure R13B**).

Figure R13. PPARγ antagonism reduces CD36 expression and function in ACM C-MSC.

A) Left panel: representative images of arrhythmogenic cardiomyopathy (ACM) cardiac mesenchymal stromal cells (C-MSC) cultured in adipogenic medium (AM) or AM+ 5 µM GW9662 and subjected to 10 µg/ml DiI oxLDL treatment. The images show the internalization of oxLDL (red), effect of CD36 functionality. Nuclei are counterstained with Hoechst 33342 (blue). Right panel: quantification of the DiI fluorescence normalized on nuclei number for each sample (n = 3). * $p < 0.05$ (Two-tailed Student's t-test).

B) Left panel: representative images of Western Blot of CD36 and GAPDH expression of protein extracts of ACM C-MSC cultured in AM or AM+ 5 µM GW9662. Right panels: densitometric analysis normalized on the housekeeping protein GAPDH (n = 7 each). * $p < 0.05$ (Two-tailed Student's t-test).

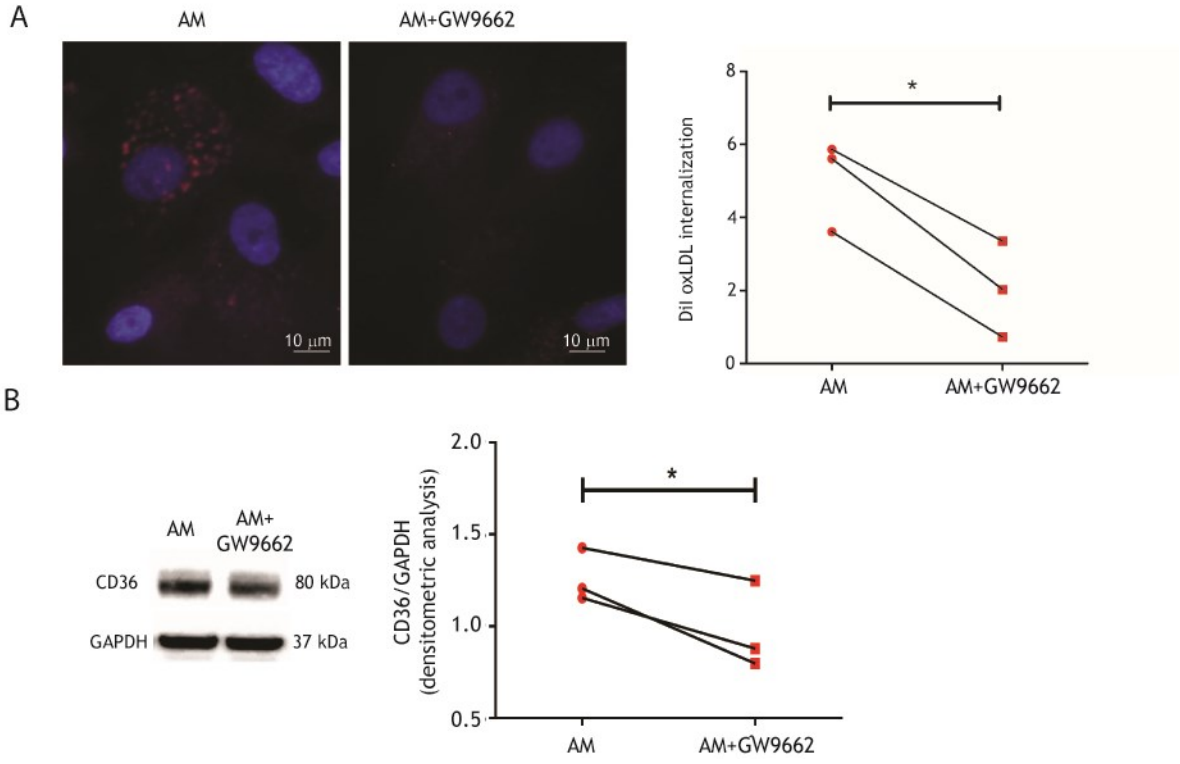

2.12 ACM hiPSC obtainment and cardiomyocyte differentiation

To understand if the mechanism mediated by oxLDL and involving CD36 and PPARγ is confirmed in human ACM cardiomyocytes, we differentiated hiPSC obtained from ACM PBMCs in cardiomyocytes (CM; **Figure R14**). PBMCs were obtained from blood samples of one ACM patient, carrying the deletion of the whole *PKP2* exon 4 leading to a predicted truncated protein (p.N346Lfs*12), and one HC of the same family (**Figure R2**). Cardiomyogenic differentiation was initially performed, as previously described (443), by hiPSC aggregation into 3D embryoid bodies (EB). Depending on the variability between different hiPSC lines and experimental repeats, the percentage of EB containing beating clusters varied between 5-15%. After single cell dissociation, CM percentage indicated by FACS positivity for the cardiac markers Troponin I (TnTI) and α-Actinin fluctuated between 10-20%.

The relatively low efficiency of cardiomyogenic differentiation led us to apply another protocol, based on monolayer differentiation in feeder-free conditions, using PSC Cardiomyocyte Differentiation Kit. Beating CM in the monolayer at 28-30 days of differentiation were then dissociated as single cells and re-plated onto Matrigel-coated dishes in basal medium supplemented with 2% FBS. Specifically, this procedure allowed us to obtain between approximatively the 50% of cells positive for TnTI organized in evident sarcomere, and thus identifiable as CM. To further increase CM purity, cells were treated with PSC-Derived Cardiomyocyte Isolation Kit and passed through the QuadroMACS™ Separator; the final population of CM had a purity of 90-95%.

Figure R14. Generation and characterization of a hiPSC line obtained from skin fibroblasts of one ACM patient (from Meraviglia et al., Journal of Visualized Experiments, 2015; doi: 10.3791/52885).

A) Representative image showing the hiPSC positive staining for alkaline phosphatase, marker of pluripotent cells (scale bar 500 µm).

B) Representative picture of normal karyogramm by Q-banding karyotype analysis.

C) Representative immunofluorescence staining showing significant expression of pluripotency proteins SSEA-4, OCT3/4, TRA-1-81, TRA-1-60 and SOX-2. Nuclei are counterstained with DAPI; scale bar 100 µm.

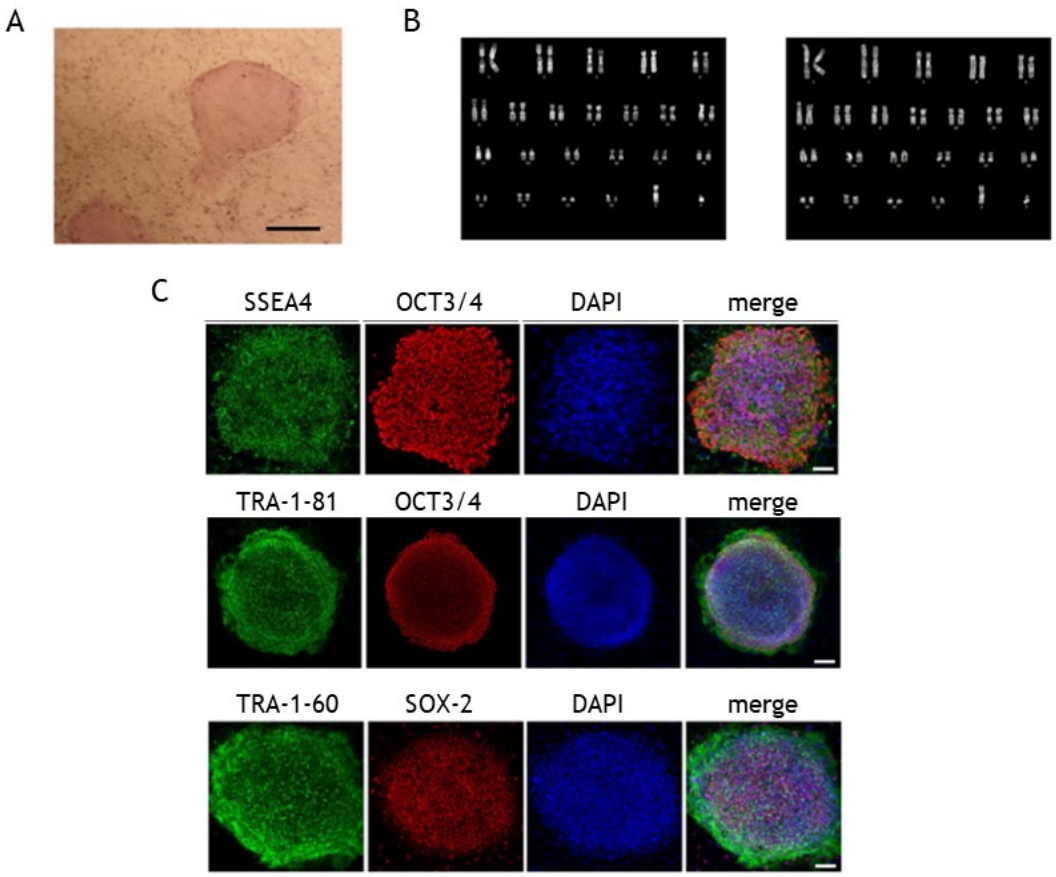

2.13 Lipid accumulation and CD36 levels in ACM hiPSC-CM upon PPARγ agonism.

CD36 membrane expression was evaluated in hiPSC-CM derived from ACM patients and unaffected relatives after adipogenic stimulation (**Figure R15**). While limited lipid accumulation was detected in GM, in analogy to what observed in C-MSC, CD36 expression showed a trend of increase in ACM hiPSC-CM than in controls. When exposed to AM containing the PPARγ agonist rosiglitazone, ACM hiPSC-CM exhibited a higher content of intracellular lipids compared to HC hiPSC-CM, as previously reported (240) (relative BODIPY staining ACM hiPSC-CM 24.02 ± 4.94 vs. HC hiPSC-CM 10.38 ± 1.94; p = 0.01). AM+rosiglitazone treatment led to CD36 expression increase both in HC (MFI 6.21 ± 1.59, p = 0.004 vs. GM) and ACM hiPSC-CM (MFI 6.10 ± 0.94, p = 0.01 vs. GM).

Figure R15. Lipid accumulation and CD36 levels increase in hiPSC-CM upon PPARγ agonism.

A) Representative images of lipid accumulation, detected with BODIPY (green), and cardiomyocyte marker αSARC (red) co-localization in arrhythmogenic cardiomyopathy (ACM) and healthy control (HC) hiPSC-CM cultured in growth (GM) or adipogenic medium (AM) supplemented with 5 µM rosiglitazone. Nuclei are stained with DAPI. On the right, the relative quantification of lipid accumulation is shown. Relative lipid accumulation is presented as normalized to GM HC. * $p < 0.05$, *** $p<0.001$.

B) Left panels: exemplificative FACS analysis of the PE fluorescence of unstained HC and ACM hiPSC-CM (autofluorescence; gray), in GM stained with CD36 antibodies (purple), and in AM added with 5 µM rosiglitazone stained with CD36 antibodies (light blue). Right panel: quantification of the median CD36 fluorescence of HC and ACM hiPSC-CM both in GM and in AM added with 5 µM rosiglitazone. Relative median CD36 fluorescence is presented as normalized to GM HC. * $p < 0.05$, ** $p < 0.01$, *** $p < 0.001$.

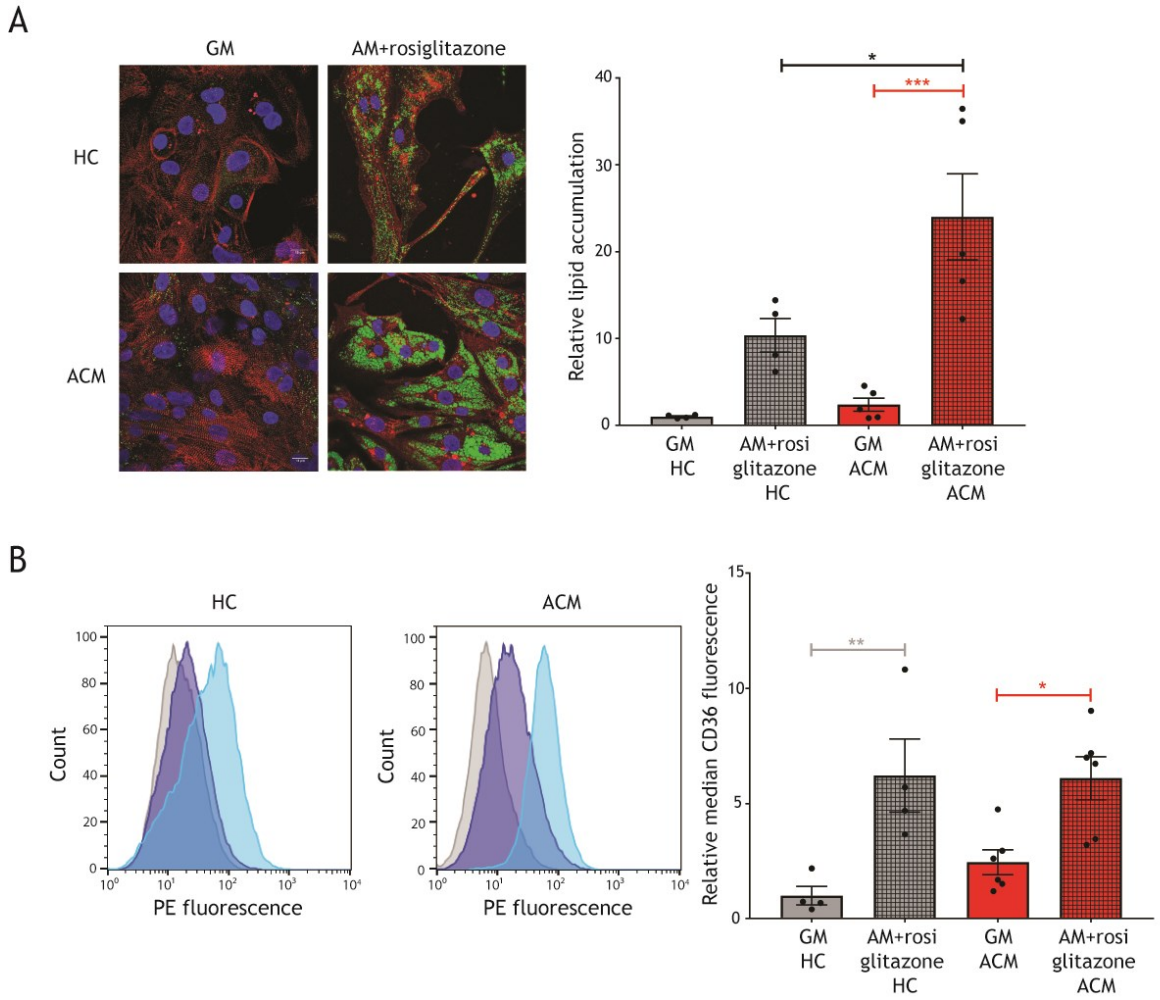

2.14 Transcriptomic analysis of ACM and HC hiPSC-CM.

The analysis of the whole transcriptome of hiPSC-CM exposed to GM and AM+rosiglitazone was performed. Table R5 reports the results of this analysis on a subset of genes of interest, comparing gene expression in ACM hiPSC-CM samples grown in AM+rosiglitazone vs. GM. The results indicate that the AM+rosiglitazone treatment significantly (FDR < 15%) modulates the expression of genes involved in apoptosis, lipid metabolism and sarcomere structure.

In addition, a considerable number of genes were found differentially expressed between ACM and HC hiPSC-CM cultured either in GM or AM+rosiglitazone (FDR = 10%). Table R6A reports significantly modulated genes in GM, while Table R6B lists the modulated genes in AM+rosiglitazone.

ACOT1 (Acyl-CoA thioesterase 1) seems particularly interesting and deserves further validation, resulting differentially expressed between ACM and HC hiPSC-CM in both adipogenic and basal conditions. ACOT are enzymes associated to Metabolism of Lipids, Fatty Acyl-CoA Biosynthesis, and Mitochondrial Fatty Acid Beta-Oxidation pathways. Interestingly, *ACOT1* and *CD36* have both been reported as downstream genes of PPARγ (444), thus sustaining the important role of this pathway in the ACM pathogenesis.

Table R5. Effect of culture conditions (AM+rosiglitazone vs. GM) on the expression of a subset of selected genes in ACM hiPSC-CM.

gene_name		log2 Fold Change	p value	p adjusted
BAX	apoptosis	-0.2051	0.527	0.7
CASP9	apoptosis	0.9343	0.032	0.101
BCL2	apoptosis	2.1891	4E-09	2E-07
MEF2C	early cardiac gene	-0.1442	0.514	0.69
GATA4	early cardiac gene	-0.1185	0.636	0.779
NKX2-5	early cardiac gene	0.3058	0.262	0.448
FABP4	lipid metabolism	2.8163	0.009	0.037
SREBF1	lipid metabolism	3E-06	3E-06	5E-05
CPT1A	lipid metabolism	1.48	1E-08	4E-07
CD36	lipid metabolism	0.6598	0.208	0.384
FASN	lipid metabolism	1.1348	1E-03	0.007
CPT1C	lipid metabolism	0.0956	0.771	0.87
PPARGC1A	lipid metabolism	-0.0437	0.827	0.905
PPARA	lipid metabolism	0.3567	0.152	0.31
CEBPZ	lipid metabolism	0.1398	0.373	0.565
CEBPB	lipid metabolism	0.2466	0.624	0.771
CEBPD	lipid metabolism	0.2531	0.323	0.515
CEBPZOS	lipid metabolism	0.2553	0.431	0.618
CEBPG	lipid metabolism	0.237	0.542	0.711
ACTC1	sarcomere	-0.6968	0.036	0.11
MYH6	sarcomere	2.222	3E-07	8E-06
MYL2	sarcomere	-0.6106	0.141	0.296
MYH7	sarcomere	-5.4594	1E-14	2E-12

Table R6A. List of the most significantly regulated genes in hiPSC CM cultured in GM from ACM and HC individuals.

gene	description	log2 Fold Change	p value	p adjusted
NOP56P1	NOP56 ribonucleoprotein pseudogene 1	7.0286	1E-14	1E-10
SPECC1L	sperm antigen with calponin homology and coiled-coil domains 1 like	0.6661	5E-07	0.003
STAG3L4	stromal antigen 3-like 4 (pseudogene)	-0.9744	4E-06	0.016
NR2C2	nuclear receptor subfamily 2 group C member 2	0.7844	1E-05	0.032
BHLHE40	basic helix-loop-helix family member e40	-2.0296	1E-05	0.032
ACOT1	acyl-coA thioesterase 1	3.8044	2E-05	0.038
CSRNP1	cysteine and serine rich nuclear protein 1	-1.7499	5E-05	0.075
CCZ1B	CCZ1 homolog B, vacuolar protein trafficking and biogenesis associated	-4.398	6E-05	0.075
RPS28	ribosomal protein S28	-1.9554	6E-05	0.075
MRPS14	mitochondrial ribosomal protein S14	-1.3841	7E-05	0.075
HLA-C	major histocompatibility complex, class I, C	-5.2285	7E-05	0.075
PLPP7	phospholipid phosphatase 7 (inactive)	1.593	9E-05	0.088
YTHDF3	YTH N6-methyladenosine RNA binding protein 3	0.5707	1E-04	0.09

Table R6B. List of the most significantly regulated genes in hiPSC-CM cultured in AM+rosiglitazone from ACM and HC individuals.

gene	description	log2 Fold Change	p value	p adjusted
NOP56P1	NOP56 ribonucleoprotein pseudogene 1	5.749	5.4E-20	6.2E-16
ACOT1	acyl-coA thioesterase 1	4.373	2.7E-08	0.0001
RPS28	ribosomal protein S28	-2.277	3.0E-06	0.0114
CPNE1	copine 1	0.834	2.8E-05	0.0797

3. *In vivo* studies

3.1 *Pkp2*+/- mice characterization.

To validate our hypothesis on an ACM *in vivo* model, we took advantage of the well-established *Pkp2*+/- mouse (257) (445). In *Pkp2*+/- hearts from mice 14.30±1.46 months old, we found similar levels of lipid accumulation, despite an increase of PPARγ immunoreactive signal in ACM mice when compared to wild type (WT; n = 5 each; PPARγ densitometric sum/nuclei number WT 1 ± 0.45 vs. *Pkp2*+/- 3.96 ± 1.04; p = 0.03). Comparable expression of MDA and CD36 were found in the two strains (**Figure R16A-D**). Moreover, at 2D echocardiography, RV and LV functions were similar in WT and *Pkp2*+/- mice (**Figure R16E**).

Figure R16. *Pkp2*+/- mice show no cardiac adipogenesis, although PPARγ high expression, and low oxidative stress and CD36 levels

A) Left panels: representative images of ventricular sections of wild type (WT) and plakophilin2 heterozygous knock out (*Pkp2*+/-) mice, stained with Oil Red O (ORO). Right panel: quantification of the percentage of ORO positive cardiac tissue area (n = 5 each).

B) Left panels: representative images of PPARγ (green) immunostaining on ventricular tissue sections of WT and *Pkp2*+/- mice. Nuclei are counterstained with Hoechst 33342 (blue). Right panel: image quantification (n = 5 each).

C) Left panels: representative images of malondialdehyde (MDA; green) immunostaining on ventricular tissue sections of WT and *Pkp2*+/- mice. Nuclei are counterstained with Hoechst 33342 (blue). Right panel: image quantification (n = 5 each).

D) Left panels: representative images of CD36 immunostaining (green) on ventricular tissue sections of WT and *Pkp2*+/- mice. Nuclei are counterstained with Hoechst 33342 (blue). Right panel: image quantification (n = 5 each).

E) Echocardiographic parameters of WT and *Pkp2*+/- mice. The percentages of RV EF % and LV EF % are shown (n = 5 each).

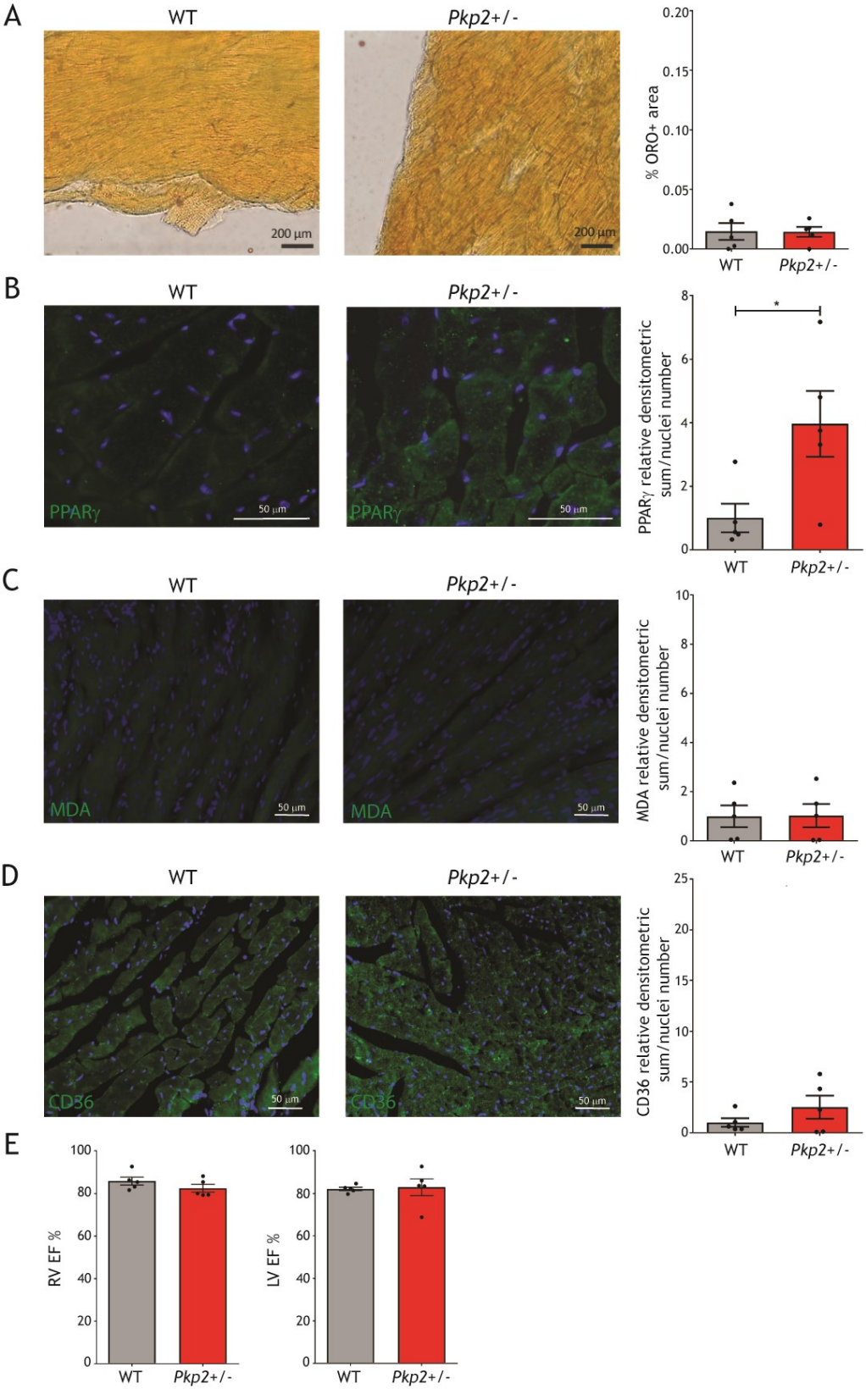
A
WT
Pkp2+/-
200 µm
200 µm
% ORO+ area
0.20
0.15
0.10
0.05
0.00
WT
Pkp2+/-
B
WT
Pkp2+/-
PPARγ
50 µm
PPARγ
50 µm
PPARγ relative densitometric sum/nuclei number
*
8
6
4
2
0
WT
Pkp2+/-
C
WT
Pkp2+/-
MDA
50 µm
MDA
50 µm
MDA relative densitometric sum/nuclei number
10
8
6
4
2
0
WT
Pkp2+/-
D
WT
Pkp2+/-
CD36
50 µm
CD36
50 µm
CD36 relative densitometric sum/nuclei number
25
20
15
10
5
0
WT
Pkp2+/-
E
RV EF %
100
80
60
40
20
0
WT
Pkp2+/-
LV EF %
100
80
60
40
20
0
WT
Pkp2+/-

3.2 Murine C-MSC isolation and adipogenic differentiation.

According to the basal higher cardiac expression of PPARγ and in analogy with human C-MSC, isolated *Pkp2*+/- mouse C-MSC cultured in AM for 6 days, accumulated higher neutral lipids than WT C-MSC (n = 5 each; ORO relative lipid accumulation *Pkp2*+/- 34.61 ± 9.23 vs. WT 1.00 ± 0.43; p = 0.007; **Figure R17**), indicating that mouse *Pkp2*+/- C-MSC are genetically predisposed to lipid accumulation.

Figure R17. ***Pkp2*+/- C-MSC are prone to adipogenic differentiation *in vitro*.**

Left panels: representative images of Oil Red O (ORO)-stained cardiac mesenchymal stromal cells (C-MSC) isolated from wild type (WT) and plakophilin2 heterozygous knock out (*Pkp2*+/-) mice and cultured in adipogenic medium for 5 days. Right panel: quantification of C-MSC lipid accumulation (n = 5 each). ** p < 0.01.

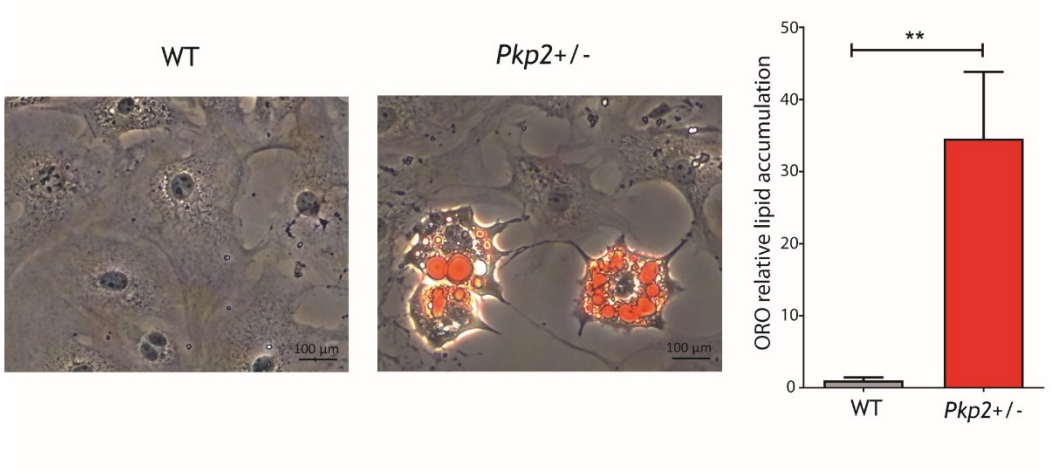

3.3 HFD administration effects on cardiac lipid accumulation and dysfunction in *Pkp2*+/- mice.

We fed *Pkp2*+/- mice a HFD for 3 months to test the hypothesis that increasing cholesterol and oxidative stress levels (446) would promote cardiac lipid accumulation.

In both strains, plasma total cholesterol concentrations, measured in the lipoprotein fractions, comparably increased after HFD (n = 8; **Figure R18A**, left). In particular, higher cholesterol was measured in HFD in fractions 29-32, representing VLDL-IDL-LDL (n = 8; $p < 0.0001$ each fraction; **Figure R18A**, right). Of note, HFD also increased oxLDL (n = 6; oxLDL nmol/ml HFD 1.29 ± 0.11 vs. CD 0.83 ± 0.05; p = 0.049; **Figure R18B**). Following HFD, cardiac sections from *Pkp2*+/- mice showed larger areas of fatty substitution compared to WT siblings (n = 10 vs. n = 10; % ORO positive area *Pkp2*+/- 1.04 ± 0.24 vs. WT 0.13 ± 0.02; p = 0.0002; **Figure R18C**), prevalently in sub-epicardial areas. As expected, the cells undergoing adipogenic differentiation in murine hearts are of mesenchymal origin (**Figure R19**). Accordingly, the difference in PPARγ immunoreactivity between WT and *Pkp2*+/- hearts substantially increased with HFD (n = 10 each; PPARγ densitometric sum/nuclei number *Pkp2*+/- 6.62 ± 1.22 vs. WT 1.64 ± 0.14; p = 0.0007).

Pkp2+/- mouse hearts also showed oxidative stress (n = 9 vs. n = 8; MDA relative densitometric sum/nuclei number *Pkp2*+/- 4.42 ± 0.88 vs. WT 0.19 ± 0.07; p = 0.003; **Figure R18D**) and CD36 level increase (n = 9 vs. n = 10; CD36 relative densitometric sum/nuclei number *Pkp2*+/- 7.48 ± 1.88 vs. WT 2.99 ± 0.68; p = 0.02; **Figure R18E**). Moreover, HFD induced RV dysfunction but no changes in LV function, as assessed by 2D echocardiography. In particular, ACM mice after 3 months of diet presented a lower RV ejection fraction (EF) compared to WT (n = 10 each; % RV EF *Pkp2*+/- 73.81 ± 3.43 vs. WT 82.69 ± 1.37; p = 0.03; **Figure R18F**). Morphometric analyses showed a trend of higher mid-chamber RV diastolic area in *Pkp2*+/- mice fed a HFD, while no differences were detected in wall thickness compared to WT (**Figure R20**).

Figure R18. HFD increases plasma oxLDL, cardiac adipose substitution, PPARγ, lipid peroxidation and oxLDL receptor expression, and impairs RV function in ACM mice.

A) Left panel: plasma total cholesterol in the different lipoprotein fractions of wild type (WT) and plakophilin2 heterozygous knock out (*Pkp2*+/-) mice fed a chow diet (CD; green line) or a 3-month high fat diet (HFD; blue line). Right panel: plasma total cholesterol quantity in fractions 29-32, corresponding to low, very low and intermediate density lipoproteins, of WT and *Pkp2*+/- mice fed a CD (green line) or a 3-month HFD (blue line). *** $p < 0.001$ (Mann-Whitney test).

B) Plasma concentration of oxLDL in WT and *Pkp2*+/- mice samples, fed a CD and a 3-month HFD (n = 5 each). * $p < 0.05$ (Two-tailed Student's t-test).

C) Left panels: representative images of Oil Red O (ORO) staining of HFD-fed WT and *Pkp2*+/- cardiac sections. Right panel: quantification of ORO positive area percentage (n = 10 each). For comparison, quantification of ORO positive area of cardiac sections of WT and *Pkp2*+/- mice fed CD (n = 5 each) is shown (Figure R16). * $p<0.05$ (Two-Way Anova).

D) Left panels: representative images of PPARγ (green) immunostaining on cardiac sections of WT and *Pkp2*+/- mice, fed a HFD (n = 10 each). Nuclei are counterstained with Hoechst 33342 (blue). Right panel: quantification of the PPARγ staining in HFD is shown relative to the values of CD (n = 5 each). *** $p < 0.001$ (Two-Way Anova).

E) Left panels: representative images of malondialdehyde (MDA; green) immunostaining on cardiac sections of WT and *Pkp2*+/- mice, fed a HFD (n = 10 each). Nuclei are counterstained with Hoechst 33342 (blue). Right panel: quantification of the MDA staining in HFD is shown relative to the values of CD (n = 5 each). * $p < 0.05$ ** $p < 0.01$ (Two-Way Anova).

F) Left panels: representative images of CD36 immunostaining (green) on cardiac sections of WT and *Pkp2*+/- mice, fed a HFD (n = 10 each). Nuclei are counterstained with Hoechst 33342 (blue). Right panel: quantification of the staining in HFD is shown relative to the values of CD (n=5 each). * $p < 0.05$ (Two-Way Anova).

G) Right ventricular (RV) and left ventricular (LV) ejection fraction (EF) percentages of WT and *Pkp2*+/- mice during (left panel) and after (right) 3-month HFD feeding. * $p < 0.05$ (Two-tailed Student's t-test).

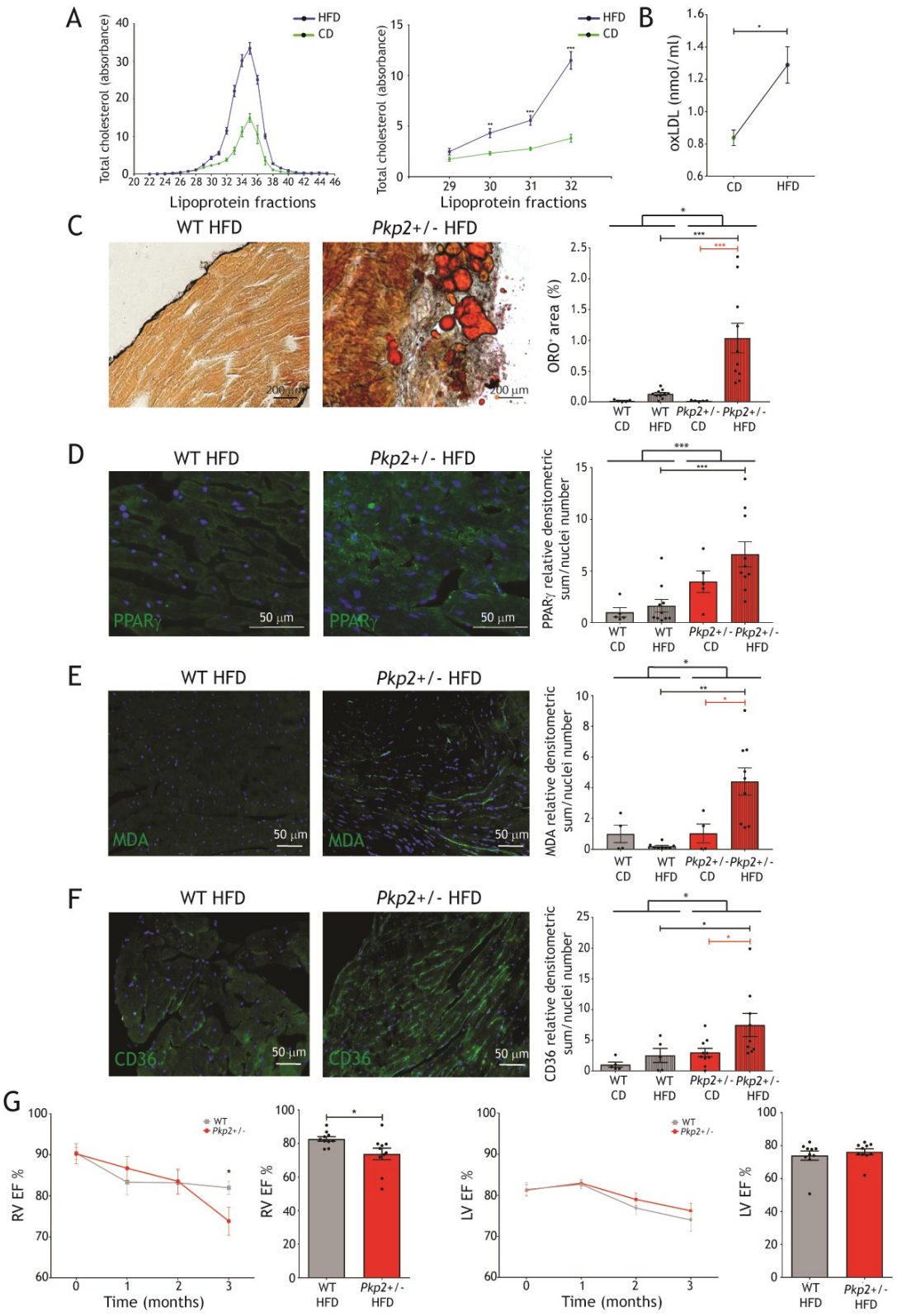

Figure R19. C-MSC undergo adipogenic differentiation in murine hearts with HFD.

A) Representative image of adipose accumulation, detected with perilipin 1 (PLIN1) antibody (green), and mesenchymal marker CD105 (red) co-localization in plakophilin2 heterozygous knockout (*Pkp2*+/-) heart section after high fat diet (HFD). Nuclei are stained with Hoechst 33258.

B) Representative image of immunofluorescence staining of *Pkp2*+/- heart section after HFD with PLIN1 antibody (green) for fat droplets membranes and Troponin T antibody (red) for cardiomyocytes. Nuclei are stained with Hoechst 33258. No co-localization was detected.

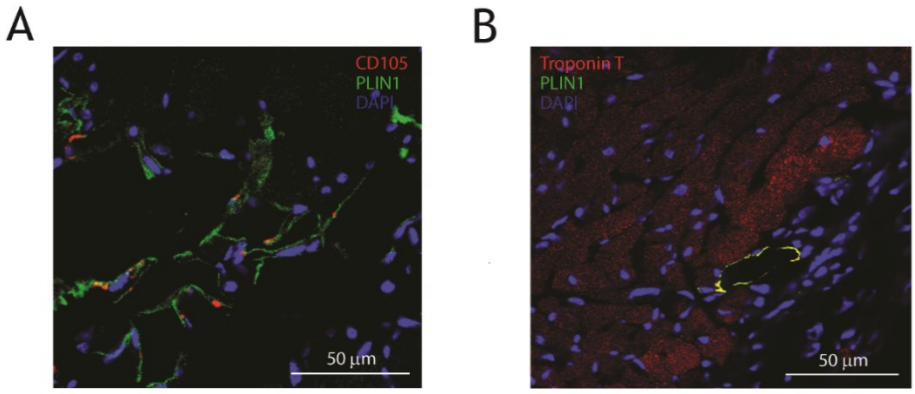

Figure R20. Echocardiographic and morphometric parameters of WT and *Pkp2*+/- mice before and after HFD.

A) Representative two-dimensional echocardiograms (M-mode, left panels; B-mode, right panels) of wild type (WT) and plakophilin2 heterozygous knockout (*Pkp2*+/-) mice in chow diet (CD; upper panels) and after 3 months of high fat diet (HFD; lower panels). The right ventricular internal diameter in systole (RVIDs) and in diastole (RVIDd) and the right ventricle (RV) are depicted.

B) Upper panels: Oil Red O–stained representative sections from the cardiac mid-chamber of WT and *Pkp2*+/- mice in CD and after HFD. Middle panel: mid-chamber RV diastolic area. Lower panel: mid-chamber RV wall thickness (n = 3 each for CD and n = 5 each for HFD).

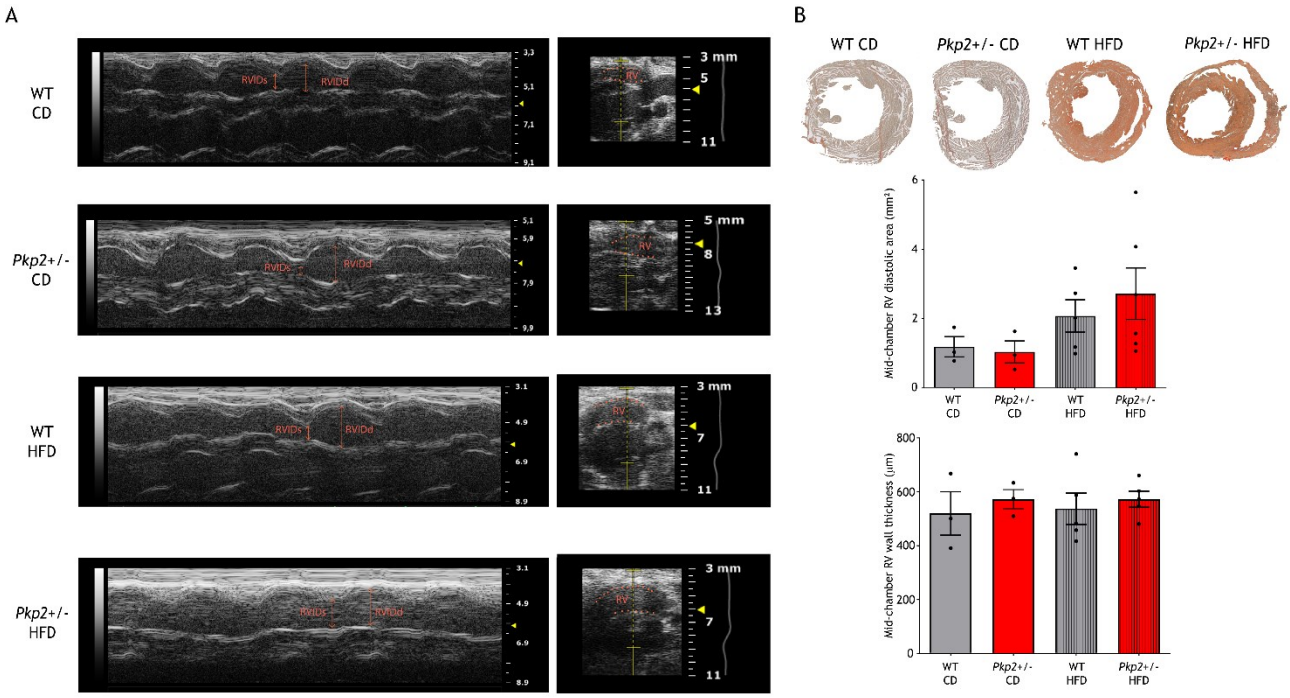

3.4 Atorvastatin administration effects on ACM manifestation in HFD-fed *Pkp2*+/- mice.

To evaluate the effect of the pharmacological counteraction of high oxLDL levels (447), we fed WT and *Pkp2*+/- mice a HFD supplemented with 20 mg/kg atorvastatin for 3 months. In both strains, lower cholesterol was measured in HFD+atorvastatin in fractions 29-32, representing VLDL-IDL-LDL ($n = 8$; $p < 0.001$; **Figure R21A**). Moreover, in parallel with plasma oxLDL concentration reduction ($n = 6$ vs. $n = 8$; oxLDL nmol/ml HFD 1.29 ± 0.11 vs. HFD+atorva 0.56 ± 0.05; $p = 0.009$; **Figure R21B**), we observed lower cardiac lipid accumulation ($n = 10$ vs. $n = 9$; % ORO positive area *Pkp2*+/- HFD 1.04 ± 0.24 vs. *Pkp2*+/- HFD+atorva 0.02 ± 0.001; $p = 0.001$; **Figure R21C**), and a dramatic decrease of PPARγ expression levels ($n = 10$ vs. $n = 9$; PPARγ densitometric sum/nuclei number *Pkp2*+/- HFD 6.62 ± 1.22 vs. *Pkp2*+/- HFD+atorva 0.01 ± 0.005; $p < 0.0001$; **Figure R21D**). MDA expression also significantly decreased ($n = 10$ vs. $n = 9$; MDA relative densitometric sum/nuclei number *Pkp2*+/- HFD 4.42 ± 0.88 vs. *Pkp2*+/- HFD+atorva 0.008 ± 0.003; $p = 0.0001$; **Figure R21E**) as well as CD36 levels ($n = 10$ vs. $n = 9$; CD36 relative densitometric sum/nuclei number *Pkp2*+/- HFD 7.48 ± 1.88 vs. *Pkp2*+/- HFD+atorva 0.03 ± 0.01; $p = 0.001$; **Figure R21F**).Moreover, RV EF improved in *Pkp2*+/- HFD+atorva respect to HFD only ($n = 10$ vs. $n = 9$; % RV EF *Pkp2*+/- HFD 73.81 ± 3.43 vs. *Pkp2*+/- HFD+atorva 83.93 ± 1.86; $p = 0.04$; **Figure R21G**).

Figure R21. HFD plus atorvastatin prevented ACM phenotype in *Pkp2*+/- mice.

A) Left panel: plasma total cholesterol in the different lipoprotein fractions of wild type (WT) and plakophilin2 heterozygous knockout (*Pkp2*+/-) mice fed a 3-month high fat diet (HFD; blue line) or a 3-month HFD+atorvastatin (red line). Right panel: plasma total cholesterol quantity in fractions 29-32, corresponding to low, very low and intermediate density lipoproteins, of WT and *Pkp2*+/- mice fed a 3-month HFD (blue line) or a 3-month HFD+atorvastatin (red line). *** $p < 0.001$ (Mann-Whitney test).

B) oxLDL plasma concentration in WT and *Pkp2*+/- mouse samples, fed for 3 months a HFD plus atorvastatin (n = 8). For comparison, plasma concentration of oxLDL in WT and *Pkp2*+/- mice samples fed HFD for 3 months is shown (as in **Figure R18B**). ** $p < 0.01$ (Two-tailed Student's t-test).

C) Left panel: representative images of Oil Red O (ORO) staining of cardiac sections of *Pkp2*+/- mice, fed 3-month HFD plus atorvastatin. Right panel: quantification of the percentage of ORO positive area (n = 9). For comparison, quantification of ORO positive area of cardiac sections of *Pkp2*+/- mice fed a HFD for 3 months is shown (as in **Figure R18C**). * $p < 0.05$ (Two-tailed Student's t-test).

D) Representative images of PPARγ immunostaining (green) on cardiac sections of *Pkp2*+/- mice fed a 3-month HFD plus atorvastatin (n = 9). Nuclei are counterstained with Hoechst 33342 (blue). For comparison, quantification of PPARγ signal of cardiac sections of *Pkp2*+/- mice fed a HFD for 3 months (as in **Figure R18D**) is shown. *** $p < 0.001$ (Two-tailed Student's t-test).

E) Representative images of malondialdehyde (MDA) immunostaining (green) on cardiac sections of *Pkp2*+/- mice fed a 3-month HFD plus atorvastatin (n = 9). Nuclei are counterstained with Hoechst 33342 (blue). For comparison, quantification of MDA immunostaining of cardiac sections of *Pkp2*+/- mice fed a HFD for 3 months (as in **Figure R18E**) is shown. *** $p < 0.001$ (Two-tailed Student's t-test).

F) Representative images of CD36 immunostaining (green) on cardiac sections of *Pkp2*+/- mice fed for 3 months a HFD plus atorvastatin (n = 9). Nuclei are counterstained with Hoechst 33342 (blue). For comparison, quantification of CD36 immunostaining of cardiac sections of *Pkp2*+/- mice fed a HFD for 3 months is shown (as in **Figure R18F**). ** $p < 0.01$ (Two-tailed Student's t-test).

G) Right ventricular ejection fraction (RV EF) percentage of *Pkp2*+/- mice during (left panel) and after (right panel) 3-month HFD plus atorvastatin feeding (n = 9). For comparison RV EF of *Pkp2*+/- mice fed a HFD is shown (as in **Figure R18G**). * p < 0.05 (Two-tailed Student's t-test).

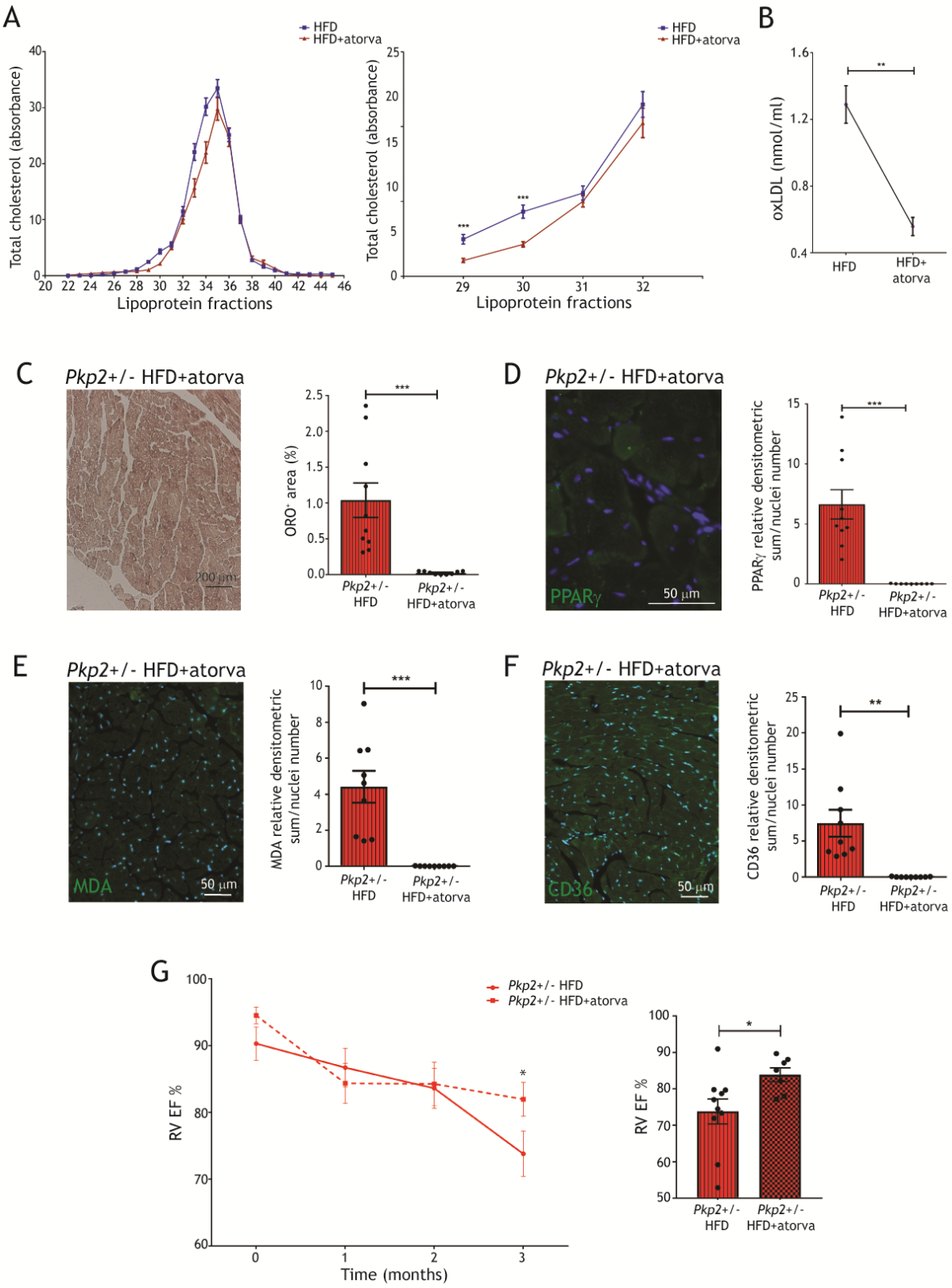

4. Elevated oxLDL plasma concentrations are associated with structural and functional impairment, and arrhythmic burden in ACM patients

Since *in vitro* and *in vivo* data demonstrated the role of oxLDL in ACM phenotype worsening, we retrospectively investigated the association between plasmatic oxLDL levels and structural, functional and arrhythmic features in the whole cohort of our ACM population. A ROC curve analysis identified the cut-off value of 86 ng/ml which best discriminates ACM patients vs. HC (n = 36 each; 63.41% sensitivity and 65.85% specificity; **Figure R22A**). Based on this cut-off value, we subdivided our ACM patient cohort in two groups (n = 26 < 86ng/ml oxLDL and n = 41 > 86ng/ml oxLDL). In the sub-cohort of ACM patients for which CMR was performed in our hospital, we quantified the mass of ventricular fat infiltration. Strikingly, patients with oxLDL plasma concentrations above the cut-off showed significantly higher myocardial fat infiltration (n = 14 vs. n = 25; fat infiltration mass < oxLDL 2.27 ± 1.35 vs. > oxLDL 15.32 ± 4.62 grams; p = 0.04; **Figure R22B**). Beside greater structural impairment, the group with higher oxLDL also showed a higher frequency of RV dysfunction defined as in (448) (n = 26 vs. n = 41; % of patients with RV dysfunction < oxLDL 26.9% (7/26) vs. > oxLDL 53.7% (22/41); p = 0.04; **Figure R22C**), biventricular dysfunction (n = 26 vs. n = 41; % of patients with biventricular dysfunction < oxLDL 0% (0/26) vs. > oxLDL 19.5% (8/41); p = 0.02; **Figure R22D**), and RV wall motion abnormalities (n = 26 vs. n = 41; % RV wall motion abnormalities < oxLDL 38.4% (19/26) vs. > oxLDL 70.7% (29/41); p = 0.01; **Figure R22E**). Accordingly, RV ejection fraction (EF) was significantly reduced in patients with higher levels of oxLDL (n = 23 vs. n = 39; % RV EF < oxLDL 50.71 ± 2.40 vs. > oxLDL 44.5 ± 1.72; p = 0.04; **Figure R22F**), confirming that higher oxLDL is associated with functional impairment.

Accordingly, stratifying ACM patients for CMR-based RV dysfunction task force criteria (163), the patients who have a greater influence in determining the difference in oxLDL values with controls are those with RV dysfunction (n = 36 vs. n = 28 vs. n = 28; oxLDL HC 66.74 ± 5.79 vs. no RV dysfunction 185.5 ± 38.68 vs. RV dysfunction 315.0 ± 88.42 ng/ml; HC vs. RV dysfunction p = 0.0004; **Figure R22G**).

A Kaplan Meier analysis revealed that ACM patient survival free from Major Arrhythmic Events (MAE) over 5-year follow up was significantly higher in the subset of patients with low amount of oxLDL (n = 67; mean

follow up 7.99 ± 0.39 years; $p < 0.0001$; **Figure R22H**), demonstrating the association between oxLDL levels and the occurrence of MAE in ACM patients.

Figure R22. Plasmatic oxLDL cut-off value of 86 ng/ml defines two patients' subpopulation with different severity of ACM phenotypes.

A) ROC curve shows accuracy of plasmatic oxLDL concentration in discriminating arrhythmogenic cardiomyopathy (ACM) vs. healthy control (HC) subjects (data as in Figure R1A). The red dot indicates the oxLDL value (86 ng/ml) which has the best sensitivity and specificity in discriminating the two populations. This value was used to divide the whole ACM cohort in two subpopulations.

B) Left panels: representative images of two cases of ACM in Steady State Free Precession (SSFP) sequences at cardiac magnetic resonance. On the left, a case with regional bulging of the right ventricular (RV) wall without fat infiltration and oxLDL levels below the cut-off; on the right, a case with fat infiltration in the RV wall (arrowheads) and oxLDL levels above the cut-off. Right panel: quantification of the myocardial fat mass of the two ACM subpopulations (above or below the cut-off) whose CMR was available for re-analysis (n = 14 oxLDL < 86 ng/ml vs. n = 25 oxLDL > 86 ng/ml; * $p < 0.05$; Two-tailed Student's *t*-test).

C) Frequency of patients showing RV dysfunction (defined as in (448)) in the two ACM cohort subgroups (n = 26 oxLDL < 86 ng/ml vs. n = 41 oxLDL > 86 ng/ml; * $p < 0.05$; Fisher's exact test).

D) Frequency of patients showing biventricular dysfunctions in the two ACM cohort subgroups (n = 26 oxLDL < 86 ng/ml vs. n = 41 oxLDL > 86 ng/ml; * $p < 0.05$; Fisher's exact test).

E) Frequency of patients showing RV wall motion abnormalities in the two ACM cohort subgroups (n = 26 oxLDL < 86 ng/ml vs. n = 41 oxLDL > 86 ng/ml; * $p < 0.05$; Fisher's exact test).

F) RV ejection fraction percentage of the patients classified in the two ACM cohort subgroups (n = 23 oxLDL < 86 ng/ml vs. n = 39 oxLDL > 86 ng/ml; * $p < 0.05$; Two-tailed Student's *t*-test).

G) oxLDL concentrations in healthy controls (HC) and arrhythmogenic cardiomyopathy (ACM) patients stratified for CMR-based RV dysfunction task force criteria (163) (n = 36 HC vs. n = 28 ACM without RV dysfunction vs. n = 28 ACM with RV dysfunction; *** $p < 0.001$; One-way ANOVA).

H) Kaplan-Meier analysis of actual MAE free survival of patient belonging to the two ACM cohort subgroups in the first 5-year follow-up (n = 26 oxLDL < 86 ng/ml vs. n = 41 oxLDL > 86 ng/ml; p < 0.0001; Log-rank (Mantel-Cox) Test).

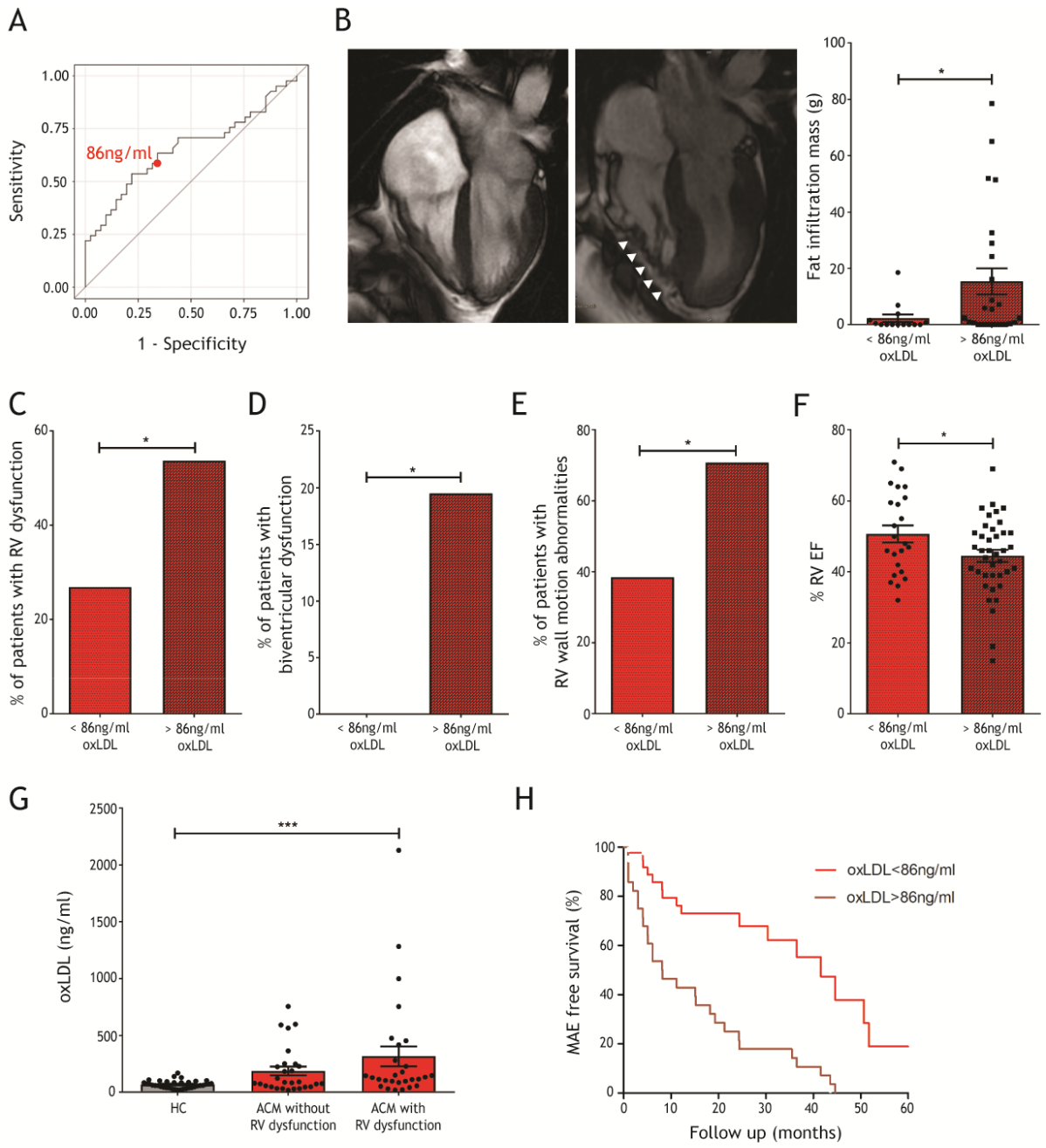

5. SEARCH (EffectS of n-acEtylcysteine on ARrhythmogenIc Cardiomyopathy pHenotypes) clinical trial

Based on the results obtained on patients', *in vitro* and *in vivo* studies, we designed and submitted to AIFA (Agenzia Italiana del Farmaco) a Phase II clinical trial to test if oxidative stress reduction may be achieved in ACM patients and may contribute to attenuate the ventricular predisposition to accumulate fat, through a drug-repositioning trial evaluating the safety and effectiveness of NAC in ACM. The overview of the SEARCH (EffectS of n-acEtylcysteine on ARrhythmogenIc Cardiomyopathy pHenotypes) study flow-chart is presented in **Figure R23**.

This would be a 3-year national, bi-center, prospective, randomized, double-blind, placebo-controlled Phase II study. The study would entail the screening of patients in the context of hospitalization for ACM diagnostic purposes. The inclusion criteria comprise:

1. Diagnosis of ACM based on Task Force Criteria 2010 (163),

2. oxLDL plasma levels ≥ 86 ng/ml (cut-off value calculated by the ROC curve analysis reported in **Figure R22A**),

3. Age ≥ 18 years,

4. A signed consent form.

The exclusion criteria include:

1. Contraindication to NAC or to any of the excipients,

2. Concomitant antioxidant drugs intake,

3. Previous or current documented history of peptic ulcer,

4. Phenylketonuria,

5. Known intolerance to histamine,

6. Pregnancy or breastfeeding,

7. Enrolment in another study that may interfere with this study.

24 patients will be enrolled and randomized in a 1:1 ratio to 600 mg twice daily of effervescent tablets of

NAC (Group A; n=12) or placebo (Group B; n=12) for 12 months.

The primary objectives of this study would be to evaluate whether NAC treatment is safe in ACM patients and superior to placebo in reducing systemic oxidative stress status in terms of oxLDL plasma levels. The secondary efficacy objectives would be to evaluate whether NAC treatment is effective in reducing lipid accumulation in C-MSC and is associated with clinical and functional preservation in terms of arrhythmia profile, cardiac function and fibro-fatty substitution. Outpatient visits will be scheduled at 3, 6 and 9 months after randomization to perform safety and tolerability assessment and to monitor adverse events, serious adverse events and suspected unexpected serious adverse events. In addition, patients will be contacted by telephone or email monthly to monitor treatment adherence. After 12 months, both groups will be re-hospitalized to perform safety and efficacy assessment including: i) oxLDL plasma measurement, ii) cardiac magnetic resonance (CMR), iii) electroanatomical mapping, iv) endomyocardial biopsy, v) blood tests.

This study is aimed to demonstrate with a precision medicine approach that oral NAC treatment is safe and effective to reduce the plasma levels of oxLDL after 12 months in those ACM patients who show elevated oxidative stress. In particular, NAC is expected to be able to reduce oxLDL concentrations at least by 60% with respect to baseline, in line with a previous randomized controlled trial by Tepel et al. demonstrating a decrease of oxLDL plasma levels after prolonged NAC treatment using the same regimen of this study (449). In addition, we expect to correlate reduction of oxLDL levels with right ventricular C-MSC lipid accumulation, according to our *in vitro* studies, in which NAC treatment was able to strongly reduce C-MSC lipid accumulation (**Figure R10**). Patient functional and electrical disease hallmarks will be also investigated in relation to treatment, since we demonstrated the association between higher concentrations of plasma oxLDL and structural and functional impairments, and arrhythmic risk (**Figure R22**). Thus, NAC-induced oxLDL plasma reduction is expected to have an effect in avoiding substrate degeneration progression in ACM patients.

Figure R23. Overview of the SEARCH (EffectS of n-acEtylcysteine on ARrhythmogenIc Cardiomyopathy pHenotypes) study flow-chart.

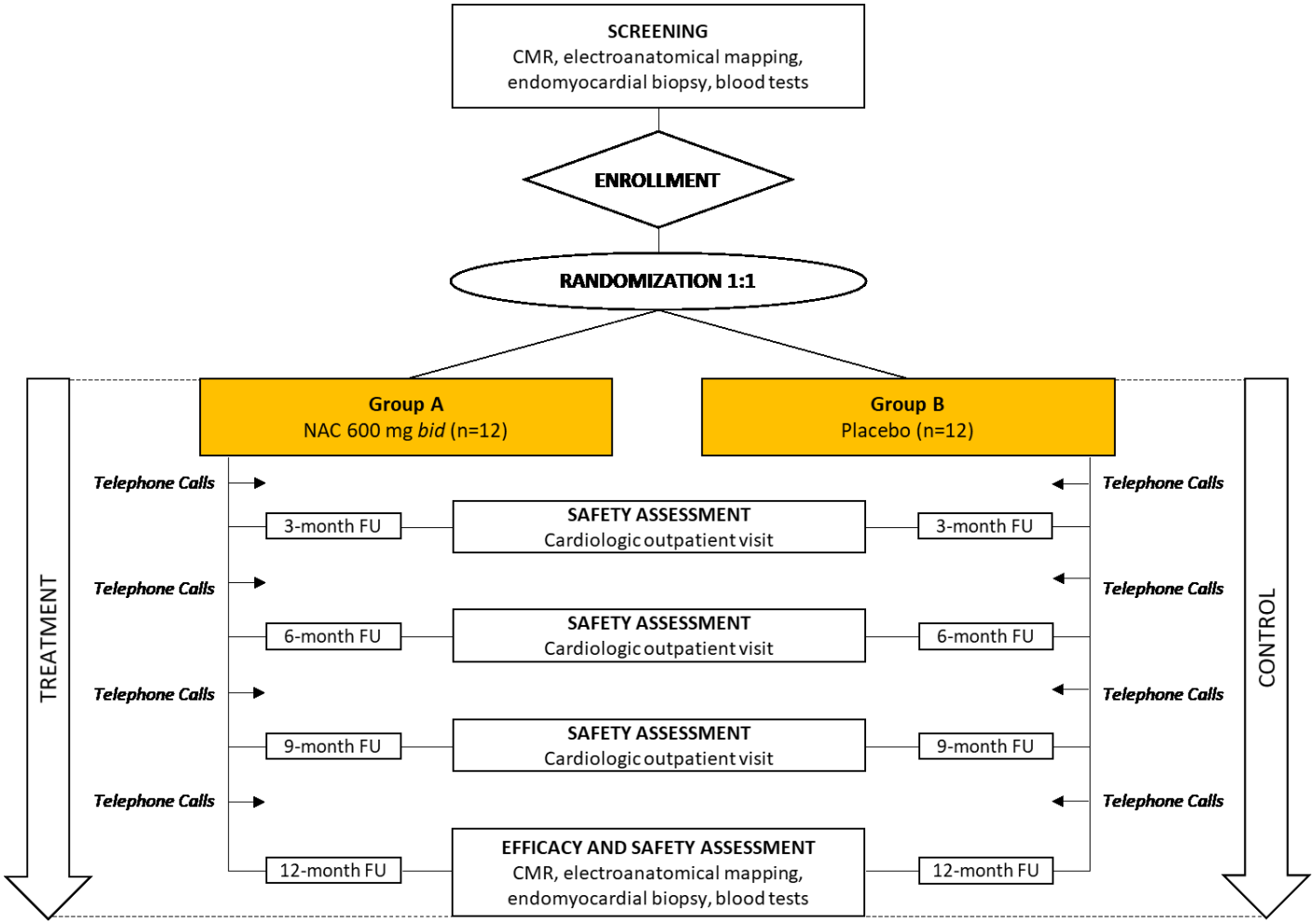

Discussion

Incomplete penetrance and variable expressivity characterize ACM, but the current information about its genetic basis is not sufficient to explain disease phenotypic variability (1) (74) (75) (76) (77). Few genetic and environmental cofactors are known to play a modifying role in ACM context: compound and digenic heterozygosity (39) (65) (71) (80) (81), modifier genes (84), physical exercise (88), β-adrenergic signalling (105) (106), sexual hormones (115), and inflammation (120). None of them is directly associated with ACM cardiac adipose substitution modulation. Indeed, to date, no adipogenesis cofactors have been identified, and no drugs are available to counteract this process. However, the adipose substitution in the heart of ACM patients alters the mechanical properties of the myocardium, thus impairing its functionality in terms of adequate contraction/relaxation, and the cardiac conduction properties, creating re-entry mechanisms, thus worsening the arrhythmic phenotype (450) (451). The understanding of the risk factors that predispose to a great amount of cardiac adipose deposits represents a key clinical need for ACM patients.

The master regulator of adipogenesis is PPARγ, known to be highly expressed in ACM hearts due to genetically-dependent Wnt pathway impairment (133). PPARγ is a ligand-activated transcription factor and regulates several physiological processes, including cellular development and differentiation, glucose and cholesterol metabolism, and fatty acid storage (452) (453). For this reason, a direct pharmacological inhibition of PPARγ could be deleterious, also in ACM patients characterized by a pathological higher expression of this receptor, and accordingly no drugs are used in the clinical practice to this purpose. Conversely, some upstream activators of PPARγ can be pharmacologically targeted.

oxLDL are PPARγ activators and their effects on lipid accumulation are well described in atherosclerosis during foam cell formation. Briefly, oxLDL accumulate in the *intima* of arteries, leading endothelial cells to recruit monocytes. In the subendothelial space, monocytes differentiate into macrophages, which internalize oxLDL, through specific receptors, as CD36, becoming lipid-laden foam cells. Since high intracellular concentrations of lipids can provoke lipotoxicity (454), lipid homeostasis-related transcription factors, as PPARγ, are upregulated by oxLDL and their components, such as 13HODE, in a dose-dependent manner (455). A feed forward loop is then created, leading to the transcriptional increase of PPARγ itself and CD36, facilitating a further internalization of oxLDL (368) (369). Intriguingly, CD36 can directly activate PPARγ, reinforcing this

positive feedback loop (456). In murine models, PPARγ deletion prompted atherosclerosis development (457), confirming the essential role of this transcription factor in mediating intracellular lipid storage.

Several hints link ACM pathogenesis to oxLDL. Most of ACM patients are athletes or very active people, and intense physical exercise can induce ROS overproduction, increasing LDL susceptibility to oxidation, and 13HODE release (384) (385) (386) (390). In other contexts, oxLDL and 13HODE have been associated with lipid accumulation (240) (392), apoptosis (393) (394) (395), fibrotic remodelling (398) (399), and inflammation (403) (404) (405). All these features are typical ACM manifestations, thus the role of oxLDL and 13HODE deserved to be explored in this context. To this purpose, the aim of the present project was to assess the potential involvement of oxLDL in ACM pathogenesis, with patients', *in vitro* and *in vivo* studies, evaluating the contribution of oxLDL/CD36/PPARγ circuitry as ACM adipogenesis co-factor.

Starting from the characterization of our ACM patient cohort, we found higher plasma concentration of oxLDL and its component 13HODE, as compared to HC. No differences in total and LDL cholesterol were detected, indicating no imbalance in the plasma lipid profile of ACM patients, but rather a crucial role of oxidative stress. Interestingly, oxLDL concentration in ACM patients' plasma is not a mere consequence of the ACM-causative genetic defect. No differences in oxLDL levels between ACM patients with and without a mutation in known ACM genes have been found. In addition, oxLDL plasma levels are higher in clinically affected ACM patients than in their unaffected relatives, carriers of the same ACM-causative genetic mutation. Nevertheless, we identified variants in genes associated with oxidative stress or dyslipidemia co-segregating with the ACM phenotype, suggesting, beyond primary causative mutations, the potential influence of the genetic background on oxLDL increase. Thus, our data support the hypothesis that oxLDL are a contributory cause of phenotype worsening. However, since the number of families and individuals per family was small, these results are preliminary and need confirmation with larger cohorts. It cannot be excluded that other factors, including lifestyle and diet, may play a role in modulating oxLDL concentrations. Moreover, the contribution of protective variants in asymptomatic relatives needs to be evaluated.

In line with the increased circulating oxidative stress, ACM ventricular tissue showed considerable lipid peroxidation, indicated by MDA levels, if compared to HC cardiac samples. In other conditions, such as

myocardial infarction, cardiac oxidative stress has been reported to intensify the myocardial remodelling, worsening ventricular dysfunction (320) (458). Moreover, lipid peroxidation has been reported to provoke redox gene overexpression, intracellular calcium overload and DNA fragmentation, damaging cardiac cells (459).

In addition, the oxLDL receptor CD36 is more expressed in ACM ventricles than in HC cardiac tissues, perhaps in response to the increased concentration of plasma oxLDL, and this indicates a possible increased internalization of oxLDL into cardiac cells.

To test the effects of increased oxLDL and oxidative stress, detected in ACM plasma and ventricular samples, on cardiac adipogenesis, and unravel which mechanisms are involved, we used human C-MSC obtained from ACM and HC heart biopsies as *in vitro* model, as they subsidize ACM-driven cardiac adipogenesis and represent a reliable cell model to study pathogenic mechanisms (20) (73).

In line with elevated lipid peroxidation in ACM ventricular tissues, we described higher oxidative stress also in ACM C-MSC, without changes in their anti-oxidant capability, pointing to an unbalanced ROS production, potentially related to an impaired mitochondrial metabolism in ACM. Indeed, the transcriptome analysis of ACM C-MSC indicated the upregulation of mitochondria-associated pathways, thus, a systematic investigation on the potential mitochondrial dysfunction need to be performed (335). In addition, the structural relationship between desmosomes and mitochondria has been shown (460) (461) (462) pointing to potential direct repercussions of ACM genetic causative mutations on mitochondria structure and function.

As previously demonstrated in other cell models (133) (139), in ACM C-MSC we confirmed a higher expression of PPARγ, but we also assessed, for the first time, the increased expression of the oxLDL receptor CD36. The interdependence between this receptor and PPARγ is largely described in the literature, predominantly for cardiovascular atherogenic conditions (367) (463). Conversely, we did not obtain statistically significant differences in the expression of other oxLDL receptors, as TLR4, SR-A and LOX1, from HC cells. This result narrows the field on CD36 as a mediator of oxLDL effect in ACM.

Accordingly, we demonstrated in ACM C-MSC the existence of a linear correlation between the activation of PPARγ, with consequent lipid accumulation, and CD36 expression and function. The proposed mechanism was

confirmed by CD36 silencing, which entailed a significant reduction of lipid accumulation in ACM C-MSC, as well as decreased PPARγ levels, and by PPARγ inhibition, which led to reduced CD36 expression and function. By means of our *in vitro* model, we then demonstrated that oxLDL and 13HODE supplementation enhances ACM C-MSC adipogenic differentiation. Interestingly, ACM C-MSC susceptibility to oxLDL treatment is dependent on their genetically determined low PKP2 levels. These results are in accordance to Parhami et al., that showed oxLDL-mediated adipogenic differentiation in bone marrow-derived mesenchymal cells (392). Furthermore, 13HODE was previously administered as *in vitro* supplement to activate PPARγ in ACM hiPSC-CM carrying *PKP2* mutation (240). Our work showed in C-MSC that 13HODE and PPARγ-dependent adipogenesis is an intrinsic ACM pathogenic mechanism, involving CD36 upregulation. PPARγ agonism induces CD36 increased expression even in hiPSC-CM. Since the link between oxLDL and arrhythmias is known, we will evaluate oxLDL effects on ACM CM electrical phenotype. In addition, oxLDL action on CM apoptosis will be investigated, since our transcriptome sequencing indicated that AM+rosiglitazone treatment significantly upregulate genes involved in apoptosis, other than in lipid metabolism and sarcomere structure.

Importantly, cell exposure to the antioxidant NAC decreased not only the lipogenic phenotype mediated by 13HODE, but was also able to reduce fat accumulation and CD36/PPARγ expression to HC levels. This represents a first proof of concept for the use of drugs able to reduce oxidative stress in ACM context.

We confirmed *in vitro* findings with *in vivo* experiments by means of the *Pkp2*+/- mouse model generated by Birchmeier and coworkers (257), as *PKP2* heterozygous mutations are the most frequent in ACM patients. Notably, available ACM *in vivo* models, including the *Pkp2*+/- mouse, do not fully recapitulate the disease phenotype, showing from absence to small amount of ventricular fibro-fatty substitution, possibly due to an intrinsic protective mechanism. Since it is known that mice possess low cholesterol plasma levels (464), we hypothesized and demonstrated that a consistent increase of plasma LDL cholesterol, including the oxidized form, obtained by HFD-feeding, results in cardiac fatty substitution. This phenomenon was prevalently located in sub-epicardial regions, in line with the epicardial-endocardial gradient observed in ACM human hearts, and involved mesenchymal cells, as previously proven in human (20). In accordance with *in vitro* and patient *ex vivo* results, cardiac oxidative stress and CD36 significantly increased in mice following HFD. Importantly, HFD

treatment provoked an initial impairment of RV cardiac function, in line with the concept that substrate alterations lead to functional impairment (450).

Despite lipid accumulation were present both in the RV and LV, cardiac dysfunction spared LV probably for its thickness and physiological characteristics.

These results further confirm that mutations in ACM causative genes are necessary but not sufficient to generate an overt ACM phenotype in mice, which, when exposed to increased oxLDL levels, develop myocardial substrate alterations similar to human hearts. A possible explanation of the fat accumulation phenomenon could be the existence of a PPARγ threshold effect. Both ACM cells and mice already showed a higher PPARγ expression in basal conditions, probably secondary to PKP2 insufficiency, able to provoke Wnt pathway alterations and consequent increase of adipogenic gene expression. However, this may be not sufficient to reach the threshold leading to phenotypic evidence. The contribution of adipogenesis co-factors, such as oxLDL, could allow to reach the PPARγ activation threshold needed for phenotypic manifestation.

Our ACM murine model will be further implemented by subjecting mice to exercise, according to the protocol described in (259), since physical activity is a pejorative cofactor of ACM phenotypes (88). In addition, to strengthen our findings, we have planned to produce and characterize two murine models, by crossing *Pkp2*+/- mice with homozygous knockout mice for ApoE (*Pkp2*+/- *ApoE*-/-), to permanently raise cholesterol levels, or CD36 (*Pkp2*+/- *Cd36*-/-), to confirm the role of this receptor and the downstream activated mechanisms in ACM pathogenesis. We will test their viability, mating capability and disease phenotypes, as for cardiac adipose substitution, ventricular dysfunction and arrhythmias.

Remarkably, atorvastatin administration prevented cardiac fat accumulation and RV dysfunction in HFD-fed *Pkp2*+/- mice. To our knowledge, this is the first proof-of-concept of an etiologic pharmacologic treatment for ACM.

By means of a multilayer approach, we demonstrated, for the first time, that altered oxidized lipid metabolism and oxidative stress increase oxLDL bioavailability, which is internalized in C-MSC by CD36 receptor, thus acting, through 13HODE-mediated PPARγ activation, as a cofactor of ACM cardiac adipogenic differentiation

(Synopsis figure). This new biological axis is pharmacologically-targetable, with potential effects also on PPARγ levels and the consequent adipogenic phenotypes.

Future studies will be performed to link oxLDL contribution to ACM cardiac fibrotic remodelling and arrhythmic phenotypes, since oxidative stress involvement in these processes has been already proposed for other diseases (398) (399).

Notably, we unravelled in our ACM patients a strong association between the plasma oxLDL cut-off above 86 ng/ml and pathognomonic ACM structural and clinical features. This cut-off allowed to segregate a ACM patient population with a severe clinical phenotype in terms of fat infiltration, ventricular dysfunction and risk of major arrhythmic events in the long-term. Thus, oxLDL can be considered a new potential circulating prognostic marker in ACM (465). Unfortunately, clinical-grade methods for plasma oxLDL measurement are lacking. Since oxLDL have been proposed as a prognostic indicator also for other cardiovascular conditions (466), there is the urgent clinical need to solve this issue. Along the same line, MDA and CD36 staining in heart bioptic samples could be studied for differential diagnostic purposes as candidate indicators of ACM at tissue level.

The description of this new pathogenic pathway is relevant for the development of new therapeutic approaches. Notably, oxidative stress and oxidized lipid defects can be targeted by means of drug repositioning of available treatments, such statins (467). Remarkably, atorvastatin prevented ACM phenotype manifestation in HFD-fed *Pkp2*+/- mice. On the one hand statins would reduce LDL levels, limiting the oxidisable substrate, but they could also exert anti-oxidant and anti-inflammatory functions (468). In other studies, statin role in arrhythmias reduction has been established (469), thus we can suppose the beneficial effect of these drugs also in counteracting the arrhythmic phenotype of ACM.

Alternatively, our data may pave the way for specific CD36 receptor targeting, although no drugs are currently available in the clinical practice (470).

Since our data point mainly to the role of oxidative stress increase in ACM pathogenesis, also the potential effects of antioxidants need to be tested (471). Our clinical trial design fits in this context and will help to evaluate the safety and the efficacy of N-acetilcysteine in reducing oxLDL plasma levels in ACM patients. Based

on our data, we expected this treatment would attenuate disease progression and clinical phenotypes. The study has been conceived with a precision medicine approach, having postulated those patients with elevated oxLDL plasma levels at higher risk of disease progression, and potentially the best responders to the therapy. Although conflicting results have been obtained in clinical studies with oral anti-oxidants (472) (473) (474), NAC efficacy in oxLDL reduction has been established (449) (475) (476) (477). In addition, NAC is well tolerated orally at a chronic regimen with rare side effects.

On this basis, we deem that this study has the potential to reduce the incidence of cardiac dysfunction and sudden death, improve patients' life span as well as quality of life, and it could address the relevant unmet health issue of a young population of patients, given the dramatic consequences of ACM in young people and athletes on their prognosis. Available non-etiologic strategies (ICD implantation, electrophysiological interventional procedures, heart transplant) represent very invasive and risky solutions in such a population with a heavily affected quality of life.

In conclusion, this study is highly innovative, introducing as a new concept the potential pharmacologic modulation of the ventricular substrate phenotype, thus addressing the unmet issue of the high variability of ACM manifestation.

References

1. Hoorntje ET, Te Rijdt WP, James CA, Pilichou K, Basso C, Judge DP, et al. Arrhythmogenic cardiomyopathy: Pathology, genetics, and concepts in pathogenesis. Cardiovasc Res. 2017;113(12):1521–31.
2. van der Voorn SM, te Riele ASJM, Basso C, Calkins H, Remme CA, van Veen TAB. Arrhythmogenic cardiomyopathy: pathogenesis, pro-arrhythmic remodelling, and novel approaches for risk stratification and therapy. Cardiovasc Res. 2020;1571–84.
3. Mattesi G, Zorzi A, Corrado D, Cipriani A. Natural History of Arrhythmogenic Cardiomyopathy. J Clin Med. 2020;9(3):878.
4. Mc Rae AT, Chung MK, Asher CR. Arrhythmogenic right ventricular cardiomyopathy: a cause of sudden death in young people. Cleve Clin J Med. 2001;68(5):459–67.
5. Zorzi A, Rigato I, Pilichou K, Marra MP, Migliore F, Mazzotti E, et al. Phenotypic expression is a prerequisite for malignant arrhythmic events and sudden cardiac death in arrhythmogenic right ventricular cardiomyopathy. Europace. 2016;18(7):1086–94.
6. Bhonsale A, Groeneweg JA, James CA, Dooijes D, Tichnell C, Jongbloed JDH, et al. Impact of genotype on clinical course in arrhythmogenic right ventricular dysplasia/cardiomyopathy-associated mutation carriers. Eur Heart J. 2015;36(14):847–55.
7. Bhonsale A, te Riele ASJM, Sawant AC, Groeneweg JA, James CA, Murray B, et al. Cardiac phenotype and long-term prognosis of arrhythmogenic right ventricular cardiomyopathy/dysplasia patients with late presentation. Hear Rhythm. 2017;14(6):883–91.
8. Rizzo S, Lodder EM, Verkerk AO, Wolswinkel R, Beekman L, Pilichou K, et al. Intercalated disc abnormalities, reduced Na+ current density, and conduction slowing in desmoglein-2 mutant mice prior to cardiomyopathic changes. Cardiovasc Res. 2012;95(4):409–18.
9. Pilichou K, Remme CA, Basso C, Campian ME, Rizzo S, Barnett P, et al. Myocyte necrosis underlies progressive myocardial dystrophy in mouse dsg2-related arrhythmogenic right ventricular cardiomyopathy. J Exp Med. 2009;206(8):1787–802.
10. Bagnall RD, Weintraub RG, Ingles J, Duflou J, Yeates L, Lam L, et al. A prospective study of sudden cardiac

death among children and young adults. N Engl J Med. 2016;374(25):2441–52.

11. Migliore F, Zorzi A, Silvano M, Bevilacqua M, Leoni L, Marra MP, et al. Prognostic value of endocardial voltage mapping in patients with arrhythmogenic right ventricular cardiomyopathy/dysplasia. Circ Arrhythmia Electrophysiol. 2013;6(1):167–76.

12. Valente M, Calabrese F, Thiene G, Angelini A, Basso C, Nava A, et al. In vivo evidence of apoptosis in arrhythmogenic right ventricular cardiomyopathy. Am J Pathol. 1998;152(2):479–84.

13. Basso C, Thiene G, Corrado D, Angelini A, Nava A, Valente M. Arrhythmogenic Right Ventricular Cardiomyopathy Dysplasia, Dystrophy, or Myocarditis? Circulation. 1996;94:983–91.

14. Mallat Z, Tedgui A, Fontaliran F, Frank R, Durigon M, Fontaine G. Evidence of apoptosis in arrhythmogenic right ventricular dysplasia. N Engl J Med. 1996;335(16):1190–6.

15. Fornes P, Ratel S, Lecomte D. Pathology of arrhythmogenic right ventricular cardiomyopathy/dysplasia--an autopsy study of 20 forensic cases. J Forensic Sci. 1998;43(4):777–83.

16. Te Riele ASJM, James CA, Philips B, Rastegar N, Bhonsale A, Groeneweg JA, et al. Mutation-positive arrhythmogenic right ventricular dysplasia/ cardiomyopathy: The triangle of dysplasia displaced. J Cardiovasc Electrophysiol. 2013;24(12):1311–20.

17. Sen-Chowdhry S, Syrris P, Prasad SK, Hughes SE, Merrifield R, Ward D, et al. Left-Dominant Arrhythmogenic Cardiomyopathy. An Under-Recognized Clinical Entity. J Am Coll Cardiol. 2008;52(25):2175–87.

18. Basso C, Bauce B, Corrado D, Thiene G. Pathophysiology of arrhythmogenic cardiomyopathy. Nat Rev Cardiol. 2012;9:223–33.

19. Corrado D, Basso C, Thiene G, McKenna WJ, Davies MJ, Fontaliran F, et al. Spectrum of clinicopathologic manifestations of arrhythmogenic right ventricular cardiomyopathy/dysplasia: A multicenter study. J Am Coll Cardiol. 1997;30(6):1512–20.

20. Sommariva E, Brambilla S, Carbucicchio C, Gambini E, Meraviglia V, Dello Russo A, et al. Cardiac mesenchymal stromal cells are a source of adipocytes in arrhythmogenic cardiomyopathy. Eur Heart J. 2016;57(23):1835–46.

21. Stadiotti I, Piacentini L, Vavassori C, Chiesa M, Scopece A, Guarino A, et al. Human Cardiac Mesenchymal Stromal Cells From Right and Left Ventricles Display Differences in Number, Function, and Transcriptomic Profile. Front Physiol. 2020;11(June).

22. Maione AS, Pilato CA, Casella M, Gasperetti A, Stadiotti I, Pompilio G, et al. Fibrosis in Arrhythmogenic Cardiomyopathy: The Phantom Thread in the Fibro-Adipose Tissue. Front Physiol. 2020;11(April):1–11.

23. Pilichou K, Thiene G, Bauce B, Rigato I, Lazzarini E, Migliore F, et al. Arrhythmogenic cardiomyopathy. Orphanet J Rare Dis. 2016;11(1):1–17.

24. Campuzano O, Alcalde M, Berne P, Castro V, Guzzo G, Iglesias A, et al. Genetic testing of candidate genes in arrhythmogenic right ventricular cardiomyopathy/dysplasia. Eur J Med Genet. 2012;55(4):225–34.

25. Marcus FI, Fontaine GH, Guiraudon G, Frank R, Laurenceau JL, Malergue C, et al. Right ventricular dysplasia: A report of 24 adult cases. Ann Noninvasive Electrocardiol. 1999;4(1):97–111.

26. Paul M, Schulze-Bahr E. Arrhythmogenic right ventricular cardiomyopathy: Evolving from unique clinical features to a complex pathophysiological concept. Herz. 2020;45(3):243–51.

27. Okabe M, Fukuda K, Nakashima Y, Arakawa K, Kikuchi M. An isolated left ventricular lesion associated with left ventricular tachycardia--arrhythmogenic 'left' ventricular dysplasia? Jpn Circ J. 1995;59:49–54.

28. Suzuki H, Sumiyoshi M, Kawai S, Takagi A, Wada A, Nakazato Y, et al. Arrhythmogenic right ventricular cardiomyopathy with an initial manifestation of severe left ventricular impairment and normal contraction of the right ventricle. Vol. 64, Japanese Circulation Journal. 2000. p. 209–13.

29. Sen-Chowdhry S, Syrris P, Ward D, Asimaki A, Sevdalis E, McKenna WJ. Clinical and genetic characterization of families with arrhythmogenic right ventricular dysplasia/cardiomyopathy provides novel insights into patterns of disease expression. Circulation. 2007;115(13):1710–20.

30. Sen-Chowdhry S, Prasad SK, Syrris P, Wage R, Ward D, Merrifield R, et al. Cardiovascular Magnetic Resonance in Arrhythmogenic Right Ventricular Cardiomyopathy Revisited. Comparison With Task Force Criteria and Genotype. J Am Coll Cardiol. 2006;48(10):2132–40.

31. Stevens TL, Wallace MJ, El Refaey M, Roberts JD, Koenig SN, Mohler PJ. Arrhythmogenic Cardiomyopathy: Molecular Insights for Improved Therapeutic Design. J Cardiovasc Dev Dis. 2020;7(2):21.

32. Protonotarios N, Tsatsopoulou A. Naxos disease and Carvajal syndrome: Cardiocutaneous disorders that highlight the pathogenesis and broaden the spectrum of arrhythmogenic right ventricular cardiomyopathy. Cardiovasc Pathol. 2004;13(4):185–94.

33. McKoy G, Protonotarios N, Crosby A, Tsatsopoulou A, Anastasakis A, Coonar A, et al. Identification of a deletion in plakoglobin in arrhythmogenic right ventricular cardiomyopathy with palmoplantar keratoderma and woolly hair (Naxos disease). Lancet. 2000;355(9221):2119–24.

34. Groeneweg JA, van der Heijden JF, Dooijes D, van Veen TAB, van Tintelen JP, Hauer RN. Arrhythmogenic cardiomyopathy: Diagnosis, genetic background, and risk management. Netherlands Hear J. 2014;22(7–8):316–25.

35. Groeneweg JA, Bhonsale A, James CA, Te Riele AS, Dooijes D, Tichnell C, et al. Clinical Presentation, Long-Term Follow-Up, and Outcomes of 1001 Arrhythmogenic Right Ventricular Dysplasia/Cardiomyopathy Patients and Family Members. Circ Cardiovasc Genet. 2015;8(3):437–46.

36. Garrod D, Chidgey M. Desmosome structure, composition and function. Biochim Biophys Acta - Biomembr. 2008;1778(3):572–87.

37. Dubash AD, Green KJ. Desmosomes. Curr Biol. 2011;21(14):529–31.

38. Matthes SA, Taffet S, Delmar M. Plakophilin-2 and the migration, differentiation and transformation of cells derived from the epicardium of neonatal rat hearts. Cell Commun Adhes. 2011;18(4):73–84.

39. Lazzarini E, Jongbloed JDH, Pilichou K, Thiene G, Basso C, Bikker H, et al. The ARVD/C genetic variants database: 2014 update. Hum Mutat. 2015;36(4):403–10.

40. van Lint FHM, Murray B, Tichnell C, Zwart R, Amat N, Lekanne Deprez RH, et al. Arrhythmogenic Right Ventricular Cardiomyopathy-Associated Desmosomal Variants Are Rarely De Novo. Circ Genomic Precis Med. 2019;12(8):e002467.

41. Fressart V, Duthoit G, Donal E, Probst V, Deharo JC, Chevalier P, et al. Desmosomal gene analysis in

arrhythmogenic right ventricular dysplasia/cardiomyopathy: Spectrum of mutations and clinical impact in practice. Europace. 2010;12(6):861–8.

42. Bao JR, Wang JZ, Yao Y, Wang YL, Fan XH, Sun K, et al. Screening of pathogenic genes in Chinese patients with arrhythmogenic right ventricular cardiomyopathy. Chin Med J (Engl). 2013;126(22):4238–41.

43. Kapplinger JD, Landstrom AP, Salisbury BA, Callis TE, Pollevick GD, Tester DJ, et al. Distinguishing arrhythmogenic right ventricular cardiomyopathy/dysplasia- associated mutations from background genetic noise. J Am Coll Cardiol. 2011;57(23):2317–27.

44. Cerrone M, Montnach J, Lin X, Zhao YT, Zhang M, Agullo-Pascual E, et al. Plakophilin-2 is required for transcription of genes that control calcium cycling and cardiac rhythm. Nat Commun. 2017;8(1).

45. Kim JC, Pérez-Hernández M, Alvarado FJ, Maurya SR, Montnach J, Yin Y, et al. Disruption of Ca2+i Homeostasis and Connexin 43 Hemichannel Function in the Right Ventricle Precedes Overt Arrhythmogenic Cardiomyopathy in Plakophilin-2-Deficient Mice. Circulation. 2019;140(12):1015–30.

46. Bass-Zubek AE, Hobbs RP, Amargo E V., Garcia NJ, Hsieh SN, Chen X, et al. Plakophilin 2: A critical scaffold for PKCα that regulates intercellular junction assembly. J Cell Biol. 2008;181(4):605–13.

47. Mertens C, Hofmann I, Wang Z, Teichmann M, Chong SS, Schnölzer M, et al. Nuclear particles containing RNA polymerase III complexes associated with the junctional plaque protein plakophilin 2. Proc Natl Acad Sci U S A. 2001;98(14):7795–800.

48. Patel DM, Dubash AD, Kreitzer G, Green KJ. Disease mutations in desmoplakin inhibit Cx43 membrane targeting mediated by desmoplakin-EB1 interactions. J Cell Biol. 2014;206(6):779–97.

49. Kam CY, Dubash AD, Magistrati E, Polo S, Satchell KJF, Sheikh F, et al. Desmoplakin maintains gap junctions by inhibiting Ras/MAPK and lysosomal degradation of connexin-43. J Cell Biol. 2018;217(9):3219–35.

50. Rampazzo A, Calore M, Van Hengel J, Van Roy F. Intercalated discs and arrhythmogenic cardiomyopathy. Circ Cardiovasc Genet. 2014;7(6):930–40.

51. Van Hengel J, Calore M, Bauce B, Dazzo E, Mazzotti E, De Bortoli M, et al. Mutations in the area composita protein at-catenin are associated with arrhythmogenic right ventricular cardiomyopathy.

Eur Heart J. 2013;34(3):201–10.

52. Mayosi BM, Fish M, Shaboodien G, Mastantuono E, Kraus S, Wieland T, et al. Identification of Cadherin 2 (CDH2) Mutations in Arrhythmogenic Right Ventricular Cardiomyopathy. Circ Cardiovasc Genet. 2017;10(2).

53. De Bortoli M, Postma A V., Poloni G, Calore M, Minervini G, Mazzotti E, et al. Whole-Exome Sequencing Identifies Pathogenic Variants in TJP1 Gene Associated With Arrhythmogenic Cardiomyopathy. Circ Genomic Precis Med. 2018;11(10):e002123.

54. Te Riele ASJM, Agullo-Pascual E, James CA, Leo-Macias A, Cerrone M, Zhang M, et al. Multilevel analyses of SCN5A mutations in arrhythmogenic right ventricular dysplasia/cardiomyopathy suggest non-canonical mechanisms for disease pathogenesis. Cardiovasc Res. 2017;113(1):102–11.

55. Baskin B, Skinner JR, Sanatani S, Terespolsky D, Krahn AD, Ray PN, et al. TMEM43 mutations associated with arrhythmogenic right ventricular cardiomyopathy in non-Newfoundland populations. Hum Genet. 2013;132(11):1245–52.

56. Tiso N, Stephan DA, Nava A, Bagattin A, Devaney JM, Stanchi F, et al. Identification of mutations in the cardiac ryanodine receptor gene in families affected with arrhythmogenic right ventricular cardiomyopathy type 2 (ARVD2). Hum Mol Genet. 2001;10(3):189–94.

57. van der Zwaag PA, van Rijsingen IAW, de Ruiter R, Nannenberg EA, Groeneweg JA, Post JG, et al. Recurrent and founder mutations in the Netherlands-Phospholamban p.Arg14del mutation causes arrhythmogenic cardiomyopathy. Netherlands Hear J. 2013;21(6):286–93.

58. Taylor M, Graw S, Sinagra G, Barnes C, Slavov D, Brun F, et al. Genetic variation in titin in arrhythmogenic right ventricular cardiomyopathy-overlap syndromes. Circulation. 2011;124(8):876–85.

59. Quarta G, Syrris P, Ashworth M, Jenkins S, Zuborne Alapi K, Morgan J, et al. Mutations in the Lamin A/C gene mimic arrhythmogenic right ventricular cardiomyopathy. Eur Heart J. 2012;33(9):1128–36.

60. Beffagna G, Occhi G, Nava A, Vitiello L, Ditadi A, Basso C, et al. Regulatory mutations in transforming growth factor-β3 gene cause arrhythmogenic right ventricular cardiomyopathy type 1. Cardiovasc Res.

2005;65(2):366–73.

61. van Tintelen JP, Van Gelder IC, Asimaki A, Suurmeijer AJH, Wiesfeld ACP, Jongbloed JDH, et al. Severe cardiac phenotype with right ventricular predominance in a large cohort of patients with a single missense mutation in the DES gene. Hear Rhythm. 2009;6(11):1574–83.

62. Hall CL, Akhtar MM, Sabater-Molina M, Futema M, Asimaki A, Protonotarios A, et al. Filamin C variants are associated with a distinctive clinical and immunohistochemical arrhythmogenic cardiomyopathy phenotype. Int J Cardiol. 2020;307:101–8.

63. Cerrone M, Remme CA, Tadros R, Bezzina CR, Delmar M. Beyond the one gene-one disease paradigm complex genetics and pleiotropy in inheritable cardiac disorders. Circulation. 2019;140(7):595–610.

64. Bennett RG, Haqqani HM, Berruezo A, Della Bella P, Marchlinski FE, Hsu CJ, et al. Arrhythmogenic Cardiomyopathy in 2018–2019: ARVC/ALVC or Both? Hear Lung Circ. 2019;28(1):164–77.

65. Xu T, Yang Z, Vatta M, Rampazzo A, Beffagna G, Pillichou K, et al. Compound and Digenic Heterozygosity Contributes to Arrhythmogenic Right Ventricular Cardiomyopathy. J Am Coll Cardiol. 2010;55(6):587–97.

66. König E, Volpato CB, Motta BM, Blankenburg H, Picard A, Pramstaller P, et al. Exploring digenic inheritance in arrhythmogenic cardiomyopathy. BMC Med Genet. 2017;18(1):1–12.

67. Andreasen C, Nielsen JB, Refsgaard L, Holst AG, Christensen AH, Andreasen L, et al. New population-based exome data are questioning the pathogenicity of previously cardiomyopathy-associated genetic variants. Eur J Hum Genet. 2013;21(9):918–28.

68. Van Der Zwaag PA, Jongbloed JDH, Van Den Berg MP, Van Der Smagt JJ, Jongbloed R, Bikker H, et al. A genetic variants database for arrhythmogenic right ventricular dysplasia/cardiomyopathy. Hum Mutat. 2009;30(9):1278–83.

69. Xu Z, Zhu W, Wang C, Huang L, Zhou Q, Hu J, et al. Genotype-phenotype relationship in patients with arrhythmogenic right ventricular cardiomyopathy caused by desmosomal gene mutations: A systematic review and meta-analysis. Sci Rep. 2017;7(January):1–8.

70. Ortiz-Genga MF, Cuenca S, Dal Ferro M, Zorio E, Salgado-Aranda R, Climent V, et al. Truncating FLNC

Mutations Are Associated With High-Risk Dilated and Arrhythmogenic Cardiomyopathies. J Am Coll Cardiol. 2016;68(22):2440–51.

71. Rigato I, Bauce B, Rampazzo A, Zorzi A, Pilichou K, Mazzotti E, et al. Compound and digenic heterozygosity predicts lifetime arrhythmic outcome and sudden cardiac death in desmosomal gene-related arrhythmogenic right ventricular cardiomyopathy. Circ Cardiovasc Genet. 2013;6(6):533–42.

72. Limongelli G, Nunziato M, Mazzaccara C, Intrieri M, D'argenio V, Esposito MV, et al. Genotype-phenotype correlation: A triple DNA mutational event in a boy entering sport conveys an additional pathogenicity risk. Genes (Basel). 2020;11(5):1–9.

73. Sommariva E, Stadiotti I, Perrucci GL, Tondo C, Pompilio G. Cell models of arrhythmogenic cardiomyopathy: advances and opportunities. Dis Model Mech. 2017 Jul 1;10(7):823–35.

74. Dalal D, James C, Devanagondi R, Tichnell C, Tucker A, Prakasa K, et al. Penetrance of Mutations in Plakophilin-2 Among Families With Arrhythmogenic Right Ventricular Dysplasia/Cardiomyopathy. J Am Coll Cardiol. 2006;48(7):1416–24.

75. Te Riele ASJM, James CA, Groeneweg JA, Sawant AC, Kammers K, Murray B, et al. Approach to family screening in arrhythmogenic right ventricular dysplasia/cardiomyopathy. Eur Heart J. 2016;37(9):755–63.

76. B-Lundqvist C, Eneström S, Edvardsson N, Olsson SB. Arrhythmogenic right ventricular dysplasia presenting with ventricular tachycardia in a father and son. Clin Cardiol. 1987;10(4):277–85.

77. Nava A, Scognamiglio R, Thiene G, Canciani B, Daliento L, Buja G, et al. A polymorphic form of familial arrhythmogenic right ventricular dysplasia. Am J Cardiol. 1987;59(15):1405–9.

78. Wlodarska EK, Konka M, Zaleska T, Ploski R, Cedro K, Pucilowska B, et al. Arrhythmogenic right ventricular cardiomyopathy in two pairs of monozygotic twins. Int J Cardiol. 2005;105(2):126–33.

79. Buja G, Nava A, Daliento L, Scognamiglio R, Miorelli M, Canciani B, et al. Right ventricular cardiomyopathy in identical and nonidentical young twins. Am Heart J. 1993;126(5):1187–93.

80. Quarta G, Muir A, Pantazis A, Syrris P, Gehmlich K, Garcia-Pavia P, et al. Familial evaluation in arrhythmogenic right ventricular cardiomyopathy: Impact of genetics and revised task force criteria.

Circulation. 2011;123(23):2701–9.

81. Bauce B, Nava A, Beffagna G, Basso C, Lorenzon A, Smaniotto G, et al. Multiple mutations in desmosomal proteins encoding genes in arrhythmogenic right ventricular cardiomyopathy/dysplasia. Hear Rhythm. 2010;7(1):22–9.

82. Rasmussen TB, Palmfeldt J, Nissen PH, Magnoni R, Dalager S, Jensen UB, et al. Mutated Desmoglein-2 Proteins are Incorporated into Desmosomes and Exhibit Dominant-Negative Effects in Arrhythmogenic Right Ventricular Cardiomyopathy. Hum Mutat. 2013;34(5):697–705.

83. Génin E, Feingold J, Clerget-Darpoux F. Identifying modifier genes of monogenic disease: Strategies and difficulties. Hum Genet. 2008;124(4):357–68.

84. Sen-Chowdhry S, Syrris P, Pantazis A, Quarta G, McKenna WJ, Chambers JC. Mutational heterogeneity, modifier genes, and environmental influences contribute to phenotypic diversity of arrhythmogenic cardiomyopathy. Circ Cardiovasc Genet. 2010;3(4):323–30.

85. Furlanello F, Bertoldi A, Dallago M, Furlanello C, Fernando F, Inama G, et al. Cardiac Arrest and Sudden Death in Competitive Athletes with Arrhythmogenic Right Ventricular Dysplasia. Pacing Clin Electrophysiol. 1998;21(1):331–5.

86. James CA, Bhonsale A, Tichnell C, Murray B, Russell SD, Tandri H, et al. Exercise increases age-related penetrance and arrhythmic risk in arrhythmogenic right ventricular dysplasia/cardiomyopathy-associated desmosomal mutation carriers. J Am Coll Cardiol. 2013;62(14):1290–7.

87. Ruwald AC, Marcus F, Estes NAM, Link M, McNitt S, Polonsky B, et al. Association of competitive and recreational sport participation with cardiac events in patients with arrhythmogenic right ventricular cardiomyopathy: Results from the North American multidisciplinary study of arrhythmogenic right ventricular cardiomyopath. Eur Heart J. 2015;36(27):1735–43.

88. Haugaa KH. Exercise and detraining are modifiable factors for arrhythmic risk in arrhythmogenic cardiomyopathy needing correct dosage. Hear Rhythm. 2020;17(8):1260–1.

89. La Gerche A, Rakhit DJ, Claessen G. Exercise and the right ventricle: A potential Achilles' heel. Cardiovasc Res. 2017;113(12):1499–508.

90. Stewart GM, Yamada A, Haseler LJ, Kavanagh JJ, Chan J, Koerbin G, et al. Influence of exercise intensity and duration on functional and biochemical perturbations in the human heart. J Physiol. 2016;594(11):3031–44.

91. Claessen G, Claus P, Ghysels S, Vermeersch P, Dymarkowski S, La Gerche A, et al. Right ventricular fatigue developing during endurance exercise: An exercise cardiac magnetic resonance study. Med Sci Sports Exerc. 2014;46(9):1717–26.

92. Saberniak J, Hasselberg NE, Borgquist R, Platonov PG, Sarvari SI, Smith H-J, et al. Vigorous physical activity impairs myocardial function in patients with arrhythmogenic right ventricular cardiomyopathy and in mutation positive family members. Eur J Heart Fail. 2014 Dec;16(12):1337–44.

93. Lie ØH, Dejgaard LA, Saberniak J, Rootwelt C, Stokke MK, Edvardsen T, et al. Harmful Effects of Exercise Intensity and Exercise Duration in Patients With Arrhythmogenic Cardiomyopathy. JACC Clin Electrophysiol. 2018;4(6):744–53.

94. Sawant AC, Riele ASJM, Tichnell C, Murray B, Bhonsale A, Tandri H, et al. Safety of American Heart Association-recommended minimum exercise for desmosomal mutation carriers. Hear Rhythm. 2016;13(1):199–207.

95. Sawant AC, Bhonsale A, te Riele ASJM, Tichnell C, Murray B, Russell SD, et al. Exercise has a Disproportionate Role in the Pathogenesis of. J Am Heart Assoc. 2014;3(6):1–10.

96. La Gerche A, Robberecht C, Kuiperi C, Nuyens D, Willems R, De Ravel T, et al. Lower than expected desmosomal gene mutation prevalence in endurance athletes with complex ventricular arrhythmias of right ventricular origin. Heart. 2010;96(16):1268–74.

97. Heidbuchel H, Prior DL, La Gerche A. Ventricular arrhythmias associated with long-term endurance sports: What is the evidence? Br J Sports Med. 2012;46(SUPPL. 1).

98. Apostolaki NE, Melita H, Manolis AS. The role of the autonomic nervous system in cardiac arrhythmias: The neuro-cardiac axis, more foe than friend? Trends Cardiovasc Med]. 2020;(xxxx):1–13.

99. Silvani A, Calandra-Buonaura G, Dampney RAL, Cortelli P. Brain–heart interactions: physiology and clinical implications. Philos Trans R Soc A Math Phys Eng Sci. 2016 May 13;374(2067):20150181.

100. Kawashima T. The autonomic nervous system of the human heart with special reference to its origin, course, and peripheral distribution. Anat Embryol (Berl). 2005 Jul 11;209(6):425–38.

101. Chamberlain PD, Jennings KH, Paul F, Cordell J, Berry A, Holmes SD, et al. The tissue distribution of the human β3-adrenoceptor studied using a monoclonal antibody: Direct evidence of the β3-adrenoceptor in human adipose tissue, atrium and skeletal muscle. Int J Obes. 1999;23(10):1057–65.

102. Mary-Rabine L, Hordof AJ, Bowman FO, Malm JR, Rosen MR. Alpha and beta adrenergic effects on human atrial specialized conducting fibers. Circulation. 1978;57(1):84–90.

103. Hedberg A, Kempf F, Josephson ME, Molinoff PB. Coexistence of beta-1 and beta-2 adrenergic receptors in the human heart: effects of treatment with receptor antagonists or calcium entry blockers. J Pharmacol Exp Ther. 1985 Sep;234(3):561–8.

104. Wichter T, Borggrefe M, Haverkamp W, Chen X, Breithardt G. Efficacy of antiarrhythmic drugs in patients with arrhythmogenic right ventricular disease: Results in patients with inducible and noninducible ventricular tachycardia. Circulation. 1992;86(1):29–37.

105. Wichter T, Hindricks G, Lerch H, Bartenstein P, Borggrefe M, Schober O, et al. Regional myocardial sympathetic dysinnervation in arrhythmogenic right ventricular cardiomyopathy: An analysis using 123I-meta- iodobenzylguanidine scintigraphy. Circulation. 1994;89(2):667–83.

106. Todica A, Siebermair J, Schiller J, Zacherl MJ, Fendler WP, Massberg S, et al. Assessment of right ventricular sympathetic dysfunction in patients with arrhythmogenic right ventricular cardiomyopathy: An 123I-metaiodobenzylguanidine SPECT/CT study. J Nucl Cardiol. 2018;

107. Wichter T, Schäfers M, Rhodes CG, Borggrefe M, Lerch H, Lammertsma AA, et al. Abnormalities of Cardiac Sympathetic Innervation in Arrhythmogenic Right Ventricular Cardiomyopathy. Circulation. 2000 Apr 4;101(13):1552–8.

108. Dusi V, Ferrari GM De. The sympathetic nervous system and arrhythmogenic right ventricular cardiomyopathy : Further evidence of a strong tie. Hear Rhythm. 2019;16(7):1011–2.

109. Shen MJ, Zipes DP. Role of the autonomic nervous system in modulating cardiac arrhythmias. Vol. 114, Circulation Research. 2014. p. 1004–21.

110. Manolis AS, Manolis AA. Exercise and Arrhythmias: A Double-Edged Sword. PACE - Pacing Clin Electrophysiol. 2016;39(7):748–62.

111. Buckley U, Shivkumar K. Stress-induced cardiac arrhythmias: The heart-brain interaction. Vol. 26, Trends in Cardiovascular Medicine. 2016. p. 78–80.

112. Bauce B, Frigo G, Marcus FI, Basso C, Rampazzo A, Maddalena F, et al. Comparison of Clinical Features of Arrhythmogenic Right Ventricular Cardiomyopathy in Men Versus Women. Am J Cardiol. 2008;102(9):1252–7.

113. Maceira AM, Prasad SK, Khan M, Pennell DJ. Reference right ventricular systolic and diastolic function normalized to age, gender and body surface area from steady-state free precession cardiovascular magnetic resonance. Eur Heart J. 2006;27(23):2879–88.

114. Natori S, Lai S, Finn JP, Gomes AS, Hundley WG, Jerosch-Herold M, et al. Cardiovascular function in multi-ethnic study of atherosclerosis: Normal values by age, sex, and ethnicity. Am J Roentgenol. 2006;186(6 SUPPL. A).

115. Akdis D, Saguner AM, Shah K, Wei C, Medeiros-Domingo A, Von Eckardstein A, et al. Sex hormones affect outcome in arrhythmogenic right ventricular cardiomyopathy/dysplasia: Froma stemcell derived cardiomyocyte-based model to clinical biomarkers of disease outcome. Eur Heart J. 2017;38(19):1498–508.

116. Herring MJ, Oskui PM, Hale SL, Kloner RA. Testosterone and the cardiovascular system: a comprehensive review of the basic science literature. Vol. 2, Journal of the American Heart Association. 2013. p. 1–11.

117. Giordano S, Hage FG, Xing D, Chen YF, Allon S, Chen C, et al. Estrogen and cardiovascular disease: Is timing everything? In: American Journal of the Medical Sciences. 2015. p. 27–35.

118. Ren J, Chen L, Zhang N, Chen X, Zhao Q, Chen K, et al. Plasma testosterone and arrhythmic events in male patients with arrhythmogenic right ventricular cardiomyopathy. ESC Hear Fail. 2020;(May):1547–59.

119. Nava A, Bauce B, Basso C, Muriago M, Rampazzo A, Bs C, et al. Clinical Profile and Long-term Follow-up

of 37 Families With Arrhythmogenic Right Ventricular Cardiomyopathy. J Am Coll Cardiol. 2000;36(7):2226–33.

120. Lubos N, van der Gaag S, Gerçek M, Kant S, Leube RE, Krusche CA. Inflammation shapes pathogenesis of murine arrhythmogenic cardiomyopathy. Basic Res Cardiol. 2020;115(4):1–19.

121. Campian ME, Hardziyenka M, De Bruin K, Van Eck-Smit BLF, De Bakker JMT, Verberne HJ, et al. Early inflammatory response during the development of right ventricular heart failure in a rat model. Eur J Heart Fail. 2010;12(7):653–8.

122. Campian ME, Verberne HJ, Hardziyenka M, De Groot EAA, Van Moerkerken AF, Van Eck-Smit BLF, et al. Assessment of inflammation in patients with arrhythmogenic right ventricular cardiomyopathy/dysplasia. Eur J Nucl Med Mol Imaging. 2010;37(11):2079–85.

123. Chelko SP, Asimaki A, Lowenthal J, Bueno-Beti C, Bedja D, Scalco A, et al. Therapeutic Modulation of the Immune Response in Arrhythmogenic Cardiomyopathy. Circulation. 2019;140(18):1491–505.

124. Campuzano O, Alcalde M, Iglesias A, Barahona-Dussault C, Sarquella-Brugada G, Benito B, et al. Arrhythmogenic right ventricular cardiomyopathy: severe structural alterations are associated with inflammation. J Clin Pathol. 2012 Dec;65(12):1077–83.

125. Francis Stuart SD, De Jesus NM, Lindsey ML, Ripplinger CM. The crossroads of inflammation, fibrosis, and arrhythmia following myocardial infarction. Vol. 91, Journal of Molecular and Cellular Cardiology. 2016. p. 114–22.

126. Thiene G, Basso C, Calabrese F, Angelini A, Valente M. Pathology and pathogenesis of arrhythmogenic right ventricular cardiomyopathy. Herz. 2000;25(3):210–5.

127. Herren T, Gerber PA, Duru F. Arrhythmogenic right ventricular cardiomyopathy/dysplasia: A not so rare 'disease of the desmosome' with multiple clinical presentations. Vol. 98, Clinical Research in Cardiology. 2009. p. 141–58.

128. Frangogiannis NG. Matricellular proteins in cardiac adaptation and disease. Vol. 92, Physiological Reviews. 2012. p. 635–88.

129. Turner NA, Mughal RS, Warburton P, O'Regan DJ, Ball SG, Porter KE. Mechanism of TNFα-induced IL-

1α, IL-1β and IL-6 expression in human cardiac fibroblasts: Effects of statins and thiazolidinediones. Cardiovasc Res. 2007;76(1):81–90.

130. Hulsmans M, Clauss S, Xiao L, Aguirre AD, King KR, Hanley A, et al. Macrophages Facilitate Electrical Conduction in the Heart. Cell. 2017;169(3):510-522.e20.

131. Skiöldebrand E, Lundqvist A, Björklund U, Sandstedt M, Lindahl A, Hansson E, et al. Inflammatory activation of human cardiac fibroblasts leads to altered calcium signaling, decreased connexin 43 expression and increased glutamate secretion. Heliyon. 2017;3(10):e00406.

132. Mazurek T, Zhang LF, Zalewski A, Mannion JD, Diehl JT, Arafat H, et al. Human Epicardial Adipose Tissue Is a Source of Inflammatory Mediators. Circulation. 2003;108(20):2460–6.

133. Garcia-Gras E. Suppression of canonical Wnt/ -catenin signaling by nuclear plakoglobin recapitulates phenotype of arrhythmogenic right ventricular cardiomyopathy. J Clin Invest. 2006 Jul 3;116(7):2012–21.

134. MacDonald BT, Tamai K, He X. Wnt/β-Catenin Signaling: Components, Mechanisms, and Diseases. Vol. 17, Developmental Cell. Elsevier Inc.; 2009. p. 9–26.

135. Asimaki A, Tandri H, Huang H, Halushka MK, Gautam S, Basso C, et al. A new diagnostic test for arrhythmogenic right ventricular cardiomyopathy. N Engl J Med. 2009;360(11):1075–84.

136. Swope D, Li J, Radice GL. Beyond cell adhesion: The role of armadillo proteins in the heart. Vol. 25, Cellular Signalling. 2013. p. 93–100.

137. Xiao Y, Leach J, Wang J, Martin JF. Hippo/Yap Signaling in Cardiac Development and Regeneration. Vol. 18, Current Treatment Options in Cardiovascular Medicine. Current Treatment Options in Cardiovascular Medicine; 2016. p. 1–9.

138. Chopra A, Tabdanov E, Patel H, Janmey PA, Kresh JY. Cardiac myocyte remodeling mediated by N-cadherin-dependent mechanosensing. Am J Physiol - Hear Circ Physiol. 2011;300(4):1252–66.

139. Chen SN, Gurha P, Lombardi R, Ruggiero A, Willerson JT, Marian AJ. The hippo pathway is activated and is a causal mechanism for adipogenesis in arrhythmogenic cardiomyopathy. Circ Res. 2014;114(3):454–68.

140. Bermúdez-Jiménez FJ, Carriel V, Brodehl A, Alaminos M, Campos A, Schirmer I, et al. Novel Desmin Mutation p.Glu401Asp Impairs Filament Formation, Disrupts Cell Membrane Integrity, and Causes Severe Arrhythmogenic Left Ventricular Cardiomyopathy/Dysplasia. Circulation. 2018;137(15):1595–610.

141. Mestroni L, Sbaizero O. Arrhythmogenic Cardiomyopathy: Mechanotransduction Going Wrong. Circulation. 2018;137(15):1611–3.

142. Ma S, Meng Z, Chen R, Guan KL. The hippo pathway: Biology and pathophysiology. Vol. 88, Annual Review of Biochemistry. 2019. p. 577–604.

143. Saffitz JE. Dependence of electrical coupling on mechanical coupling in cardiac myocytes: Insights gained from cardiomyopathies caused by defects in cell-cell connections. In: Annals of the New York Academy of Sciences. 2005. p. 336–44.

144. Oxford EM, Musa H, Maass K, Coombs W, Taffet SM, Delmar M. Connexin43 remodeling caused by inhibition of plakophilin-2 expression in cardiac cells. Circ Res. 2007;101(7):703–11.

145. Lyon RC, Mezzano V, Wright AT, Pfeiffer E, Chuang J, Banares K, et al. Connexin defects underlie arrhythmogenic right ventricular cardiomyopathy in a novel mouse model. Hum Mol Genet. 2014;23(5):1134–50.

146. Gehmlich K, Lambiase PD, Asimaki A, Ciaccio EJ, Ehler E, Syrris P, et al. A novel desmocollin-2 mutation reveals insights into the molecular link between desmosomes and gap junctions. Hear Rhythm. 2011;8(5):711–8.

147. Cerrone M, Noorman M, Lin X, Chkourko H, Liang FX, Van Der Nagel R, et al. Sodium current deficit and arrhythmogenesis in a murine model of plakophilin-2 haploinsufficiency. Cardiovasc Res. 2012;95(4):460–8.

148. Noorman M, Hakim S, Kessler E, Groeneweg JA, Cox MGPJ, Asimaki A, et al. Remodeling of the cardiac sodium channel, connexin43, and plakoglobin at the intercalated disk in patients with arrhythmogenic cardiomyopathy. Hear Rhythm. 2013;10(3):412–9.

149. Moccia F, Lodola F, Stadiotti I, Pilato CA, Bellin M, Carugo S, et al. Calcium as a key player in

arrhythmogenic cardiomyopathy: Adhesion disorder or intracellular alteration? Vol. 20, International Journal of Molecular Sciences. 2019.

150. van Opbergen CJM, Delmar M, van Veen TAB. Potential new mechanisms of pro-arrhythmia in arrhythmogenic cardiomyopathy: Focus on calcium sensitive pathways. Vol. 25, Netherlands Heart Journal. 2017. p. 157–69.

151. Godsel LM, Dubash AD, Bass-Zubek AE, Amargo E V., Klessner JL, Hobbs RP, et al. Plakophilin 2 Couples Actomyosin Remodeling to Desmosomal Plaque Assembly via RhoA. Omary MB, editor. Mol Biol Cell. 2010 Aug 15;21(16):2844–59.

152. Dorn T, Kornherr J, Parrotta EI, Zawada D, Ayetey H, Santamaria G, et al. Interplay of cell–cell contacts and RhoA/ MRTF -A signaling regulates cardiomyocyte identity. EMBO J. 2018;37(12):1–19.

153. Zhang H, Liu S, Dong T, Yang J, Xie Y, Wu Y, et al. Profiling of differentially expressed microRNAs in arrhythmogenic right ventricular cardiomyopathy. Sci Rep. 2016;6:1–11.

154. Thum T, Gross C, Fiedler J, Fischer T, Kissler S, Bussen M, et al. MicroRNA-21 contributes to myocardial disease by stimulating MAP kinase signalling in fibroblasts. Nature. 2008;456(7224):980–4.

155. Kawakita A, Yanamoto S, Yamada SI, Naruse T, Takahashi H, Kawasaki G, et al. MicroRNA-21 promotes oral cancer invasion via the wnt/β-catenin pathway by targeting DKK2. Pathol Oncol Res. 2014;20(2):253–61.

156. Lin CW, Chang YL, Chang YC, Lin JC, Chen CC, Pan SH, et al. MicroRNA-135b promotes lung cancer metastasis by regulating multiple targets in the Hippo pathway and LZTS1. Nat Commun. 2013;4(May).

157. Gurha P, Chen X, Lombardi R, Willerson JT, Marian AJ. Knockdown of plakophilin 2 downregulates MIR-184 through CpG hypermethylation and suppression of the E2F1 pathway and leads to enhanced adipogenesis in vitro. Circ Res. 2016;119(6):731–50.

158. Sommariva E, D'Alessandra Y, Farina FM, Casella M, Cattaneo F, Catto V, et al. MiR-320a as a Potential Novel Circulating Biomarker of Arrhythmogenic CardioMyopathy. Sci Rep. 2017;7(1):1–10.

159. Hamam D, Ali D, Vishnubalaji R, Hamam R, Al-Nbaheen M, Chen L, et al. MicroRNA-320/RUNX2 axis regulates adipocytic differentiation of human mesenchymal (skeletal) stem cells. Cell Death Dis.

2014;5(10):1–12.

160. Sun JY, Huang Y, Li JP, Zhang X, Wang L, Meng YL, et al. MicroRNA-320a suppresses human colon cancer cell proliferation by directly targeting β-catenin. Biochem Biophys Res Commun. 2012;420(4):787–92.

161. Chatterjee D, Fatah M, Akdis D, Spears DA, Koopmann TT, Mittal K, et al. An autoantibody identifies arrhythmogenic right ventricular cardiomyopathy and participates in its pathogenesis. Eur Heart J. 2018;39(44):3932–44.

162. McKenna WJ, Thiene G, Nava A, Fontaliran F, Blomstrom-Lundqvist C, Fontaine G, et al. Diagnosis of arrhythmogenic right ventricular dysplasia/cardiomyopathy. Vol. 71, British Heart Journal. 1994. p. 215–8.

163. Marcus FI, McKenna WJ, Sherrill D, Basso C, Bauce B, Bluemke DA, et al. Diagnosis of arrhythmogenic right ventricular cardiomyopathy/Dysplasia: Proposed modification of the task force criteria. Circulation. 2010;121(13):1533–41.

164. Ward D, Syrris P, Sen-Chowdhry S, McKenna WJ. Diagnosis: Task Force Criteria including Modifications for Family Members. In: Arrhythmogenic RV Cardiomyopathy/Dysplasia. 2007. p. 87–96.

165. Marcus FI, Sherrill D. Strengths and Weaknesses of the Task Force Criteria — Proposed Modifications. In: Arrhythmogenic RV Cardiomyopathy/Dysplasia. 2007. p. 97–104.

166. Bomma C, Rutberg J, Tandri H, Nasir K, Roguin A, Tichnell C, et al. Misdiagnosis of arrhythmogenic right ventricular dysplasia/cardiomyopathy. J Cardiovasc Electrophysiol. 2004;15(3):300–6.

167. Femia G, Sy RW, Puranik R. Systematic review: Impact of the new task force criteria in the diagnosis of arrhythmogenic right ventricular cardiomyopathy. Int J Cardiol. 2017 Aug;241:311–7.

168. Bosman LP, Cadrin-Tourigny J, Bourfiss M, Aliyari Ghasabeh M, Sharma A, Tichnell C, et al. Diagnosing arrhythmogenic right ventricular cardiomyopathy by 2010 Task Force Criteria: clinical performance and simplified practical implementation. Europace. 2020;22(5):787–96.

169. Corrado D, Perazzolo Marra M, Zorzi A, Beffagna G, Cipriani A, Lazzari M De, et al. Diagnosis of arrhythmogenic cardiomyopathy: The Padua criteria. Int J Cardiol. 2020;

170. Oomen AWGJ, Semsarian C, Puranik R, Sy RW. Diagnosis of Arrhythmogenic Right Ventricular

Cardiomyopathy: Progress and Pitfalls. Vol. 27, Heart Lung and Circulation. Australian and New Zealand Society of Cardiac and Thoracic Surgeons (ANZSCTS) and the Cardiac Society of Australia and New Zealand (CSANZ); 2018. p. 1310–7.

171. Gandjbakhch E, Redheuil A, Pousset F, Charron P, Frank R. Clinical Diagnosis, Imaging, and Genetics of Arrhythmogenic Right Ventricular Cardiomyopathy/Dysplasia: JACC State-of-the-Art Review. Vol. 72, Journal of the American College of Cardiology. 2018. p. 784–804.

172. Borgquist R, Haugaa KH, Gilljam T, Bundgaard H, Hansen J, Eschen O, et al. The diagnostic performance of imaging methods in ARVC using the 2010 task force criteria. Eur Heart J Cardiovasc Imaging. 2014;15(11):1219–25.

173. Mooij CF, De Wit CJ, Graham DA, Powell AJ, Geva T. Reproducibility of MRI measurements of right ventricular size and function in patients with normal and dilated ventricles. J Magn Reson Imaging. 2008;28(1):67–73.

174. Sugeng L, Mor-Avi V, Weinert L, Niel J, Ebner C, Steringer-Mascherbauer R, et al. Multimodality Comparison of Quantitative Volumetric Analysis of the Right Ventricle. JACC Cardiovasc Imaging. 2010;3(1):10–8.

175. Tandri H, Saranathan M, Rodriguez ER, Martinez C, Bomma C, Nasir K, et al. Noninvasive detection of myocardial fibrosis in arrhythmogenic right ventricular cardiomyopathy using delayed-enhancement magnetic resonance imaging. J Am Coll Cardiol. 2005;45(1):98–103.

176. Etoom Y, Govindapillai S, Hamilton R, Manlhiot C, Yoo SJ, Farhan M, et al. Importance of CMR within the task force criteria for the diagnosis of ARVC in children and adolescents. J Am Coll Cardiol. 2015;65(10):987–95.

177. Peters S, Trümmel M, Koehler B, Westermann KU. The value of different electrocardiographic depolarization criteria in the diagnosis of arrhythmogenic right ventricular dysplasia/cardiomyopathy. J Electrocardiol. 2007;40(1):34–7.

178. Te Riele ASJM, James CA, Bhonsale A, Groeneweg JA, Camm CF, Murray B, et al. Malignant Arrhythmogenic Right Ventricular Dysplasia/Cardiomyopathy with a normal 12-lead

electrocardiogram: A rare but underrecognized clinical entity. Hear Rhythm. 2013;10(10):1484–91.

179. Peters S, Trümmel M, Koehler B. QRS fragmentation in standard ECG as a diagnostic marker of arrhythmogenic right ventricular dysplasia-cardiomyopathy. Hear Rhythm. 2008;5(10):1417–21.

180. Asimaki A, Saffitz JE. The role of endomyocardial biopsy in ARVC: Looking beyond histology in search of new diagnostic markers. Vol. 22, Journal of Cardiovascular Electrophysiology. 2011. p. 111–7.

181. Basso C, Ronco F, Marcus F, Abudureheman A, Rizzo S, Frigo AC, et al. Quantitative assessment of endomyocardial biopsy in arrhythmogenic right ventricular cardiomyopathy/dysplasia: An in vitro validation of diagnostic criteria. Eur Heart J. 2008;29(22):2760–71.

182. Avella A, D'Amati G, Pappalardo A, Re F, Silenzi PF, Laurenzi F, et al. Diagnostic value of endomyocardial biopsy guided by electroanatomic voltage mapping in arrhythmogenic right ventricular cardiomyopathy/dysplasia. J Cardiovasc Electrophysiol. 2008;19(11):1127–34.

183. Casella M, Dello Russo A, Vettor G, Lumia G, Catto V, Sommariva E, et al. Electroanatomical mapping systems and intracardiac echo integration for guided endomyocardial biopsy. Vol. 14, Expert Review of Medical Devices. Taylor & Francis; 2017. p. 609–19.

184. Casella M, Pizzamiglio F, Dello Russo A, Carbucicchio C, Al-Mohani G, Russo E, et al. Feasibility of Combined Unipolar and Bipolar Voltage Maps to Improve Sensitivity of Endomyocardial Biopsy. Circ Arrhythmia Electrophysiol. 2015 Jun;8(3):625–32.

185. Pilato CA, Stadiotti I, Maione AS, Saverio V, Catto V, Tundo F, et al. Isolation and Characterization of Cardiac Mesenchymal Stromal Cells from Endomyocardial Bioptic Samples of Arrhythmogenic Cardiomyopathy Patients. J Vis Exp. 2018 Feb 28;(132).

186. Lin T, Conti S, Cipolletta L, Marino V, Zucchetti M, Russo E, et al. Right Ventricular Outflow Tract Arrhythmias: Benign Or Early Stage Arrhythmogenic Right Ventricular Cardiomyopathy/Dysplasia? J Atr Fibrillation. 2014;7(4):1161.

187. Aliot EM, Stevenson WG, Almendral-Garrote JM, Bogun F, Calkins CH, Delacretaz E, et al. EHRA/HRS expert consensus on catheter ablation of ventricular arrhythmias. Vol. 11, Europace. 2009. p. 771–817.

188. Morin DP, Mauer AC, Gear K, Zareba W, Markowitz SM, Marcus FI, et al. Usefulness of Precordial T-

Wave Inversion to Distinguish Arrhythmogenic Right Ventricular Cardiomyopathy from Idiopathic Ventricular Tachycardia Arising from the Right Ventricular Outflow Tract. Am J Cardiol. 2010;105(12):1821–4.

189. Patrianakos AP, Protonotarios N, Nyktari E, Pagonidis K, Tsatsopoulou A, Parthenakis FI, et al. Arrhythmogenic right ventricular cardiomyopathy/dysplasia and troponin release. Myocarditis or the 'hot phase' of the disease? Int J Cardiol. 2012;157(2):e26–8.

190. Vasaiwala SC, Finn C, Delpriore J, Leya F, Gagermeier J, Akar JG, et al. Prospective study of cardiac sarcoid mimicking arrhythmogenic right ventricular dysplasia. J Cardiovasc Electrophysiol. 2009;20(5):473–6.

191. Ladyjanskaia GA, Basso C, Hobbelink MGG, Kirkels JH, Lahpor JR, Cramer MJ, et al. Sarcoid myocarditis with ventricular tachycardia mimicking ARVD/C. J Cardiovasc Electrophysiol. 2010;21(1):94–8.

192. Mohsen A, Panday M, Wetherold S, Jimenez A. Cardiac Sarcoidosis Mimicking Arrhythmogenic Right Ventricular Dysplasia With High Defibrillation Threshold Requiring Subcutaneous Shocking Coil Implantation. Hear Lung Circ. 2012;21(1):46–9.

193. Corrado D, Zorzi A, Cerrone M, Rigato I, Mongillo M, Bauce B, et al. Relationship between arrhythmogenic right ventricular cardiomyopathy and brugada syndrome. Circ Arrhythmia Electrophysiol. 2016;9(4):1–10.

194. Peters S. Is Brugada syndrome a variant of arrhythmogenic cardiomyopathy? Int J Cardiol. 2015;189(1):88–90.

195. Catalano O, Antonaci S, Moro G, Mussida M, Frascaroli M, Baldi M, et al. Magnetic resonance investigations in Brugada syndrome reveal unexpectedly high rate of structural abnormalities. Eur Heart J. 2009;30(18):2241–8.

196. Yu J, Hu J, Dai X, Cao Q, Xiong Q, Liu X, et al. SCN5A mutation in Chinese patients with arrhythmogenic right ventricular dysplasia. Herz. 2014;39(2):271–5.

197. Cerrone M, Lin X, Zhang M, Agullo-Pascual E, Pfenniger A, Chkourko Gusky H, et al. Missense mutations in plakophilin-2 cause sodium current deficit and associate with a brugada syndrome phenotype.

Circulation. 2014;129(10):1092–103.

198. Spezzacatene A, Sinagra G, Merlo M, Barbati G, Graw SL, Brun F, et al. Arrhythmogenic phenotype in dilated cardiomyopathy: Natural history and predictors of life-threatening arrhythmias. J Am Heart Assoc. 2015;4(10):1–9.

199. Patel H, Shah P, Rampal U, Shamoon F, Tiyyagura S. Arrythmogenic right ventricular dysplasia/cardiomyopathy (ARVD/C) and cathecholaminergic polymorphic ventricular tachycardia (CPVT): A phenotypic spectrum seen in same patient. Vol. 48, Journal of Electrocardiology. Elsevier B.V.; 2015. p. 874–8.

200. Bhuiyan ZA, Van Den Berg MP, Van Tintelen JP, Bink-Boelkens MTE, Wiesfeld ACP, Alders M, et al. Expanding spectrum of human RYR2-related disease: New electrocardiographic, structural, and genetic features. Circulation. 2007;116(14):1569–76.

201. Baggish AL. Exercise-induced cardiac remodeling. Vol. 9, Circulation: Cardiovascular Imaging. 2016. p. 1–3.

202. Maron BJ, Udelson JE, Bonow RO, Nishimura RA, Ackerman MJ, Estes NAM, et al. Eligibility and Disqualification Recommendations for Competitive Athletes with Cardiovascular Abnormalities: Task Force 3: Hypertrophic Cardiomyopathy, Arrhythmogenic Right Ventricular Cardiomyopathy and Other Cardiomyopathies, and Myocarditis: A Scientif. Vol. 132, Circulation. 2015. p. e273–80.

203. Corrado D, Basso C, Pavei A, Michieli P, Schiavon M TG. Trends in Sudden Cardiovascular Death in Young Competitive Athletes. Jama. 2006;296(13):1593–601.

204. Mascia G, Arbelo E, Porto I, Brugada R, Brugada J. The arrhythmogenic right ventricular cardiomyopathy in comparison to the athletic heart. Vol. 31, Journal of Cardiovascular Electrophysiology. 2020. p. 1836–43.

205. D'Ascenzi F, Solari M, Corrado D, Zorzi A, Mondillo S. Diagnostic Differentiation Between Arrhythmogenic Cardiomyopathy and Athlete's Heart by Using Imaging. Vol. 11, JACC: Cardiovascular Imaging. 2018. p. 1327–39.

206. Corrado D, Wichter T, Link MS, Hauer R, Marchlinski F, Anastasakis A, et al. Treatment of

arrhythmogenic right ventricular cardiomyopathy/dysplasia: An international task force consensus statement. Eur Heart J. 2015;36(46):3227–37.

207. Corrado D, Wichter T, Link MS, Hauer RNW, Marchlinski FE, Anastasakis A, et al. Treatment of arrhythmogenic right ventricular cardiomyopathy/dysplasia: An international task force consensus statement. Circulation. 2015;132(5):441–53.

208. Heidbüchel H, Hoogsteen J, Fagard R, Vanhees L, Ector H, Willems R, et al. High prevalence of right ventricular involvement in endurance athletes with ventricular arrhythmias: Role of an electrophysiologic study in risk stratification. Eur Heart J. 2003;24(16):1473–80.

209. Corrado D, Basso C, Schiavon M, Thiene G. Does sports activity enhance the risk of sudden cardiac death? Vol. 7, Journal of Cardiovascular Medicine. 2006. p. 228–33.

210. Marcus GM, Glidden D V., Polonsky B, Zareba W, Smith LM, Cannom DS, et al. Efficacy of Antiarrhythmic Drugs in Arrhythmogenic Right Ventricular Cardiomyopathy. A Report From the North American ARVC Registry. J Am Coll Cardiol. 2009;54(7):609–15.

211. Ermakov S, Scheinman M. Arrhythmogenic right ventricular cardiomyopathy - antiarrhythmic therapy. Arrhythmia Electrophysiol Rev. 2015;4(2):86–9.

212. Schinkel AFL. Implantable cardioverter defibrillators in arrhythmogenic right ventricular dysplasia/cardiomyopathy: Patient outcomes, incidence of appropriate and inappropriate interventions, and complications. Circ Arrhythmia Electrophysiol. 2013;6(3):562–8.

213. Boriani G, Artale P, Biffi M, Martignani C, Frabetti L, Valzania C, et al. Outcome of cardioverter-defibrillator implant in patients with arrhythmogenic right ventricular cardiomyopathy. Heart Vessels. 2007;22(3):184–92.

214. Piccini JP, Dalal D, Roguin A, Bomma C, Cheng A, Prakasa K, et al. Predictors of appropriate implantable defibrillator therapies in patients with arrhythmogenic right ventricular dysplasia. Hear Rhythm. 2005;2(11):1188–94.

215. Hodgkinson KA, Parfrey PS, Bassett AS, Kupprion C, Drenckhahn J, Norman MW, et al. The impact of implantable cardioverter-defibrillator therapy on survival in autosomal-dominant arrhythmogenic right

ventricular cardiomyopathy (ARVD5). J Am Coll Cardiol. 2005 Feb;45(3):400–8.

216. Corrado D, Leoni L, Link MS, Della Bella P, Gaita F, Curnis A, et al. Implantable Cardioverter-Defibrillator Therapy for Prevention of Sudden Death in Patients with Arrhythmogenic Right Ventricular Cardiomyopathy/Dysplasia. Circulation. 2003;108(25):3084–91.

217. Philips B, Riele ASJM, Sawant A, Kareddy V, James CA, Murray B, et al. Outcomes and ventricular tachycardia recurrence characteristics after epicardial ablation of ventricular tachycardia in arrhythmogenic right ventricular dysplasia / cardiomyopathy. Hear Rhythm. 2015;12(4):716–25.

218. Santangeli P, Zado ES, Supple GE, Haqqani HM, Garcia FC, Tschabrunn CM, et al. Long-Term Outcome with Catheter Ablation of Ventricular Tachycardia in Patients with Arrhythmogenic Right Ventricular Cardiomyopathy. Circ Arrhythmia Electrophysiol. 2015;8(6):1413–21.

219. Bai R, Biase L Di, Shivkumar K, Mohanty P, Tung R, Santangeli P, et al. Ablation of ventricular arrhythmias in arrhythmogenic right ventricular dysplasia/cardiomyopathy: Arrhythmia-free survival after endo-epicardial substrate based mapping and ablationablation of ventricular arrhythmias in arrhythmogenic right ventricular dy. Circ Arrhythmia Electrophysiol. 2011;4(4):478–85.

220. Dalal D, Jain R, Tandri H, Dong J, Eid SM, Prakasa K, et al. Long-Term Efficacy of Catheter Ablation of Ventricular Tachycardia in Patients With Arrhythmogenic Right Ventricular Dysplasia/Cardiomyopathy. J Am Coll Cardiol. 2007 Jul;50(5):432–40.

221. Calkins H, Corrado D, Marcus F. Risk stratification in arrhythmogenic right ventricular cardiomyopathy. Circulation. 2017;136(21):2068–82.

222. Bezzerides VJ, Prondzynski M, Carrier L, Pu WT. Gene Therapy for Inherited Arrhythmias. Cardiovasc Res. 2020;1635–50.

223. Te Riele ASJM, James CA, Rastegar N, Bhonsale A, Murray B, Tichnell C, et al. Yield of serial evaluation in at-risk family members of patients with ARVD/C. J Am Coll Cardiol. 2014;64(3):293–301.

224. Cadrin-Tourigny J, Bosman LP, Nozza A, Wang W, Tadros R, Bhonsale A, et al. A new prediction model for ventricular arrhythmias in arrhythmogenic right ventricular cardiomyopathy. Eur Heart J. 2019;40(23):1850–8.

225. Field LJ. Atrial natriuretic factor-SV40 T antigen transgenes produce tumors and cardiac arrhythmias in mice. Science. 1988;239(4843):1029–33.

226. Beffagna G, De Bortoli M, Nava A, Salamon M, Lorenzon A, Zaccolo M, et al. Missense mutations in Desmocollin-2 N-terminus, associated with arrhythmogenic right ventricular cardiomyopathy, affect intracellular localization of desmocollin-2 in vitro. BMC Med Genet. 2007;8:1–10.

227. De Bortoli M, Beffagna G, Bauce B, Lorenzon A, Smaniotto G, Rigato I, et al. The p.A897KfsX4 frameshift variation in desmocollin-2 is not a causative mutation in arrhythmogenic right ventricular cardiomyopathy. Eur J Hum Genet. 2010;18(7):776–82.

228. Gehmlich K, Syrris P, Peskett E, Evans A, Ehler E, Asimaki A, et al. Mechanistic insights into arrhythmogenic right ventricular cardiomyopathy caused by desmocollin-2 mutations. Cardiovasc Res. 2011;90(1):77–87.

229. Kirchner F, Schuetz A, Boldt LH, Martens K, Dittmar G, Haverkamp W, et al. Molecular insights into arrhythmogenic right ventricular cardiomyopathy caused by plakophilin-2 missense mutations. Circ Cardiovasc Genet. 2012;5(4):400–11.

230. Schlipp A, Schinner C, Spindler V, Vielmuth F, Gehmlich K, Syrris P, et al. Desmoglein-2 interaction is crucial for cardiomyocyte cohesion and function. Cardiovasc Res. 2014;104(2):245–57.

231. Forleo C, Carmosino M, Resta N, Rampazzo A, Valecce R, Sorrentino S, et al. Clinical and functional characterization of a novel mutation in lamin a/C gene in a multigenerational family with arrhythmogenic cardiac laminopathy. PLoS One. 2015;10(4):1–18.

232. Notari M, Hu Y, Sutendra G, Dedeić Z, Lu M, Dupays L, et al. iASPP, a previously unidentified regulator of desmosomes, prevents arrhythmogenic right ventricular cardiomyopathy (ARVC)-induced sudden death. Proc Natl Acad Sci U S A. 2015;112(9):E973–81.

233. Spampanato C. A case of polimalformed fetus with a microdeletion of CTNNA3 gene. J Prenat Med. 2016;10(3/4):20.

234. Fidler LM, Wilson GJ, Liu F, Cui X, Scherer SW, Taylor GP, et al. Abnormal connexin43 in arrhythmogenic right ventricular cardiomyopathy caused by plakophilin-2 mutations. J Cell Mol Med.

2009;13(10):4219–28.

235. Zhang Q, Deng C, Rao F, Modi RM, Zhu J, Liu X, et al. Silencing of desmoplakin decreases connexin43/Nav1.5 expression and sodium current in HL-1 cardiomyocytes. Mol Med Rep. 2013;8(3):780–6.

236. Wang L, Liu S, Zhang H, Hu S, Wei Y. RhoA activity increased in myocardium of arrhythmogenic cardiomyopathy patients and affected connexin 43 protein expression in HL-1 cells. Int J Clin Exp Med. 2015;8(8):12906–13.

237. Swope D, Cheng L, Gao E, Li J, Radice GL. Loss of Cadherin-Binding Proteins -Catenin and Plakoglobin in the Heart Leads to Gap Junction Remodeling and Arrhythmogenesis. Mol Cell Biol. 2012;32(6):1056–67.

238. Gomes J, Finlay M, Ahmed AK, Ciaccio EJ, Asimaki A, Saffitz JE, et al. Electrophysiological abnormalities precede overt structural changes in arrhythmogenic right ventricular cardiomyopathy due to mutations in desmoplakin-A combined murine and human study. Eur Heart J. 2012;33(15):1942–53.

239. Ma D, Wei H, Lu J, Ho S, Zhang G, Sun X, et al. Generation of patient-specific induced pluripotent stem cell-derived cardiomyocytes as a cellular model of arrhythmogenic right ventricular cardiomyopathy. Eur Heart J. 2013;34(15):1122–33.

240. Kim C, Wong J, Wen J, Wang S, Wang C, Spiering S, et al. Studying arrhythmogenic right ventricular dysplasia with patient-specific iPSCs. Nature. 2013 Feb 27;494(7435):105–10.

241. Caspi O, Huber I, Gepstein A, Arbel G, Maizels L, Boulos M, et al. Modeling of arrhythmogenic right ventricular cardiomyopathy with human induced pluripotent stem cells. Circ Cardiovasc Genet. 2013;6(6):557–68.

242. Giacomelli E, Meraviglia V, Campostrini G, Cochrane A, Cao X, van Helden RWJ, et al. Human-iPSC-Derived Cardiac Stromal Cells Enhance Maturation in 3D Cardiac Microtissues and Reveal Non-cardiomyocyte Contributions to Heart Disease. Cell Stem Cell. 2020;26(6):862-879.e11.

243. Sebastião MJ, Serra M, Pereira R, Palacios I, Gomes-Alves P, Alves PM. Human cardiac progenitor cell activation and regeneration mechanisms: Exploring a novel myocardial ischemia/reperfusion in vitro

model. Stem Cell Res Ther. 2019;10(1):1–16.

244. Lombardi R, Da Graca Cabreira-Hansen M, Bell A, Fromm RR, Willerson JT, Marian AJ. Nuclear plakoglobin is essential for differentiation of cardiac progenitor cells to adipocytes in arrhythmogenic right ventricular cardiomyopathy. Circ Res. 2011;109(12):1342–53.

245. Lepilina A, Coon AN, Kikuchi K, Holdway JE, Roberts RW, Burns CG, et al. A Dynamic Epicardial Injury Response Supports Progenitor Cell Activity during Zebrafish Heart Regeneration. Cell. 2006;127(3):607–19.

246. Rao KS, Spees JL. Harnessing Epicardial Progenitor Cells and Their Derivatives for Rescue and Repair of Cardiac Tissue After Myocardial Infarction. Curr Mol Biol Reports. 2017;3(3):149–58.

247. Lombardi R, Chen SN, Ruggiero A, Gurha P, Czernuszewicz GZ, Willerson JT, et al. Cardiac fibro-adipocyte progenitors express desmosome proteins and preferentially differentiate to adipocytes upon deletion of the desmoplakin gene. Circ Res. 2016;119(1):41–54.

248. Souders CA, Bowers SLK, Baudino TA. Cardiac fibroblast: The renaissance cell. Circ Res. 2009;105(12):1164–76.

249. Brown RD, Ambler SK, Mitchell MD, Long CS. The cardiac fibroblast: Therapeutic target in myocardial remodeling and failure. Annu Rev Pharmacol Toxicol. 2005;45(1):657–87.

250. Pittenger MF, Martin BJ. Mesenchymal stem cells and their potential as cardiac therapeutics. Circ Res. 2004;95(1):9–20.

251. Koop A, Goldmann P, Chen SRW, Thieleczek R, Varsáni M. ARVC-related mutations in divergent region 3 alter functional properties of the cardiac ryanodine receptor. Biophys J. 2008;94(12):4668–77.

252. Rajkumar R, Sembrat JC, McDonough B, Seidman CE, Ahmad F. Functional effects of the TMEM43 Ser358Leu mutation in the pathogenesis of arrhythmogenic right ventricular cardiomyopathy. BMC Med Genet. 2012;13.

253. Basso C, Fox PR, Meurs KM, Towbin JA, Spier AW, Calabrese F, et al. Arrhythmogenic Right Ventricular Cardiomyopathy Causing Sudden Cardiac Death in Boxer Dogs: A New Animal Model of Human Disease. Circulation. 2004;109(9):1180–5.

254. Meurs KM, Lacombe VA, Dryburgh K, Fox PR, Reiser PRPR, Kittleson MD. Differential expression of the cardiac ryanodine receptor in normal and arrhythmogenic right ventricular cardiomyopathy canine hearts. Hum Genet. 2006;120(1):111–8.

255. Gerull B, Brodehl A. Genetic Animal Models for Arrhythmogenic Cardiomyopathy. Front Physiol. 2020;11(June):1–20.

256. Van Tintelen JP, Entius MM, Bhuiyan ZA, Jongbloed R, Wiesfeld ACP, Wilde AAM, et al. Plakophilin-2 mutations are the major determinant of familial arrhythmogenic right ventricular dysplasia/cardiomyopathy. Circulation. 2006;113(13):1650–8.

257. Grossmann KS, Grund C, Huelsken J, Behrend M, Erdmann B, Franke WW, et al. Requirement of plakophilin 2 for heart morphogenesis and cardiac junction formation. J Cell Biol. 2004 Oct 11;167(1):149–60.

258. Leo-Macias A, Liang FX, Delmar M. Ultrastructure of the intercellular space in adult murine ventricle revealed by quantitative tomographic electron microscopy. Cardiovasc Res. 2015;107(4):442–52.

259. Cruz FM, Sanz-Rosa D, Roche-Molina M, García-Prieto J, García-Ruiz JM, Pizarro G, et al. Exercise Triggers ARVC Phenotype in Mice Expressing a Disease-Causing Mutated Version of Human Plakophilin-2. J Am Coll Cardiol. 2015 Apr;65(14):1438–50.

260. Moncayo-Arlandi J, Guasch E, la Garza MS de, Casado M, Garcia NA, Mont L, et al. Molecular disturbance underlies to arrhythmogenic cardiomyopathy induced by transgene content, age and exercise in a truncated PKP2 mouse model. Hum Mol Genet. 2016;25(17):3676–88.

261. Moriarty MA, Ryan R, Lalor P, Dockery P, Byrnes L, Grealy M. Loss of plakophilin 2 disrupts heart development in zebrafish. Int J Dev Biol. 2012;56(9):711–8.

262. Ian Gallicano G, Kouklis P, Bauer C, Yin M, Vasioukhin V, Degenstein L, et al. Desmoplakin is required early in development for assembly of desmosomes and cytoskeletal linkage. J Cell Biol. 1998;143(7):2009–22.

263. Yang Z, Bowles NE, Scherer SE, Taylor MD, Kearney DL, Ge S, et al. Desmosomal dysfunction due to mutations in desmoplakin causes arrhythmogenic right ventricular dysplasia/cardiomyopathy. Circ Res.

2006;99(6):646–55.

264. Martherus R, Jain R, Takagi K, Mendsaikhan U, Turdi S, Osinska H, et al. Accelerated cardiac remodeling in desmoplakin transgenic mice in response to endurance exercise is associated with perturbed wnt/β-catenin signaling. Am J Physiol - Hear Circ Physiol. 2016;310(2):H174–87.

265. Giuliodori A, Beffagna G, Marchetto G, Fornetto C, Vanzi F, Toppo S, et al. Loss of cardiac Wnt/β-catenin signalling in desmoplakin-deficient AC8 zebrafish models is rescuable by genetic and pharmacological intervention. Cardiovasc Res. 2018;114(8):1082–97.

266. Eshkind L, Tian Q, Schmidt A, Franke WW, Windoffer R, Leube RE. Loss of desmoglein 2 suggests essential functions for early embryonic development and proliferation of embryonal stem cells. Eur J Cell Biol. 2002;81(11):592–8.

267. Krusche CA, Holthöfer B, Hofe V, Van De Sandt AM, Eshkind L, Bockamp E, et al. Desmoglein 2 mutant mice develop cardiac fibrosis and dilation. Basic Res Cardiol. 2011;106(4):617–33.

268. Kant S, Krull P, Eisner S, Leube RE, Krusche CA. Histological and ultrastructural abnormalities in murine desmoglein 2-mutant hearts. Cell Tissue Res. 2012;348(2):249–59.

269. Chelko SP, Asimaki A, Andersen P, Bedja D, Amat-Alarcon N, DeMazumder D, et al. Central role for GSK3β in the pathogenesis of arrhythmogenic cardiomyopathy. JCI Insight. 2016;1(5).

270. Calore M, Lorenzon A, Vitiello L, Poloni G, Khan MAF, Beffagna G, et al. A novel murine model for arrhythmogenic cardiomyopathy points to a pathogenic role of Wnt signalling and miRNA dysregulation. Cardiovasc Res. 2019;115(4):739–51.

271. Brodehl A, Belke DD, Garnett L, Martens K, Abdelfatah N, Rodriguez M, et al. Transgenic mice overexpressing desmocollin-2 (DSC2) develop cardiomyopathy associated with myocardial inflammation and fibrotic remodeling. PLoS One. 2017;12(3):1–19.

272. Heuser A, Plovie ER, Ellinor PT, Grossmann KS, Shin JT, Wichter T, et al. Mutant desmocollin-2 causes arrhythmogenic right ventricular cardiomyopathy. Am J Hum Genet. 2006;79(6):1081–8.

273. Ruiz P, Brinkmann V, Ledermann B, Behrend M, Grund C, Thalhammer C, et al. Targeted mutation of plakoglobin in mice reveals essential functions of desmosomes in the embryonic heart. J Cell Biol.

1996;135(1):215–25.

274. Bierkamp C, McLaughlin KJ, Schwarz H, Huber O, Kemler R. Embryonic heart and skin defects in mice lacking plakoglobin. Dev Biol. 1996;180(2):780–5.

275. Kirchhof P, Fabritz L, Zwiener M, Witt H, Schäfers M, Zellerhoff S, et al. Age- and training-dependent development of arrhythmogenic right ventricular cardiomyopathy in heterozygous plakoglobin-deficient mice. Circulation. 2006;114(17):1799–806.

276. Fabritz L, Hoogendijk MG, Scicluna BP, Van Amersfoorth SCM, Fortmueller L, Wolf S, et al. Load-reducing therapy prevents development of arrhythmogenic right ventricular cardiomyopathy in plakoglobin-deficient mice. J Am Coll Cardiol [Internet]. 2011;57(6):740–50. Available from: http://dx.doi.org/10.1016/j.jacc.2010.09.046

277. Li J, Swope D, Raess N, Cheng L, Muller EJ, Radice GL. Cardiac Tissue-Restricted Deletion of Plakoglobin Results in Progressive Cardiomyopathy and Activation of -Catenin Signaling. Mol Cell Biol. 2011;31(6):1134–44.

278. Li D, Liu Y, Maruyama M, Zhu W, Chen H, Zhang W, et al. Restrictive loss of plakoglobin in cardiomyocytes leads to arrhythmogenic cardiomyopathy. Hum Mol Genet. 2011;20(23):4582–96.

279. Takeshima H, Komazaki S, Hirose K, Nishi M, Noda T, Iino M. Embryonic lethality and abnormal cardiac myocytes in mice lacking ryanodine receptor type 2. EMBO J. 1998;17(12):3309–16.

280. Kannankeril PJ, Mitchell BM, Goonasekera SA, Chelu MG, Zhang W, Sood S, et al. Mice with the R176Q cardiac ryanodine receptor mutation exhibit catecholamine-induced ventricular tachycardia and cardiomyopathy. Proc Natl Acad Sci U S A. 2006;103(32):12179–84.

281. Shan J, Xie W, Betzenhauser M, Reiken S, Chen BX, Wronska A, et al. Calcium leak through ryanodine receptors leads to atrial fibrillation in 3 mouse models of catecholaminergic polymorphic ventricular tachycardia. Circ Res. 2012;111(6):708–17.

282. Hesse M, Kondo CS, Clark RB, Su L, Allen FL, Geary-Joo CTM, et al. Dilated cardiomyopathy is associated with reduced expression of the cardiac sodium channel Scn5a. Cardiovasc Res. 2007;75(3):498–509.

283. Watanabe H, Yang T, Stroud DM, Lowe JS, Harris L, Atack TC, et al. Striking in vivo phenotype of a

disease-associated human scn5a mutation producing minimal changes in vitro. Circulation. 2011;124(9):1001–11.

284. Huttner IG, Trivedi G, Jacoby A, Mann SA, Vandenberg JI, Fatkin D. A transgenic zebrafish model of a human cardiac sodium channel mutation exhibits bradycardia, conduction-system abnormalities and early death. J Mol Cell Cardiol. 2013;61:123–32.

285. Wan E, Garan H, Marx SO, Wan E, Abrams J, Weinberg RL, et al. Aberrant sodium influx causes cardiomyopathy and atrial fibrillation in mice Find the latest version : Aberrant sodium influx causes cardiomyopathy and atrial fibrillation in mice. J Clin Invest. 2016;126(1):112–22.

286. Papadatos GA, Wallerstein PMR, Head CEG, Ratcliff R, Brady PA, Benndorf K, et al. Slowed conduction and ventricular tachycardia after targeted disruption of the cardiac sodium channel gene Scn5a. Proc Natl Acad Sci U S A. 2002;99(9):6210–5.

287. Haghighi K, Kolokathis F, Gramolini AO, Waggoner JR, Pater L, Lynch RA, et al. A mutation in the human phospholamban gene, deleting arginine 14, results in lethal, hereditary cardiomyopathy. Proc Natl Acad Sci U S A. 2006;103(5):1388–93.

288. Chu G, Ferguson DG, Edes I, Kiss E, Sato Y, Kranias EG. Phospholamban Ablation and Compensatory Responses in the Mammalian Heart. Ann N Y Acad Sci. 2006;853(1):49–62.

289. Stroud MJ, Fang X, Zhang J, Guimarães-Camboa N, Veevers J, Dalton ND, et al. Luma is not essential for murine cardiac development and function. Cardiovasc Res. 2018;114(3):378–88.

290. Zheng G, Jiang C, Li Y, Yang D, Ma Y, Zhang B, et al. TMEM43-S358L mutation enhances NF-κB-TGFβ signal cascade in arrhythmogenic right ventricular dysplasia/cardiomyopathy. Protein Cell. 2019;10(2):104–19.

291. Padrón-Barthe L, Villalba-Orero M, Gómez-Salinero JM, Domínguez F, Román M, Larrasa-Alonso J, et al. Severe Cardiac Dysfunction and Death Caused by Arrhythmogenic Right Ventricular Cardiomyopathy Type 5 Are Improved by Inhibition of Glycogen Synthase Kinase-3β. Circulation. 2019;140(14):1188–204.

292. Chen SN, Sbaizero O, Taylor MRG, Mestroni L. Lamin A/C Cardiomyopathy: Implications for Treatment.

Vol. 21, Current Cardiology Reports. 2019. p. 1–9.

293. Psarras S, Mavroidis M, Sanoudou D, Davos CH, Xanthou G, Varela AE, et al. Regulation of adverse remodelling by osteopontin in a genetic heart failure model. Eur Heart J. 2012;33(15):1954–63.

294. Li J, Goossens S, van Hengel J, Gao E, Cheng L, Tyberghein K, et al. Loss of αT-catenin alters the hybrid adhering junctions in the heart and leads to dilated cardiomyopathy and ventricular arrhythmia following acute ischemia. J Cell Sci. 2012;125(4):1058–67.

295. Kostetskii I, Li J, Xiong Y, Zhou R, Ferrari VA, Patel V V., et al. Induced deletion of the N-cadherin gene in the heart leads to dissolution of the intercalated disc structure. Circ Res. 2005;96(3):346–54.

296. Li J, Patel V V., Kostetskii I, Xiong Y, Chu AF, Jacobson JT, et al. Cardiac-specific loss of N-cadherin leads to alteration in connexins with conduction slowing and arrhythmogenesis. Circ Res. 2005;97(5):474–81.

297. Zhou Y, Chen Z, Zhang L, Zhu M, Tan C, Zhou X, et al. Loss of filamin c is catastrophic for heart function. Circulation. 2020;869–71.

298. Gerull B, Gramlich M, Atherton J, McNabb M, Trombitás K, Sasse-Klaassen S, et al. Mutations of TTN, encoding the giant muscle filament titin, cause familial dilated cardiomyopathy. Nat Genet. 2002;30(2):201–4.

299. Gramlich M, Michely B, Krohne C, Heuser A, Erdmann B, Klaassen S, et al. Stress-induced dilated cardiomyopathy in a knock-in mouse model mimicking human titin-based disease. J Mol Cell Cardiol. 2009 Sep;47(3):352–8.

300. Zou J, Tran D, Baalbaki M, Tang LF, Poon A, Pelonero A, et al. An internal promoter underlies the difference in disease severity between N- and C-terminal truncation mutations of Titin in zebrafish. Elife. 2015 Oct 16;4.

301. Shih Y-H, Dvornikov A V., Zhu P, Ma X, Kim M, Ding Y, et al. Exon- and contraction-dependent functions of titin in sarcomere assembly. Development. 2016 Dec 15;143(24):4713–22.

302. Huttner IG, Wang LW, Santiago CF, Horvat C, Johnson R, Cheng D, et al. A-Band Titin Truncation in Zebrafish Causes Dilated Cardiomyopathy and Hemodynamic Stress Intolerance. Circ Genomic Precis

Med. 2018 Aug;11(8).

303. Kaartinen V, Voncken JW, Shuler C, Warburton D, Bu D, Heisterkamp N, et al. Abnormal lung development and cleft palate in mice lacking TGF–β3 indicates defects of epithelial–mesenchymal interaction. Nat Genet. 1995 Dec;11(4):415–21.

304. Proetzel G, Pawlowski SA, Wiles M V., Yin M, Boivin GP, Howles PN, et al. Transforming growth factor–β3 is required for secondary palate fusion. Nat Genet. 1995 Dec;11(4):409–14.

305. Ghosh A, Shcherbik N. Effects of Oxidative Stress on Protein Translation: Implications for Cardiovascular Diseases. Int J Mol Sci. 2020 Apr 11;21(8):2661.

306. Forrester SJ, Kikuchi DS, Hernandes MS, Xu Q, Griendling KK. Reactive Oxygen Species in Metabolic and Inflammatory Signaling. Circ Res. 2018 Mar 16;122(6):877–902.

307. Di Meo S, Reed TT, Venditti P, Victor VM. Role of ROS and RNS Sources in Physiological and Pathological Conditions. Oxid Med Cell Longev. 2016;2016:1–44.

308. Levitan I, Volkov S, Subbaiah P V. Oxidized LDL: Diversity, Patterns of Recognition, and Pathophysiology. Antioxid Redox Signal. 2010 Jul;13(1):39–75.

309. West AP, Brodsky IE, Rahner C, Woo DK, Erdjument-Bromage H, Tempst P, et al. TLR signalling augments macrophage bactericidal activity through mitochondrial ROS. Nature. 2011;472(7344):476–80.

310. Zhang J, Wang X, Vikash V, Ye Q, Wu D, Liu Y, et al. ROS and ROS-Mediated Cellular Signaling. Oxid Med Cell Longev. 2016;2016:1–18.

311. ZIMA A, BLATTER L. Redox regulation of cardiac calcium channels and transporters. Cardiovasc Res. 2006 Jul 15;71(2):310–21. A

312. D'Oria R, Schipani R, Leonardini A, Natalicchio A, Perrini S, Cignarelli A, et al. The Role of Oxidative Stress in Cardiac Disease: From Physiological Response to Injury Factor. Oxid Med Cell Longev. 2020 May 14;2020:1–29.

313. Ellah MRA. Involvement of oxidative stress in cardiovascular diseases. J Adv Vet Res. 2018;8(1):1–5.

314. Schieber M, Chandel NS. ROS Function in Redox Signaling and Oxidative Stress. Curr Biol. 2014

May;24(10):R453–62.

315. Moris D, Spartalis M, Tzatzaki E, Spartalis E, Karachaliou G-S, Triantafyllis AS, et al. The role of reactive oxygen species in myocardial redox signaling and regulation. Ann Transl Med. 2017 Aug;5(16):324–324.

316. Giordano FJ. Oxygen, oxidative stress, hypoxia, and heart failure. J Clin Invest. 2005 Mar 1;115(3):500–8.

317. Panth N, Paudel KR, Parajuli K. Reactive Oxygen Species: A Key Hallmark of Cardiovascular Disease. Adv Med. 2016;2016:1–12.

318. Taverne YJHJ, Bogers AJJC, Duncker DJ, Merkus D. Reactive Oxygen Species and the Cardiovascular System. Oxid Med Cell Longev. 2013;2013:1–15.

319. Ide T, Tsutsui H, Kinugawa S, Utsumi H, Kang D, Hattori N, et al. Mitochondrial Electron Transport Complex I Is a Potential Source of Oxygen Free Radicals in the Failing Myocardium. Circ Res. 1999 Aug 20;85(4):357–63.

320. Sawyer DB, Siwik DA, Xiao L, Pimentel DR, Singh K, Colucci WS. Role of Oxidative Stress in Myocardial Hypertrophy and Failure. J Mol Cell Cardiol. 2002 Apr;34(4):379–88.

321. Sabri A, Hughie HH, Lucchesi PA. Regulation of Hypertrophic and Apoptotic Signaling Pathways by Reactive Oxygen Species in Cardiac Myocytes. Antioxid Redox Signal. 2003 Dec;5(6):731–40.

322. Suematsu N, Tsutsui H, Wen J, Kang D, Ikeuchi M, Ide T, et al. Oxidative Stress Mediates Tumor Necrosis Factor-α–Induced Mitochondrial DNA Damage and Dysfunction in Cardiac Myocytes. Circulation. 2003 Mar 18;107(10):1418–23.

323. Ruzzenente B, Rötig A, Metodiev MD. Mouse models for mitochondrial diseases. Hum Mol Genet. 2016 Oct 1;25(R2):R115–22.

324. Cesselli D, Jakoniuk I, Barlucchi L, Beltrami AP, Hintze TH, Nadal-Ginard B, et al. Oxidative Stress–Mediated Cardiac Cell Death Is a Major Determinant of Ventricular Dysfunction and Failure in Dog Dilated Cardiomyopathy. Circ Res. 2001 Aug 3;89(3):279–86.

325. Liu Q, Berchner-Pfannschmidt U, Moller U, Brecht M, Wotzlaw C, Acker H, et al. A Fenton reaction at the endoplasmic reticulum is involved in the redox control of hypoxia-inducible gene expression. Proc

Natl Acad Sci. 2004 Mar 23;101(12):4302–7.

326. Scortegagna M, Ding K, Oktay Y, Gaur A, Thurmond F, Yan L-J, et al. Multiple organ pathology, metabolic abnormalities and impaired homeostasis of reactive oxygen species in Epas1−/− mice. Nat Genet. 2003 Dec 9;35(4):331–40.

327. Lee PJ, Jiang BH, Chin BY, Iyer N V, Alam J, Semenza GL, et al. Hypoxia-inducible factor-1 mediates transcriptional activation of the heme oxygenase-1 gene in response to hypoxia. J Biol Chem. 1997 Feb 28;272(9):5375–81.

328. Goncharov N, Avdonin P, Nadeev A, Zharkikh I, Jenkins R. Reactive Oxygen Species in Pathogenesis of Atherosclerosis. Curr Pharm Des. 2015 Jan 3;21(9):1134–46.

329. Kaneto H, Katakami N, Matsuhisa M, Matsuoka T. Role of Reactive Oxygen Species in the Progression of Type 2 Diabetes and Atherosclerosis. Mediators Inflamm. 2010;2010:1–11.

330. Allen CL, Bayraktutan U. Oxidative Stress and Its Role in the Pathogenesis of Ischaemic Stroke. Int J Stroke. 2009 Dec;4(6):461–70.

331. Sharma S, Adrogue J V., Golfman L, Uray I, Lemm J, Youker K, et al. Intramyocardial lipid accumulation in the failing human heart resembles the lipotoxic rat heart. FASEB J. 2004 Nov;18(14):1692–700.

332. Kumagai T, Matsukawa N, Kaneko Y, Kusumi Y, Mitsumata M, Uchida K. A lipid peroxidation-derived inflammatory mediator: Identification of 4-hydroxy-2-nonenal as a potential inducer of cyclooxygenase-2 in macrophages. J Biol Chem. 2004;279(46):48389–96.

333. Yadav UCS, Ramana K V. Regulation of NF-B-Induced Inflammatory Signaling by Lipid Peroxidation-Derived Aldehydes. Oxid Med Cell Longev. 2013;2013:1–11.

334. Furnkranz A, Leitinger N. Regulation of Inflammatory Responses by Oxidized Phospholipids: Structure-Function Relationships. Curr Pharm Des. 2004 Mar 1;10(8):915–21.

335. van Opbergen CJM, den Braven L, Delmar M, van Veen TAB. Mitochondrial Dysfunction as Substrate for Arrhythmogenic Cardiomyopathy: A Search for New Disease Mechanisms. Front Physiol. 2019 Dec 10;10.

336. Williams GSB, Boyman L, Lederer WJ. Mitochondrial calcium and the regulation of metabolism in the

heart. J Mol Cell Cardiol. 2015 Jan;78:35–45.

337. Tsutsui H, Kinugawa S, Matsushima S. Oxidative stress and heart failure. Am J Physiol Circ Physiol. 2011 Dec;301(6):H2181–90.

338. Sugden PH, Clerk A. Oxidative Stress and Growth-Regulating Intracellular Signaling Pathways in Cardiac Myocytes. Antioxid Redox Signal. 2006 Nov;8(11–12):2111–24.

339. Landmesser U, Drexler H. The clinical significance of endothelial dysfunction. Curr Opin Cardiol. 2005 Nov;20(6):547–51.

340. Jialal I, Devaraj S. Low-density lipoprotein oxidation, antioxidants, and atherosclerosis: a clinical biochemistry perspective. Clin Chem. 1996 Apr 1;42(4):498–506.

341. Hevonoja T, Pentikäinen MO, Hyvönen MT, Kovanen PT, Ala-Korpela M. Structure of low density lipoprotein (LDL) particles: Basis for understanding molecular changes in modified LDL. Biochim Biophys Acta - Mol Cell Biol Lipids. 2000 Nov;1488(3):189–210.

342. Gough PJ, Greaves DR, Suzuki H, Hakkinen T, Hiltunen MO, Turunen M, et al. Analysis of Macrophage Scavenger Receptor (SR-A) Expression in Human Aortic Atherosclerotic Lesions. Arterioscler Thromb Vasc Biol. 1999 Mar;19(3):461–71.

343. Hiltunen TP, Luoma JS, Nikkari T, Ylä-Herttuala S. Expression of LDL Receptor, VLDL Receptor, LDL Receptor–Related Protein, and Scavenger Receptor in Rabbit Atherosclerotic Lesions. Circulation. 1998 Mar 24;97(11):1079–86.

344. Naito M, Suzuki H, Mori T, Matsumoto A, Kodama T, Takahashi K. Coexpression of type I and type II human macrophage scavenger receptors in macrophages of various organs and foam cells in atherosclerotic lesions. Am J Pathol [Internet]. 1992 Sep;141(3):591–9. Available from: http://www.ncbi.nlm.nih.gov/pubmed/1519666

345. Dejager S, Mietus-Synder M, Pitas RE. Oxidized low density lipoproteins bind to the scavenger receptor expressed by rabbit smooth muscle cells and macrophages. Arterioscler Thromb A J Vasc Biol. 1993 Mar;13(3):371–8.

346. Li H, Freeman MW, Libby P. Regulation of smooth muscle cell scavenger receptor expression in vivo by

atherogenic diets and in vitro by cytokines. J Clin Invest. 1995 Jan 1;95(1):122–33.

347. Hughes DA, Fraser IP, Gordon S. Murine macrophage scavenger receptor:in vivo expression and function as receptor for macrophage adhesion in lymphoid and non-lymphoid organs. Eur J Immunol. 1995 Feb;25(2):466–73.

348. Boullier A, Gillotte KL, Hörkkö S, Green SR, Friedman P, Dennis EA, et al. The Binding of Oxidized Low Density Lipoprotein to Mouse CD36 Is Mediated in Part by Oxidized Phospholipids That Are Associated with Both the Lipid and Protein Moieties of the Lipoprotein. J Biol Chem. 2000 Mar 31;275(13):9163–9.

349. Podrez EA, Febbraio M, Sheibani N, Schmitt D, Silverstein RL, Hajjar DP, et al. Macrophage scavenger receptor CD36 is the major receptor for LDL modified by monocyte-generated reactive nitrogen species. J Clin Invest. 2000 Apr 15;105(8):1095–108.

350. Podrez EA, Hoppe G, O'Neil J, Hoff HF. Phospholipids in oxidized LDL not adducted to apoB are recognized by the CD36 scavenger receptor. Free Radic Biol Med. 2003 Feb;34(3):356–64.

351. Endemann G, Stanton LW, Madden KS, Bryant CM, White RT, Protter AA. CD36 is a receptor for oxidized low density lipoprotein. J Biol Chem. 1993 Jun 5;268(16):11811–6.

352. Nicholson AC, Frieda S, Pearce A, Silverstein RL. Oxidized LDL Binds to CD36 on Human Monocyte-Derived Macrophages and Transfected Cell Lines. Arterioscler Thromb Vasc Biol. 1995 Feb;15(2):269–75.

353. Hoosdally SJ, Andress EJ, Wooding C, Martin CA, Linton KJ. The Human Scavenger Receptor CD36. J Biol Chem. 2009 Jun 12;284(24):16277–88.

354. Acton S, Rigotti A, Landschulz KT, Xu S, Hobbs HH, Krieger M. Identification of Scavenger Receptor SR-BI as a High Density Lipoprotein Receptor. Science. 1996 Jan 26;271(5248):518–20.

355. Rigotti A, Trigatti BL, Penman M, Rayburn H, Herz J, Krieger M. A targeted mutation in the murine gene encoding the high density lipoprotein (HDL) receptor scavenger receptor class B type I reveals its key role in HDL metabolism. Proc Natl Acad Sci. 1997 Nov 11;94(23):12610–5.

356. Trigatti B, Rigotti A. Scavenger receptor class B type I (SR-BI) and high-density lipoprotein metabolism:

recent lessons from genetically manipulated mice. Int J Tissue React. 2000;22(2–3):29–37.

357. Varban ML, Rinninger F, Wang N, Fairchild-Huntress V, Dunmore JH, Fang Q, et al. Targeted mutation reveals a central role for SR-BI in hepatic selective uptake of high density lipoprotein cholesterol. Proc Natl Acad Sci. 1998 Apr 14;95(8):4619–24.

358. Zhang Y. Hepatic expression of scavenger receptor class B type I (SR-BI) is a positive regulator of macrophage reverse cholesterol transport in vivo. J Clin Invest. 2005 Oct 1;115(10):2870–4.

359. Chen M, Masaki T, Sawamura T. LOX-1, the receptor for oxidized low-density lipoprotein identified from endothelial cells: implications in endothelial dysfunction and atherosclerosis. Pharmacol Ther. 2002 Jul;95(1):89–100.

360. Sawamura T, Kume N, Aoyama T, Moriwaki H, Hoshikawa H, Aiba Y, et al. An endothelial receptor for oxidized low-density lipoprotein. Nature. 1997 Mar;386(6620):73–7.

361. Moriwaki H, Kume N, Sawamura T, Aoyama T, Hoshikawa H, Ochi H, et al. Ligand Specificity of LOX-1, a Novel Endothelial Receptor for Oxidized Low Density Lipoprotein. Arterioscler Thromb Vasc Biol. 1998 Oct;18(10):1541–7.

362. Kakutani M, Ueda M, Naruko T, Masaki T, Sawamura T. Accumulation of LOX-1 Ligand in Plasma and Atherosclerotic Lesions of Watanabe Heritable Hyperlipidemic Rabbits: Identification by a Novel Enzyme Immunoassay. Biochem Biophys Res Commun. 2001 Mar;282(1):180–5.

363. Hijiya N, Miyake K, Akashi S, Matsuura K, Higuchi Y, Yamamoto S. Possible Involvement of Toll-Like Receptor 4 in Endothelial Cell Activation of Larger Vessels in Response to Lipopolysaccharide. Pathobiology. 2002;70(1):18–25.

364. Tsukumo DML, Carvalho-Filho MA, Carvalheira JBC, Prada PO, Hirabara SM, Schenka AA, et al. Loss-of-Function Mutation in Toll-Like Receptor 4 Prevents Diet-Induced Obesity and Insulin Resistance. Diabetes. 2007 Aug;56(8):1986–98.

365. Vitseva OI, Tanriverdi K, Tchkonia TT, Kirkland JL, McDonnell ME, Apovian CM, et al. Inducible Toll-like Receptor and NF-κB Regulatory Pathway Expression in Human Adipose Tissue. Obesity. 2008 May 21;16(5):932–7.

366. Choi S-H, Harkewicz R, Lee JH, Boullier A, Almazan F, Li AC, et al. Lipoprotein Accumulation in Macrophages via Toll-Like Receptor-4–Dependent Fluid Phase Uptake. Circ Res. 2009 Jun 19;104(12):1355–63.

367. Thorne RF, Mhaidat NM, Ralston KJ, Burns GF. CD36 is a receptor for oxidized high density lipoprotein: Implications for the development of atherosclerosis. FEBS Lett. 2007 Mar 20;581(6):1227–32.

368. Tontonoz P, Nagy L, Alvarez JG., Thomazy VA, Evans RM. PPARγ Promotes Monocyte/Macrophage Differentiation and Uptake of Oxidized LDL. Cell. 1998 Apr;93(2):241–52.

369. Nagy L, Tontonoz P, Alvarez JG., Chen H, Evans RM. Oxidized LDL Regulates Macrophage Gene Expression through Ligand Activation of PPARγ. Cell. 1998 Apr;93(2):229–40.

370. Lee HS, Song CY. Oxidized Low-Density Lipoprotein and Oxidative Stress in the Development of Glomerulosclerosis. Am J Nephrol. 2009;29(1):62–70.

371. Villa M, Cerda-Opazo P, Jimenez-Gallegos D, Garrido-Moreno V, Chiong M, Quest AF, et al. Pro-fibrotic effect of oxidized LDL in cardiac myofibroblasts. Biochem Biophys Res Commun. 2020 Apr;524(3):696–701.

372. Jialal I, Devaraj S. Low-density lipoprotein oxidation, antioxidants, and atherosclerosis: a clinical biochemistry perspective. Clin Chem. 1996 Apr;42(4):498–506.

373. Higashi Y, Peng T, Du J, Sukhanov S, Li Y, Itabe H, et al. A redox-sensitive pathway mediates oxidized LDL-induced downregulation of insulin-like growth factor-1 receptor. J Lipid Res. 2005 Jun;46(6):1266–77.

374. Park YM, Febbraio M, Silverstein RL. CD36 modulates migration of mouse and human macrophages in response to oxidized LDL and may contribute to macrophage trapping in the arterial intima. J Clin Invest. 2008 Dec 8.

375. Nishio E, Arimura S, Watanabe Y. Oxidized LDL Induces Apoptosis in Cultured Smooth Muscle Cells: A Possible Role for 7-Ketocholesterol. Biochem Biophys Res Commun. 1996 Jun;223(2):413–8.

376. Hsieh C-C, Yen M-H, Liu H-W, Lau Y-T. Lysophosphatidylcholine induces apoptotic and non-apoptotic death in vascular smooth muscle cells: in comparison with oxidized LDL. Atherosclerosis. 2000

Aug;151(2):481–91.

377. Björkerud B, Björkerud S. Contrary Effects of Lightly and Strongly Oxidized LDL With Potent Promotion of Growth Versus Apoptosis on Arterial Smooth Muscle Cells, Macrophages, and Fibroblasts. Arterioscler Thromb Vasc Biol. 1996 Mar;16(3):416–24.

378. Dandapat A, Hu C, Sun L, Mehta JL. Small Concentrations of oxLDL Induce Capillary Tube Formation From Endothelial Cells via LOX-1–Dependent Redox-Sensitive Pathway. Arterioscler Thromb Vasc Biol. 2007 Nov;27(11):2435–42.

379. Camaré C, Trayssac M, Garmy-Susini B, Mucher E, Sabbadini R, Salvayre R, et al. Oxidized LDL-induced angiogenesis involves sphingosine 1-phosphate: prevention by anti-S1P antibody. Br J Pharmacol. 2015 Jan;172(1):106–18.

380. Camaré C, Augé N, Pucelle M, Saint-Lebes B, Grazide M-H, Nègre-Salvayre A, et al. The neutral sphingomyelinase-2 is involved in angiogenic signaling triggered by oxidized LDL. Free Radic Biol Med. 2016 Apr;93:204–16.

381. Nègre-Salvayre A, Augé N, Camaré C, Bacchetti T, Ferretti G, Salvayre R. Dual signaling evoked by oxidized LDLs in vascular cells. Free Radic Biol Med. 2017 May;106:118–33.

382. Kokkinos PF, Fernhall B. Physical Activity and High Density Lipoprotein Cholesterol Levels. Sport Med. 1999;28(5):307–14.

383. Radak Z, Chung HY, Goto S. Exercise and hormesis: oxidative stress-related adaptation for successful aging. Biogerontology. 2005 Jan;6(1):71–5.

384. Sánchez-Quesada JL, Homs-Serradesanferm R, Serrat-Serrat J, Serra-Grima JR, González-Sastre F, Ordóñez-Llanos J. Increase of LDL susceptibility to oxidation occurring after intense, long duration aerobic exercise. Atherosclerosis. 1995 Dec;118(2):297–305.

385. Powers SK, Jackson MJ. Exercise-Induced Oxidative Stress: Cellular Mechanisms and Impact on Muscle Force Production. Physiol Rev. 2008 Oct;88(4):1243–76.

386. Sugama K, Suzuki K, Yoshitani K, Shiraishi K, Miura S, Yoshioka H, et al. Changes of thioredoxin, oxidative stress markers, inflammation and muscle/renal damage following intensive endurance exercise. Exerc

Immunol Rev. 2015;21:130–42.

387. Morillas-Ruiz JM, Villegas García JA, López FJ, Vidal-Guevara ML, Zafrilla P. Effects of polyphenolic antioxidants on exercise-induced oxidative stress. Clin Nutr. 2006 Jun;25(3):444–53.

388. Pimentel DR, Amin JK, Xiao L, Miller T, Viereck J, Oliver-Krasinski J, et al. Reactive Oxygen Species Mediate Amplitude-Dependent Hypertrophic and Apoptotic Responses to Mechanical Stretch in Cardiac Myocytes. Circ Res. 2001 Aug 31;89(5):453–60.

389. Mastaloudis A, Leonard SW, Traber MG. Oxidative stress in athletes during extreme endurance exercise. Free Radic Biol Med. 2001 Oct;31(7):911–22.

390. Nieman DC, Shanely RA, Luo B, Meaney MP, Dew DA, Pappan KL. Metabolomics approach to assessing plasma 13- and 9-hydroxy-octadecadienoic acid and linoleic acid metabolite responses to 75-km cycling. Am J Physiol Integr Comp Physiol. 2014 Jul 1;307(1):R68–74.

391. Djouadi F, Lecarpentier Y, Hebert J-L, Charron P, Bastin J, Coirault C. A potential link between peroxisome proliferator-activated receptor signalling and the pathogenesis of arrhythmogenic right ventricular cardiomyopathy. Cardiovasc Res. 2009 Oct 1;84(1):83–90.

392. Parhami F, Jackson SM, Tintut Y, Le V, Balucan JP, Territo M, et al. Atherogenic Diet and Minimally Oxidized Low Density Lipoprotein Inhibit Osteogenic and Promote Adipogenic Differentiation of Marrow Stromal Cells. J Bone Miner Res. 1999 Dec 1;14(12):2067–78.

393. Jostarndt K, Rubic T, Kuhn H, Anthosen M., Andera L, Gellert N, et al. Enzymatically modified low-density lipoprotein upregulates CD36 in low-differentiated monocytic cells in a peroxisome proliferator-activated receptor-γ-dependent way. Biochem Pharmacol. 2004 Mar;67(5):841–54.

394. Hampel JKA, Brownrigg LM, Vignarajah D, Croft KD, Dharmarajan AM, Bentel JM, et al. Differential modulation of cell cycle, apoptosis and PPARγ2 gene expression by PPARγ agonists ciglitazone and 9-hydroxyoctadecadienoic acid in monocytic cells. Prostaglandins, Leukot Essent Fat Acids. 2006 May;74(5):283–93.

395. Jostarndt K, Gellert N, Rubic T, Weber C, Kühn H, Johansen B, et al. Dissociation of Apoptosis Induction and CD36 Upregulation by Enzymatically Modified Low-Density Lipoprotein in Monocytic Cells.

Biochem Biophys Res Commun. 2002 Jan;290(3):988–93.

396. Hussain SP, Amstad P, He P, Robles A, Lupold S, Kaneko I, et al. p53-Induced Up-Regulation of MnSOD and GPx but not Catalase Increases Oxidative Stress and Apoptosis. Cancer Res. 2004 Apr 1;64(7):2350–6.

397. Li J, Li Y, Chen L, Yu B, Xue Y, Guo R, et al. p53/PGC-1α-mediated mitochondrial dysfunction promotes PC3 prostate cancer cell apoptosis. Mol Med Rep. 2020 May 5.

398. Paulus WJ, Tschöpe C. A Novel Paradigm for Heart Failure With Preserved Ejection Fraction. J Am Coll Cardiol. 2013 Jul;62(4):263–71.

399. Louzao-Martinez L, Vink A, Harakalova M, Asselbergs FW, Verhaar MC, Cheng C. Characteristic adaptations of the extracellular matrix in dilated cardiomyopathy. Int J Cardiol. 2016 Oct;220:634–46.

400. Arad U, Madar-Balakirski N, Angel-Korman A, Amir S, Tzadok S, Segal O, et al. Galectin-3 is a sensor-regulator of toll-like receptor pathways in synovial fibroblasts. Cytokine. 2015 May;73(1):30–5.

401. de Boer RA, Daniels LB, Maisel AS, Januzzi JL. State of the Art: Newer biomarkers in heart failure. Eur J Heart Fail. 2015 Jun;17(6):559–69.

402. Oz F, Onur I, Elitok A, Ademoglu E, Altun I, Bilge AK, et al. Galectin-3 correlates with arrhythmogenic right ventricular cardiomyopathy and predicts the risk of ventricular -arrhythmias in patients with implantable defibrillators. Acta Cardiol. 2017 Jul 4;72(4):453–9.

403. Wenzel P, Kossmann S, Münzel T, Daiber A. Redox regulation of cardiovascular inflammation – Immunomodulatory function of mitochondrial and Nox-derived reactive oxygen and nitrogen species. Free Radic Biol Med. 2017 Aug;109:48–60.

404. Karbach S, Wenzel P, Waisman A, Munzel T, Daiber A. eNOS Uncoupling in Cardiovascular Diseases - the Role of Oxidative Stress and Inflammation. Curr Pharm Des. 2014 Jun;20(22):3579–94.

405. Agita A, Alsagaff MT. Inflammation, Immunity, and Hypertension. Acta Med Indones. 2017 Apr;49(2):158–65.

406. Guzik TJ, Touyz RM. Oxidative Stress, Inflammation, and Vascular Aging in Hypertension. Hypertension. 2017 Oct;70(4):660–7.

407. Wu J, Saleh MA, Kirabo A, Itani HA, Montaniel KRC, Xiao L, et al. Immune activation caused by vascular oxidation promotes fibrosis and hypertension. J Clin Invest. 2015 Nov 23;126(1):50–67.

408. Bulua AC, Simon A, Maddipati R, Pelletier M, Park H, Kim K-Y, et al. Mitochondrial reactive oxygen species promote production of proinflammatory cytokines and are elevated in TNFR1-associated periodic syndrome (TRAPS). J Exp Med. 2011 Mar 14;208(3):519–33.

409. Zhou R, Yazdi AS, Menu P, Tschopp J. A role for mitochondria in NLRP3 inflammasome activation. Nature. 2011 Jan 1;469(7329):221–5.

410. Li H, Durbin R. Fast and accurate long-read alignment with Burrows–Wheeler transform. Bioinformatics. 2010 Mar 1;26(5):589–95.

411. DePristo MA, Banks E, Poplin R, Garimella K V, Maguire JR, Hartl C, et al. A framework for variation discovery and genotyping using next-generation DNA sequencing data. Nat Genet. 2011 May 10;43(5):491–8.

412. Auwera GA, Carneiro MO, Hartl C, Poplin R, del Angel G, Levy-Moonshine A, et al. From FastQ Data to High-Confidence Variant Calls: The Genome Analysis Toolkit Best Practices Pipeline. Curr Protoc Bioinforma. 2013 Oct 15;43(1).

413. García-Alcalde F, Okonechnikov K, Carbonell J, Cruz LM, Götz S, Tarazona S, et al. Qualimap: evaluating next-generation sequencing alignment data. Bioinformatics. 2012 Oct 15;28(20):2678–9.

414. Jun G, Flickinger M, Hetrick KN, Romm JM, Doheny KF, Abecasis GR, et al. Detecting and Estimating Contamination of Human DNA Samples in Sequencing and Array-Based Genotype Data. Am J Hum Genet. 2012 Nov;91(5):839–48.

415. Weichenberger CX, Blankenburg H, Palermo A, D'Elia Y, König E, Bernstein E, et al. Dintor: functional annotation of genomic and proteomic data. BMC Genomics. 2015 Dec 21;16(1):1081.

416. Lek M, Karczewski KJ, Minikel E V., Samocha KE, Banks E, Fennell T, et al. Analysis of protein-coding genetic variation in 60,706 humans. Nature. 2016 Aug;536(7616):285–91.

417. The 1000 Genomes Project Consortium . A global reference for human genetic variation. Nature. 2015 Oct 30;526(7571):68–74.

418. Squellerio I, Caruso D, Porro B, Veglia F, Tremoli E, Cavalca V. Direct glutathione quantification in human blood by LC–MS/MS: comparison with HPLC with electrochemical detection. J Pharm Biomed Anal. 2012 Dec;71:111–8.

419. Dobin A, Davis CA, Schlesinger F, Drenkow J, Zaleski C, Jha S, et al. STAR: ultrafast universal RNA-seq aligner. Bioinformatics. 2013 Jan;29(1):15–21.

420. Langmead B, Salzberg SL. Fast gapped-read alignment with Bowtie 2. Nat Methods. 2012 Apr 4;9(4):357–9.

421. Liao Y, Smyth GK, Shi W. featureCounts: an efficient general purpose program for assigning sequence reads to genomic features. Bioinformatics. 2014 Apr 1;30(7):923–30.

422. Robinson MD, Oshlack A. A scaling normalization method for differential expression analysis of RNA-seq data. Genome Biol. 2010;11(3):R25.

423. McCarthy DJ, Chen Y, Smyth GK. Differential expression analysis of multifactor RNA-Seq experiments with respect to biological variation. Nucleic Acids Res. 2012 May 1;40(10):4288–97.

424. Risso D, Ngai J, Speed TP, Dudoit S. Normalization of RNA-seq data using factor analysis of control genes or samples. Nat Biotechnol. 2014 Sep 24;32(9):896–902.

425. Leek JT, Storey JD. A general framework for multiple testing dependence. Proc Natl Acad Sci. 2008 Dec 2;105(48):18718–23.

426. Subramanian A, Tamayo P, Mootha VK, Mukherjee S, Ebert BL, Gillette MA, et al. Gene set enrichment analysis: A knowledge-based approach for interpreting genome-wide expression profiles. Proc Natl Acad Sci. 2005 Oct 25;102(43):15545–50.

427. Merico D, Isserlin R, Stueker O, Emili A, Bader GD. Enrichment Map: A Network-Based Method for Gene-Set Enrichment Visualization and Interpretation. Ravasi T, editor. PLoS One. 2010 Nov 15;5(11):e13984.

428. Shannon P. Cytoscape: A Software Environment for Integrated Models of Biomolecular Interaction Networks. Genome Res. 2003 Nov 1;13(11):2498–504.

429. Sunitha K, Suresh P, Santhosh MS, Hemshekhar M, Thushara RM, Marathe GK, et al. Inhibition of

hyaluronidase by N-acetyl cysteine and glutathione: Role of thiol group in hyaluronan protection. Int J Biol Macromol. 2013 Apr;55:39–46.

430. Meraviglia V, Zanon A, Lavdas AA, Schwienbacher C, Silipigni R, Di Segni M, et al. Generation of Induced Pluripotent Stem Cells from Frozen Buffy Coats using Non-integrating Episomal Plasmids. J Vis Exp. 2015 Jun 5;(100).

431. Khan-Merchant N, Penumetcha M, Meilhac O, Parthasarathy S. Oxidized Fatty Acids Promote Atherosclerosis Only in the Presence of Dietary Cholesterol in Low-Density Lipoprotein Receptor Knockout Mice. J Nutr. 2002 Nov 1;132(11):3256–62.

432. Milano G, Raucci A, Scopece A, Daniele R, Guerrini U, Sironi L, et al. Doxorubicin and Trastuzumab Regimen Induces Biventricular Failure in Mice. J Am Soc Echocardiogr. 2014 May;27(5):568–79.

433. Seta F, Rahmani M, Turner P V., Funk CD. Pulmonary Oxidative Stress Is Increased in Cyclooxygenase-2 Knockdown Mice with Mild Pulmonary Hypertension Induced by Monocrotaline. Bogyo M, editor. PLoS One. 2011 Aug 5;6(8):e23439.

434. Urboniene D, Haber I, Fang Y-H, Thenappan T, Archer SL. Validation of high-resolution echocardiography and magnetic resonance imaging vs. high-fidelity catheterization in experimental pulmonary hypertension. Am J Physiol Cell Mol Physiol. 2010 Sep;299(3):L401–12.

435. Hansmann G, Fernandez-Gonzalez A, Aslam M, Vitali SH, Martin T, Mitsialis SA, et al. Mesenchymal Stem Cell-Mediated Reversal of Bronchopulmonary Dysplasia and Associated Pulmonary Hypertension. Pulm Circ. 2012 Apr;2(2):170–81.

436. Aquaro GD, Todiere G, Strata E, Barison A, Di Bella G, Lombardi M. Usefulness of india ink artifact in steady-state free precession pulse sequences for detection and quantification of intramyocardial fat. J Magn Reson Imaging. 2014 Jul;40(1):126–32.

437. Aquaro GD, Nucifora G, Pederzoli L, Strata E, De Marchi D, Todiere G, et al. Fat in left ventricular myocardium assessed by steady-state free precession pulse sequences. Int J Cardiovasc Imaging. 2012 Apr 12;28(4):813–21.

438. Sekihara K. Steady-State Magnetizations in Rapid NMR Imaging Using Small Flip Angles and Short

Repetition Intervals. IEEE Trans Med Imaging. 1987 Jun;6(2):157–64.

439. Park YM. CD36, a scavenger receptor implicated in atherosclerosis. Exp Mol Med. 2014 Jun 6;46(6):e99–e99.

440. Dominici M, Le Blanc K, Mueller I, Slaper-Cortenbach I, Marini F., Krause DS, et al. Minimal criteria for defining multipotent mesenchymal stromal cells. The International Society for Cellular Therapy position statement. Cytotherapy. 2006;8(4):315–7.

441. Beltrami AP, Cesselli D, Bergamin N, Marcon P, Rigo S, Puppato E, et al. Multipotent cells can be generated in vitro from several adult human organs (heart, liver, and bone marrow). Blood. 2007 Nov 1;110(9):3438–46.

442. Sung HJ, Kim J, Kim Y, Jang S-W, Ko J. N-acetyl cysteine suppresses the foam cell formation that is induced by oxidized low density lipoprotein via regulation of gene expression. Mol Biol Rep. 2012 Mar 17;39(3):3001–7.

443. Kim C, Majdi M, Xia P, Wei KA, Talantova M, Spiering S, et al. Non-Cardiomyocytes Influence the Electrophysiological Maturation of Human Embryonic Stem Cell-Derived Cardiomyocytes During Differentiation. Stem Cells Dev. 2010 Jun;19(6):783–95.

444. Strand DW, Jiang M, Murphy TA, Yi Y, Konvinse KC, Franco OE, et al. PPARγ isoforms differentially regulate metabolic networks to mediate mouse prostatic epithelial differentiation. Cell Death Dis. 2012 Aug 9;3(8):e361–e361.

445. Sato PY, Musa H, Coombs W, Guerrero-Serna G, Patiño GA, Taffet SM, et al. Loss of Plakophilin-2 Expression Leads to Decreased Sodium Current and Slower Conduction Velocity in Cultured Cardiac Myocytes. Circ Res. 2009 Sep 11;105(6):523–6.

446. Matsuzawa-Nagata N, Takamura T, Ando H, Nakamura S, Kurita S, Misu H, et al. Increased oxidative stress precedes the onset of high-fat diet–induced insulin resistance and obesity. Metabolism. 2008 Aug;57(8):1071–7.

447. Tsimikas S, Witztum JL, Miller ER, Sasiela WJ, Szarek M, Olsson AG, et al. High-Dose Atorvastatin Reduces Total Plasma Levels of Oxidized Phospholipids and Immune Complexes Present on

Apolipoprotein B-100 in Patients With Acute Coronary Syndromes in the MIRACL Trial. Circulation. 2004 Sep 14;110(11):1406–12.

448. Basso C, Corrado D, Marcus FI, Nava A, Thiene G. Arrhythmogenic right ventricular cardiomyopathy. Lancet. 2009 Apr;373(9671):1289–300.

449. Tepel M, van der Giet M, Statz M, Jankowski J, Zidek W. The Antioxidant Acetylcysteine Reduces Cardiovascular Events in Patients With End-Stage Renal Failure. Circulation. 2003 Feb 25;107(7):992–5.

450. Pabon MA, Manocha K, Cheung JW, Lo JC. Linking Arrhythmias and Adipocytes: Insights, Mechanisms, and Future Directions. Front Physiol. 2018 Dec 5;9.

451. te Riele AS, Tandri H, Bluemke DA. Arrhythmogenic right ventricular cardiomyopathy (ARVC): cardiovascular magnetic resonance update. J Cardiovasc Magn Reson. 2014 Dec 20;16(1):50.

452. Derosa G, Sahebkar A, Maffioli P. The role of various peroxisome proliferator-activated receptors and their ligands in clinical practice. J Cell Physiol. 2018 Jan;233(1):153–61.

453. FINCK B. The PPAR regulatory system in cardiac physiology and disease. Cardiovasc Res. 2007 Jan 15;73(2):269–77.

454. Borradaile NM, Han X, Harp JD, Gale SE, Ory DS, Schaffer JE. Disruption of endoplasmic reticulum structure and integrity in lipotoxic cell death. J Lipid Res. 2006 Dec;47(12):2726–37.

455. Taketa K, Matsumura T, Yano M, Ishii N, Senokuchi T, Motoshima H, et al. Oxidized Low Density Lipoprotein Activates Peroxisome Proliferator-activated Receptor-α (PPARα) and PPARγ through MAPK-dependent COX-2 Expression in Macrophages. J Biol Chem. 2008 Apr 11;283(15):9852–62.

456. Lee K-J, Kim H-A, Kim P-H, Lee H, Ma K-R, Park JH, et al. Ox-LDL suppresses PMA-induced MMP-9 expression and activity through CD36-mediated activation of PPAR-γ. Exp Mol Med. 2004 Dec 1;36(6):534–44.

457. Chawla A, Boisvert WA, Lee C-H, Laffitte BA, Barak Y, Joseph SB, et al. A PPARγ-LXR-ABCA1 Pathway in Macrophages Is Involved in Cholesterol Efflux and Atherogenesis. Mol Cell. 2001 Jan;7(1):161–71.

458. Hori M, Nishida K. Oxidative stress and left ventricular remodelling after myocardial infarction.

Cardiovasc Res. 2008 Oct 29;81(3):457–64.

459. Tofas T, Draganidis D, Deli CK, Georgakouli K, Fatouros IG, Jamurtas AZ. Exercise-Induced Regulation of Redox Status in Cardiovascular Diseases: The Role of Exercise Training and Detraining. Antioxidants. 2019 Dec 23;9(1):13.

460. Rassat J, Robenek H, Themann H. Structural relationship between desmosomes and mitochondria in human livers exhibiting a wide range of diseases. Am J Pathol. 1981 Dec;105(3):207–11.

461. Freddo T. Mitochondria attached to desmosomes in the ciliary epithelia of human, monkey, and rabbit eyes. Cell Tissue Res. 1988 Mar;251(3):671–5.

462. Pinali C, Bennett HJ, Davenport JB, Caldwell JL, Starborg T, Trafford AW, et al. Three-Dimensional Structure of the Intercalated Disc Reveals Plicate Domain and Gap Junction Remodeling in Heart Failure. Biophys J. 2015 Feb;108(3):498–507.

463. Nicholson AC, Hajjar DP. CD36, oxidized LDL and PPARγ: pathological interactions in macrophages and atherosclerosis. Vascul Pharmacol. 2004 May;41(4–5):139–46.

464. Kashyap VS, Santamarina-Fojo S, Brown DR, Parrott CL, Applebaum-Bowden D, Meyn S, et al. Apolipoprotein E deficiency in mice: gene replacement and prevention of atherosclerosis using adenovirus vectors. J Clin Invest. 1995 Sep 1;96(3):1612–20.

465. Stadiotti I, Pompilio G, Maione AS, Pilato CA, D'Alessandra Y, Sommariva E. Arrhythmogenic cardiomyopathy: what blood can reveal? Hear Rhythm. 2019 Mar;16(3):470–7.

466. Tsutsui T, Tsutamoto T, Wada A, Maeda K, Mabuchi N, Hayashi M, et al. Plasma oxidized low-density lipoprotein as a prognostic predictor in patients with chronic congestive heart failure. J Am Coll Cardiol. 2002 Mar;39(6):957–62.

467. Ky B, Burke A, Tsimikas S, Wolfe ML, Tadesse MG, Szapary PO, et al. The Influence of Pravastatin and Atorvastatin on Markers of Oxidative Stress in Hypercholesterolemic Humans. J Am Coll Cardiol. 2008 Apr;51(17):1653–62.

468. Oesterle A, Laufs U, Liao JK. Pleiotropic Effects of Statins on the Cardiovascular System. Circ Res. 2017 Jan 6;120(1):229–43.

469. KOSTAPANOS M, LIBEROPOULOS E, GOUDEVENOS J, MIKHAILIDIS D, ELISAF M. Do statins have an antiarrhythmic activity? Cardiovasc Res. 2007 Jul 1;75(1):10–20.

470. Mansor LS, Sousa Fialho M da L, Yea G, Coumans WA, West JA, Kerr M, et al. Inhibition of sarcolemmal FAT/CD36 by sulfo-N-succinimidyl oleate rapidly corrects metabolism and restores function in the diabetic heart following hypoxia/reoxygenation. Cardiovasc Res. 2017 Jun;113(7):737–48.

471. Shafiei E, Bahtoei M, Raj P, Ostovar A, Iranpour D, Akbarzadeh S, et al. Effects of N-acetyl cysteine and melatonin on early reperfusion injury in patients undergoing coronary artery bypass grafting. Medicine (Baltimore). 2018 Jul;97(30):e11383.

472. Schmidt HHHW, Stocker R, Vollbracht C, Paulsen G, Riley D, Daiber A, et al. Antioxidants in Translational Medicine. Antioxid Redox Signal. 2015 Nov 10;23(14):1130–43.

473. Münzel T, Gori T, Bruno RM, Taddei S. Is oxidative stress a therapeutic target in cardiovascular disease? Eur Heart J. 2010 Nov;31(22):2741–8.

474. Daiber A, Steven S, Weber A, Shuvaev V V., Muzykantov VR, Laher I, et al. Targeting vascular (endothelial) dysfunction. Br J Pharmacol. 2017 Jun;174(12):1591–619.

475. Thiele H, Hildebrand L, Schirdewahn C, Eitel I, Adams V, Fuernau G, et al. Impact of High-Dose N-Acetylcysteine Versus Placebo on Contrast-Induced Nephropathy and Myocardial Reperfusion Injury in Unselected Patients With ST-Segment Elevation Myocardial Infarction Undergoing Primary Percutaneous Coronary Intervention. J Am Coll Cardiol. 2010 May;55(20):2201–9.

476. Hsu S-P, Chiang C-K, Yang S-Y, Chien C-T. N-Acetylcysteine for the Management of Anemia and Oxidative Stress in Hemodialysis Patients. Nephron Clin Pract. 2010;116(3):c207–16.

477. Cui Y, Narasimhulu CA, Liu L, Zhang Q, Liu PZ, Li X, et al. N-acetylcysteine inhibits in vivo oxidation of native low-density lipoprotein. Sci Rep. 2015 Dec 5;5(1):16339.